

**MEASUREMENTS AND MODELING OF GAS FLUXES
IN UNSATURATED MINE WASTE MATERIALS**

by

LOUIS KATELE KABWE

Dipl., Institut de Recherche Scientifique, 1977
B.Sc., Université du Québec à Montréal, 1983
M.Sc., M.Sc., The University of Saskatchewan, 1994, 2001

A THESIS SUBMITTED IN PARTIAL FULFILMENT OF
THE REQUIREMENTS FOR THE DEGREE OF

DOCTOR OF PHILOSOPHY

in

THE FACULTY OF GRADUATE STUDIES

(Mining Engineering)

THE UNIVERSITY OF BRITISH COLUMBIA

June 2007

© Louis Katele Kabwe, 2007

Abstract

Accurate measurements and predictions of surface CO₂ fluxes are needed to quantify biogeochemical reaction rates in unsaturated geologic media and soils. However, no standard appears to exist for establishing the accuracy of field measurements of soil respiration rates. As a result, a technique to measure CO₂ fluxes from the soil surface to the atmosphere was recently developed and verified in mesocosms over the range of CO₂ fluxes reported for field conditions. The method, termed the dynamic closed chamber (DCC), was shown to accurately measure CO₂ fluxes from ground surface to the atmosphere in mesocosms. The main advantage of this direct technique is the almost instantaneous estimation of the CO₂ flux. Although the DCC is a promising technique, its ability to accurately quantify surface CO₂ flux under field conditions remains to be verified.

The field application of the DCC is investigated in this thesis with a particular focus on quantifying reaction rates in waste-rock piles at the Key Lake uranium mine in northern Saskatchewan, Canada. It should, however, be noted that the dominant geochemical reactions in the two waste-rock piles at the Key Lake mine were not typical of acid rock drainage (ARD) waste-rock piles. The CO₂ fluxes measured in this study occur in the organic material underlying the waste rocks, in contrast to ARD waste-rock piles where O₂ consumption and CO₂ production are the results of sulphide oxidation and carbonate buffering. This work provided a complete suite of measurements required to characterize spatial distribution of CO₂ fluxes on larger-scale studies of waste-rock piles. There has been no previous field-scale study to quantify CO₂ fluxes across a waste-rock pile.

The ability of the DCC method to accurately quantify field soil respiration was demonstrated by comparing the DCC fluxes to those obtained using two other CO₂ flux measurement techniques: the static closed chamber (SCC) and eddy covariance (EC) methods. The DCC yielded comparable data but had distinct advantages over the two other methods in terms of speed and repeatability.

The DCC was also used to investigate CO₂ fluxes under the climatic variables (e.g., rainfall and evaporation) that affect soil water content at the Deilmann north (DNWR) and Deilmann south (DSWR) waste-rock piles, at the Key Lake uranium mine. The effects of rainfall events on waste-rock surface-water conditions and CO₂ fluxes were of short duration.

A simple model for predicting the effects of soil water content on CO₂ diffusion coefficient and concentration profiles was developed. The model was verified with measured CO₂ fluxes obtained from meso-scale columns of unsaturated sand. Verification of the model showed good agreement between predicted and measured data. The model was subsequently used to predict CO₂ diffusion and concentration profiles in response to changes in soil water contents in the piles and also to predict surface CO₂ fluxes from the DNWR and DSWR for a 6-d test period [August 1 (day 3) to August 6 (day 8) 2002] following a 72.9 mm precipitation event over the initial 48-h [July 30 (day 1) to July 31 (day 2) 2002]. The model predicted surface CO₂ fluxes trends that were very similar to the measured surface CO₂ fluxes from the DNWR and DSWR piles during the test period

Based on the tests conducted in this thesis the DCC method has shown to be suitable for field applications to quantify CO₂ fluxes and to characterize the spatial and temporal dynamics of CO₂ fluxes from unsaturated C-horizon soils and waste-rock piles.

Table of Contents

	Page
Abstract	ii
Table of Contents	iv
List of Tables	ix
List of Figures	x
Abbreviations and Symbols	xxiii
Acknowledgements	xxvii
Dedication	xxviii
CHAPTER 1: Introduction	1
1.1 Introduction.....	1
1.2 Research Objectives.....	3
1.3 Organization of the Thesis.....	5
CHAPTER 2: Literature Review	7
2.1 Introduction.....	7
2.2 Waste-Rock Piles.....	8
2.3 Sources of CO ₂ in Subsurface Soils and Waste-Rock Piles.....	19
2.3.1 CO ₂ Production by Microbial Respiration (Biotic).....	20
2.3.2 CO ₂ Production by Pyrite Oxidation-Carbonate Buffering (Abiotic).....	24
2.4 Studies of CO ₂ in Subsurface Pore Gas and Associated Surface Gas Fluxes from Waste Rock and non Waste-Rock Systems.....	27
2.4.1 Studies of Subsurface CO ₂ Gas and Surface CO ₂ Fluxes from Waste Rock Piles.....	28
2.4.2 Studies of Subsurface CO ₂ from Non-Waste-Rock Material.....	31

2.5	Climatic Variables Affecting Subsurface and Surface Gas Fluxes: Precipitation and Evaporation.....	39
2.5.1	Evaporation.....	40
2.5.2	Methods of Predicting Evaporation.....	44
2.5.3	SoilCover Program.....	47
2.5.4	Chapter Summary.....	50
CHAPTER 3: Materials and Methods		53
3.1	Introduction.....	53
3.2	Laboratory Program.....	53
3.2.1	Sample Collection.....	53
3.2.2	Grain-Size Analysis.....	54
3.2.3	Water Retention Curve.....	56
3.2.4	Saturated Hydraulic Conductivity.....	58
3.3	Laboratory Mesocosm and Minicosms (sand columns).....	62
3.4	Field Program.....	65
3.4.1	Site Location and Description.....	66
3.4.2	Field CO ₂ Flux Measurements Methods.....	72
	3.4.2.1 Measuring CO ₂ Fluxes using Dynamic Closed Chamber (DCC) Method.....	74
	3.4.2.2 Measuring CO ₂ Fluxes using Static Closed Chamber (SCC) Method.....	77
	3.4.2.3 Measuring CO ₂ Fluxes using Eddy Covariance (EC) Method.....	80
	3.4.2.4 Gravimetric Water Content Measurement.....	83
	3.4.2.5 Meteorological Weather Station.....	83
	3.4.2.6 Chapter Summary.....	84

CHAPTER 4: Results and Data Interpretation	86
4.1 Laboratory Tests Program.....	86
4.1.1 Grain-Size Distribution.....	86
4.1.2 Water Retention Curve.....	91
4.1.3 Hydraulic Conductivity.....	99
4.2 Field Tests Program.....	104
4.2.1 Diurnal Variation In CO ₂ Flux.....	104
4.2.2 Spatial and Temporal Variation in CO ₂ Flux Measured using the Dynamic Closed Chamber at the Deilmann South Waste-Rock Pile.....	107
4.2.3 Spatial and Temporal Variations in CO ₂ Flux Measured using the Dynamic Closed Chamber at the Deilmann North Waste-Rock Pile.....	112
4.2.4 Cross-Statistical Comparison Between CO ₂ Fluxes Measured from across the DNWR and DSWR.....	115
4.3. Comparison of CO ₂ Fluxes Measured using the DCC to those Measured using Static Closed Chamber (SCC) and Eddy Covariance (EC) Methods on the Deilmann South Waste Rock Pile (DSWR).....	117
4.3.1 Introduction.....	117
4.3.2 DCC Fluxes.....	118
4.3.3. SCC Fluxes.....	118
4.3.4 EC Fluxes.....	123
4.3.4 Summary of the advantages and disadvantages of the dynamic closed chamber (DCC) method.....	129
CHAPTER 5: Analysis and Discussion	131
5.1. Introduction.....	131

5.2	Effects of Rainfall Events on Waste-Rock Surface Water Conditions and CO ₂ Fluxes Across the Surfaces of the Deilmann North (DNWR) and Deilmann South (DSWR) Waste Rock Piles.....	131
5.2.1	Short Term Effects of Rainfall Events on Near Surface-Water Conditions.....	132
5.2.2	Short Term Effects of Rainfall Events on CO ₂ Fluxes.....	138
5.3	Predictions of Evaporative Fluxes and Near-Surface Water Contents Profiles.....	142
5.3.1	Short Term Predictions of Evaporative Fluxes	144
5.3.2	Short Term Predictions of Near Surface Water Contents Profiles	150
5.4	CO ₂ Diffusion Prediction and Model Proposed.....	153
5.4.1	CO ₂ Diffusion.....	153
5.4.2	Biotic CO ₂ Production Rate.....	159
5.4.3	Development of the Partial Differential Equation.....	163
5.4.4	Finite Difference Formulation.....	166
5.5	Computer Code Program.....	169
5.6	Application of the "CO ₂ " Model Using Measured Values in Sand Minicosms ..	173
5.6.1	Prediction of CO ₂ Concentration Profiles in Response to Changes in Water Contents Profiles.	173
5.6.2	Simulations of CO ₂ Concentrations Profiles using Sand Minicosms Measured Data.....	176
5.7	Prediction of CO ₂ Diffusion and Concentration-Depth Profiles in Response to Changes in Water-Depth Profiles in the DSWR.....	181

5.8	Predictions of CO ₂ Diffusion and Surface CO ₂ Flux from the DNWR and DSWR Piles Following Rainfall Events.....	188
5.9	Chapter Summary.....	192
	CHAPTER 6: Summary and Conclusions.....	193
	References.....	197
	Appendices.....	219
	Appendix A: Measuring O ₂ Fluxes Using the Dynamic Closed Chamber (DCC) System.....	219
	Appendix B: Eddy Correlation Method: a Brief Theory.....	227
	Appendix C: Computer Code for CO ₂ Diffusion Model.....	231
	Appendix D: Waste-Rock Samples Analyses Results.....	244
	Appendix E: CO ₂ Flux Measurements Results obtained at the Deilmann south (DSWR) and Deilmann north (DNWR) Waste-rock Piles using the Dynamic Closed Chamber (DCC), Static Closed Chamber (SCC) and Eddy Covariance (EC) Methods.	252
	Appendix F: Data for Measurements of Water Contents and CO ₂ Fluxes Across the Surfaces of the DSWR and DNWR Piles after Rainfall Events.....	257
	Appendix G: Minicosms Data used for Validation of the CO ₂ Diffusion Model	259
	Appendix H: Climatic Parameters used in Simulations with SoilCover and recorded at the weather station installed on the Deilmann south waste-rock (DSWR) pile.....	262
	Appendix I: SoilCover Run Summary Pages for Simulations of Evaporative Fluxes At the DSWR and DNWR Piles during the Field Tests.....	254

List of Tables

	Page
Table 2.1 In-situ thermal conductivity measurements in waste-rock dumps material.....	15
Table 2.2 In-situ air permeability measurements in waste-rock dump material...	15
Table 2.3 In-situ oxygen diffusion coefficient measurements in waste-rock dumps.....	15
Table 2.4 Typical physical properties of ARD waste-rock piles (Ritchie, 1994a).	16
Table 2.5 Physicochemical properties of the Doyon and Nordhalde waste rock piles (Lefebvre et al., 2001).....	17
Table 2.6 Typical characteristics of ARD (Ritchie, 1994a).....	18
Table 2.7 Summary of CO ₂ concentrations for waste-rock material.....	28
Table 2.8 Summary of CO ₂ concentrations for non-waste-rock material.....	31
Table 2.9 Summary of surface CO ₂ fluxes for non-waste-rock material	33
Table 4.1 Nature, origin, and basic geotechnical properties of various granular materials.....	87
Table 4.2 Nature and origin of data for the hydraulic conductivity “k” value of various granular materials.....	103
Table 4.3 Summary of results of CO ₂ flux measurements using the dynamic closed chamber system (DCC) for the test period of 2000-2002 at Deilmann south waste-rock pile (DSWR).....	112
Table 4.4 Summary of results of CO ₂ flux measurements using the dynamic closed chamber system (DCC) for the test period of 2000-2002 at Deilmann north waste-rock pile (DNWR).....	113

List of Figures

		Page
Figure 2.1	Diagram describing the complex flow system develop within the waste-rock dump in response to precipitation and climatic conditions.....	9
Figure 2.2	Conceptual model of water flow and vapour transport in a waste-rock dumps	11
Figure 2.3	(A) Depth geologic profile for Deilmann south waste-rock (DSWR) pile (Adapted from Birkham et al., 2003 and (B) Map showing the Deilmann north (DNWR), Deilmann south (DSWR) and outline of former lake bed at the Key Lake mine, Saskatchewan, Canada.....	22
Figure 2.4	O ₂ consumption rates vs CO ₂ production rates for forest soils, lake bottom sediments, and gneissic waste rocks units: $\mu\text{mol/kg/week}$; x represents gneissic waste rocks (DNWR); Δ represents lake bottom sediments collected from beneath the waste-rock pile (DNWR); \square represents forest soils (natural forest site adjacent to the DNWR) (Lee et al., 2003b).	23
Figure 2.5	(A) Relation of evaporation (flux) to time under different evaporativities. (B) Relation of relative evaporation rate (actual rate as a function of the potential rate) to time, indicating the three stages of the drying process.....	42
Figure 3.1	Photographs showing the mechanical sieve machine and sedimentation process setups.....	55

Figure 3.2	Schematic diagram and photograph of Tempe cell setup for measurement of soil water characteristic curve.....	57
Figure 3.3	Schematic diagram and photograph of permeameter cell setup for measurement of saturated hydraulic conductivity.....	60
Figure 3.4	Schematic diagram and photographs of the columns (mesocosm and minicosms) used to calibrate and verify the dynamic closed chamber method.....	63
Figure 3.5	Map of Saskatchewan showing the location of the Key Lake uranium mine, Saskatchewan, Canada.....	67
Figure 3.6	Photograph showing the Deilmann pit, the Deilmann north waste-rock (DNWR) and Deilmann south waste-rock (DSWR) piles at the Key Lake uranium mine, Saskatchewan, Canada	69
Figure 3.7	Depth geologic profile for Deilmann south waste-rock (DSWR pile at the Key Lake mine, Saskatchewan, Canada (Adapted from Birkham et al., 2003).....	71
Figure 3.8	Map of the Deilmann north waste-rock (DNWR) and Deilmann south waste-rock (DSWR) piles at the Key Lake mine, Saskatchewan, Canada, showing the chambers and the meteorological weather station locations.	73
Figure 3.9	Schematic diagram and photograph of the dynamic closed chamber (DCC) setup for surface CO ₂ flux measurements.....	75

Figure 3.10	(A) Typical slopes of direct measurement of concentration versus time using the dynamic closed chamber (DCC) method (B) schematic diagram and (C) photograph of the DCC method setup for measuring surface CO ₂ gas fluxes	78
Figure 3.11	Photograph showing the meteorological weather station and the eddy covariance (EC) sensors for measuring CO ₂ flux installed on Deilmann south waste-rock (DSWR).....	81
Figure 3.12	(A) Schematic diagram and (B) photograph of meteorological weather station installed on Deilmann south waste-rock (DSWR) pile at the Key Lake mine, Saskatchewan, Canada.....	85
Figure 4.1	Particle size distribution curves (without gravel and boulder-sized) for the samples of waste-rock from Deilmann south waste-rock pile (DSWR) for ground surface sand (curve with symbols) and core sand/sandstone (curves with full lines). Symbols represent the measured data from this thesis. The full lines show the one standard deviation range of grain-size data obtained by Birkhman et al. (2002).....	88
Figure 4.2	Particle size (without gravel and boulder-sized) distribution curves for the samples of waste-rock from Deilmann north waste-rock pile (DNWR) for ground surface sand (curve with broken line and symbols) and core basement-rock (curves with solid lines). Symbols represent the measured data from this thesis. The full lines show the one standard deviation range of grain-size data obtained by Birkhman et al. (2002).....	89

Figure 4.3	Water retention curve (WRC) of the sample of waste-rock (with fine fraction only) from the Deilmann north waste-rock (DNWR) pile. Symbols represent the measured data and the solid line the best fit curve generated with SoilCover (SoilCover, 1997).	92
Figure 4.4	Water retention curve (WRC) of the sample of waste-rock (with fine fraction only) from the Deilmann south waste-rock (DSWR) pile. Symbols represent the measured data and the solid line the best fit curve generated with SoilCover (SoilCover, 1997).....	93
Figure 4.5	Water Retention Curve (WRC) of the sample of waste-rock from the Deilmann north (DNWR) pile: Symbols represent the measured data and the solid line represents the best fit curve generated with SoilCover(SoilCover, 1997).....	95
Figure 4.6	Water Retention Curve (WRC) of the sample of waste-rock from the Deilmann south (DSWR) pile: Symbols represent the measured data for and the solid line represens the best fit curve generated with SoilCover (SoilCover, 1997).....	96
Figure 4.7	Characteristic of the sample of the waste-rock from the Deilmann north waste-rock pile (DNWR): hydraulic conductivity curve (K). The value of saturated hydraulic conductivity (K_{sat}) was measured in the laboratory but the unsaturated hydraulic conductivity (K) was derived from the Brooks and Corey mode (Brooks and Corey, 1964).....	101

Figure 4.8	Characteristic of the sample of the waste-rock from the Deilmann north waste-rock pile (DNWR): hydraulic conductivity curve (K). The value of saturated hydraulic conductivity (K_{sat}) was measured in the laboratory but the unsaturated hydraulic conductivity (K) was derived from the Brooks and Corey mode (Brooks and Corey, 1964).....	102
Figure 4.9	Short-term (hourly) variations in the CO_2 flux measured at DSF1 on August 6, 2000. Fluxes were determined using the dynamic closed chamber (DCC) method and averaging a series of four to eight measurement cycles, with each cycle lasting from 2- to 8-min (depending on the magnitude of the flux). The shaded box represents the 95% confidence interval ($\pm 17 \text{ mg } CO_2 \text{ m}^{-2} \text{ h}^{-1}$) around the calculated daily mean ($235 \text{ mg } CO_2 \text{ m}^{-2} \text{ h}^{-1}$).....	106
Figure 4.10	(A) CO_2 fluxes measured using the dynamic closed chamber (DCC) at twenty selected sampling stations (DSF1 – DSF20) at the Deilmann south waste-rock pile (DSWR) (Figure 3.8) during the summers of 2000 and 2002 (B) average flux values ($\text{mg } CO_2 \text{ m}^{-2} \text{ h}^{-1}$) measured from sampling locations (●) on the DSWR.....	108

- Figure 4.11** Daily variations in the CO₂ flux measured at the Deilmann south waste rock (DSWR) pile in (A) July, (B) August, and (C) September 2000. Flux measurements were obtained at three to four locations on each sampling date. At each location, the flux was determined using the dynamic closed chamber (DCC) method and averaging a series of four to eight measurement cycles, with each cycle lasting from 2- to 8-min (depending on the magnitude of the flux). The overall mean for each monthly sampling period is represented by the dashed lines (- - -). Within months, symbols labeled with the same letter are not significantly different at the $P \leq 0.05$ level of probability. 109
- Figure 4.12** Box & Whisker plot characterizing the spatial and long-term temporal variability in the CO₂ flux measured using the dynamic closed chamber (DCC) method at the Deilmann south waste-rock (DSWR) pile in 2000 and 2002. The estimated, time-averaged flux = 170 (\pm 51) mg CO₂ m⁻² h⁻¹. The minimum and maximum flux values are marked by asterisks (*). Note: values occurring beyond the “whiskers” were identified as outliers and were not included in the analysis of variance..... 111
- Figure 4.13** CO₂ fluxes measured using the dynamic closed chamber (DDC) at nine sampling stations (DNF1 – DNF9) at the Deilmann north waste-rock pile (Figure 3.6) during the summers of 2000 and 2002: (A) Data points presented on a XY (scatter) and (B) average flux values (mg CO₂ m⁻² h⁻¹) from samplings locations on the DNWR. ... 114

Figure 4.14	Spatial and temporal variations in CO ₂ fluxes measured during the summer of 2000 and summer 2002: box-and-wisker plots showing the mean, standard deviation, and extreme values for Deilmann north waste-rock (DNWR) pile data.....	116
Figure 4.15	Box-and-wisker plot for flux measurements obtained using the DCC method at the Deilmann south waste-rock (DSWR) pile during the period from August 24 th to August 25 th , 2002 (set of data for comparison with the other two methods: SCC and EC). The minimum and maximum flux values are marked by asterisks (*). Note: values occurring beyond the “whiskers” were identified as outliers and were not included in the analysis of variance.....	119
Figure 4.16	(A) CO ₂ flux values (mg m ⁻² h ⁻¹) obtained using the static closed chamber (SCC) at eleven selected sampling stations (●) at the Deilmann south waste-rock (DSWR) pile in the morning (AM) (between 10:00 and 11:00) and afternoon (PM) between 16:30 and 17:30) on August 24, 2002 (B) averages fluxes (mg CO ₂ m ² h ⁻¹) from the sampling locations.....	120
Figure 4.17	Box-and-wisker plots for CO ₂ flux measurements obtained from the Deilmann south waste rock pile on August/24/2002. Measurements were obtained using the static closed chamber method between the hours of 10:00 and 11:00 AM and 16:30 and 17:30 PM. The minimum and maximum flux values are marked by asterisks *. Note: values occurring beyond the “whiskers” were identified as outliers and were not included in the analysis of variance.....	121

- Figure 4.18** Comparison of the dynamic closed chamber (DCC) and static closed chamber (SCC) methods for measuring CO₂ fluxes. Flux measurements were obtained at the Deilmann south waste-rock (DSWR) pile site during the period from August 24th to August 25th, 2002. The minimum and maximum flux values are marked by asterisks (*). Note: values occurring beyond the “whiskers” were identified as outliers and were not included in the analysis of variance..... 122
- Figure 4.19** Diurnal variations in the CO₂ flux measured from 10:00 to 17:00 on August 25, 2002 using the EC method at the Deilmann south waste-rock (DSWR) pile. The shaded box represents the 95% confidence interval ($\pm 24 \text{ mg CO}_2 \text{ m}^{-2} \text{ h}^{-1}$) around the calculated daily mean ($150 \text{ mg CO}_2 \text{ m}^{-2} \text{ h}^{-1}$)..... 124
- Figure 4.20** Measured CO₂ fluxes using Eddy covariance (EC) at the Deilmann south waste-rock (DSWR) pile. Measurements were obtained on a continuous basis during the period from June 25th to August 25th 2002. Each data point represents the daily mean value averaged over the period from 10:00 to 17:00 hours: The shaded box (B) represents the 95% confidence interval ($\pm 10 \text{ mg CO}_2 \text{ m}^{-2} \text{ h}^{-1}$) around the overall mean ($150 \text{ mg CO}_2 \text{ m}^{-2} \text{ h}^{-1}$). Note: gaps in the data set represent precipitation events during which no useful data were collected by the EC system. 125

Figure 4.21	Comparison of the eddy covariance (EC) and chamber-based methods for measuring the CO ₂ flux from the Deilmann south waste-rock (DSWR) pile.....	127
Figure 5.1	Rainfall and volumetric water contents measured over an 8-day test period [July 30 (day 1) to August 6 (day 8), 2002] at station DNF1 with time at the Deilmann north waste-rock (DNWR) pile.....	133
Figure 5.2	Rainfall and volumetric water contents measured over an 8-day test period [July 30 (day 1) to August 6 (day 8), 2002] at sampling station DSF1 with time at the Deilmann south waste-rock pile (DSWR)	134
Figure 5.3	Volumetric water content profiles measured over an 8-d test period (30 July (day 1) to 6 August (day 8) 2002 at station: (A) DSF1 at the Deilmann south waste-rock (DSWR) pile and (B) DNF1 at the Deilmann north waste-rock (DNWR) pile with time.....	137
Figure 5.4	Rainfall, water contents, and CO ₂ fluxes measured at sampling station DNF1 over an 8-d test period (30 July (day 1) to 6 August (day 8) 2002) at the Deilmann north waste-rock (DNWR) pile with time.....	139
Figure 5.5	Rainfall, water contents, and CO ₂ fluxes measured at sampling station DSF1 over an 8-d test period (30 July (day 1) to 6 August (day 8) 2002) at the Deilmann south waste-rock (DSWR) pile with time.....	140

Figure 5.6	Variations in CO ₂ flux measurements with surface-water saturation (S=θ/n) measured over an 8-d test period [July 30 (day 1) to August 6 (day 8), 2002] at DSF1 and DNF1 at the Deilmann south waste-rock pile (DSWR) and Deilmann north waste-rock pile (DNWR) respectively.....	143
Figure 5.7	(A) Rainfall, water contents measured, and SoilCover predicted evaporative fluxes at the Deilmann north waste-rock (DNWR) pile (B) ratio of actual (AE) and potential (PE) evaporation as a function of time over an 8-d test period [30 July (day 1) to 6 August (day 8) 2002].	145
Figure 5.8	(A) Rainfall, water contents measured, and SoilCover predicted evaporative fluxes at the Deilmann north waste-rock (DSWR) pile (B) ratio of actual (AE) and potential (PE) evaporation as a function of time over an 8-d test period [30 July (day 1) to 6 August (day 8) 2002].	146
Figure 5.9	SoilCover predicted evaporative fluxes (actual AE and potential (PE) and (B) ratio of AE/PE at the Deilmann south waste-rock pile (DSWR) over a 27-d test period (29 July (day 1) to 24 August (day 27) 2002) with time.....	148
Figure 5.10	SoilCover predicted evaporative fluxes (actual AE and potential (PE) and (B) ratio of AE/PE at the Deilmann north waste-rock pile (DNWR) over a 27-d test period (29 July (day 1) to 24 August (day 27) 2002) with time.....	149

Figure 5.11	Comparison of (A) measured and (B) SoilCover simulated water content profiles and (B) SoilCover predicted water contents for a 6-d test period [30 July (day 3) to 4 August (day 8), 2002] at the Deilmann north waste-rock (DNWR) pile.....	151
Figure 5.12	Comparison of (A) measured and (B) SoilCover simulated water content profiles and (B) SoilCover predicted water contents for a 6-d test period [30 July (day 3) to 4 August (day 8), 2002] at the Deilmann south waste-rock (DSWR) pile.....	152
Figure 5.13	(A) Hypothetical water content profiles obtained by reducing the initial water profile (d1) by a factor of 0.8 consecutively (B) Simulated effective diffusion coefficient (D_e) of CO_2 as a function of water content using artificial data presented above.....	158
Figure 5.14	Simulated microbial respiration rates as a function of temperature and water content using Equation 5.21.....	163
Figure 5.15	Representative elementary volume, REV, for derivation of partial differential equation.....	164
Figure 5.16	Three nodes and the mass fluxes entering and exiting node 1 for development of the finite difference formulation.....	167
Figure 5.17	Flowchart for Visual Basic program.....	170
Figure 5.18	Stability curves generated by the model for different iterations using time steps of 0.05 day.....	172

Figure 5.19	(A) Hypothetical water contents profiles in a sand material described in Figure 5.13A (B) Model predicted CO ₂ concentrations profiles in a HT sand column obtained with hypothetical simulated water contents profiles (Figure 5.19A) and an initial measured CO ₂ concentrations profiles (d1) in HT column (Kabwe et al., 2002).....	175
Figure 5.20	Measured volumetric water content profiles in the low (A) temperature (LT) (thermostat set at 5 °C) and (B) high (21 temperature (HT) (room temperature) minicosms. ∇ represent the water table.....	177
Figure 5.21	Measured CO ₂ concentration profiles in the (A) high temperature (HT) (21 – 23 °C) and low temperature (LT) (5 °C) minicosms (Richards, 1998; Kabwe, 2001).....	179
Figure 5.22	Model predicted CO ₂ concentration profiles in the (A) high temperature (HT) (21 – 23 °C) and (B) low temperature (LT) (5°C) minicosms	180
Figure 5.23	Relationship between measured and simulated CO ₂ concentrations from (A) low temperature (LT) and (B) high temperature (HT) minicosms plotted on a 1:1 scale	182
Figure 5.24	Depth profiles for Deilmann south waste-rock (DSWR) pile (A) Geologic profile (B) mean CO ₂ concentration (Vol.) and (C) mean volumetric water contents values (Adapted from Birkham et al, 2003).....	184

Figure 5.25	(A) Hypothetical water-depth profiles in DSWR pile and (B) model predicted effective diffusion coefficients (D_e) in response to changes in water contents (Figure 5.32A). Curve d1 represents the actual measured mean water- depth profile (Birkham et al., 2003). The subsequent profiles were generated by reducing the initial measured water-depth profile by a factor of 0.1 consecutively.....	186
Figure 5.26	Model predicted changes in: (A) effective diffusion coefficient (D_e) and (B) CO_2 concentrations profiles in response to changes in water contents profiles described in Figure 5.32A.....	187
Figure 5.27	Rainfall, measured surface water content and CO_2 flux and predicted effective diffusion coefficient (D_e) and surface CO_2 flux at the Deilmann North waste-rock (DNWR) pile over an 8-day test period [30 July (day 1) to 6 August (day 8) 2002] with time.....	189
Figure 5.28	Rainfall, measured surface water content and CO_2 flux and predicted effective diffusion coefficient (D_e) and surface CO_2 flux at the Deilmann South waste-rock (DSWR) pile over an 8-day test period [30 July (day 1) to 6 August (day 8) 2002] with time.....	190

Abbreviation and Symbols

1. Abbreviations	Meaning
A	Area
A_{rh}	Inverse of relative humidity of air
AE	Actual evaporation
AEV	Air entry value
B_{rh}	Inverse of relative humidity of soil surface
C	Concentration
C_p	Specific heat capacity
C_u	Uniformity coefficient
C_v	Specific heat of the soil
C_h	Volumetric specific heat of the soil
C_w	Coefficient of consolidation with respect to water phase
CV	Coefficient of variation
D*	Bulk diffusion coefficient
D_e	Effective diffusion coefficient
D_a	Diffusion coefficient through air phase
D_H	Equivalent particle diameter
D_w	Diffusion coefficient through water phase
D_v	Diffusion coefficient of water vapor
D_{vap}	Molecular diffusion of water vapor
DAS	Data acquisition system
DCC	Dynamic closed chamber
DNF#	Collar location # at Deilmann north
DSF#	Collar location # at Deilmann south
DNWR	Deilmann north waste-rock
DSWR	Deilmann south waste-rock
E	Vertical Evaporative flux
E_a	Actual evaporation
E_p	Potential evaporation
E_h	Sensible heat flux

EC	Eddy covariance
e	Void ratio
e_s	Vapour pressure at the soil surface
e_a	Vapour pressure of the air above the evaporating surface
f(u)	Wind mixing function
F_{CO2}	Flux of carbon dioxide
g	Acceleration due to gravity
G	Production rate
G_o	Reference production rate
G_r	Ground heat flux
G_s	Ground heat flux
h	Height
h_r	Relative humidity of the soil surface
h_w	Total head
H_h	Pressure head
H	Henry's Law coefficient
HT	High temperature
k	Hydraulic conductivity
k_r	Constant in Arrhenius equation
k_s	Saturated hydraulic conductivity
L	Pore-size distribution index
L_v	Latent heat of evaporation of water
m	Total mass of gas
P	Total Pressure
PE	Potential evaporation
P_s	Saturation vapour pressure of the soil
P_{sv}	Saturation vapour pressure of soil
P_v	Vapor pressure within the soil
q	Humidity
Q_n	Net radiant energy available at the surface
R	Universal gas constant
REV	Representative elementary volume
R_c	Concentration ratio of two isotopes

S	Degree of saturation
S_r	Residual saturation
S_e	Effective saturation
SCC	Static closed chamber
SWCC	Soil water characteristic curve
t	time
T	Temperature
T_a	Air temperature
T_s	Surface temperature
T_{ra}	Tortuosity coefficient for air
T_{rw}	Tortuosity coefficient for water phase
U_a	wind speed
U*	Friction velocity.
V	Volume
V_s	Volume of voids
V_v	Volume of solids
W_v	Molecular weight of water
w	Vertical wind

2. Symbols

Meaning

αTortuosity factor of the soil
βCross-sectional area of the soil available for vapor transfer
ΔSlope of the saturation vapor pressure versus temperature curve
γ Psychrometric constant
ρ_wMass density of water
ρ_sMass density of soil
ρ_aDensity of dry air
λThermal conductivity of the soil
ψTotal suction
ψ_rResidual suction
θTotal porosity
θ_{eq} Equivalent porosity
θ_a Air porosity
θ_wWater porosity
δFactor representing the ratios of ^{13}C and ^{12}C

Acknowledgements

I would like to express my sincere gratitude to my supervisor Dr. Ward Wilson for the time and energy he has expended, along with his willingness to share his expertise, experience, guidance, encouragement and support throughout the course of my MSc and this PhD thesis works. His constant enthusiasm, positive attitude and Christian faith were a source of inspiration for me.

My thanks are also extended to all members of my Advisory Committee: Dr Scott Dunbar, Dr. Bern Klein and Dr Marek Pawlik for their valuable suggestions and constructive feedbacks.

I gratefully acknowledge the assistance and guidance of my former MSc thesis co-supervisor and co-author, Dr. Jim Hendry from the University of Saskatchewan.

Cogema Resources Ltd, Cameco Corporation, and Natural Sciences and Engineering Research Council of Canada are acknowledged for providing financial support through an Industrial Research Council (IRC).

The assistance by the mine staff of Cameco at the Key Lake uranium mine, and Ray Kirkland and Tyler Birkham from the University of Saskatchewan, is gratefully acknowledged. My sincere thanks are also extended to Dr Henrique Rubio and Dr Bruno Bussière who reviewed my thesis draft.

May those who have contributed either directly or indirectly to this work, especially, my sister Bernadette Kapembe and Dr Musangu Ngeleka, and whom I have failed to mention individually, find in this work the fruit of their conjugated efforts (none mentioned, none forgotten).

Finally I would like to thank my wife Florence Chabu Kabwe for her patience, understanding and for the support throughout the course my studies. My son Fiston, my daughter Berthe, and my grand-daughter Joy Makayla were a source of joy and inspiration for me.

Dedication

To my late mother Saya Kasuba and my late father Jonas Mumba Katele:
their dreams have been fulfilled.

(Romans 5: 1-5)

...knowing that suffering produces endurance, and endurance produces character, and character produces hope, and hope does not disappoint us, because God's love has been poured into our hearts through the Holy Spirit that has been given to us.

To my Creator and Saviour, Jesus Christ.

CHAPTER I

INTRODUCTION

1.1 Introduction

Accurate measurements and predictions of surface gas fluxes such as CO₂ and O₂ are of great importance to the mining engineers and/or researchers in the development of a long-term management plan for reactive mine waste dumps.

Measurements of CO₂ fluxes are needed to quantify biogeochemical reaction rates in unsaturated geologic media and soils (Hendry et al., 1993, 1999, 2001; Wood et al., 1993; Wood and Petraitis, 1984; Affek et al., 1998; Keller and Bacon, 1998; Lee et al., 2003, Birkham et al., 2003). These flux measurements can also provide needed input for global warming models (Hanson et al., 1993; Sundquist, 1993; Holland et al., 1995; Sellers et al., 1995; Thierron et al., 1996; Wickland and Striegl, 1997; Buchmann et al., 1999).

Quantification of gas (e.g., O₂) diffusion rates can be used to determine the extent of sulfide oxidation in unsaturated waste-rock piles (e.g., Harries and Ritchie, 1985; Davis and Ritchie, 1987; Hockley et al., 2000; Timms and Bennett, 2000; Bennett et al., 2003; Molson et al., 2005) and mine tailings impoundments (Elberling and Nicholson, 1996; Wunderly et al., 1996; Elberling et al., 2000; Elberling and Damgaard, 2001). Oxygen gas diffusion rates can also be used to establish how effective soil cover systems would be at reducing gas diffusion into the waste rock and tailing profile (Harries and Ritchie, 1985; Yanful et al., 1993a; O'Kane et al., 1995; Smolensky and Hockley, 1999; Aubertin et al., 2000; Timms and Bennett, 2000; Mbonimpa et al., 2002,

2003; Bussi re et al., 2002, 2003; Cook et al., 2004; Martin et al., 2006; Aubertin et al., 2006).

Soil CO₂ flux is a complex process controlled by biotic and abiotic factors (Buchmann, 2000). The presence of CO₂ also exerts an important control on the pH of the pore water in unsaturated zones (Lowson et al., 1982; Neal and Whitehead, 1988). The CO₂ dissolved in water has a major influence on water chemistry (Neal and Whitehead, 1988) and soil acidification (Elberling and Jakobsen, 2000) and it drives carbonic acid weathering of silicate and carbonate minerals (Reardon et al., 1979).

Over the past two decades considerable attention has focused on radiatively important biogenic trace gas such CO₂ because of the concern of global warming (Blake and Rowland, 1988; Matson and Harris, 1995; Trumbore et al., 1996, Brooks et al., 1997; Fahnstock et al., 1998; Hobbie et al., 2000; Burkins et al., 2001). Similarly, because of the concern over acid rock drainage (ARD), most studies involving pore gases in mine wastes (including waste-rock piles) have focused on O₂ consumption rates as an indication of the rate of sulfide mineral oxidation. To date, there has been comparatively little attention paid to the CO₂ side of biotic and abiotic gas production and fluxes from the subsurface C-horizon soils and mine waste dumps.

Monitoring of O₂-CO₂ fluxes may provide a practical tool for identifying and understand the different important mechanisms in the waste dumps such as the zones of microbial respiration and pyrite oxidation-carbonate buffering in mine waste dumps (Lee et al., 2003) as well as providing an indication as to the extent of microbial activity in the waste dumps. Fluxes of CO₂ from waste-rock piles, though important in determining geochemical reactions rates, are poorly characterized and standards establishing the accuracy of field measurements of CO₂ surface fluxes are lacking

(Nakayama, 1990; Norman et al., 1992; Rayment and Jarvis, 1997; Janssens et al., 2000; Scott-Denton et al., 2003).

In previous work, the author (Kabwe, 2001, and Kabwe et al., 2002) developed and verified in mesocosms a technique to measure CO₂ fluxes from the soil surface to the atmosphere. The technique termed the dynamic closed chamber (DCC) method is based on direct measurement of the change in CO₂ concentration with time in the headspace of a chamber installed on ground surface over a relatively short period of time. The DCC method was shown to accurately measure CO₂ surface fluxes from ground surface to the atmosphere in mesocosms. This is a direct technique of measurements and it provides an almost instantaneous indication of the reaction rate under field conditions, regardless of climatic or moisture conditions in the waste dumps. This laboratory-verified technique provided the opportunity to quantify temporal and spatial CO₂ fluxes under field conditions and at the same time, compare these fluxes measurements to those obtained from two other methods: the static closed chamber (SCC) and eddy covariance (EC) methods.

This thesis work presents the results of the field applications of the DCC to quantify reaction rates and other processes at work in mine waste-rock piles at the Key Lake uranium mine in northern Saskatchewan. The work provided a complete suite of measurements required to characterize spatial distribution of CO₂ fluxes on waste rock. The author is not aware of any larger-scale studies that quantify CO₂ fluxes across a waste-rock pile.

1.2 Research Objectives

The main objective of this thesis was to extend the application of a novel and laboratory-verified device (the dynamic closed chamber DCC system) designed and developed by the author (Kabwe, 2001; Kabwe et al., 2002) for CO₂ flux measurements under field conditions on the DSWR and DNWR mine dumps at the Key Lake mine in northern Saskatchewan. It should be noted that this thesis represents the Phase II work of a 'Collaborative Research Program in the Mining Industry for Waste-Rock Hydrology', between the University of Saskatchewan and the University of British Columbia and funded by Cameco Mining and Cogema Resources. Phase I of the research work (Kabwe, 2001, and Kabwe et al., 2002) involved the design and testing of a dynamic closed chamber method for measurements of CO₂ flux in mesocosms.

The specific objectives of this thesis were:

- (1) To compare the DCC field CO₂ fluxes data with those obtained using two other field soil respiration techniques: static closed chamber (SCC) and eddy covariance (EC) methods.
- (2) To measure the drying rate on surfaces of waste-rock piles after rainfall events
- (3) To predict evaporation on the surfaces of waste-rock piles using the SoilCover (Unsaturated Soils Group, 1997) computer model.
- (4) To predict changes in water content profiles on waste-rock piles after rainfall events using SoilCover computer model.

-
- (5) To design and develop a numerical model for CO₂ gas production and diffusion in unsaturated materials.
 - (6) To validate the CO₂ model using measured data.
 - (7) To use the CO₂ model to predict CO₂ diffusion and concentration-depth profiles in the waste-rock piles in response to changes in water-depth profiles at the Key Lake mine.
 - (8) To use the CO₂ model to predict the effects of rainfall events on the surface effective diffusion coefficient and surface CO₂ flux on the waste-rock piles at the Key Lake mine.

The work presented in this thesis applies the DCC method that was previously developed and verified in mesocosms to measure CO₂ flux from ground surface to the atmosphere (Kabwe et al., 2002) and was shown to accurately measure CO₂ surface fluxes. In this study the DCC will be tested under field conditions to quantify and determine biogeochemical reaction rates in waste-rock piles. The method can be of great value to the mine engineer in the development of closure designs for mine waste-rock piles at the Key Lake mine. The method can also be extended to other mine waste dumps to quantify biogeochemical reaction rates in unsaturated geologic media and soils at other mine sites in Canada and world wide.

1.3 Organization of the Thesis

Chapter 2 of the thesis presents a literature review for studies of subsurface CO₂ and O₂ production and consumption rates and the associated fluxes in waste-rock

systems and other soil ecosystems. The chapter ends with a brief review of climatic variables affecting the gas fluxes: precipitation and evaporation.

Chapter 3 presents material characterizations. The objective was to determine the soil properties and characteristics of near-surface waste rock which influence the CO₂ gas flux. The tests conducted include: grain size analysis, water retention curve (WRC) (or soil water characteristic curve), and saturated hydraulic conductivity.

Chapter 4 discusses results of field application of the dynamic closed chamber (DCC) method for measurements of CO₂ fluxes. The chapter ends with a comparison of the DCC fluxes to those obtained from two other methods: static closed chamber (SCC) and eddy covariance (EC) methods.

Chapter 5 presents results of the investigations for the climatic variables affecting CO₂ fluxes (e.g., effects of rainfall and evaporation on soil moisture and CO₂ fluxes) precipitation and evaporation. The "CO₂" diffusion model developed in this work is discussed at the end of Chapter 5. The theoretical background, development of the partial differential equation including verification of the model developed are also presented. Final conclusions are summarized in Chapter 6.

CHAPTER II

Literature Review

2.1 Introduction

This chapter presents a literature review for studies of subsurface CO₂ and O₂ production, consumption rates and the associated surface fluxes in waste-rock systems and establishes the need for the research.

Section 2.2 presents a physical description of a waste-rock pile to help conceptualize the complex flow developed within the waste rock in response to climatic conditions. Section 2.3 discusses the sources of CO₂ in waste-rock piles, more specifically on biotic and abiotic reactions in waste-rock piles. Section 2.4 presents results of studies for CO₂ production and O₂ consumption rates and surface fluxes in waste-rock and non-waste-rock systems reported in literature. Section 2.5 provides a discussion on the two important climatic variables that affect subsurface and surface gas fluxes namely, precipitation and evaporation. The chapter summary is presented in section 2.6.

2.2 Waste-Rock Piles

Waste-rock piles from mining operations are constructed from the excavation and surface deposit of overburden rock, which commonly contain sulfide minerals. These above-ground, coarse-grained deposits tend to be heterogeneous in structure as a result of placement methods (e.g., end dumping, lift placement and compaction). The volume of a waste rock dump can be as large as hundreds of millions of cubic meters, making its size several kilometers in width and hundreds of meters in depth. These unsaturated and exposed to atmospheric precipitation, energy (e.g., solar energy) and gases (oxygen, carbon dioxide) and have the potential for generating sulfuric acid (H_2SO_4) in the presence of sulfide minerals (e.g., FeS_2 , $Fe_{1-x}S$) (Nordstrom and Alpers, 1999; Keit and Vaughan, 2000; Rimstidt and Vaughan, 2003; Elberling, 2005) (see Figure 2.1). This acid can dissolve heavy metals in the mine waste and produce acid rock drainage (ARD), which is potentially toxic to plants, animals and humans. The oxidation rate of sulphide minerals (e.g., pyrite, FeS_2) depends on a number of factors which define the environment within the waste-rock dumps, including temperature, pH, oxygen concentration, chemical composition of the pore water, and microbial population (Ritchie, 1994). Oxidation is an exothermic process that produces a large amount of heat (Elberling, 2005). Field measurements show that the temperature can be as much as 63 K warmer than the atmosphere in waste-rock piles with heights of 20-30 m (Harries and Ritchie, 1981; Gelinis and Choquette, 1992). Another factor that complicates the oxidation process is the presence of bacteria. Certain species of bacteria (e.g., *Thiobacillus ferrooxidans*) were found to increase the rate of oxidation by two orders of magnitude (Lorenz and Tarpley, 1963; Brierley, 1978).

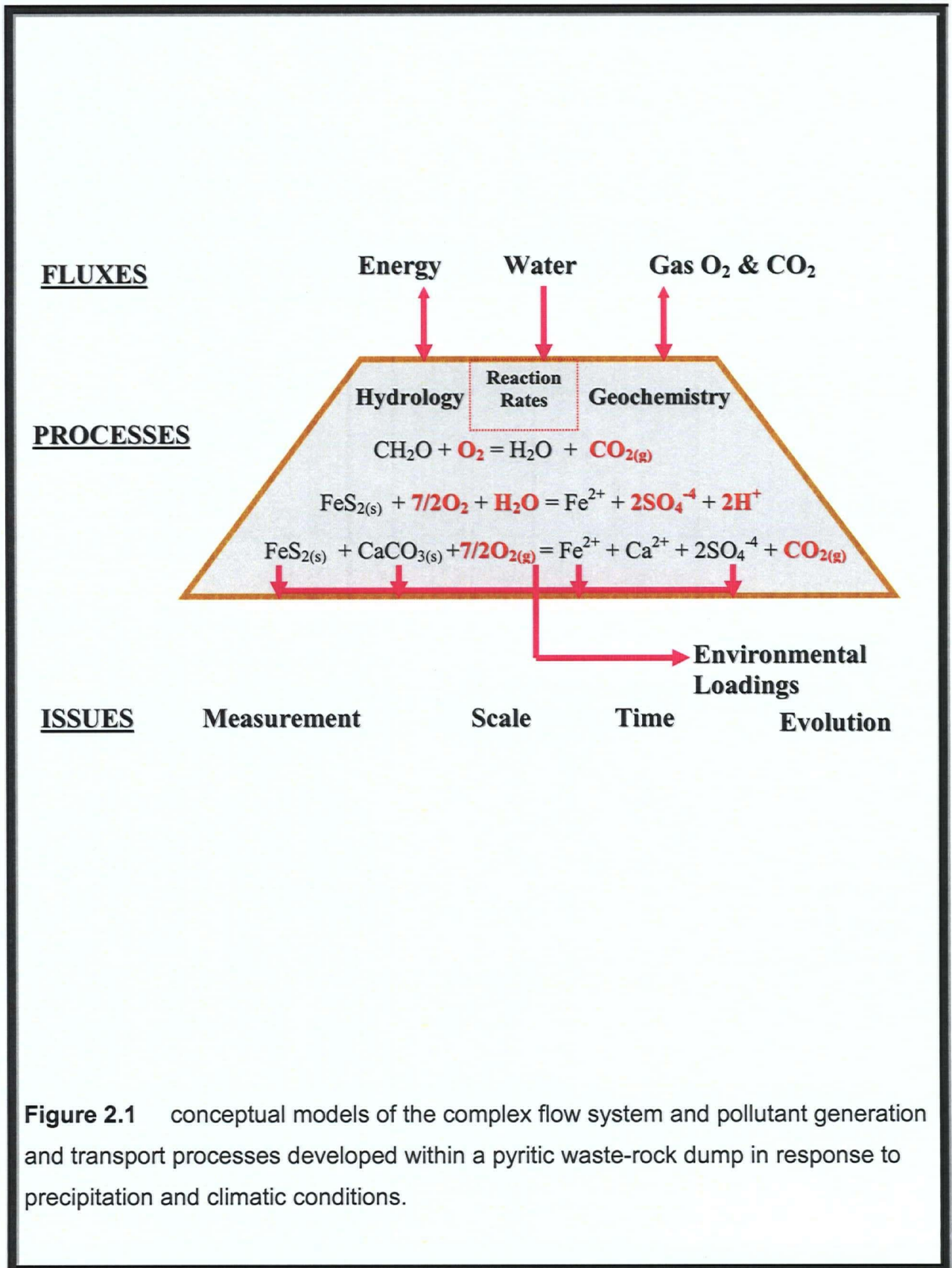


Figure 2.1 conceptual models of the complex flow system and pollutant generation and transport processes developed within a pyritic waste-rock dump in response to precipitation and climatic conditions.

In short, the physico-chemical-microbial environment within a waste-rock dump determines the sulfide mineral oxidation rate, which in turn determines the physico-chemical-microbiological environment (Ritchie, 1994).

Figure 2.2 shows a conceptual model of water and gas flow, and vapour transport in a waste-rock dump and internal structure and material segregation of a waste rock pile (Herasymuik, 1995; Fala et al., 2005). MEND (2001) proposed four hydrostratigraphic types to characterize waste-rock piles. The types differ depending upon the materials and construction methods, and the characteristics of flow. The four types are:

- i. Non-segregated coarse-grained rock piles that transmit water rapidly to the base of the pile;
- ii. Non-segregated fine-grained rock piles that are likely to contain a basal saturated zone;
- iii. The segregated rock piles that contain a fine-grained crest zone that may not permit the passage of significant quantities of water; and
- iv. Layered, segregated dumps that contain a finer-grained crest and sandy gravel layers to the face of the rock pile.

Segregated waste-rock dumps exhibit a graded stratigraphy caused by the segregation that occurs as materials roll down the pile at the angle-of-repose (Figure 2.2A). Finer sandy gravels are present at the crest, while coarser materials accumulate further down-slope. Dawson and Morgenstern (1995) have shown that when materials consisting mostly of finer sandy gravel are end-dumped, little segregation occurs and a finer grained layer is formed in the dump. A layer of finer material is typically found on the surface of the rock and a layer of coarser material is found at the base (Fala et al.,

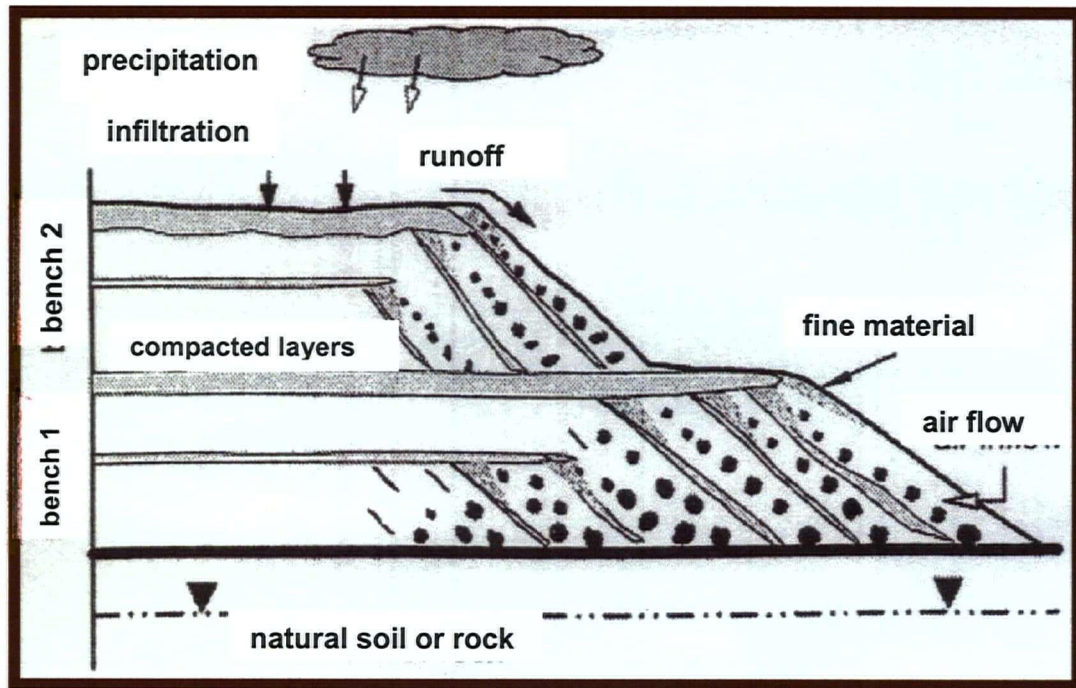


Figure 2.2. Conceptual model of internal structure and material segregation of a waste rock pile.

2005). The bulk grain size distribution then includes alternating fine and coarse-grained material layers (see Figure 2.2) (Morin et al., 1991). When the grain size distribution is more variable, the vertical pile profile can be irregular and the structure of alternating fine and coarse layers less distinct. Layering inside the pile can be locally enhanced by construction traffic (heavy equipment), which tends to crush and compact the surface material, creating layers that can be up to 1 m thick (Aubertin et al., 2002; Martin, 2004; Fala et al., 2005).

The grain and pore size distribution within a waste rock piles affects its hydraulic properties, which in turn control internal flow. Preferential flow can be caused by continuous macropores or by vertical, horizontal, or inclined layers of relatively high hydraulic conductivity that often control the movement of water within a pile. When the layering occurs as a fine-grained unit above a coarse-grained zone, a capillary barrier is formed in which water is preferentially retained in the fine grained material due to capillary forces (Nicholson et al., 1989; Buissonière et al., 2003; Fala et al., 2005). Capillary barriers have been proposed for use in waste rock piles to control air and water flow (Poulin et al., 1996; Lefebvre et al., 2001b). The unsaturated condition and heterogeneous, coarse-grained nature of the waste rock deposits often make geochemical and geotechnical parameters difficult to measure (Pantelis et al., 2002). The problem is exacerbated when the dump is > 10 m high, as this is as high as a column of water can be supported by atmospheric pressure. For these reasons, few data on the chemical composition of pore water within waste-rock dumps are in the literature. Monitoring the chemistry of the gas phase in unsaturated environments is a relatively easy process. The gas can be easily drawn from sampling ports within the pile and the technology to measure chemically important components (i.e. O₂ and CO₂) is

readily accessible (Russell and Appleyard, 1915; Enock and Dasberg, 1971; de Jong and Schappert, 1972; Rightmire and Hanshaw, 1973; Rightmire, 1978; Hass et al., 1983; Jaynes et al., 1983a; Wallick, 1983; Wood and Petraitis, 1984; Harries and Ritchie, 1985; Cerling et al., 1991; Gelinis et al., 1992; Elberling et al., 1993; Hendry et al., 1993, 2001; Ritchie, 1994a, 1994b; Elberling and Nicholson, 1996; Lee, 1997; Keller and Bacon, 1998; Russell and Voroney, 1998; Helgen et al., 2000; Hockley et al., 2000; Kabwe et al., 2002).

The O₂ and CO₂ concentrations in the pore gas can be expected to vary because there are sinks and sources for these within the waste-rock dumps. The source of O₂ in a waste-rock dump is at the outer surface of the dump. O₂ concentrations vary with increasing distance into a dump in a manner that depends on the prevailing O₂ transport mechanisms and on the oxidation rates. It should be noted that O₂ concentrations less than 0.2% mole fraction have been measured (Bennett et al., 1999), and values as low as 0.01% mole fraction have been reported (Goodman et al., 1992). CO₂ concentrations in the pore space of a waste-rock dump can range up to about 20% mole fraction and are frequently in the range 1-10% (Harries and Ritchie, 1983; Schuman et al., 1992). This is much higher than atmospheric levels of 0.03%. Elevated concentrations of CO₂ increase the oxidation rate of pyrite by moderate thermophiles (Norris, 1989), some workers have reported increased growth rate of *thiobacillus ferrooxidans* with increasing levels of CO₂ (Holuigue et al., 1987; Beyer et al., 1990), but others have reported little change up to 7% (Kelly and Jones, 1978; Norris, 1989). Haddadin et al. (1993) observed that increased CO₂ concentrations increased the pyrite oxidation rates, but that concentrations of 4% were inhibitory to all three of the microbial populations involved in pyrite oxidation in the system studied.

The monitoring of O₂ and CO₂ concentrations in pore gas is commonly used as an indication of the occurrence, location, rate and type of chemical reactions occurring in subsurface environments (Ritchie, 1994). O₂ consumption by sulphide mineral oxidation is of particular importance in assessing the impact of waste-rock piles on the environment because of the associated acid generation (Molson et al., 2005). A decrease in O₂ concentrations in waste-rock piles does not necessarily indicate the occurrence of sulphide mineral oxidation. Organic oxidation is another common, but less environmentally harmful, process during which O₂ is consumed. CO₂ in pore gas is an indicator of the types of oxidation processes occurring. For example, for a given amount of O₂ consumed, carbonate buffering of acid generated from sulphide mineral oxidation will typically produce less CO₂ than organic oxidation (discussed further in this Chapter). In addition, carbonate minerals and organic molecules have different ratios of stable carbon isotopes (discussed briefly in section 2.3): consequently, the stable carbon isotope signature of pore gas CO₂ may be used to trace the CO₂ source (Hendry et al., 2002).

Ritchie (1994a) and Lefebvre et al. (2001) provided a summary of typical physical properties and typical characteristics of ARD waste-rock with data on bulk properties of waste-rock dumps (Tables 2.1, 2.2, 2.3, 2.4 and 2.5). The gas concentration and temperature profiles in a waste-rock dump depend on the magnitude of a number of physical properties of the dump material, including air permeability, the gas diffusion coefficient, and the thermal conductivity. Ritchie (1994a) pointed out that the set of data in these Tables indicate that, at least for the parameters measured

Table 2.1. In-situ thermal conductivity measurements in waste-rock dumps material

Mine site location	# of measurement points in waste dump	Range ($\text{Wm}^{-1} \text{K}^{-1}$)	Average ($\text{Wm}^{-1} \text{K}^{-1}$)
Aitik mine, Sweden ^x	8	0.71 -1.63	1.2 ± 0.4
Heath Steele, Canada ^x	3	1.04 – 1.22	1.2 ± 0.1
Kelian, Kalimantan ^x	7	1.57 – 3.31	2.1 ± 0.6
Rum Jungle, Australia ^x	6	1.77 – 3.12	2.2 ± 0.5
Doyen mine, Canada ^y	6		2.5
Nordhalde, Germany ^y	8		1.0

Table 2.2. In-situ air permeability measurements in waste-rock dumps material

Mine site location	# of measurement points in waste dump	Range (m^2)
Aitik mine, Sweden ^x	27	$(0.6 \pm 0.2) \times 10^{-11} - (1.4 \pm 0.1) \times 10^{-9}$
Heath Steele, Canada ^x	24	$(1.6 \pm 0.15) \times 10^{-11} - (4.7 \pm 0.5) \times 10^{-9}$
Kelian, Kalimantan ^x	18	$(3.9 \pm 0.1) \times 10^{-9}$
Rum Jungle, Australia ^y	144	$(8.89 \pm 0.19) \times 10^{-13} - (1.49 \pm 0.21) \times 10^{-9}$
Doyen mine, Canada ^y		8.1×10^{-10}
Nordhalde, Germany ^y		2.5×10^{-12}

Table 2.3. In-situ oxygen diffusion coefficient measurements in waste-rock dumps

Mine site location	# of measurement points in waste dump	Range $\text{m}^2 \text{s}^{-1} (\times 10^{-6})$
Aitik mine, Sweden ^x	2	$(2.25 \pm 1.04) - (6.85 - 1.02)$
Heath Steele, Canada ^x	3	$(2.65 + 0.55) - (3.35 - 0.25)$
Woodlawn, Australia ^x	2	$(3.49 \pm 1.64) - (5.07 - 0.39)$
Doyen mine, Canada ^y	6	2.85
Nordhalde, Germany ^y	8	5.70

X = Ritchie, 1994; y = Lefebvre et al., 2001

Table 2.4. Typical physical properties of ARD waste-rock piles (Ritchie, 1994a)

Property	Unit	Typical value	Approximate Range of values
Height	m	20	2 to 150
Area	ha	30	0.1 to 150
Density	Kg/m ³	1500	1300 to 1900
Sulfur content as pyrite	Wt. %	2	0.5 to 30
Climate type			Tropical to polar
Rainfall	m/yr		0.1 to 5
Water content within dump	Vol. %	10 (at infiltration of 0.5 m yr ⁻¹)	5 to 25
Porosity	%	40	
Carbonate density		0.6 kg m ⁻³ 0.04 %	
O ₂ diffusion coefficient	m ² /s	5 x 10 ⁻⁶	2 x 10 ⁻⁶ to 6x10 ⁻⁶
Air permeability	m ²		1x10 ⁻¹² to 1x10 ⁻⁹
Temperature within dump	°C		-7 to 65

Table 2.5. Physicochemical properties of the Doyon and Nordhalde waste rock piles (Lefebvre et al., 2001)

Properties	Unit	Doyon	Nordhalde
Volume of waste rocks	m ³	11.5x10 ⁶	27.0x10 ⁶
Maximum thickness	m	35	80
Main Rock Type		Sericite schists	Slates
Solid density	Kg/m ³	2740	2751
Porosity	Dim.	0.00	0.30
Average water saturation	%	42	63
Effective vertical air permeability	m ²	8.1x10 ⁻¹⁰	2.5x10 ⁻¹²
Water infiltration rate	m/year	0.350	0.166
Average thermal conductivity	W/m °C	2.5	1.0
Effective oxygen diffusivity	m ² /s	2.13x10 ⁻⁵	2.13x10 ⁻⁵
Range of Temperature within dumps	°C	1 - 65	3-16
Sulfur content as pyrite	%		1 – 2%

Table 2.6. Typical characteristics of ARD (Ritchie, 1994a).

Property	Typical associated chemical species	Range	Impact
Acidity (pH)	Sulfuric acid	2 to 4	Mobilization of metal ions
Iron	Ferrous and ferric ions; ferric oxides, hydroxides; jarosites	Concentration 100 to 3000 mg L ⁻¹	Discoloration and turbidity in receiving waters as pH increases and ferric salts precipitate
Heavy metals	Cu, Mn, Zn, Cd, Hg, Pb, As, Ra	1 to 200 mg L ⁻¹	Reduction in aquatic flora and fauna; bioaccumulation; reduction in quality of potable groundwater supplies
Total dissolved salts	Ca, Mg, Al, SO ₄ ²⁻	100 to 30000 mg L ⁻¹	Reduction in quality of potable groundwater supplies; reduction in quality of water supplies for livestock

(though small data-set) the heterogeneity of the dump material and layering consequent on the method of dump formation do not carry through in any marked way.

These bulk properties are required both to predict the environmental conditions within a dump, and to quantify oxidation rates. The extents to which these properties vary from place to place in a dump and from dump to dump provide some insight on the impact that dump-construction methods and details of dump composition have on these bulk properties (Fala et al., 2005). The gas concentration and temperature profiles in a waste-rock dump depend on the magnitude of a number of physical properties of the dump material, including air permeability, the gas diffusion coefficient, and thermal conductivity. It was noted that the variation from dump to dump (from this data set) was about the same as that within a dump and that gas transport in a dump was dominated by diffusion when the air permeability was 10^{-10} m^2 or less (Bennett et al., 1989; Pantelis and Ritchie, 1991a).

2.3 Sources of CO₂ in Subsurface Soils and Waste-Rock Piles

The generation of soil CO₂ flux is a complex process controlled by biotic and abiotic factors (Buchmann, 2000; Shi et al., 2006). Gas-filled pores in soil typically contain 10–100 times higher concentrations of CO₂ than the atmosphere (Welles et al., 2001), primarily due to soil CO₂ production from respiration in living roots and heterotrophic soil microorganisms (Elberling, 2003). CO₂ in pore gas may be used to identify its source. The ratio of stable carbon isotopes (¹³C/¹²C) in CO₂ from pore gas indicates if the CO₂ source is organic, inorganic, or a combination of both. It should be noted that the carbon isotopes technique was used by Birkham et al. (2003) to determine the source of CO₂ in the waste-rock piles (DNWR & DSWR) and beneath at

the Key Lake mine. Birkham et al. (2003) presented measured values of carbon isotopes ratio for the waste-rock piles at the Key Lake mine and concluded that pore gas CO₂ in the DNWR pile (see Figure 2.3) likely originated from a combination of organic (biotic) and inorganic (abiotic) sources (Birkham et al., 2003). Carbon isotopes ratio values for the DSWR indicated the majority of pore gas CO₂ from DSWR originated from an organic source underlying the waste rock (e.g., Figure 2.3, dewatered lake) (Birkham et al., 2003).

2.3.1 CO₂ production by microbial respiration (biotic)

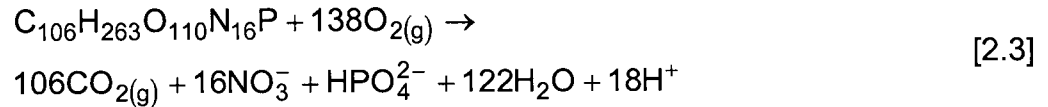
Microbial aerobic respiration and oxidation of organic matter are generally considered to be the primary sinks for O₂ and the main sources of elevated biogenic CO₂ concentrations in the subsurface. Rates of aerobic microbial degradation of organic matter and contaminants in the subsurface are greater than anaerobic degradation (Hendry et al., 2002). An understanding of the physical transport mechanisms and the biochemical processes that control CO₂ and O₂ concentrations and fluxes to and within the subsurface are needed (Bennet and Ritchie, 1990; Hendry et al., 1999; Hendry et al., 2002; Pantelis et al., 2002; Lee et al., 2003b).

O₂ consumption and CO₂ production by microbial respiration in unsaturated media can be represented by the general biotic reaction (Stumm and Morgan, 1981; Lee et al., 2003b):



where CH₂O represents a simple carbohydrate. In this simple case of organic oxidation

one mole of O₂ consumed results in the production of one mole of CO₂. More complex organic molecules (e.g., C₁₀₆H₂₆₃O₁₁₀N₁₆P) may have molar ratios of O₂ consumption to CO₂ production of closer to 1:0.77 (Drever, 1997):



Based on the Equations 2.2 and 2.3, respiratory consumption of 1 mol of O₂ should produce 0.8 or 1 mol of CO₂.

It was noted in the literature review that mine waste-rock piles are, in some cases, constructed upon organic carbon-rich dewatered lake bottoms (Birkham et al., 2003; Lee et al., 2003b) (see Figure 2.3). Microbial respiration in these buried deposits can also consume O₂ and produce CO₂. Lee and co-workers (Lee et al., 2003) found that these stoichiometric ratios are very similar to those observed for microbial respiration in forest soils (1O₂:0.7CO₂) (see Figure 2.3B) and in buried lake sediments beneath mine waste-rock piles (1O₂:0.5CO₂). They found a positive correlation between the rates of O₂ consumption and CO₂ production and organic carbon content (i.e., higher organic carbon contents in forest soil than lake bottom sediments) and suggested that the difference in O₂/CO₂ ratios were due to differences in the stoichiometry of the organic carbon. Other researchers (Amundson et al., 1988; Wang et al., 1999) reported positive correlation between respiration rates and organic carbon content in unsaturated zones. Measurements of O₂-CO₂ fluxes, therefore, may provide an indication of the zones of respiration and the extent of microbial activity in the waste-rock pile.

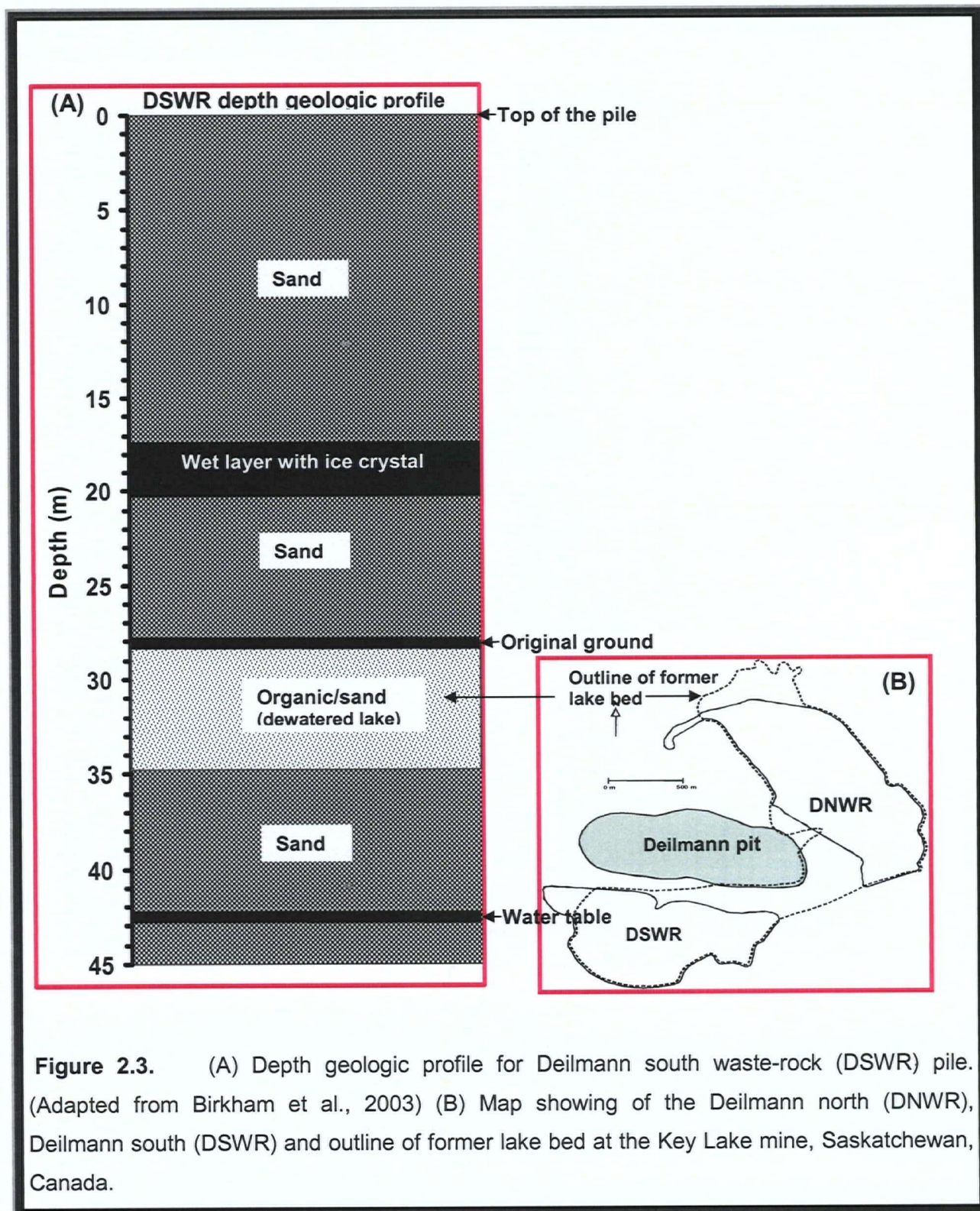


Figure 2.3. (A) Depth geologic profile for Deilmann south waste-rock (DSWR) pile. (Adapted from Birkham et al., 2003) (B) Map showing of the Deilmann north (DNWR), Deilmann south (DSWR) and outline of former lake bed at the Key Lake mine, Saskatchewan, Canada.

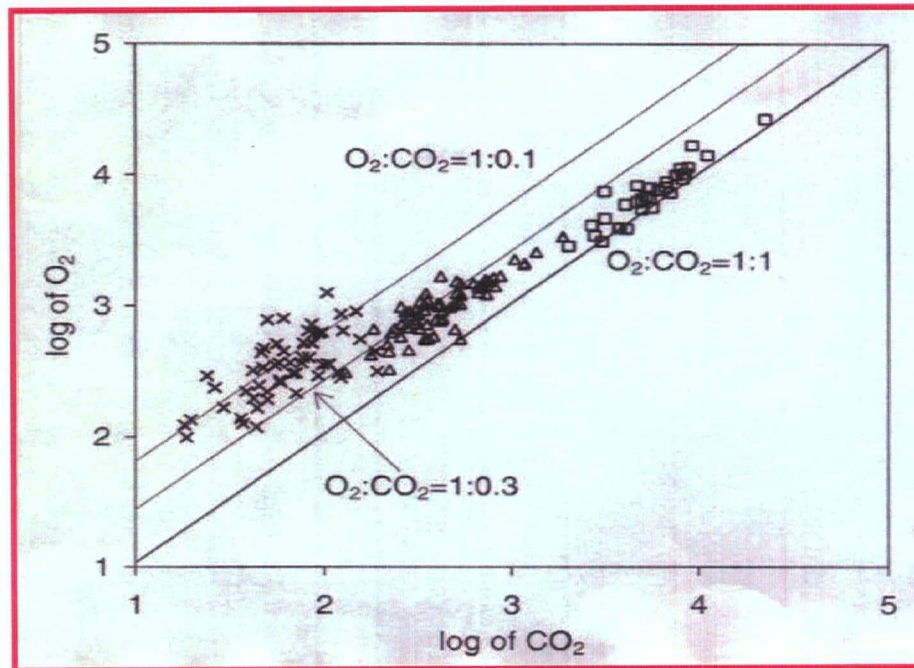
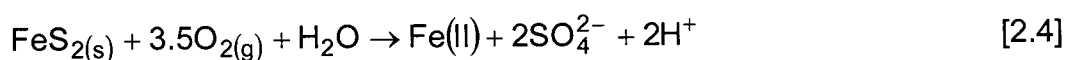


Figure 2.4. O₂ consumption rates vs CO₂ production rates for forest soils, lake bottom sediments, and gneissic waste rocks (units: $\mu\text{mol}/\text{kg}/\text{week}$; x represents gneissic waste rocks (DNWR); Δ represents lake bottom sediments collected from beneath the waste-rock pile (DNWR); \square represents forest soils (natural forest site adjacent to the DNWR) (Lee et al., 2003b).

2.3.2 CO₂ production by pyrite oxidation-carbonate buffering (abiotic)

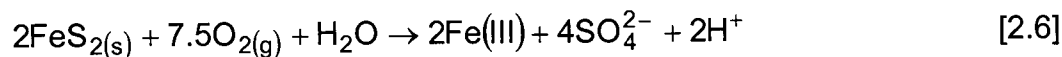
Soil CO₂ derived from unsaturated mine waste-rock piles can also be produced in abiotic (e.g. sulfide minerals) reactions in situ (Elberling and Nicholson, 1996; Timms and Bennett, 2000; Birkham et al., 2003; Lee et al., 2003b). If gaseous O₂ is present in the unsaturated waste-rock piles, the oxygen can be consumed by microorganisms in the chemical oxidation of minerals (e.g. pyrite) and can lead to formation of acid and sulfate (Stumm and Morgan, 1981; Ritchie, 1994b; Lee et al., 2003b):



The resulting Fe(II) in Equation 2.4 can be oxidized to Fe(III) by :



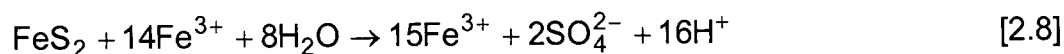
Combining Equations 2.4 and 2.5 we obtain:



In a solution with pH > 3, Fe³⁺ can precipitate from solution to produce additional acid (Dubrovsky et al., 1984; Janzen et al., 2000) by:



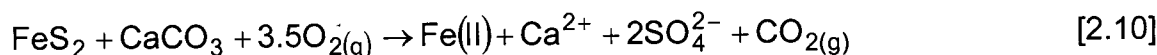
Precipitation of other Fe(III)-bearing phases, such as goethite (α -FeOOH) or schwertmannite (Fe₈O₈(OH)₆SO₄), may occur in acid mine waters (Bigham et al., 1990). Alternatively, Fe(III) can be consumed through further oxidation of sulphide minerals in acidic water (Wiersma and Rimstidt, 1984; Blowes et al., 1995) by:



Carbonate minerals are often present in natural subsurface environments and have a buffering effect on the pH of subsurface pore water (Freeze and Cherry, 1979). The acid generated by pyrite oxidation can dissolve available carbonates to produce CO₂ gas by:



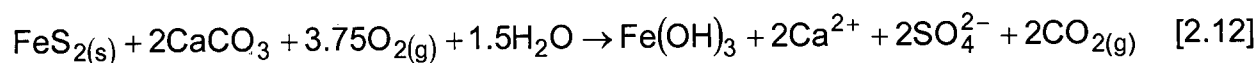
Combining Equations 2.4 and 2.9 yields Equation 2.10:



In addition, combining Equations 2.6 and 2.9 yields Equation 2.11



Furthermore, combining Equations 2.6, 2.7, and 2.9 yields Equation 2.13 for near neutral pH solution:



Based on Equations 2.10 – 2.12, consumption of 1 mol of O₂ by pyrite oxidation with carbonate buffering may produce 0.1, 0.3, or 0.5 mol of CO₂ and between 0.5 and 0.6 mol of sulphate.

The CO₂ produced is thus an indirect measure for the carbonate buffering and an indicator of the types of oxidation processes occurring. It is therefore suggested that both sulfide oxidation-carbonate buffering and microbial respiration may control O₂ and CO₂ gas concentrations in the unsaturated waste-rock piles (Lee et al., 2003b).

CO₂ produced in unsaturated soils and waste-rock piles undergoes redistribution via gas transport and geochemical reactions with water and various mineral phases

(Hendry et al., 1993) and will diffuse upward to the atmosphere (soil respiration) and downward to the water table under concentration gradients. Microbially produced CO_2 can dissolve in the recharging water and react to produce bicarbonate (HCO_3^-). These species are then transported to the water table in the dissolved state. In addition to sinks attributed to CO_2 -carbonate mineral reactions, CO_2 also dissolves in water to produce carbonic acid. Although this latter flux is small compared to the soil CO_2 efflux, it has a major influence on water chemistry (Neal and Whitehead, 1988) and soil acidification (Elberling and Jakobsen, 2000) and it drives carbonic acid weathering of silicate and carbonate minerals (Reardon et al., 1979; Elberling, 2003).

Many studies have shown that the dominant sink for CO_2 from unsaturated zones is the atmosphere (Solomon and Cerling, 1987; Hendry et al., 2001). For example, Hendry et al. (1993) showed that 2% of the CO_2 produced in a 3.2 m thick sandy unsaturated zone under high recharge conditions was removed by the recharging ground water. Solomon and Cerling (1987) determined that about 4% of the CO_2 produced in an unsaturated zone was removed by the recharging ground water.

The dominant mechanism for gas transport in soil pores is generally accepted to be concentration controlled molecular diffusion through air-filled pores (Keen, 1931; Grable, 1966; Weeks et al., 1982; Elberling, 2003). Variations in pore gas composition due to thermal convection and atmospheric pressure variations were observed by Harries and Ritchie (1985), Bell et al. (1991), Hockley et al. (2000), Lefebvre et al. (2001), and Molson et al. (2005). While diffusion is typically limited to a near-surface zone of a few meters depth, advection (due to a thermal gradient and/or wind pressure gradients or barometric pumping) and barometric pumping have the potential to move air (and oxygen) to much greater depths into the pile. In general, the more permeable

general, the more permeable the waste-rock material, and the greater the height-to-width ratio of the waste-rock pile, the greater is the potential for advective air movement. The reactivity of the waste-rock material as well as the coarseness (hence air permeability), and the spatial variability of these properties within a pile, have a strong influence on the magnitude of thermally induced advection (Wels and Robertson, 2003). In contrast, air movement due to barometric pumping is controlled by the waste rock porosity, changes in ambient air pressure and the heterogeneity of air permeability of the waste-rock dump.

2.4 Studies of CO₂ in Subsurface Pore Gas and Associated Surface Gas Fluxes from Waste-Rock and non Waste-Rock Systems

The following sections present literature review of studies of CO₂ in subsurface pore gas and associated surface gas fluxes from waste-rock and non waste-rock systems.

It should be noted that this literature review serves to establish the need for surface CO₂ fluxes measurements on both mine waste-rock and non-waste-rock systems. This is because the dominant oxidation reactions and associated CO₂ fluxes measured at the DSWR occur in the organic material underlying the waste-rock pile (Birkham et al., 2003). Birkham et al. (2003) also suggested that pyrite oxidation-carbonate buffering and the resulting O₂ consumption and CO₂ production are more likely to be observed in the gneissic waste rocks at the DNWR.

Many studies have investigated CO₂ in pore gas in subsurface and surface gas fluxes for non waste-rock material and only few attempts have been made to quantify CO₂ production or surface flux (Birkham et al., 2003) in waste-rock piles.

2.4.1 Studies of subsurface CO₂ gas and surface gas fluxes from waste-rock piles

The following section along with Tables provide the literature review results for typical studies of CO₂ production and consumption rates and surface fluxes for waste-rock piles.

Table 2.7. Summary of CO₂ concentrations for waste-rock material.

Sources	Locations	Waste Rock: size and geologic material	CO ₂ maximum concentration (%)
Harries and Ritchie (1985)	Rum Jungle Australia	15 to 25 m high waste-rock piles silty sand to rocks, 1 to 3% pyrite	> 20
Gelinas et al. (1992)	La Mine Doyen, Quebec	30 to 35 m high waste-rock pile, 3.5 to 4.5% pyrite	7
Hockley et al. (2000)	Germany	1 to 3% sulphides, high conc. of carbonates	60
Birham et al. (2003)	Key Lake mine Saskatchewan Canada	20 to 28 m high, sand/sandstone	8

Harries and Ritchie (1985) measured pore gas CO₂ and O₂ concentrations in the within a pyritic waste-rock pile (average height 25 m) at the Rum Jungle uranium mine in Australia to identify oxidation zones and measure rates of oxidation. The waste-rock pile consisted mainly of pyritic, graphitic shale. CO₂ concentrations varied from near

atmospheric levels to greater than 20 %. O₂ concentrations varied from near atmospheric levels to 0 %. Important conclusions of this study were that O₂ supply was a rate-limiting factor for oxidation and that both diffusion and advection (due to thermal and atmospheric effects) resulted in gas migration through the pile. Advection due to thermal effects (buoyancy forces) was significant in regions where temperatures were elevated (>50 °C) relative to monthly mean temperatures (25 to 30 °C). Advection due to changes in atmospheric pressure was observed at depths of up to 7.5 m where O₂ concentration fluctuations matched the semidiurnal changes in atmospheric pressure.

Gelinas et al. (1992) studied the physico-chemical conditions for La Mine Doyon in Quebec. ARD from the waste-rock piles had pH values around 2 and total dissolved solids (mainly sulfates, Fe, Al and Mg) values up to 200 000 mg/L; pyrite concentrations in the waste-rock piles were approximately 3.5 to 4.5 % (by mass). Porosity of the piles and the dry bulk density were estimated at 35 % and 1850 kg/m³, respectively. Maximum temperatures typically ranged from 40 to 50°C, CO₂ pore gas concentrations typically increased to about 7 % at a depth of 30 m and O₂ pore gas concentrations typically decreased to about 2.5 % at a depth of 30 m. Air convection (due to thermal effects) was identified as a key gas transport process as air venting from the waste piles was observed during cold weather.

Hockley et al. (2000) measured temperature, CO₂ and O₂ pore-gas concentrations, and air pressure in a waste-rock pile at a uranium mine in Germany. Typical seepage from the waste-rock pile had a pH of 2.7 and sulfate concentrations above 10 000 mg/L. Acid generating material had sulfide mineral concentrations ranging from 1 to 3 % (by mass). Thermal convection of pore gas was observed at some sites during winter months as stable temperatures deeper in the pile were

between the summer and winter ambient temperatures. Gas transport due to barometric pressure fluctuations was also observed. CO₂ concentrations typically increased (up to 60%) with increasing depth. CO₂ production was attributed to high concentrations of carbonate material. O₂ concentrations typically decreased (down to 0%) with increasing depth;

Birkham et al. (2003) measured CO₂ concentrations profiles, CO₂ consumption and production rates, and CO₂ fluxes from two waste-rock (the Deilmann south waste-rock (DSWR) and Gaertner (GWR) piles at the Key Lake Uranium Mine in northern Saskatchewan. The concentrations exhibited a linear increase for CO₂ in concentrations with depth through the piles and suggested that the dominant sites of reactions occurred below the piles. Mean CO₂ concentrations at the DSWR changed little with depth (change in CO₂ concentrations less than 1% from atmospheric concentrations). CO₂ concentration increased from 10 to 20 m, decrease from 20 to 30 m, and increased from 30 to 40 m. They found that oxidation of organic matter beneath the waste-rock pile dominated the pore-gas chemistry and that significant changes in O₂ and CO₂ concentrations within mine waste piles may not be the result of sulfide mineral oxidation/carbonate buffering. The gas consumption and production values ranged between 0.04 and 0.15 $\mu\text{g CO}_2/\text{g soil/day CO}_2$.

CO₂ concentration depth profiles at the Key Lake mine were similar to those presented in other waste-rock studies (Harries and Ritchie, 1985; Hockley et al., 2000) in that CO₂ concentrations were negatively correlated to O₂ concentrations. Although CO₂ concentrations increased to a maximum of 20 % at the Rum Jungle mine in Australia (Harries and Ritchie, 1985), O₂+CO₂ values were usually less than 15 %. CO₂ concentration depth profiles presented by Hockley et al. (2000) had CO₂ concentrations

that usually increased to much greater than 20 % (up to 60 %) at depths below 20 m; O₂+CO₂ values ranged from approximately 5 % to approximately 60 %.

In summary, waste-rock studies in the literature indicated that only one attempts have been made to quantify CO₂ production and CO₂ concentration depth profiles (Birkham et al., 2003) and surface flux. A need, therefore, exists for measurements of surface CO₂ fluxes for large waste-rock piles.

2.4.2 Studies of subsurface CO₂ from non waste-rock material

The following section along with Tables provide the literature review results for typical studies of CO₂ production and consumption rates and surface fluxes for non waste-rock piles. It should be noted that the range of non-waste-rock systems is wide, and only selected literature review results will be presented.

Table 2.8. Summary of CO₂ concentrations for non-waste-rock material.

Source	Location	Waste rock size and geologic material	Max. CO ₂ conc. (%)
De Jong and Schappert (1972)	Canadian prairie	(1.5 m of unsaturated heavy clay)	2.26
Rightmire and Hanshaw (1973)	Florida	(sand, forest and grassland)	
Atkinson (1977)	England	(limestone soils, depths to 130 m)	1.8

Table 2.8 Continued.

Source	Location	Waste rock size and geologic material	Max. CO ₂ conc. (%)
Reardon et al. (1979)	Ontario	(up to 11 m of unsaturated, calcareous sand, forest region)	0.8
Jaynes et al. (1983b)	Eastern United States	(reclaimed coal strip mine)	18.7
Haas et al. (1983)	North Dakota)	Great Plains(greater than 13 m of calcareous claystone and siltstone, lignite present, vegetated.	19 to 20
Wallick (1983)	Alberta	(less than 13 m thick unsaturated zone, reclaimed coal mine area, high carbonate content in some areas)	24
Wood and Petraitis (1984)	Southern High Plains, Texas	(51 to 77 m of calcareous geologic material)	3.02
Solomon and Cerling (1987)	Utah	(approximately 2 m of unsaturated montane soil, vegetated)	1.24
Wood et al. (1993)	Southern Saskatchewan	(7 m of unsaturated silt loam/till, vegetated)	3
Trumbore et al. (1995)	Eastern Amazonia	(45 m of unsaturated clay, forest and pastureland)	7
Lee (1997)	Massachusetts	(0.5 to 12 m of unsaturated sand)	5

Table 2.9. Summary of surface CO₂ fluxes for non waste-rock material.

Source	Location/geologic material	CO ₂ surface flux (mmol C/m ² /day)
De Jong and Schappert (1972)	Canadian prairie (at least 1.5 m of unsaturated heavy clay), (d=1710 kg/m ³)	Up to 241
Wood and Petraitis (1984)	Southern High Plains, Texas (51 to 77 m of calcareous geologic material), (d=1710 kg/m ³)	2.5x10 ⁻⁴ to 1.2x10 ⁻²
Solomon and Cerling (1987)	Utah (approximately 2 m of unsaturated montane soil, vegetated) (d=2070 kg/m ³)	7.48x10 ⁻² to 0.64
Wood et al. (1993)	Washington state (loess, vegetated) d=1869 kg/m ³)	9.63x10 ⁻⁴ to 8.18x10 ⁻²
Wood et al. (1993)	Southern Saskatchewan (7 m of unsaturated silt loam/till, vegetated)(d=2056 kg/m ³)	0 to 2.58x10 ⁻³
Trumbore et al. (1995)	Eastern Amazonia (45 m unsaturated clay, forest and pastureland)	220 to 580
Lee (1997)	Massachusetts (0.5 to 12 m of unsaturated sand)	19.6 (low veg.) 372 (golf course) 50 (woodland) 123 (grassy area)
Russell and Voroney (1998)	central Saskatchewan (calcareous till, forest)	53 to 807
Hendry et al. (1999) Southern	Saskatchewan (5.75 m of unsaturated sand)	30.8 (average)

de Jong and Schappert (1972) calculated CO₂ production rates and CO₂ surface flux in the Canadian prairies using a Fickian approach (using measured CO₂ concentration depth profiles and an estimated diffusion coefficient). The maximum CO₂ concentration measurement within the top 1.5 m was 2.26 %. CO₂ production rates ranged up to 241 $\mu\text{g C/g/day}$ and the surface flux of CO₂ ranged up to 1 473 mmol C/m²/day. The geologic material was heavy clay.

Russell and Voroney (1973) measured CO₂ surface fluxes ranging from 53 to 807 mmol C/m²/day in central Saskatchewan (forest region). Root respiration was estimated to contribute 60 % of the CO₂ production and a strong correlation was found between CO₂ surface flux and temperature, pore-gas CO₂ concentration in the humus layer (surficial organics) and moisture content. The geologic material was medium to fine-textured, medium to strongly calcareous, glacial till. Volumetric soil moisture content ranged from about 10 to 35 %.

Atkinson (1977) measured pore gas CO₂ concentrations in a limestone environment in England. CO₂ concentrations increased up to 1.8 % with measurements taken at depths as great as 130 m. Oxidation of down-washed organic matter was noted as a possible source of CO₂ at depth. Maximum total carbon content was 11 % in the limestone soils.

Reardon et al. (1979) measured pore gas CO₂ concentrations values in a forest area in Ontario. CO₂ % generally increased with depth (up to between 0.3 and 0.8 %). The water table was 6 to 11 m deep and the total porosity was approximately 0.38. At one site a CO₂ concentration gradient at the water table was observed indicating that the groundwater was a source of CO₂ (degassing). A CO₂ concentration gradient at the water table was not observed at the other site.

Jaynes et al. (1983a) measured pore-gas CO₂ concentrations at a reclaimed coal strip mine in eastern United States. CO₂ concentrations ranged from near atmospheric to greater than 15 %. O₂+CO₂ values were less than 20.9 %, and O₂ and CO₂ concentrations were negatively correlated. O₂ and CO₂ concentrations were weakly correlated to temperature. The average bulk dry density was 1560 kg/m³. The average pyritic S concentration was 0.18 % (by mass, ranging from 0.02 to 2.0 %); the average C concentration was 4.4 % (by mass, ranging from 0.4 to 22.8 %).

Haas et al. (1983) measured pore-gas CO₂ concentrations, at 8 sites in North Dakota (Great Plains region). CO₂ concentrations fluctuated seasonally indicating a relationship to root respiration. Organic and lignite (coal) oxidation were dominant sources of CO₂ in the pore gas.

Wallick (1983) measured pore-gas CO₂ concentrations in the Battle River Mine area in Alberta to indicate when a reclaimed mined area had reached geochemical equilibrium with unmined landscapes. CO₂ concentrations ranging from atmospheric to 24 % and originated from both carbonate dissolution (CO₂ degassing) and organic oxidation.

Wood and Petraitis (1984) calculated O₂ consumption rates, CO₂ production rates and CO₂ surface fluxes at two sites on the Southern High Plains of Texas. O₂ consumption rates varied from approximately 2.3×10^{-3} to 2.5×10^{-2} $\mu\text{g O}_2/\text{g/day}$ (assuming bulk dry density of 1735 kg/m³); CO₂ production rates varied from approximately 2.5×10^{-4} to 1.2×10^{-2} $\mu\text{g C/g/day}$; and surface fluxes were 2.2 mmol C/m²/day and 10.5 mmol C/m²/day. CO₂ production was calculated as a function of depth and gas migration was attributed to diffusion. CO₂ concentrations increased with depth (up to approximately 1 and 2.5 %); O₂ concentrations decreased with depth

(down to approximately 19 and 16 %). Although the sites contained significant amounts of calcium carbonate (up to 80 % in many zones), CO₂ production was attributed to oxidation of organic particles deep in the unsaturated zone. An important conclusion of this study was that a very small amount of CO₂ production at depth had a more profound effect on the geochemistry of the system than a similar production rate near the surface. The unsaturated zones studied were 51 m (gas probes to 36 m) and 77 m (gas probes to 21 m) thick.

Solomon and Cerling (1987) calculated CO₂ production rates ranging from 7.48×10^{-2} to $0.64 \mu\text{g C/g/day}$ in a montane soil in Utah using the concentration-gradient approach. Pore gas CO₂ increased to 1.24 % during the growing season and also during the winter due to the capping effect of the snowpack. CO₂ in the pore gas was noted as an important factor in the weathering of certain minerals (i.e. albite). Also, CO₂ removal by dissolution in infiltrating water was determined to be minimal (less than 4 % of annual budget of CO₂ in pore gas); as much as 15 % of the CO₂ in pore gas could be removed during periods of low CO₂ production.

Wood et al. (1993) calculated CO₂ production rates in Washington state (9.63×10^{-4} to $8.18 \times 10^{-2} \mu\text{g C/g/day}$) and south central Saskatchewan (0 to $2.58 \times 10^{-3} \mu\text{g C/g/day}$) considering diffusive fluxes and partitioning of CO₂ into infiltrating water; CO₂ sorption onto solid phase was considered negligible. CO₂ production rates were reasonably correlated with temperature and microbial abundance at the Washington site; no correlation was observed at the Saskatchewan site. Production at the Saskatchewan site was found to be isolated within 1 m above the water table (approximately 6.5 m below ground surface) and to within the top 2 m during the growing season (root respiration). The water table at the Washington site was 5 to 6 m

below the ground surface. CO₂ and O₂ pore gas concentrations were negatively correlated at both sites; CO₂ % generally increased with depth (up to approximately 2 % in Washington and 3 % in Saskatchewan). CO₂ production was attributed to root respiration and the oxidation of soil organic carbon. Total organic carbon (TOC) of the loess at the Washington site ranged from 1.5 % near the surface to 0.03 % deeper in the unsaturated zone; TOC of the till at the Saskatchewan site ranged from 1.3 % near the surface to 0.2 % deeper in the unsaturated zone. Volumetric moisture contents at the Saskatchewan site ranged from 11.78 to 21.88 %.

Trumbore et al. (1995) measured CO₂ surface fluxes (220 to 580 mmol C/m²/day) from clay soils in Eastern Amazonia by collecting CO₂ from the subsurface as it was released. The study sites ranged from pastureland to forest and CO₂ production was attributed to both root respiration and oxidation of soil organic matter. Total soil C concentrations ranged from 0.10 to 0.20 % below 3 m to 2.52 to 3.18 % near the surface. Dry bulk density ranged from 960 to 1 220 kg/m³. CO₂ concentrations in the pore gas increased (up to about 8 %) with depth (down to 8 m).

Lee (1997) calculated the surface flux of CO₂ at four different sites (gravel-pit area, woodland, golf course, and grassy area) using a Fickian approach. CO₂ surface fluxes and maximum CO₂ concentrations were: 19.6 mmol C/m²/day and 0.7 % (gravel-pit area), 372 mmol C/m²/day and 5 % (golf course), 50 mmol C/m²/day and 1.1 % (woodland), and 123 mmol C/m²/day and 3.2 % (grassy area). CO₂ concentrations were measured to a depth of 3.5 m and generally increased with depth. The geologic material in the study area was sandy (quartz and Na feldspar) with no carbonate minerals present and low organic C content (< 0.1 %).

Hendry et al. (2001) measured pore gas CO₂ concentrations, and calculated CO₂ production rates and surface fluxes, and measured field CO₂ surface fluxes for a 5.7 m thick sandy, unsaturated zone (in central Saskatchewan). Volumetric moisture content ranged from 3 % to over 6 %; mean density and porosity values were 1510 kg/m³ and 0.43, respectively. CO₂ concentrations fluctuated seasonally with maximum concentrations occurring in the summer (0.85 to 1.22 %) and minimum concentrations occurring in the winter (0.04 to 0.24 %). A numerical model constrained by measured CO₂ concentrations and fluxes, temperature and moisture contents and assuming gas migration due to diffusion was used to calculate CO₂ production rates between 5 µg C/g dry soil/day (summer respiration in the soil horizon) and less than 10⁻⁴ mg C/g dry soil/day in unsaturated sections of the C horizon. It was also noted that microbial activity (CO₂ production) might be very low despite the presence of microorganisms in the unsaturated zone.

In summary, studies indicated that CO₂ pore gas concentrations typically increased (absolute maximum of 24%) with increasing depth. Reardon et al., 1979, Wood and Petraitis, 1984, Solomon and Cerling, 1987, Hendry et al., 1993, Wood et al., 1993, Trumbore et al., 1995, Lee 1997, Hendry et al., 1999, and Birkham et al. 2003, all presented CO₂ concentration depth profiles in which CO₂ concentrations generally increased with depth. Reardon et al., 1979, Wood et al., 1993, Lee 1977, and Hendry et al., 1999 presented concentration depth profiles in which CO₂ concentrations at shallow depths were elevated due to seasonal root respiration. CO₂ concentrations were elevated at shallow depths in Hendry et al., 1993 due to increased concentrations of organic matter in the top 0.3 m.

2.5 Climatic Variables Affecting Subsurface and Surface Gas Fluxes: Precipitation and Evaporation

Climate has the potential to enhance or reduce soil CO₂ fluxes. Precipitation can create changes in soil water content and gases (e.g., CO₂) profiles within unsaturated zones; the extent of the effect depends on the intensity and duration of rainfall (Freeze 1969; Capehart and Carlson 1997). Heavy rainfall events, which close the air pathways to the atmosphere in the upper layers of the soils, may result in an inverted CO₂ profile for a short period and in lower surface CO₂ flux (Osozawa and Hasegawa, 1995). Soil CO₂ flux decreases as the soil moisture decreases (Davidson et al., 1998). The influence of the soil water content on gas flux measurements and diffusion is important only when the soil is at a high water content (Davidson and Trumbore, 1995; Moncrieff and Fan, 1999; Conen and Smith, 2000; Hutchinson et al., 2000). Moreover, Moncrieff and Fan (1999) pointed out that no available theory completely describes the influence of high water content on the CO₂ flux from each soil layer.

Evaporation from mine wastes (tailings and waste rocks) is a crucial component of the water balance, partitioning incoming precipitation into water losses back to the atmosphere and controlling water available for soil moisture storage and deep drainage (Carey et al., 2005). Soil covers are widely used in mine waste (tailings and waste rocks) to prevent the generation of acid. To assess the long-term performance of a cover, it is necessary to study the total water balance, including evaporation (Wilson et al., 1994; Wilson et al., 1997; Yanful et al., 2003a; Carey et al., 2005). For an effective soil cover, the soil must maintain a high degree of saturation (Yanful, et al., 2003a; Aubertin et al., 2006). Soil water evaporation significantly affects water content, and as

a result the degree of saturation of the soil. Therefore, knowledge of the rate of evaporation at the soil-atmosphere interface is required to estimate the water content of candidate cover soils (Wilson et al., 1994; Yanful et al., 2003a; Carey et al., 2005).

The following sections briefly present the theory and methods of estimating evaporation, including SoilCover (Unsaturated Soils Group, 1997) computer model. SoilCover was used to estimate evaporative fluxes for comparison with direct measurements of evaporation using eddy covariance (EC) method (Carey et al., 2005). SoilCover model is well-established in the literature, and has been shown by several research to give reasonable accuracy solutions to real-world problems (Rykaart et al., 2001; Scanlon et al., 2002; Noel and Rykaart, 2003; Yanful and Mousavi, 2003a; Yanful et al., 2003b; Vermaak and Beznuidenhout, 2003);

2.5.1 Evaporation

Evaporation involves the change in state of water from a liquid to a vapour. The process occurs when water molecules, which are in constant motion, possess sufficient energy to overcome the surface tension at the liquid surface and escape into the atmosphere (Gray, 1995). The evaporation demand is governed by environmental conditions, such as air temperature, relative humidity, net radiation and wind speed (Wilson, 1990; Unsaturated Soils Group, 1997). Evaporation from soil surfaces is strongly controlled by the water content and water transmission properties of the soil. The rate of movement of water from soil to air depends on the energy gradient and the resistance offered by each pathway through which water moves. Under the same climatological conditions, the evaporation rate can be expected to differ from the rate of evaporation from a free water surface because of the influence of the soil on the mass

and energy exchange processes (Hillel, 1980). For example:

1. The surfaces of soil in a natural environment usually are unsaturated, therefore the vapor pressure is less than the saturation vapor pressure at the surface temperature.
2. The capillary conductivity, which controls the rate of capillary flow of water in an unsaturated soil under a specific energy gradient, is largely a function of the soil moisture content, the size, shape and distribution of the soil pores, and fluid properties.

There is a distinct difference between potential (PE) and actual evaporation (AE). The actual rate of evaporation from a soil surface depends on the availability of water (Thornthwaite, 1948; Penman, 1948; Holmes, 1961; Bouchet, 1963; Priestley and Taylor, 1972; Brutsaert, 1982; Morton, 1983; Wilson et al., 1994 and 1997). The maximum potential rate occurs only when the soil surface is fully saturated and water is present on the ground surface. The actual rate of evaporation begins to decline once the soil surface becomes unsaturated. The rate of evaporation continues to decline as the soil surface continues to desiccate. Hillel (1980) showed typical curves for evaporation rates versus drying time for soil (Figure 2.4). The soil drying process has been observed to occur in three recognizable stages (Fisher, 1923; Pearce et al., 1949; Hillel, 1980):

- (1) An initial constant-rate stage, which occurs early in the process, while the soil is wet and conductive enough to supply water to the site of evaporation at a rate commensurate with the evaporative demand. During this stage, the evaporation rate is limited by, and hence also controlled by, external meteorological conditions (i.e., radiation, wind, air humidity, etc.)

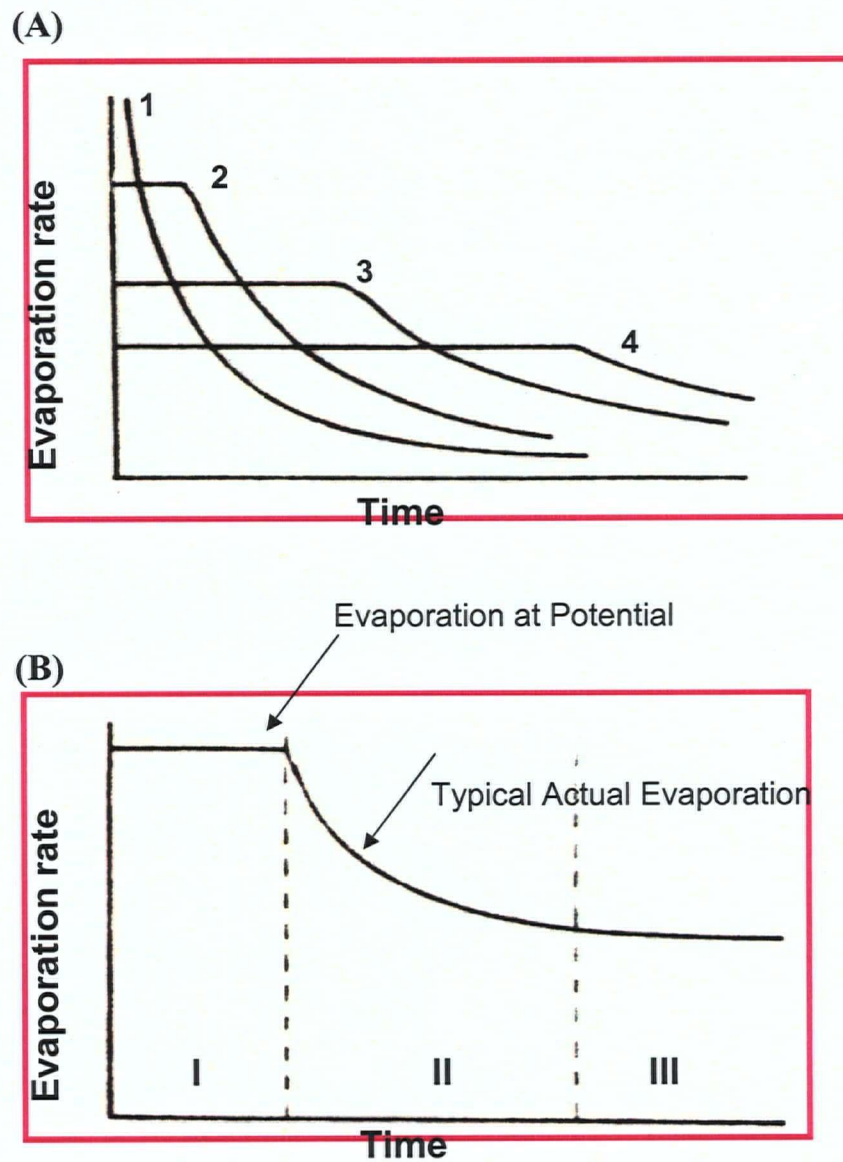


Figure 2.5. (A) Relation of evaporation (flux) to time under different evaporativities (curves 1 – 4 are in order of decreasing initial evaporation rate). (B) Relation of relative evaporation rate (actual rate as a function of the potential rate) to time, indicating the three stages of the drying process.

rather than by the properties of the soil profile.

As such, this stage, being weather controlled, is analogous to the flux-controlled stage of infiltration in contrast with the profile-controlled stage. The evaporation rate during this stage might also be influenced by soil surface conditions. In a dry climate, this stage of evaporation is generally brief and may last only a few hours to a few days.

- (2) An intermediate falling-rate stage, during which the evaporation rate falls progressively below the potential rate (the evaporativity). At this stage, the evaporation rate is limited or dictated by the rate at which the gradually drying soil profile can deliver moisture toward the evaporation zone. Hence, it can also be called the soil profile-controlled stage.
- (3) A residual slow-rate stage, which is established eventually and which may persist at a nearly steady rate for many days, weeks, or even months. This stage apparently comes about after the surface-zone has become so desiccated that further liquid-water conduction through it effectively ceases. Water transmission through the desiccated layer thereafter occurs primarily by the slow process of vapor diffusion, and it is affected by the vapor diffusivity of the dried surface zone and by the adsorptive forces acting over molecular distances at the particle surfaces (Hillel, 1980). This stage is often called the vapor diffusion stage and can be important where the surface layer is such that it becomes quickly desiccated.

The transition from the first to second stage is generally a sharp one, but the second stage generally blends into the third stage so gradually that the last two cannot be

separated so easily. This can be explained by the fact that during the initial stage, the soil surface gradually dries out and soil moisture is drawn upward in response to steepening evaporation-induced gradients (Hillel, 1980). The rate of evaporation can remain nearly constant as long as the moisture gradients toward the surface compensate for the decreasing hydraulic conductivity (resulting from the decrease in water content).

Hillel (1980) noted that since, as the evaporation process continues, both the gradients and the conductivities at each depth near the surface are decreasing at the same time, it follows that the flux toward the surface and the evaporation rate inevitably decreases as well. As shown in Figure 2.4, the end of the first, i.e., the beginning of the second stage of drying can occur rather abruptly.

2.5.2 Methods of predicting evaporation

Evaporation can be calculated with a formulation of Dalton Equation (Wilson et al., 1994):

$$E_p = f(u)(e_s^* - e_a). \quad [2.13]$$

Where:

$f(u)$ = a wind mixing function

e_s^* = vapour pressure at the soil surface

e_a = vapour pressure of the air above the evaporating surface.

The actual evaporation rate is governed by the vapor pressure difference ($e_s - e_a$) and the potential evaporation rate by the vapor pressure difference ($e_a^* - e_a$) (for a specific

set of conditions of net available energy, Q , drying power, E_A , surface temperature, T_s , and surface vapor pressure, e_s).

Penman (1948) formulated an equation for evaporation from a well-watered, short-grass surface by incorporating net radiation and energy balance into Dalton equation:

$$E = \frac{\Delta Q_n + \gamma E_a}{\Delta + \gamma} \quad [2.14]$$

where;

- E = Vertical evaporative flux (mm day^{-1}),
- Δ = Slope of the saturation vapor pressure versus, temperature curve at the mean temperature of the air ($\text{mmHg}/^\circ\text{C}$),
- Q_n = Net radiant energy available at the surface (mm day^{-1}),
- γ = Psychrometric constant,
- E_a = $f(u) (e_a^* - e_a)$

Penman equation is well-known, and many variations on it have been developed over the years (Burman and Pochop, 1994). There are several other commonly used methods for the calculation of potential evaporation, including the Thornthwaite (Thornthwaite and Mather, 1955) for monthly calculations, and Priestley-Taylor method (Priestley and Taylor, 1972; Wilson, 1990). Wilson (1990) and Burman and Pochop (1994) provide a more detailed review of potential evaporation calculation methods.

Another analytical approach to the prediction of actual evaporation was presented by Granger (1989), who suggested that the actual rate of evaporation from the soil could be determined through the Dalton equation, and the actual vapour pressure at the soil surface. Granger did not present a method for calculation of vapour

pressure at the soil surface.

Wilson et al. (1994, 1997) expanded on the work of Penman (1948) and developed a coupled thermal, vapor, and liquid water flow model for predicting actual evaporation from a bare soil. Dalton's Law was utilized to calculate evaporation rate based on the suction at the soil surface:

$$E = \frac{\Delta Q_n + \gamma E_a}{\Delta + \gamma A_{rh}} \quad [2.15]$$

where; E = Vertical evaporative flux (mm day^{-1}),

E_a = $f(u)e_a(B_{rh}-A_{rh})$ where,

$f(u)$ = Function dependent on wind speed, surface roughness, and eddy diffusion,

= $0.35(1+0.1U_a)$,

U_a = Wind speed (km hr^{-1}),

e_a = Vapor pressure in the air above the evaporating surface,

A_{rh} = Inverse of the relative humidity of the air,

B_{rh} = Inverse of the relative humidity at the soil surface.

In this equation, the parameter A_{rh} (inverse of relative humidity) at the soil surface becomes unit in the case of saturated vapour pressure in the soil surface, and the equation simplifies to the original Penman equation. In order to predict the actual evaporation with this equation, it is necessary to solve for the vapour pressure at the soil surface. The solution for evaporation events is equally complex because the rate of

potential evaporation is determined by both the rate of potential evaporation established by climatic conditions and the suction at the soil surface.

2.5.3 SoilCover program

SoilCover is a one-dimensional finite-element package that models transient liquid and water vapor flow, based on a theoretical model for predicting the rate of evaporation from soil surfaces presented by Wilson et al. (1994). The model is based on a system of equations for couple heat and mass transfer in soil (Yanful et al., 2003). The flow of water vapor and liquid water are described on the basis of Fick's Law and Darcy's as follows:

$$\frac{\delta h_w}{\delta t} = C_w^1 \frac{\delta}{\delta y} \left(K_w \frac{\delta h_w}{\delta y} \right) + C_w^2 \frac{\delta}{\delta y} \left(D_v \frac{\delta P_v}{\delta y} \right) \quad [2.16]$$

where: h_w = Total head (m)

t = Time (s)

C_w^1 = Coefficient of consolidation with respect to the liquid water phase

$$C_w^1 = \frac{1}{\rho_w g}$$

ρ_w = Mass density of water (kg m^{-3})

g = Acceleration due to gravity (m s^{-2})

y = Position (m)

K_w = Hydraulic conductivity (m s^{-1})

C_w^2 = Coefficient of consolidation with respect to the water vapour phase

$$= \frac{(P + P_v)}{P(\rho_w)^2 g m_2^w}$$

m_2^w = Slope of the moisture retention curve (1/kPa)

P = Total pressure in the air p_h

$$D_v = \alpha \beta \left(D_{vap} \frac{W_v}{RT} \right)$$

= diffusion coefficient of water vapor through the soil (kg m kN⁻¹ s⁻¹)

$\alpha = \beta^{2/3}$ is the tortuosity factor of the soil; and β is the cross-sectional area of the soil available for vapor transfer

$$D_{vap} = 0.229 \times 10^{-4} \left(1 + \frac{T}{27315} \right)^{1.75}$$

= is the molecular diffusivity of water vapor in air (m² s⁻¹)

T = temperature (K)

W_v = the molecular weight of water (0.18 kg kmol⁻¹)

R = the universal gas constant (8.314 J mol⁻¹ K⁻¹).

Temperature is evaluated on the basis of conductive and latent heat transfer as follows:

$$C_h \frac{\delta T}{\delta t} = \frac{\delta}{\delta y} \left(\lambda \frac{\delta T}{\delta y} \right) - L_v \left(\frac{(P + P_v)}{P} \right) \frac{\delta}{\delta y} \left(D_v \frac{\delta P_v}{\delta y} \right) \quad [2.17]$$

where:

T = temperature ($^{\circ}\text{C}$)

C_h = $C_v \rho_s$

= the volumetric specific heat of the soil as a function of water content ($\text{J m}^{-3} \text{ }^{\circ}\text{C}^{-1}$)

C_v = the specific heat of the soil ($\text{J kg}^{-1} \text{ }^{\circ}\text{C}$)

ρ_s = the mass density of the soil (kg m^{-3})

λ = the thermal conductivity of the soil ($\text{W m}^{-1} \text{ }^{\circ}\text{C}^{-1}$)

L_v = the latent heat of vaporization of water (J kg^{-1}).

SoilCover calculates the vapor pressure in the soil using the relationship provided by Edlefsen and Anderson (1943), in which vapor pressure is calculated on the basis of the total suction in the liquid phase:

$$P_v = P_{sv} h_r \quad [2.18]$$

Where: P_v = Actual vapour pressure within the soil

P_{sv} = Saturation vapour pressure of the soil at its temperature, T

h_r = relative humidity of the soil surface as a function of temperature

$$h_r = e^{\left(\frac{\psi g W_v}{RT}\right)}$$

ψ = Total suction in the total suction in the unsaturated soil (m).

Atmospheric coupling is achieved by calculating the soil evaporative flux. Soil evaporative flux is a function of the vapor pressure gradient between the cover surface

and the atmosphere. A modified Penman formulation proposed by Wilson (1990) in Equation 2.14 is used.

The surface temperature may be estimated using the following relationship (Wilson, 1990):

$$T_s = T_a + \frac{1}{\gamma f(u)} (Q - E - G_s) \quad [2.19]$$

where:

T_s = the temperature at the soil surface ($^{\circ}\text{C}$)

T_a = the temperature of the air above the soil surface
($^{\circ}\text{C}$)

G_s = the ground heat flux (mm day^{-1} of equivalent latent heat).

γ = Psychrometric constant,

2.5.4 Chapter Summary

In summary, from the literature review, it was noted that many studies have investigated O_2 and CO_2 in subsurface pore gas and surface O_2 and CO_2 fluxes for natural ground profiles. Very few studies have focused on quantifying surface CO_2 fluxes and CO_2 production rates for waste-rock systems. The literature review for waste-rock studies also indicated that quantification of O_2 consumption rates has been completed almost exclusively by Australian researchers using using temperature profiles. A need, therefore, exists for measurements of surface CO_2 fluxes and CO_2 production rates in waste-rock piles.

O_2 is geochemically important and active because it is a strong oxidizing agent (has strong affinity for electrons). Examples will be outlined later in the thesis to illustrate the role of O_2 as an oxidant in a waste-rock environment (e.g., oxidation of sulphide minerals and oxidation of organic matter). The production of CO_2 gas is important because it dissolves in the pore water and produces an increase in the activity of H^+ (increase acidity). It is also important to note that carbonate minerals are often present in natural subsurface environments and have a buffering effect on the pH of subsurface pore water (Freeze and Cherry, 1979). This effect will be discussed later in the thesis.

Pore gas migration in this study will be attributed to diffusion. This assumption is consistent with previous sub-surface gas studies (de Jong and Schappert, 1972; Elberling and Nicholson, 1996; Harries and Ritchie, 1985; Solomon and Cerling, 1987). Different diffusion models describe the interaction between gas molecules and the porous media through which the gas is diffusing. The Knudsen model depends upon the molecular weight and temperature of the gas as well as the pore size through which it is diffusing, but it is not influenced by the presence of other gas molecules. The molecular diffusion process assumes that gas molecules collide only with other gas molecules. Molecular diffusion depends upon the molecular weights and temperatures of all the gases in a particular system and does not consider the physical nature of the porous media. A third diffusion model assumes that gas molecules collide with each other and with the porous media. Diffusion is dependent upon pore size, molecular weights and temperatures of the gases, and the physical nature of the porous media. This gas diffusion model will be used in the present work and the development of related equations will be described later in the thesis.

The influence of soil water content on gas fluxes measurements and diffusion is important when the soil is at high water content (Davidson and Trumbore, 1995; Moncrieff and Fan, 1999). The water content of soil depends on several factors: soil texture, temperature, soil respiration rate, environmental conditions of adjacent layers. These factors, which control CO₂ fluxes, vary in different ecosystems and under different climatic conditions. As pointed above, climate has the potential to enhance or reduce soil CO₂ fluxes. The total water balance, including evaporation is necessary, example to assess the long-term performance of a cover (Wilson et al., 1994, and 1997; Aubertin et al., 2006). The dependency of the effective diffusion coefficient on soil water content for different textured soils is well documented (Klute and Letey, 1958; Rowell et al., 1967; Mbonimpa et al., 2003). The diffusion coefficient of CO₂ in water is about four orders of magnitude slower than that in the air-filled voids. The knowledge of the rate of evaporation at the soil-atmosphere interface is therefore required to estimate the water content of candidate cover soils (Wilson et al., 1994; Yanful et al., 2003a)

In conclusion, the work described in the subsequent chapters is primarily directed at the measurement of CO₂ fluxes from a waste rock surface. A review of literature shows there is need for further study in this important area of mine waste management. A new instrument is developed and tested using other methods. In addition, the new instrument is used to measure CO₂ from a waste rock surface under natural field conditions. The influence of surface water conditions with respect to the diffusion coefficient of CO₂ and associated fluxes is also investigated.

CHAPTER III

Materials and Methods

3.1 Introduction

The methods used in this thesis consist of laboratory tests and field measurements. The objective of the laboratory program was to determine the hydraulic properties and characteristics of the soil that influence the CO₂ gas surface fluxes. The tests were conducted in the geotechnical laboratory of the department of mining engineering at the University of British Columbia. The tests conducted include: grain size analysis, water retention curve (WRC) measurements, and saturated hydraulic conductivity tests. The field program consisted of (i) measuring the CO₂ surface fluxes at the Deilmann north (DNWR) and Deilmann south (DSWR) waste-rock piles using the dynamic closed chamber (DCC) method during the summers of 2000 and 2002 and compare the results with those obtained using the static closed chamber (SCC) and eddy covariance (EC) methods and (ii) investigating the effects of climatic variables (e.g., rainfall and evaporation) which affect the gas fluxes.

3.2 Laboratory Program

The laboratory program consisted of sample collection and testing for hydraulic properties.

3.2.1 Sample collection

A 5-kg sample of waste-rock material from the ground and near ground surface (0-0.15 m) was collected at three different locations around DNF1 and DSF1 (Figure

3.8) at the DNWR and DSWR using a sampling scoop. The triplicates samples from each of the waste-rock piles were combined and placed in zippered airtight plastic bags. The samples were shipped to the department of mining engineering of the University of British Columbia for laboratory tests. All samples were stored in the laboratory at room temperature. It should be noted that the waste-rock samples were not representative of the entire DNWR and DSWR piles because physical weathering of the waste rock would have occurred at the surface and near surface of each pile over the years. The grain size of the samples collected was < than 5 cm.

It should be noted that the DNWR and DSWR piles consisted of sand and sandstone, and basement gneiss rock, respectively, and that, after physical weathering, had broken down to soil with texture of a medium sand. Therefore, the samples of waste-rock material collected were not representative of the entire waste-rock piles.

3.2.2 Grain-size analysis

The particle-size analysis of the soil samples was determined by sieve analysis according to ASTM Designation: D 422-63. Two tests were performed on each sample: (i) the distribution of particle sizes larger than 75 μm (retained on the No. 200 sieve) was determined by sieving (ii) the distribution of particle smaller than 75 μm was determined by a sedimentation process, using a hydrometer to secure the necessary data (Figure 3.1).

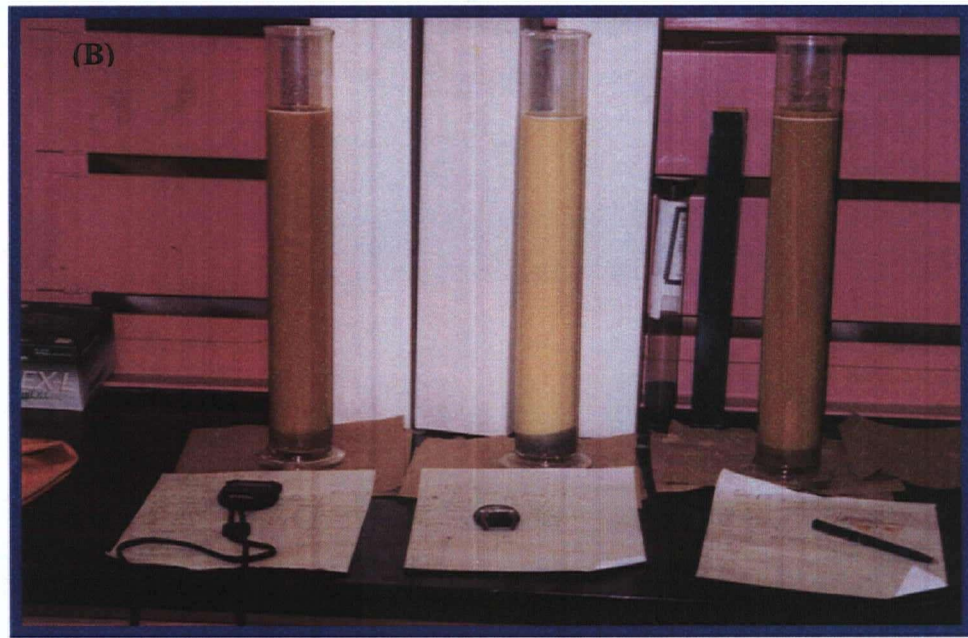


Figure 3.1. Photographs showing (A) the mechanical sieve machine and (B) sedimentation process setups.

(i) Particles larger than 75 μm : Approximately 200 g of each waste-rock sample larger than 75 μm (retained on the No. 200 mesh) was dried at 110 $^{\circ}\text{C}$ for 24 h. The oven dried sample was sieved through sieves with mesh sizes of 4, 10, 20, 40, 60, 80, 100, 140, 200 and 270 on a shaker for 10 minutes. The mass and percent of waste-rock retained on each sieve were determined by weighing and plotted against the size of the sieves openings.

(ii) Sedimentation process: Approximately 70 g of each sample passing through 200 mesh opening sieve was oven dried for 24 h and the mass was subsequently recorded. The sedimentation process was done in a 1-L glass cylinder using Sodium hexametaphosphate as a dispersing agent dissolved in distilled water (Figure 3.1). The solution was adjusted to a pH of 9.5 using sodium carbonate. After agitation of the slurry hydrometer readings were taken at specified time intervals up to 24 h. A sieve analysis was then performed on the material after the suspension was washed with tap water and oven dry at 110 $^{\circ}\text{C}$. The percentage of soil remaining in suspension at the level at which the hydrometer was measuring the density of the suspension was calculated using a formula (ASTM Standard D 422-63, 1998).

3.2.3 Water retention curve

Water retention curves (WRCs) (or soil water characteristic curves) for the two waste-rock samples were determined in a Plexiglas Tempe cell apparatus (0.1 m dia. x 0.14 m height) using standard methods (Fredlund and Rahardjo, 1993) (Figure 3.2). In this test approximately 75 percent of the cell volume was filled with the waste-rock sample. The samples were tested using a 1 bar ceramic stone conducted at room temperature of approximately 20 $^{\circ}\text{C}$. Atmospheric pressure was maintained at the

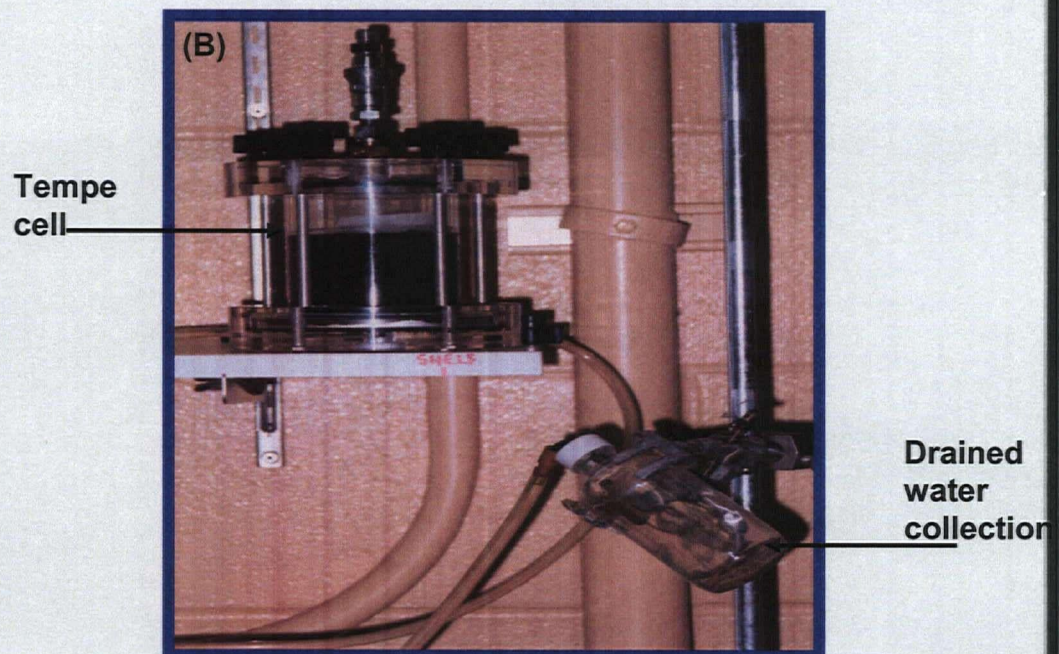
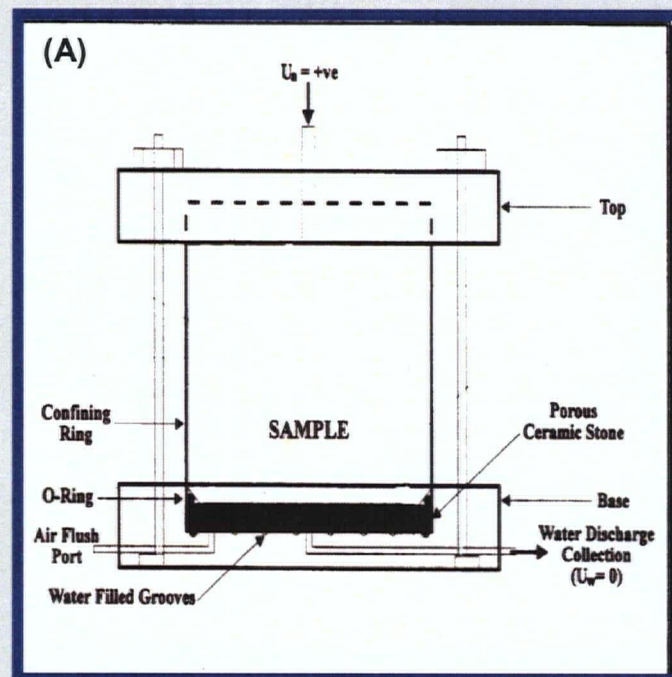


Figure 3.2. (A) Schematic diagram of Tempe cell and (b) water retention curve (SWCC) measurement setup.

discharge face of the porous stone. Air did not flow through the cell unless the air pressure exceeded the air entry value of the ceramic disk. Small amounts of the air diffused through the water in the pores of the high air entry disk and were subsequently flushed from the base of the cell. However, the test was not affected as the air pressure in the cell was maintained by the inlet pressure. The high air entry disk at the base of the apparatus must be saturated prior to the start of the test. The sample was slowly saturated from the base upwards with distilled water until the sample surface was flooded. The sample was left saturated over night prior to the measurements. After saturation of the waste-rock specimen, increasing pressures of 0.2, 0.5, 1, 2, 3, 4, 5, 6, 7, 8, 9, 10, 20, 50, 80 and 100 kPa were applied to the air phase within the cell. The total mass of the waste-rock filled Tempe cell was continually monitored during the drainage phase of each pressure increment. Equilibrium was achieved when zero discharge (measured as change in mass) was observed over a 24 to 72 hour period. Upon reaching equilibrium at 100 kPa of applied suction, the sample was removed from the Tempe cell. The water content corresponding to the highest matric suction (100 kPa) was measured by oven-drying the waste-rock sample. This water content together with the previous changes in weight were used to back-calculate the water contents corresponding to the other suction values. The matric suctions were then plotted against their corresponding water contents to yield the SWCC. Fredlund and Rahardjo (1993) provide a discussion on the measurement of the matric suction.

3.2.4. Saturated hydraulic conductivity

The saturated hydraulic conductivity (K_{sat}) of the samples was determined by performing a falling-head hydraulic conductivity test in a stainless steel permeameter

cell (0.101 m dia. x 0.116 m height) using an ASTM Standard Test Method, D 5856, 1995 (Figure 3.3). It should be noted that the falling-head test is usually recommended for soil having a $K_{\text{sat}} > 10^{-4} - 10^{-5} \text{ m s}^{-1}$ and the constant head test is recommended for coarse-grained soils. The base and top plates of the permeameter were sealed using rubber O-rings. The top plate was connected to a 100 ml standing pipe burette (0.015 m dia. x 0.70 m height). The base plate was connected to a constant head reservoir. Oven-dried waste-rock samples were uniformly and loosely poured into the cell to about 95 percent of the cell volume. The weight of the dry sample was determined by the difference between the weight of the waste-rock-filled cell and the empty cell. The sample was saturated downward with distilled water flowing from the burette through. All air bubbles were removed from the apparatus system by downward flushing of the system with distilled water. Water from the standing pipe burette was allowed to flow through the waste-rock sample using a regulated valve. The time for water to fall between two defined elevations on the standing pipe burette was recorded for each test. The test was repeated until a constant time for water to fall a given height was achieved. The final sample height was then measured before removing the sample from the permeameter cell. The K_{sat} was calculated using the following equation (ASTM Standard Test Method, D 5856, 1995):

$$K_{\text{sat}} = 2.3 * \left[\frac{aL}{A(t_1 - t_2)} \right] * \left[\text{Log} \frac{H_0}{H_1} \right] \quad [3.1]$$

where: a = cross-sectional area of the burette,

L = Length of the waste-rock sample in the permeameter,

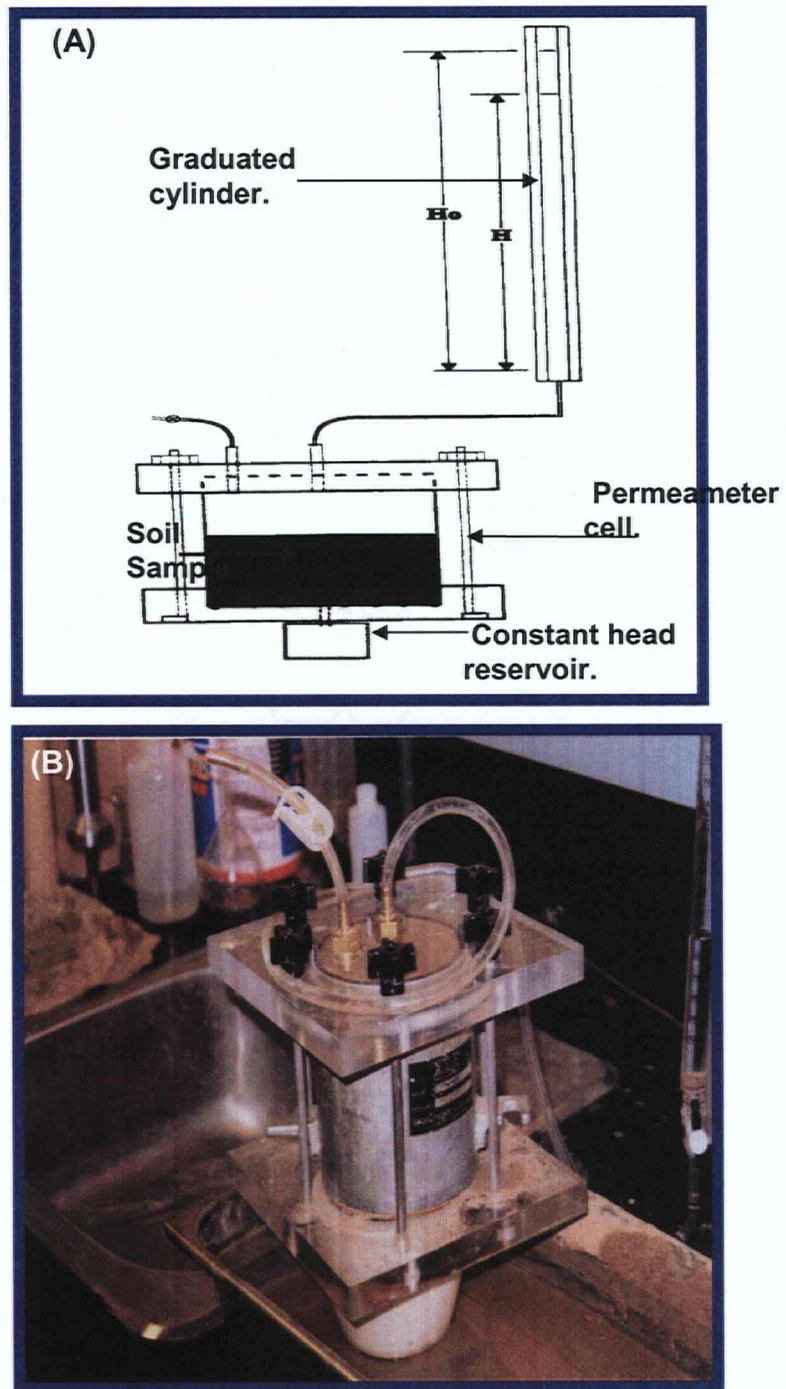


Figure 3.3. (A) Schematic diagram and (B) experimental setup of the saturated hydraulic conductivity measurement.

A = cross-sectional area of the permeameter,

T_0 = time when water in the standing pipe is at H_0 ,

T_1 = time when water in the standing pipe is at H_1 ,

H_0 and H_1 = are the heads from the stand pipe to the bottom

constant head.

The hydraulic conductivity (K) of an unsaturated soil is a function of the degree of saturation (or the volumetric water content) or soil matric suction (ψ) (Huang et al. 1998). A number of empirical relationships have been proposed to determine K as a function of volumetric water content, or matric suction or ψ (Richards 1931; Wind 1955; Gardner 1956; Davidson et al. 1969; Philip 1986; Ahuja et al. 1988, and Frudlund and Rahardjo, 1993). However, the models proposed by Brooks and Corey (1964) and Mualem (1978), appear to be of wider applicability than other models. We used the Brooks and Corey (1964) relation to calculate the unsaturated hydraulic conductivity (K):

$$K(\psi) = K_{\text{sat}} \left[\frac{\Psi_{\text{AEV}}}{\Psi} \right]^n, \quad \Psi > \Psi_{\text{AEV}} \quad [3.2]$$

in which the measured K_{sat} is defined as above at $\psi \leq \psi_{\text{AEV}}$, ψ_{AEV} is the suction corresponding to air-entry value (AEV) and,

$$n = 2 + 3L \quad [3.3]$$

L = the pore-size distribution index,

$$L = -\frac{\Delta \log(S_e)}{\Delta \log(\Psi)} \quad [3.4]$$

S_e = effective saturation,

$$S_e = \frac{S - S_r}{1 - S_r} \quad [3.5]$$

S = degree of saturation at ψ , and S_r = residual saturation.

3.3 Laboratory Mesocosm and Minicosms (sand columns)

Previously, Kabwe et al. (2002) tested the dynamic closed chamber (DCC) method in the laboratory in well-constrained mesocosm (2.4 m dia. x 3.2 m thick) and two minicosms (0.58 m dia. x 1.2 m thick) that was shown to accurately measure CO₂ fluxes from ground surface to the atmosphere (Figure 3.4). One minicosm was maintained at 18-23 °C (HT) and the other at 5 °C (LT). Data measured from these columns were used to validate the numerical model developed in this thesis [see also Appendix E]. The data include: the water contents, CO₂ and O₂ concentrations and temperature profiles measured in the columns. These large physical models, referred to as mesocosms, are considered better surrogates for the natural ecosystem because they have biogeochemical cycles and gradients representative of the natural system. They are of sufficient size that relevant physical, chemical, and biological processes are active and thus permit natural behavior under controlled conditions and can provide an important link in the validation and extrapolation of results to ecosystems (Hendry et al., 2001; Lawrence and Hendry, 1995). The description, construction and filling of the mesocosm are presented in Lawrence et al. (1993), Hendry and Lawrence et al. (1993),

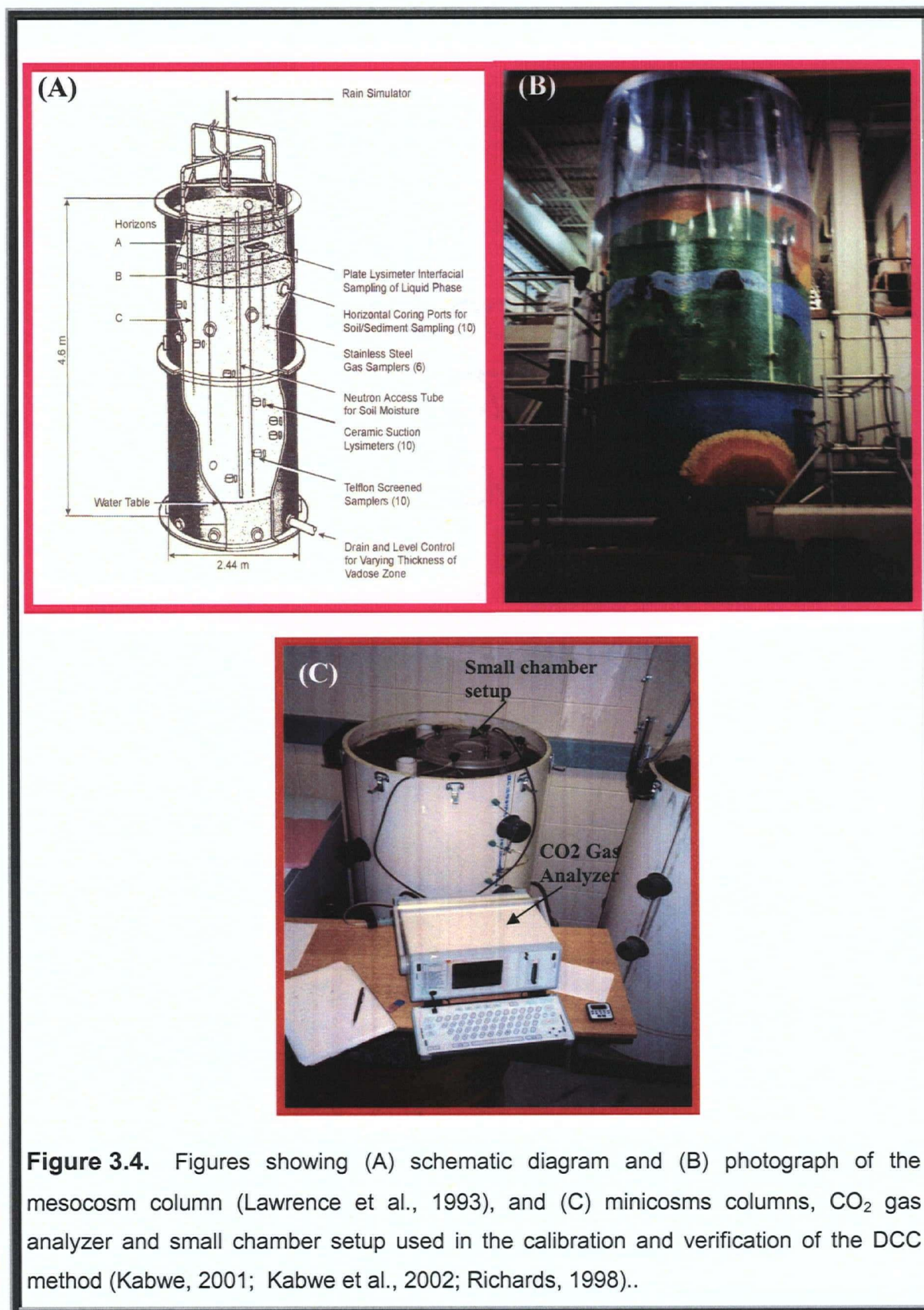


Figure 3.4. Figures showing (A) schematic diagram and (B) photograph of the mesocosm column (Lawrence et al., 1993), and (C) minicosms columns, CO₂ gas analyzer and small chamber setup used in the calibration and verification of the DCC method (Kabwe, 2001; Kabwe et al., 2002; Richards, 1998)..

Lawrence and Hendry (1995), and Hendry et al. (2001). The following section briefly presents the physical descriptions of the mesocosm and minicosms.

Mesocosm: (Figure 3.4A) Fine-grained, poorly graded sand was excavated from the C-horizon of an unsaturated zone at a field site located 10 km south of Saskatoon, Saskatchewan (Hendry et al., 2001). The sand was excavated to a depth of 6 m using a 2 m diameter solid-stem auger in November 1992. As it was excavated, the 65 tons of sand were placed on plastic sheets and transported to the laboratory. The bottom 0.5 m of the cylinder mesocosm (2.4 diameter x 4.6 m high) was filled with 6 to 12 diameter gravel to facilitate control of the water table. The sand excavated from the field site was placed on top of the gravel in the order opposite to which it was removed from the field site. The volume of the excavated material yielded a final sand thickness of 3.6 m. and minicosms shown in Figure 3.4. Biologically produced CO₂, was considered to be the primary source for the CO₂. Studies (Hendry et al., 2001) on microbial aspects of the mesocosm indicated the presence of microbial activity throughout the unsaturated zone. These results indicated that biological activity within the mesocosm was likely sufficient to account for the generation of CO₂ throughout the profile.

Minicosms: (Figure 3.4B) Two minicosms were constructed from a 0.58 m ID polyvinylchloride (PVC) tube, 1.3 m in height, fitted with removable airtight lids. The minicosms were filled with about 634 kg of sand excavated from an unsaturated C-horizon (no A or B horizons) at a field site located 10 km south of Saskatoon, Saskatchewan. The texture and chemistry of the C-horizon sand are described in Hendry et al. (1999, 2000). The methods of filling the minicosms and installation of the instrumentation are described in Richards (1998). On day 1 of the study (August 06,

1995), the water tables in the minicosms were lowered from ground surface to a depth of 0.95 m. One minicosm was maintained at room temperature (21-23°C) (HT -High Temperature) and the other minicosm at 5 ± 2 °C (LT - Low Temperature). Results of studies of microbial populations also indicated that biological activity within the minicosms was likely sufficient to account for the generation of CO₂ throughout the profile (Hendry et al., 1999; Richards, 1998).

3.4 Field Program

The field investigations were carried out at the Key Lake uranium mine, northern Saskatchewan, Canada (57° 12' latitude, 105° 35' longitude) during the summers of 2000 (June to September) and 2002 (August to September). Two waste-rock piles were selected for study: the Deilmann north waste-rock (DNWR) and the Deilmann south waste-rock (DSWR) piles. The DSRW was selected because of its overall simplicity. Specifically, (1) it is texturally uniform with a grain size similar to that of the sand used in mesocosms to verify the DCC method (Kabwe et al., 2002); (2) the surface of the pile was devoid of plant cover and there was no soil development, hence any spatial or temporal variability associated with surficial respiration was minimal.

A weather station was installed at the DSWR in April 2000 to characterize basic climatic variables. CO₂ flux collars for the dynamic close chambers (DCC) method were installed on the DNWR and DSWR in April 2000 by the author of this thesis. CO₂ flux collars for the static closed chamber (SCC) method were installed on the DNWR and DSWR in Summer 2002 by the author of this thesis. Sensors for measuring CO₂ flux using the eddy covariance (EC) technique were installed on the tripod of weather station on DSWR in Summer 2002.

The following sections describe materials and methods of the field tests along with the results and interpretation.

3.4.1 Site location and description

The Key Lake uranium mine is located at the southern rim of the Athabasca Basin in north-central Saskatchewan, approximately 750 km north of Saskatoon, Canada (57° 12' latitude, 105° 35' longitude) (Figure 3.5). The average mean annual temperature at the mine site from 1977 to 1998 was -1.33 °C. From 1977 to 1998, average winter precipitation (October to April inclusive; predominantly snow) was 163.6 mm, average summer precipitation (May to September inclusive; predominantly rain) was 294.8 mm and average total precipitation was 457.4 mm (Birkham et al., 2003). The average annual evaporation (potential) for this time period was 652.9 mm (data obtained at the Key Lake mine site).

Basement gneiss rock is unconformably overlain by Athabasca Group sandstone (Key Lake Mining Corporation, 1979). The Deilmann ore body was mined from 1984 to 1997. Predominant uranium-bearing minerals were coffinite (USiO₄) and pitchblende (UO₂) (Key Lake Mining Corporation, 1979). Arsenide, nickel and sulfide minerals associated with the Key Lake deposits included niccolite (NiAs), gersdorffite (NiAsS) and millerite (NiS) (Key Lake Mining Corporation, 1979). Dissolution of these minerals would potentially increase the concentrations of Ni and As in infiltrating waters. Minor amounts of pyrite (FeS₂) and cobaltite ((Co, Fe)AsS) were also present (Key Lake Mining Corporation, 1979)

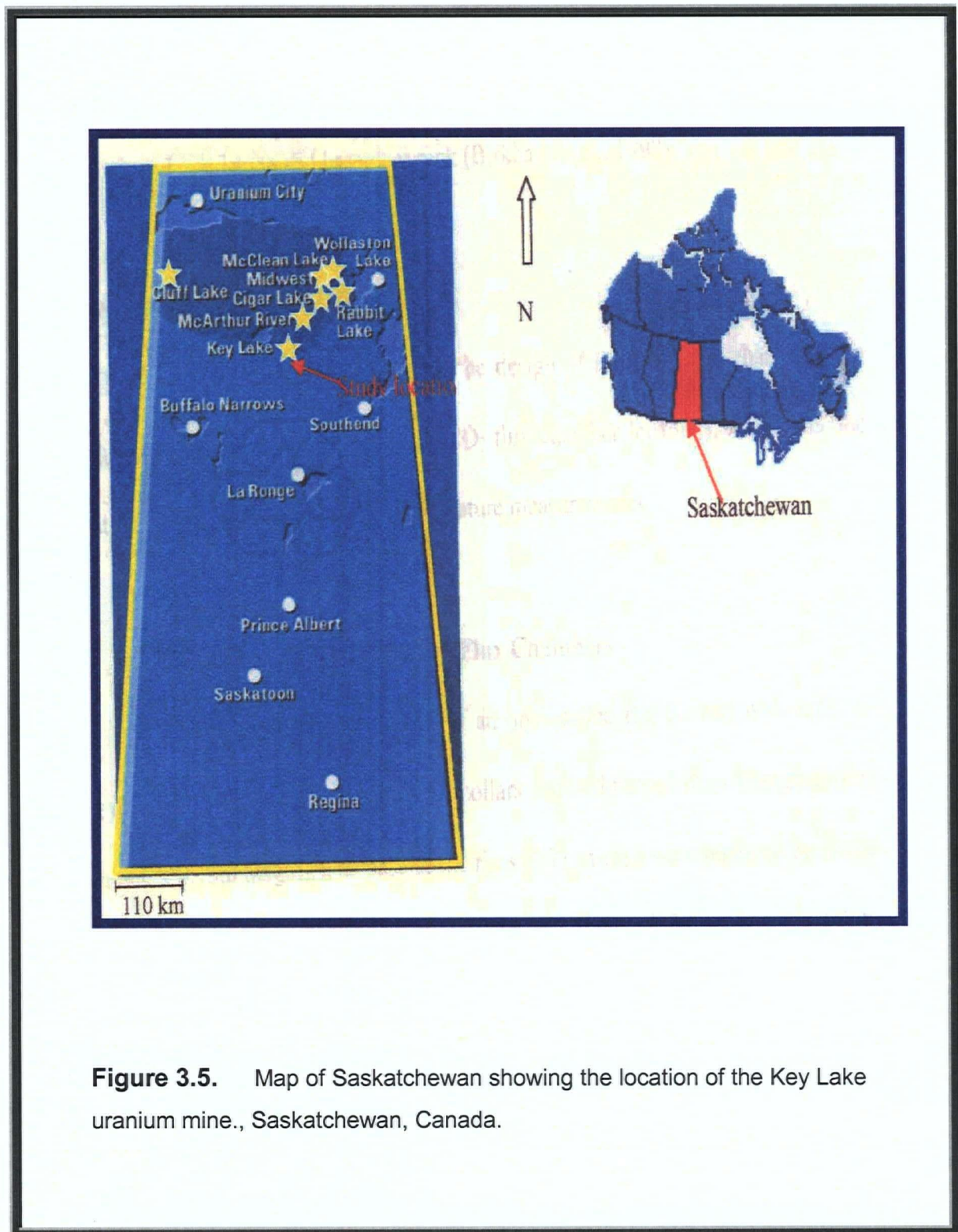


Figure 3.5. Map of Saskatchewan showing the location of the Key Lake uranium mine., Saskatchewan, Canada.

Gangue materials consisted of sandstone and basement gneiss. The minerals comprising the sandstone included quartz (SiO_2), chlorite $((\text{Mg}, \text{Fe}, \text{Al})_6(\text{Al}, \text{Si})_4\text{O}_{10}(\text{OH})_8)$, kaolinite $(\text{Al}_2\text{Si}_2\text{O}_5(\text{OH})_4)$, calcite (CaCO_3) and siderite (FeCO_3) (Key Lake mining Corporation, 1979). The basement gneiss was typically composed of quartz, muscovite $(\text{KAl}_3(\text{AlSi}_3\text{O}_{10})(\text{OH})_2)$, chlorite and feldspars (Key Lake Mining Corporation, 1979). Graphitic gneiss was also present.

Acid base accounting results for sand/outwash till, sandstone and basement rock indicated that both the sulfur and carbonate contents were very low and that the waste-rock piles were not clearly acid generating or consuming (Steffen Robertson and Kirsten (Canada) Inc., 1993). The ratio of neutralization potential to acid generation potential (NP/AP) for sand/outwash till was 1.6 with a standard deviation (s.d.) of 1.30 and a sample size (n) of 29. The mean total sulfur content was 0.03 % (s.d. = 0.02, n = 29). The NP/AP for sandstone was 0.8 (s.d. = 1.93, n = 68) and the total sulfur content was 0.04 % (s.d. = 0.02, n = 68). The NP/AP for basement rock was 1.7 (s.d. = 1.5, n = 27) and the total sulfur content was 0.11 % (s.d. = 0.05, n = 27). Temperatures within the piles ranged from 0 to 2°C.

The excavation of the Deilmann pit resulted in the concurrent construction of two main waste-rock piles from 1984 to 1997, the Deilmann north waste-rock (DNWR) and the Deilmann south waste-rock (DSWR) piles (Figure 3.6). The waste-rock piles were constructed in lifts approximately 8 m in height. Haul ramps were used to transport material to each new lift pad where the waste rock was then dumped and pushed off the edge of the pad to maintain a flat top. Compaction and physical weathering of the waste rock would have occurred at the surface of each lift as a result of machinery traffic.

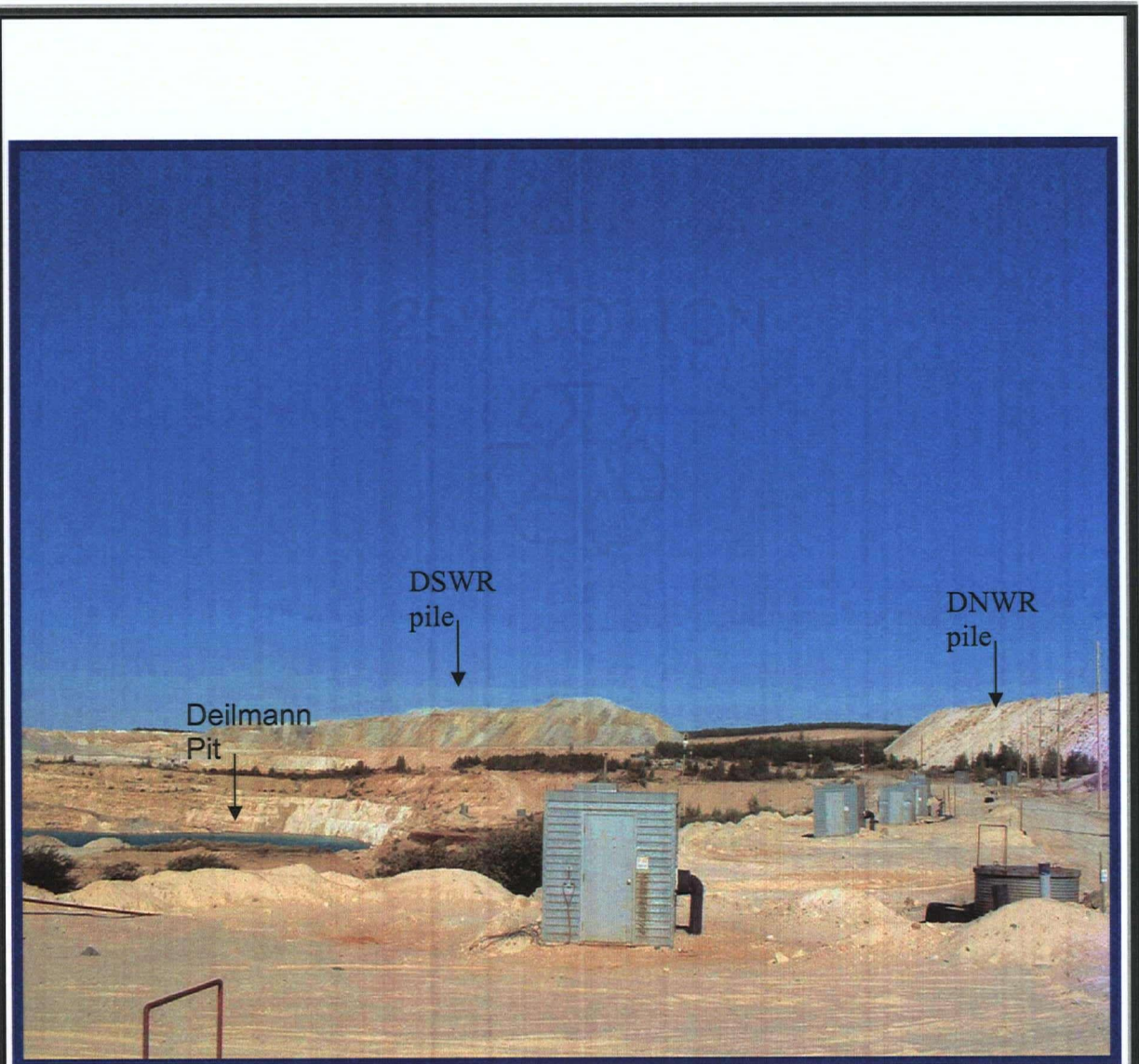


Figure 3.6. Photograph showing the Deilmann pit, the Deilmann north waste-rock (DNWR) and Deilmann south waste-rock (DSWR) piles at the Key Lake uranium mine, Saskatchewan, Canada.

The degree of compaction and weathering could be expected to be the greatest nearest the haul ramp and to decrease further from the haul ramp.

The DSWR was constructed between 1984 and 1995 and consists exclusively of sand and sandstone (Key Lake Mining Corporation, 1979) (Figure 3.7). The maximum height of the DSWR pile is 28 to 31 m above the original ground surface. The bottom of the pile has elevated concentrations of organic matter derived from both lake bottom sediments and forest soils (e.g., Figure 3.7). The original ground surface was not scraped of organic material before construction creating a layer of organic-rich sand at the bottom of a large area of the waste-rock pile (Figure 3.7)

The DNWR pile was constructed from 1984 to 1997 and consists of a mixture of sand, sandstone and basement rock. The maximum height of the DNWR pile is approximately 42 m above the original ground surface. Several lakes near the pits were drained, exposing lake bottom sediments. The bottom of the pile has also elevated concentrations of organic matter derived from both lake bottom sediments and forest soils. Similarly, the original ground surface of the DNWR was also not scraped of organic material before construction creating a layer of organic-rich sand at the bottom of a large area of the waste-rock pile (Birkham et al., 2003).

The geochemical conditions of the waste-rock piles at the Key Lake mine were unique because sulfur contents $< 0.11\%$ S (Steffen Robertson and Kirsten (Canada) Inc., 1993) were low compared to most other geochemical studies (Jaynes et al., 1983a; Gelinis et al., 1992; Elberling et al., 1993; Ritchie, 1994a; Elberling and Nicholson, 1996; Keller and Bacon, 1998; Hockley et al., 2000). Geochemical conditions are also unique because of the cold climate and, as previously mentioned, the piles are constructed of overburden sand, sandstone and gneissic basement rock

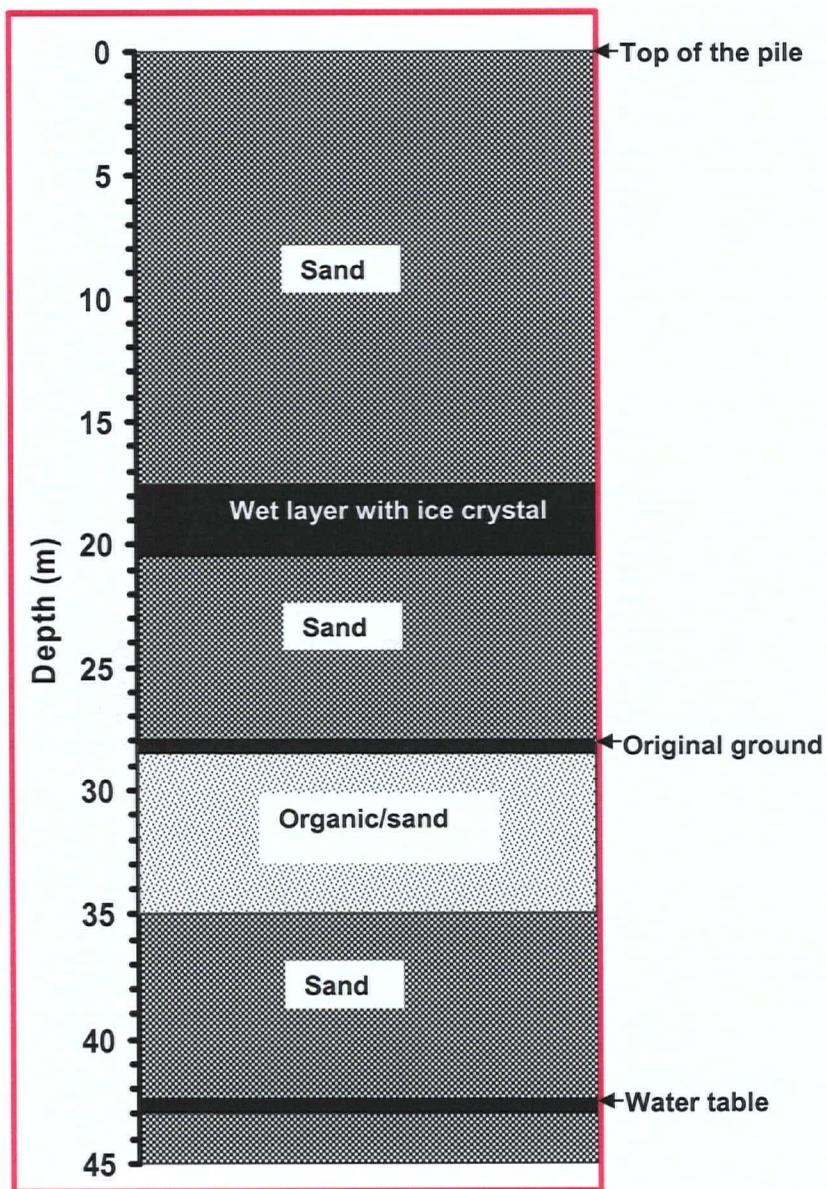


Figure 3.7. Depth geologic profile for Deilmann south waste-rock (DSWR) pile at the Key Lake uranium mine, Saskatchewan, Canada (Adapted from Birkham et al., 2003).

that were dumped on the original ground surface. Approximately 44 million cubic meters of waste rock produced at this site is more than most waste-rock volumes reported in the literature (Gelinas et al., 1992; Ritchie, 1994a; Hockley et al., 2000). Geochemical conditions are also unique because of the cold climate.

3.4.2 Field CO₂ flux measurement methods

This section presents the three methods for CO₂ flux measurements: the dynamic closed chamber (DCC), the static closed chamber (SCC), and eddy covariance (EC) methods. It should be noted again that the DCC was designed, verified and applied on field by the author of this thesis. The SCC was designed by the Department of Soil Science of the University of Saskatchewan (U of S), however, the field measurements were carried out by the author of this thesis, but the gas analysis for CO₂ were done at the Department of Soil Science of the U of S (Farrell et al., 2002). Sensors for measuring CO₂ fluxes using EC method were installed by the Department of Geography of the U of S on the tripod of the weather station installed on the DSWR by the author of this thesis on April 28, 2000 (see later in this section). Data analysis was also done at the same Department of the U of S.

Twenty collars were installed on the DNWR and nine on the DSWR, between April 27 and 29, 2000 (Figure 3.8). The collars were manually driven into the waste-rock piles, leaving the top 0.01 m of the collar above the waste-rock surface. The ground surface was leveled by rotating a straight edge template (0.01 m thick) on top of the collar. The collars were allowed to stabilize in the sand for about 60 days prior to the start of the CO₂ flux measurements.

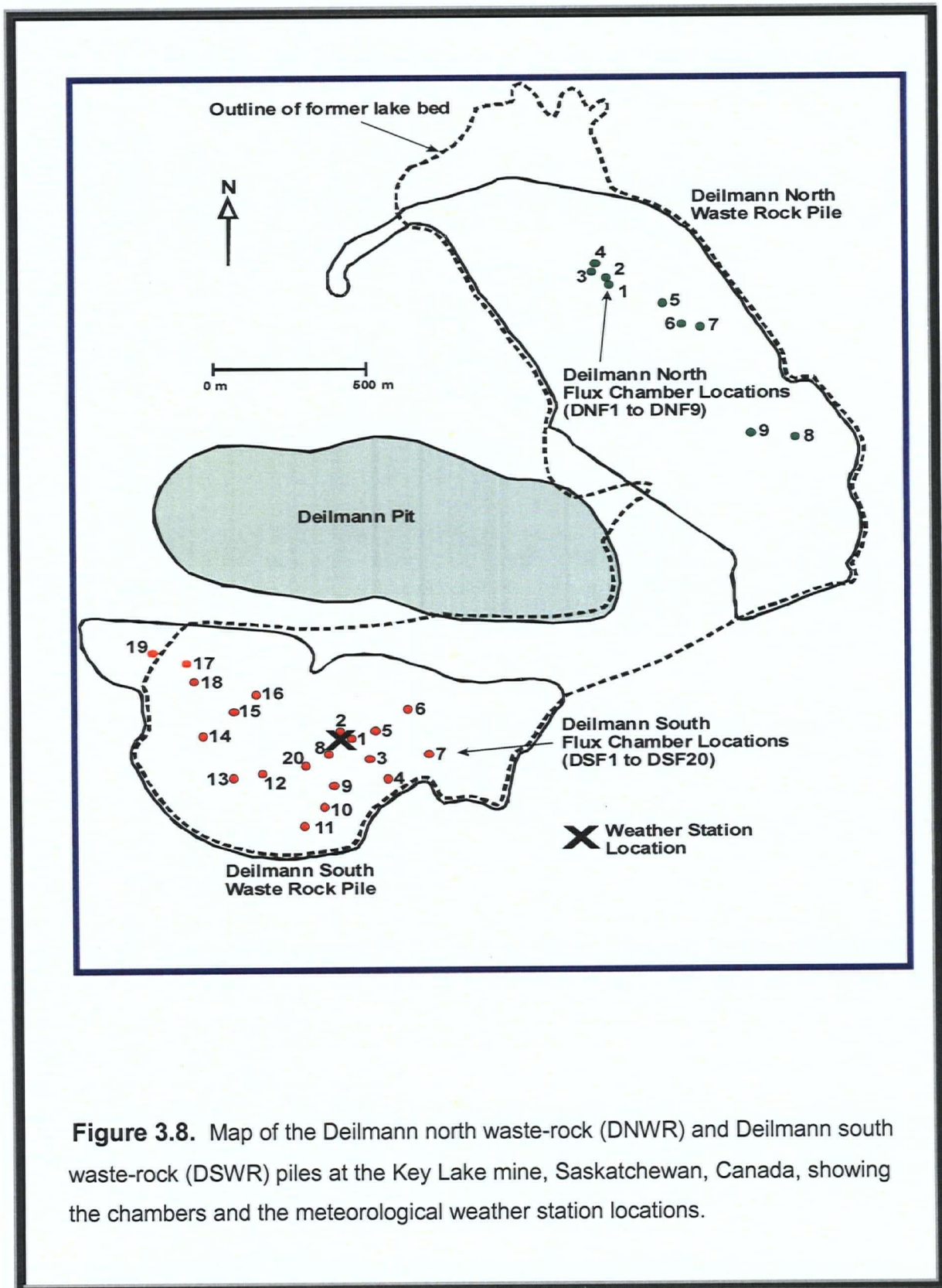


Figure 3.8. Map of the Deilmann north waste-rock (DNWR) and Deilmann south waste-rock (DSWR) piles at the Key Lake mine, Saskatchewan, Canada, showing the chambers and the meteorological weather station locations.

3.4.2.1 Measuring CO₂ fluxes using dynamic closed chamber (DCC) method

A technique to measure CO₂ fluxes from the soil surface to the atmosphere was recently developed and verified in mesocosms over the range of CO₂ fluxes reported for field conditions by the author of this thesis (Kabwe, 2001 and Kabwe et al., 2002). The technique termed the dynamic closed chamber (DCC) method, is based on direct measurement of the change in CO₂ concentration with time in the headspace of a chamber installed on ground surface. Carbon dioxide concentrations were directly measured using a portable CO₂ gas analyzer (ADC 2250, BioScientific Ltd).

The work of this thesis focused on the field application of the DCC method to quantify reaction rates in waste-rock piles. Full details of the design, construction, and operation of the DCC are presented in Kabwe (2001) and Kabwe et al. (2002). The following section briefly described the DCC method.

Chamber collars for the DCC were fabricated from fiberglass rims (0.76m dia. × 0.15m height); the chamber lid (0.76m dia. × 0.05m thick) was fabricated from Plexiglas (Figure 3.9). A rubber O-ring was installed into a groove on the underside of the lid to provide an air-tight seal between the lid and the collar. Inlet and outlet brass-fittings were installed in the lid. A perforated tube (1.20 m long) with one end connected to the inlet fitting was installed into a groove on the underside of the lid to provide air dispersion in the chamber headspace. The lid was attached to the collars with nuts and bolts. Carbon dioxide analyses were performed using an ADC 2250 differential infrared CO₂ gas analyzer (ADC BioScientific Ltd). The analyzer provided simultaneous absolute and differential gas measurements. All CO₂ measurements were corrected for pressure

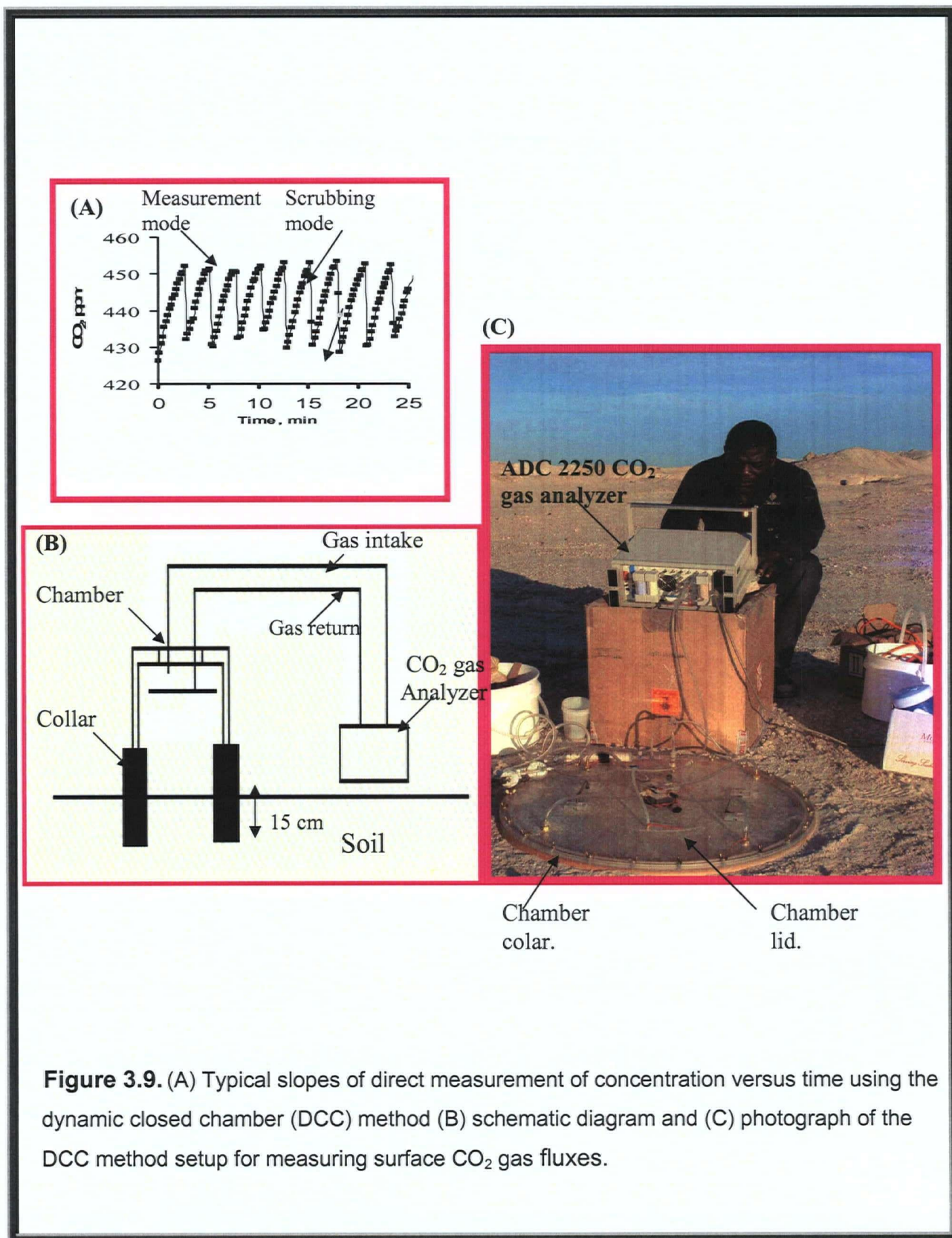


Figure 3.9. (A) Typical slopes of direct measurement of concentration versus time using the dynamic closed chamber (DCC) method (B) schematic diagram and (C) photograph of the DCC method setup for measuring surface CO₂ gas fluxes.

broadening and dilution effects caused by water vapor; single bench (CO₂) peak-to-peak noise was typically <0.2 ppmV at 350 ppmV CO₂. Measurements were made by sealing the lid onto the collar and continuously circulating air from the chamber (top, center) through the ADC 2250 CO₂ analyzer and back into the chamber through the perforated air-dispersion ring on the underside of the lid (see Figure 3.9).

Prior to measuring a flux, the ambient CO₂ concentration was measured at the collar. The CO₂ was then scrubbed from the air in the sealed chamber (using soda lime in an on-line trap) to lower the CO₂ concentration to below ambient (to yield improved accuracy at low flux levels). In the measurement mode, the analyzer measured the CO₂ concentrations in the chambers as they increased from sub-ambient to ambient and higher concentrations (Figure 3.9). During this period, the CO₂ concentration in the chamber was measured at 1 s intervals, with mean concentrations recorded every 10 s. The flow rate through the chambers was maintained at approximately 39 L h⁻¹. The flux of CO₂ from the soil surface was calculated from the rate of change in CO₂ concentrations in the chambers as follows:

$$F_{\text{CO}_2} = \left[\frac{dC}{dt} \right] \times h \quad [3.6]$$

where F_{CO_2} is the CO₂ flux from the soil surface, C is the concentration (mg m⁻³) in the chamber at ambient temperature and pressure, t is time, h is chamber height (m), and dC/dt is the slope of the best fit of the time series as time approaches zero. Fluxes were determined by averaging a series of four to eight measurement cycles. The final flux reported here equals the flux observed at the ambient air CO₂ concentration, which was determined prior to measurements. The time required to determine one series of flux

measurements ranged from 2 to 8 min, depending on the magnitude of the flux. To minimize temperature variation within the chamber, it was shielded from the sun during the measurement period. Note: in all cases, actual CO₂ concentrations were measured as mixing ratios (i.e., volume per unit volume of air) and were converted to a mass basis as described by Hutchinson and Livingston (2000).

3.4.2.2 Measuring CO₂ fluxes using static closed chamber (SCC) method

Ambient fluxes of CO₂ also were measured using a static closed chamber (SCC) consisting of a PVC cap fitted with a vent tube and Swagelok™ sampling port (see Figure 3.10). Collars (15 cm × 20.3 cm i.d.) for the chambers were manually driven into the collar. To minimize the effects of soil disturbance on the CO₂ flux, the collars were inserted into the waste rock about one week prior to the start of the measurement period. Each chamber had a volume-to-surface area ratio of about 9:1, with an internal headspace volume (including the above-ground portion of the collar) of 1750 cm³ and a surface area of 201 cm². Once the chamber was sealed to the collar, gas samples were collected at 20-min intervals. Gas samples were collected from the enclosed headspace using a disposable, 20-cc syringe equipped with a 25-gauge, ⁵/₈-inch needle. Gas samples were withdrawn through the sampling port (sealed with a gray butyl rubber septum) in the top of each chamber; injected into pre-evacuated (ca. 5 × 10⁻³ atm), 12-cc Exotainers™, and analyzed using gas chromatography (Farrell et al., 2002). The gas samples were stored under a positive pressure of approximately 2-atm (i.e., 20-cc of headspace gas was injected into each 12-cc collection tube) to minimize any gaseous exchange with atmospheric air. The gas samples were then shipped to the Department

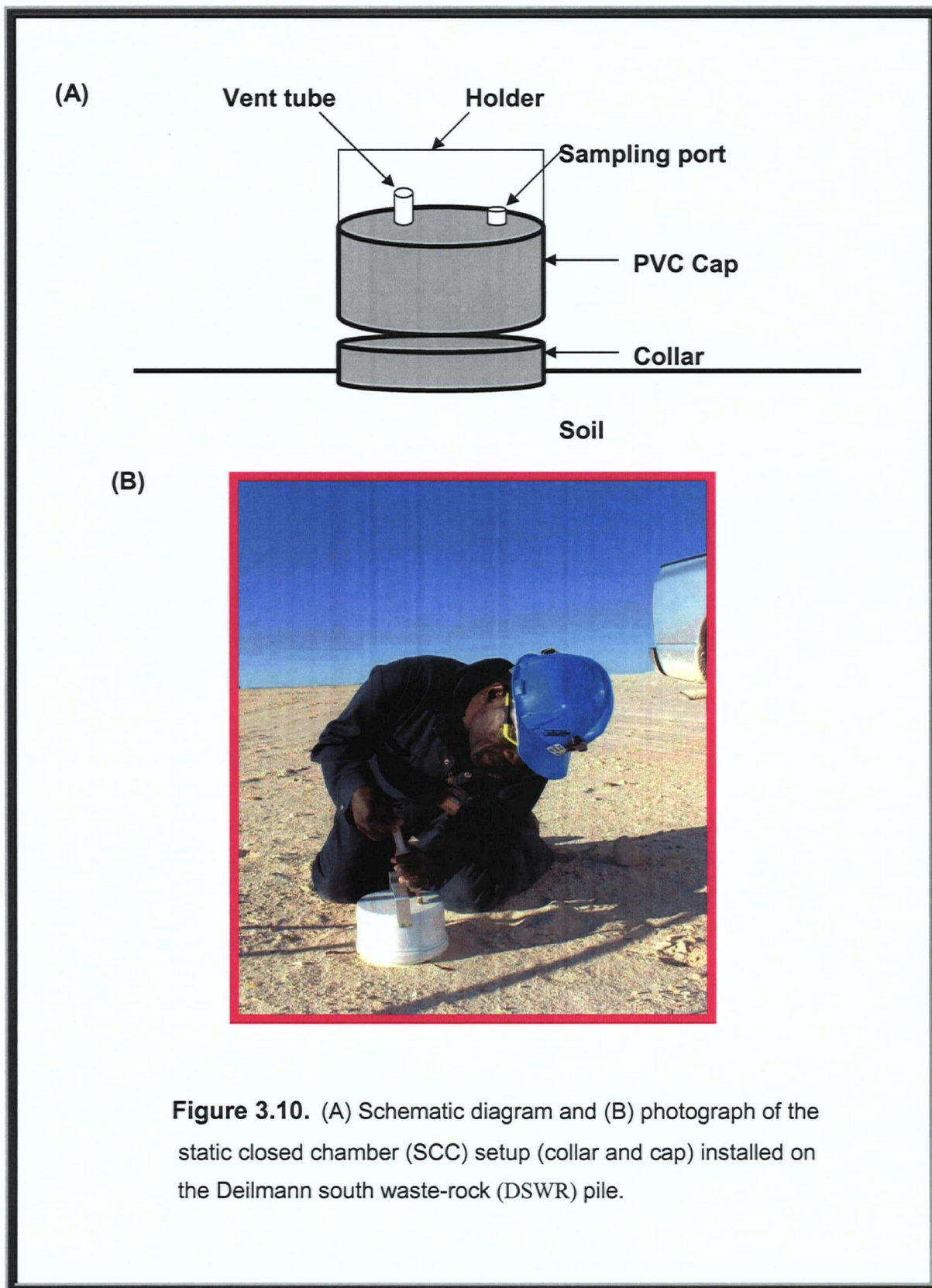


Figure 3.10. (A) Schematic diagram and (B) photograph of the static closed chamber (SCC) setup (collar and cap) installed on the Deilmann south waste-rock (DSWR) pile.

of Soil Science of U of S for CO₂ gas analysis.

Carbon dioxide concentrations were determined using a Varian Model CP2003 Micro-GC equipped with a micro-TCD and Poraplot U column (injector temperature = 110°C, column and detector temperature = 50°C). Ultra-high purity (UHP) helium was used as the carrier gas.

The vertical flux density for CO₂ above the soil surface (mg CO₂ m⁻² h⁻¹) was determined by measuring the change in gas concentration beneath the sealed chamber at set (equally spaced) time intervals. The vertical flux was then calculated using the diffusion-based estimation model proposed by Hutchinson and Mosier (1981) (see also Appendix I):

$$F_{\text{CO}_2} = \frac{V(C_1 - C_0)^2}{A t_1 (2C_1 - C_2 - C_0)} \ln \frac{(C_1 - C_0)}{(C_2 - C_1)} \quad [3.7]$$

$$\text{and } t_2 = 2t_1 \text{ and } \frac{(C_1 - C_0)}{(C_2 - C_1)} > 1 \quad [3.8]$$

where: V is the volume (m³) of enclosed chamber air, A is the area (m²) of soil that is covered by the chamber, C_0 is the initial CO₂ concentration (mg m⁻³), and C_1 and C_2 are the CO₂ concentrations (mg m⁻³) at times t_1 (0.33 h) and t_2 (0.67 h). The 20 min time interval between samples was long enough for the CO₂ concentration in the chamber headspace to increase to a measurable level, yet short enough that the CO₂ concentration in the chamber neither leveled off nor declined during the interval from t_1 to t_2 . Carbon dioxide concentrations were converted to a mass basis after correcting for variations in temperature (i.e., 15°C), vapor-pressure (to correct for wet gas), and atmospheric pressure.

3.4.2.3 Measuring CO₂ fluxes using eddy covariance (EC) method

Sensors for measuring CO₂ flux using eddy covariance (EC) technique were installed on the same tripod of weather station in 2002 between 2 July and 25 August (Figures 3.11 and 3.12). A three-dimensional sonic anemometer (CSAT3, Campbell Scientific Inc., Logan, UT) was mounted on a 1.5 m boom with the mid-point of the sonic head approximately 1.7 m above the ground surface within the constant flux layer. The instrument height is justified considering the surface is vegetation-free without wake elements and above the height of the roughness sub-layer. An open-path gas analyzer (LI-7500, LI-COR Inc., Lincoln, NB) was placed on the boom adjacent to the sonic anemometer at the same height with approximately 0.2 m separating the mid-point of each sensor. Various wind components were recorded every half hour using a CR-23X data-logger (Campbell Scientific Inc., Logan, UT). Although the DSWR site was flat, it had a fetch of only 150 to 300 m. The 'flux footprint' of a tower (which is a function of wind speed and direction and the height of the tower) was calculated as described by Schuepp et al. (1990). The peak for the flux footprint ranged from 35 to 50 m upwind, with approximately 90% of the cumulative flux footprint within 150 m upwind of the tower. The EC method was used to measure the CO₂ flux on a continuous basis (Baldocchi et al., 1988). Changes in CO₂ concentration were measured using the LI-7500 open-path CO₂/H₂O gas analyzer. Latent and sensible heat fluxes were measured concurrently. Wind speed and gas concentration measurements were obtained at a frequency of 10 Hz. The CO₂ flux (F_{CO_2}) was calculated as the product of the mean covariance of the vertical wind speed fluctuations (w') and the scalar fluctuations in CO₂

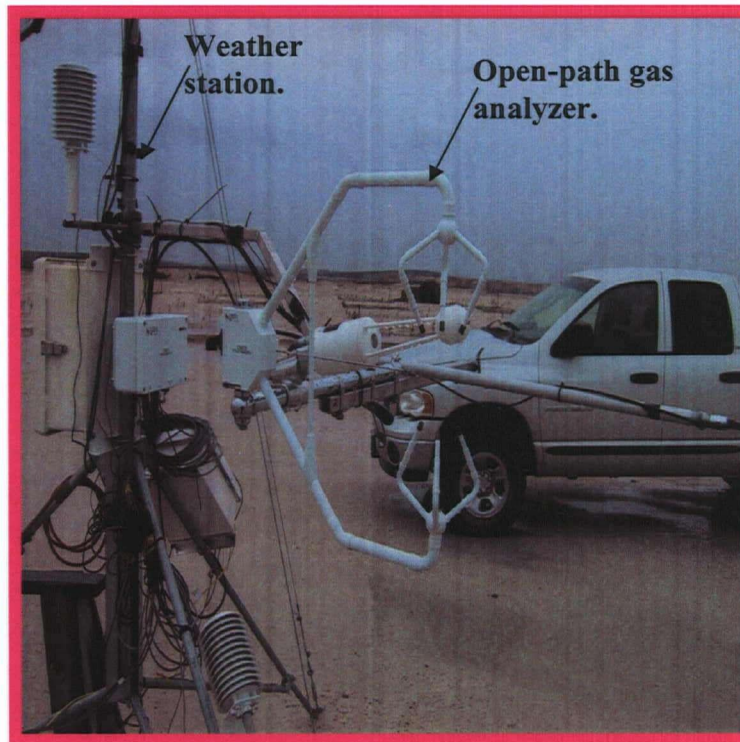


Figure 3.11. Photograph showing the meteorological weather station and the eddy covariance (EC) sensors for measuring CO_2 flux installed on Deilmann south waste-rock pile (DSWR).

$$F_{\text{CO}_2} = \rho_a \overline{w' \text{CO}_2'} \quad [3.9]$$

where ρ_a is the density of the dry air and the prime (') denotes the deviation from the mean (see also Appendix A). The running mean was based on a 300-s time constant; the resultant mean fluxes and various wind components were recorded every 30 minutes. Corrections and adjustments to the F_{CO_2} are summarized as follows. First, fluxes were corrected for changes in air density (Webb et al., 1980) and were removed when $u^* < 0.1 \text{ m s}^{-1}$ (Note: u^* is the friction velocity as measured by EC) due to poor energy balance closure at low wind speeds (Twine et al., 2000; Barr et al., 2002). Second, F_{CO_2} was corrected for underestimation by eddy covariance by adjusting for energy-balance closure, assuming that eddy covariance underestimated F_{CO_2} by the same fraction that it underestimated sensible and latent heat fluxes (Black et al., 2000, Twine et al. 2000; Barr et al., 2002), i.e., by 24% for all measurement periods ($r^2 = 0.86$, $n = 3035$). Additionally, as a check on the energy balance closure method, a power spectral density function was computed using high-frequency (20 Hz) data to determine if sampling interval was sufficient to capture low and high frequency eddies (i.e., Moore, 1986). This analysis indicates that the tower captured 79% of the energy being transferred (sampling at 10 Hz and integrating over 30 minutes). However, this high-frequency data was collected during one 6-hour period only, and as such the energy-balance method of correction was used as it was considered more representative over all stability conditions.

3.4.2.4 Gravimetric water content measurement

Waste rock samples were retrieved in triplicates from selected locations around DNF and DSF (Figure 3.8) at four different depths (0, 0.05, 0.10 and 0.15 m) at the DNWR and DSWR, from the period of July 29 to August 06, 2002. The samples weighing between 200 to 250 g were immediately placed in zippered plastic bags to preserve the in situ moisture in the samples. The samples were transported to the on site Key Lake metallurgical laboratory and kept in the refrigerator. The samples were tested within 24 h. The gravimetric water content for waste rock samples was measured according to the ASTM Standard Test Methods for Laboratory Determination of Water (Moisture) Content of Soil and Rock by Mass (D2216-05). The method consisted of taking the waste rock samples weighing between 100 and 200g. The samples were put in a container of known weight, weighed (subtracting the weight of the container gives the weight of the wet soil). The samples were then put in an oven, and dried at 105 °C for about 24 h until all the water had evaporated. After drying the samples, they were weighed again (subtracting the weight of the container gives the weight of the dry soil). The moisture content on a weight basis was the difference between the wet and dry weights divided by the dry weight. The gravimetric water contents were converted to volumetric water contents using data from the WRC and specific gravity.

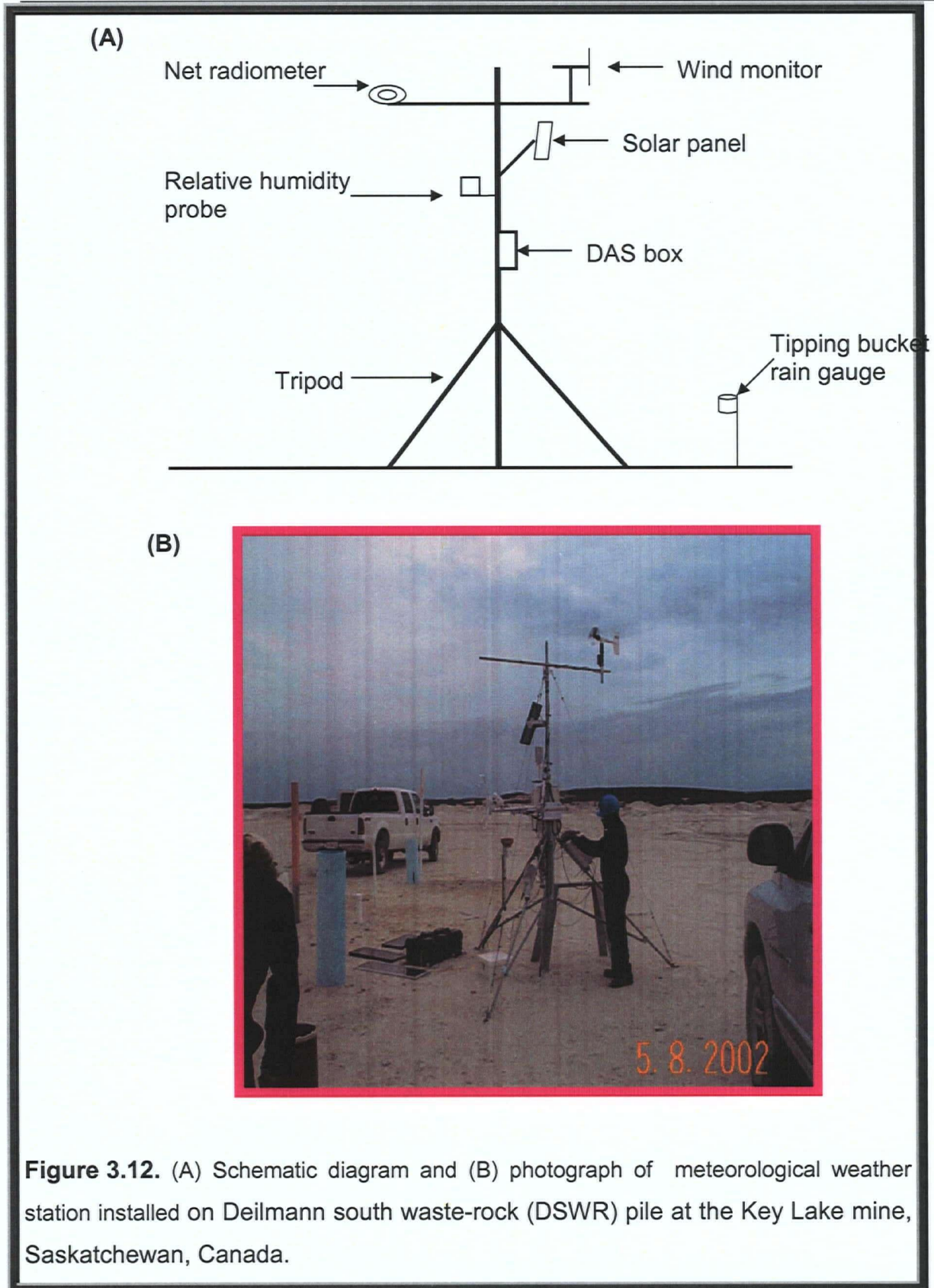
3.4.2.5 Meteorological weather station

A meteorological weather station (Campbell Scientific, Inc.) was installed on DSWR (Figure 3.12) approximately 5 m southwest of the collar located at DSF1 (Figure 3.8) on April 28, 2000 by the author of this thesis. The meteorological station sensors

and data acquisition systems (DAS) were installed on a tripod. The wind monitor and net radiometer were mounted on a steel cross-arm at a height of approximately 3 m above the ground surface. The air temperature and relative humidity probe was housed in a radiation shield (approximately 1.8 m above the ground surface) to minimize the effects of solar radiation. The tipping bucket rain gauge was installed on a wooden plank near the tripod (approximately 1 m above the ground surface). The DAS consisted of a CR10 data- logger (Campbell Scientific Inc.), a storage module and a solar panel with 12 volt battery system. The station collected hourly average air temperatures.

3.4.2.6 Chapter Summary

In summary, in a previous study using large-scale, laboratory mesocosms filled with sand [Kabwe et al., 2002], the DCC method was shown to accurately measure CO₂ fluxes from ground surface to the atmosphere. This laboratory-verified technique, therefore, provided the opportunity to quantify CO₂ fluxes under field conditions. The following chapter 4 presents results of the field application of the DCC method. The DCC method was used to determine the magnitude of spatial and, to a lesser degree, temporal variations in the CO₂ efflux on the DNWR and DSWR piles. In addition, fluxes measured using the DCC method were compared to those obtained from two other methods: static closed chamber (SCC) and eddy covariance (EC) methods.



CHAPTER IV

Results and Data Interpretation

4.1 Laboratory Tests Program

The laboratory program consisted of testing for hydraulic properties for samples from the Deilmann north (DNWR) and Deilmann south (DSWR) waste-rock piles .

4.1.1 Grain-size distribution

The laboratory tests results for the near-ground surface (0 – 0.15 m) samples from DSWR and DNWR for grain-size distribution are plotted respectively in Figures 4.1 and 4.2. The detailed tests results are presented in Appendix C. The grain-size distribution curves from DSWR sample (Figure 4.1, curve with symbols) indicated that 90% of the material was sand size with 10% silt- and clay-size particles. The sand sizes ranged from coarse (6%), medium (32%), and fine (52%). The uniformity coefficient (C_u) of the sample ($C_u = D_{60}/D_{10}$) was found to be about 3.6 (e.g., $D_{10} = 0.015$ cm is the size such that 10% of the particles are smaller than that size). For comparison, a washed beach sand would have a C_u of about 2 to 6 whereas a sample with a $C_u < 4$ is considered well sorted while a sample with a $C_u > 6$ is considered poorly sorted. The void ratio (e) of the sample ($e = V_v/V_s$) was found to be 0.560 (e.g., V_v is the volume of voids and V_s is the volume of solids). The C_u , e and D_{10} values of the sample are typical of the values for granular non-consolidated sand materials reported in Table 4.1.

Table 4.1. Nature, origin, and basic geotechnical properties of various granular materials.

Source	Material	D ₁₀ (cm)	C _u	e
Sydor (1992)	. Coarse sand.....	0.05800	1.3	0.750
	. Borden sand.....	0.00910	1.7	0.590
	. Modifield Borden sand..	0.00800	1.8	0.640
Kissiova (1996)	. Secrete sand.....	0.01450	3.5	0.570
Mackay (1997)	. Ottawa sand.....	0.00937	1.7	0.634
Bruch (1993)	. Beaver Creek sand consolidated at 5 kPa....	0.00930	2.6	0.269
	. Beaver Creek sand consolidated at 10 kPa....	0.00930	2.6	0.267
Lim et al. (1998)	. Beaver Creek sand consolidated at 5 kPa....	0.00930	2.6	0.618

The mean \pm one standard deviation grain-size distributions (curves with solid lines) obtained from 106 core samples from DSWR (Birkham, 2002) are also presented in Figure 4.1 for comparison. The partial grain-size (without gravel and boulder-sized) distribution for the material evaluated in this thesis (curve with symbols) was within the envelope of the core samples up to the grain size > 0.3 mm)..

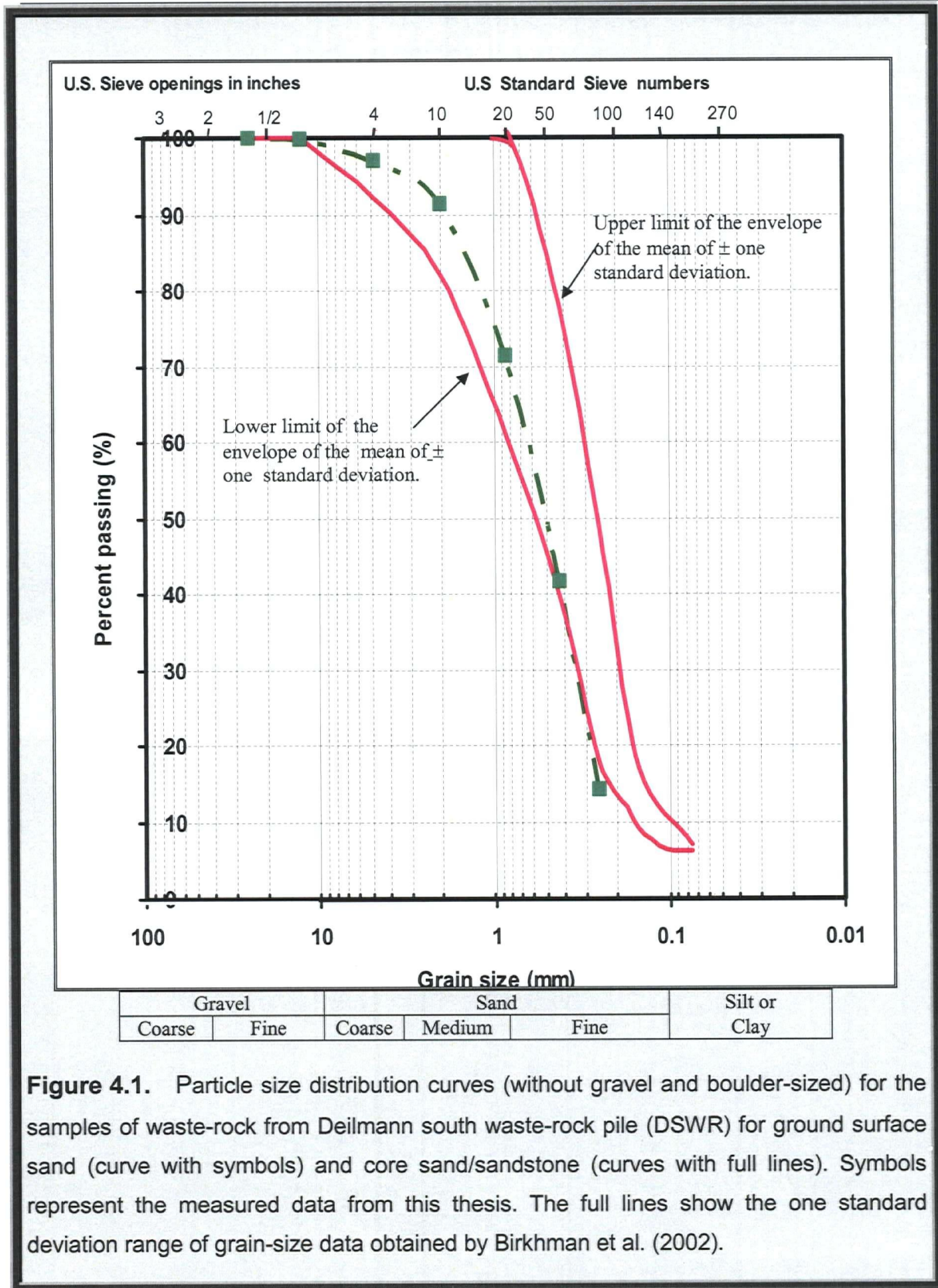


Figure 4.1. Particle size distribution curves (without gravel and boulder-sized) for the samples of waste-rock from Deilmann south waste-rock pile (DSWR) for ground surface sand (curve with symbols) and core sand/sandstone (curves with full lines). Symbols represent the measured data from this thesis. The full lines show the one standard deviation range of grain-size data obtained by Birkhman et al. (2002).

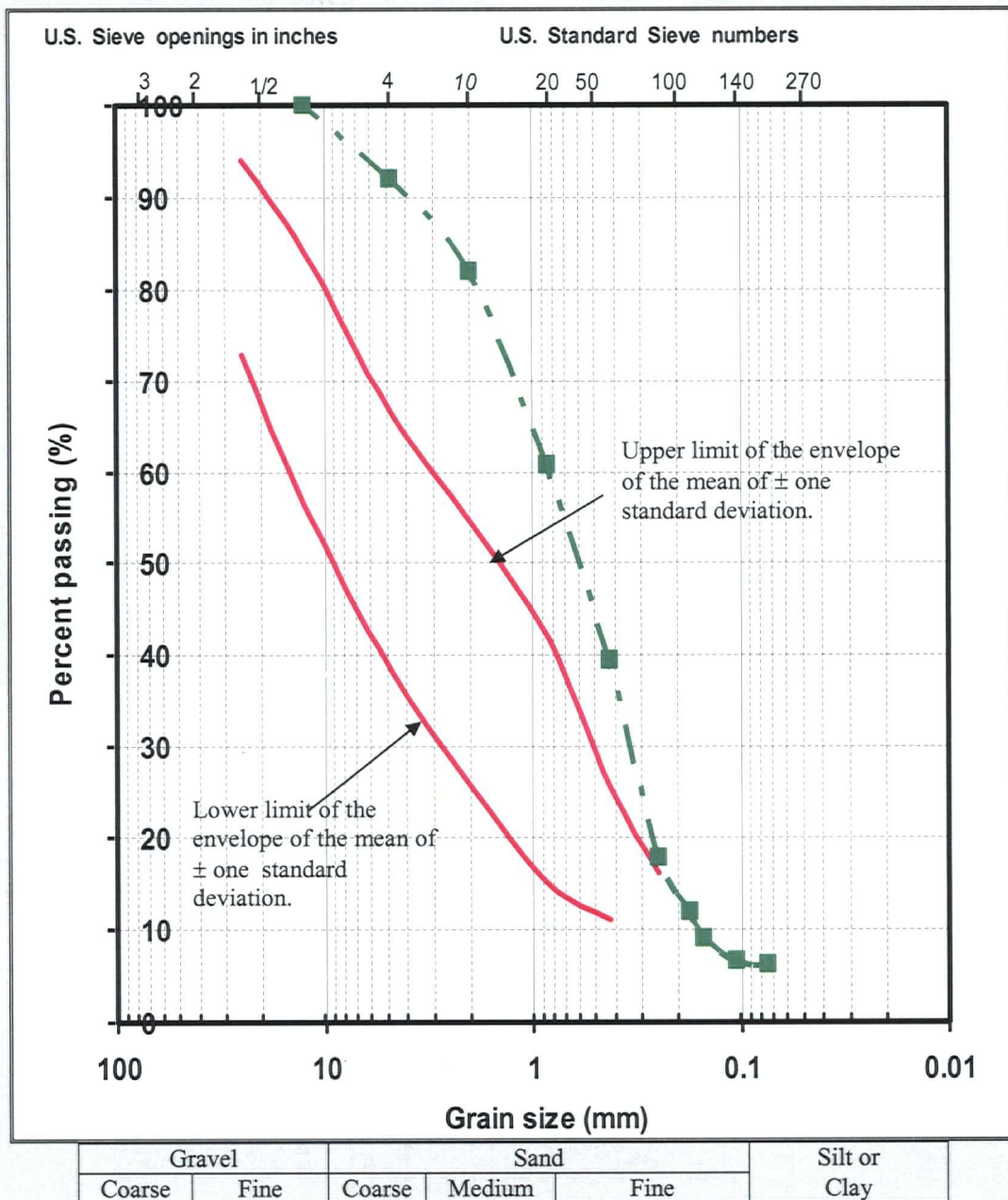


Figure 4.2. Particle size (without gravel and boulder-sized) distribution curves for the samples of waste-rock from Deilmann north waste-rock pile (DNWR) for ground surface sand (curve with broken line and symbols) and core basement-rock (curves with solid lines). Symbols represent the measured data from this thesis. The full lines show the one standard deviation range of grain-size data obtained by Birkhman et al. (2002).

The C_u of the mean grain-distribution (not presented) for the core samples was about 3.3 and was typical of the value obtained for this study. Birkham (2002) noted, however, that the grain-size distributions of waste-rock samples were not representative of the entire DSWR pile as gravel and boulder-sized particles were excluded from the analysis

The grain-size distribution for the near-surface sample collected from DNWR of (Figure 4.2, curve with symbols) indicated that 83% of the material was sand size with 17% silt- and clay-size particles. The sand sizes ranged from coarse (16%), medium (42%), and fine (25%). The C_u of the sample was found to be about 6.3 (e.g., $D_{10} = 0.018$ cm). The DNWR sample is considered to be poorly sorted than that from the DSWR. The e of the sample was found to be 0.591 and was within the range of the granular sand materials reported in Table 4.1. The mean \pm one standard deviation of 26 grain-size distributions (curves with solid lines) obtained from core samples from DNWR (Birkham, 2002) are also presented in Figure 4.2. The grain-size distribution curve measured in this study was outside the mean \pm one standard deviation envelope for the basement-rock core samples. The C_u of the mean grain-size distributions (not shown) for the basement-rock was determined to be about 30. Birkham (2002) found that 40% of the DNWR basement-rock bulk sample was coble-sized. This was consistent with the visual observation that the basement-rock in the DNWR generally had larger particles compared with the sand-sandstone material. As was the case for the grain-size distributions from the DSWR, the grain-size distributions of samples from the DNWR could not be considered representative of the entire DNWR pile because boulder-sized particles were excluded from the analysis (Birkham, 2002).

4.1.2 Water retention curve

For a given porous media, the relationship between the soil water content (θ) and the soil suction (ψ) or matric potential is known as either the water retention curve (WRC) (Marshall et al., 1996; Aubertin et al., 1998; Delleur, 1999), the soil water characteristic curve (SWCC) (Fredlund and Xing, 1994; Barbour, 1998), the soil suction curve (Yong, 2001), or the soil moisture-retention curve (Kovacs, 1993; Hillel, 1980; Looney and Falta, 2000). In this thesis, the WRC will be used to represent the relationship between θ and ψ . Figures 4.3 and 4.4 show the WRCs for the DNWR and DSWR samples respectively measured in the laboratory using Tempe cells. The solid symbols are measured data (from 0.2 to 100 kPa suction) and the solid lines (0 to 1 million kPa suction) represent the best fit curves generated with SoilCover model using an equation developed by Fredlund and Xing (1994). The water content (θ) can also be expressed in terms of saturation (S) ($S = \theta/n$), where n is the soil porosity (Figures 4.5 and 4.6). It should be noted that θ at zero suction is equivalent n . The n for the samples for DNWR and DSWR were found to be 0.36 and 0.38, respectively.

The WRC describes the soil's ability to store and release water (Fredlund and Rahardjo, 1993; Barbour, 1998). It also represents the drying curve for the soil material and provides useful information on the water retention and water transmission behavior of a waste-rock pile and helps to describe the effects of waste-rock texture and void ratio (e) on the distribution of the water phase in the waste-rock pile, and thus, the gas diffusion in this pile (Barbour, 1998). The WRC can be seen as a representation of the pore-size distribution function with assumption based on the capillary model (Mualem, 1986). Aubertin et al. (2003) also developed a model to predict the SWCC from basic

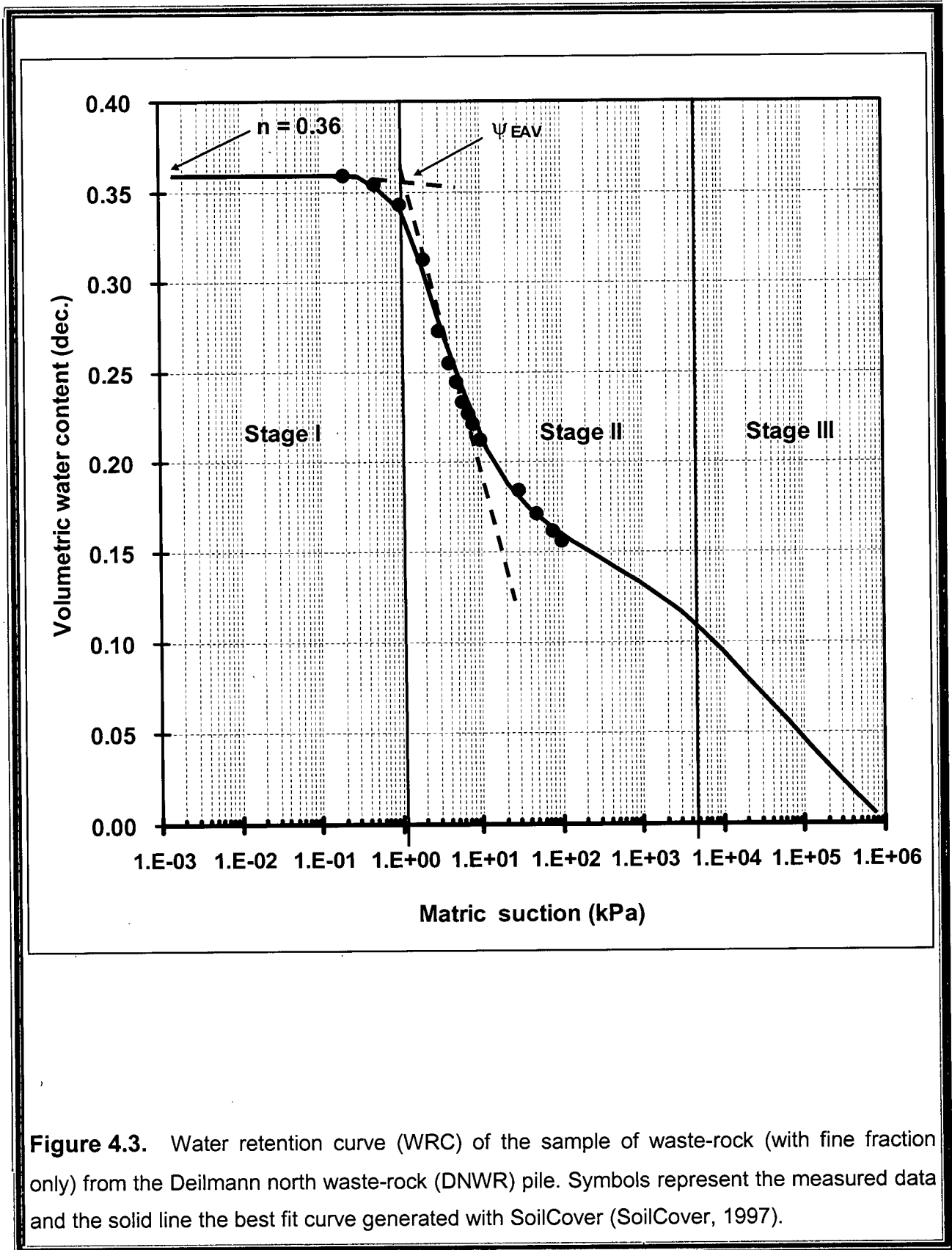


Figure 4.3. Water retention curve (WRC) of the sample of waste-rock (with fine fraction only) from the Deilmann north waste-rock (DNWR) pile. Symbols represent the measured data and the solid line the best fit curve generated with SoilCover (SoilCover, 1997).

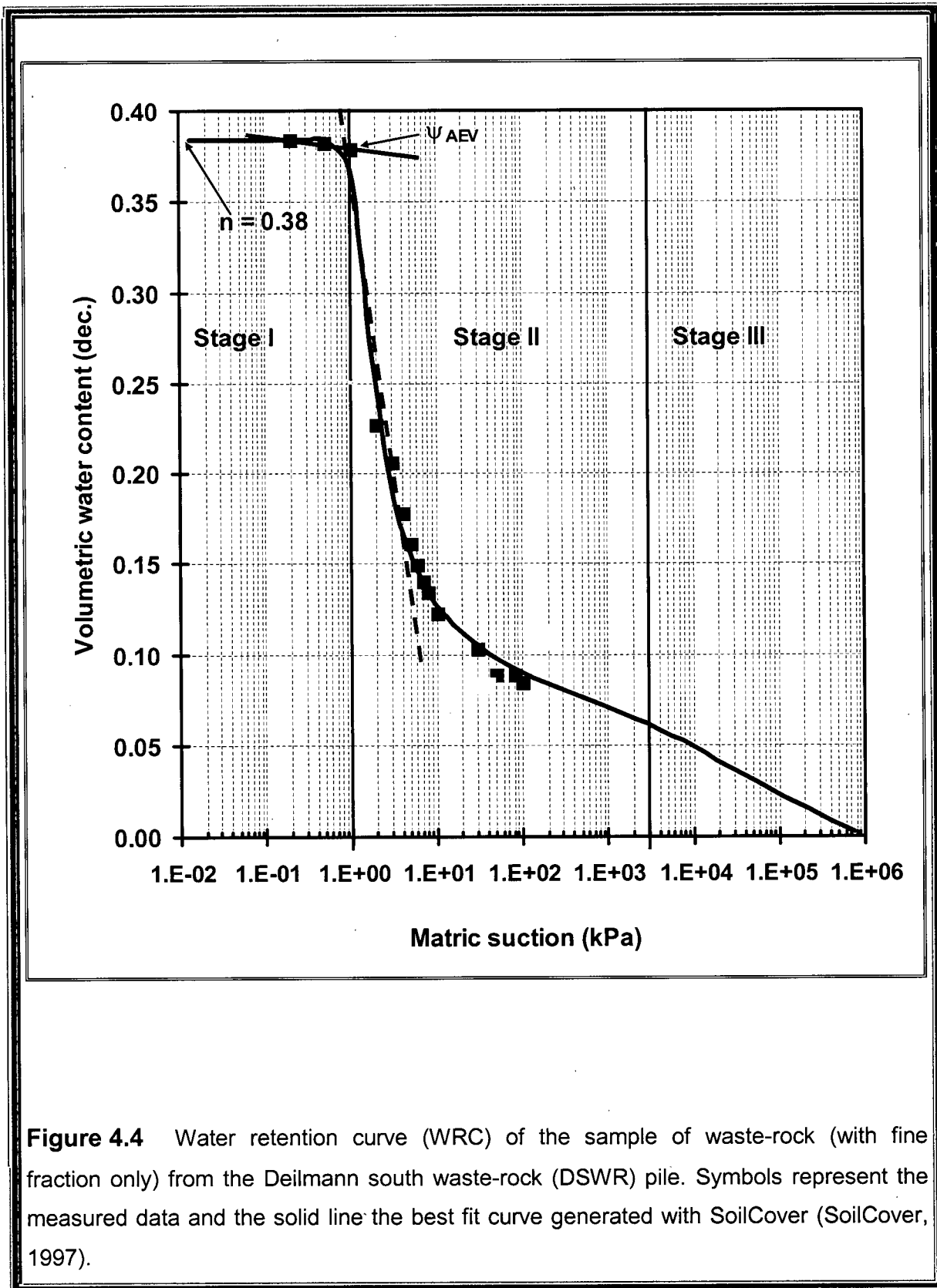


Figure 4.4 Water retention curve (WRC) of the sample of waste-rock (with fine fraction only) from the Deilmann south waste-rock (DSWR) pile. Symbols represent the measured data and the solid line the best fit curve generated with SoilCover (SoilCover, 1997).

geotechnical properties.

In general, the WRC is described as having three parts: (i), the upper horizontal line of the curve represents approximately 100% saturation of the sample (ii) the fast decreasing slope, and (iii) the slow decreasing slope represents the residual water content. The WRCs show that the soil samples remain saturated when suctions are lower than the air-entry values (AEVs). The AEV corresponds to the suction at which the soil sample will begin to desaturate and, depending on the soil type, may or not be well defined. SoilCover model calculations yielded values of AEVs of 2.4 and 1.3 kPa for the DNWR and DSWR, respectively. The capillarity of the soil allows it to remain saturated at suction less than the AEV (Aubertin et al., 2003). The slope of the curve defines the volume of water taken on or released by a change in pore-water pressure. The WRCs show that the AEV of the sample from the DSWR is better defined (with steep slope) than that from the DNWR (with smooth slope) (Figures 4.3 and 4.4). The AEV can be defined graphically as the intersection of the best-fit lines of the two linear segments of the WRC (as shown in Figures 4.3 and 4.4) (Fredlund and Xing, 1994 and Barbour, 1998). The tangent (graphical) method yielded values of approximately 1.5 and 1 kPa for the DNWR and DSWR piles respectively. SoilCover model simulations yielded values of AEVs of 2.4 and 1.3 kPa for the DNWR and DSWR, respectively. The slight difference in the AEVs values is due to slight variations in the waste rock textures and porosity. Fine grained soils tend to have flat (or smooth) functions with high AEVs, whereas coarse grained soils tend to have steep functions with low AEVs. For example, the DSWR sample contained less fine-grained (e.g., 10% silt- and clay-size particles), than the DNWR (e.g., 17% silt- and clay-size particles) and the rest of the material was sand-size.

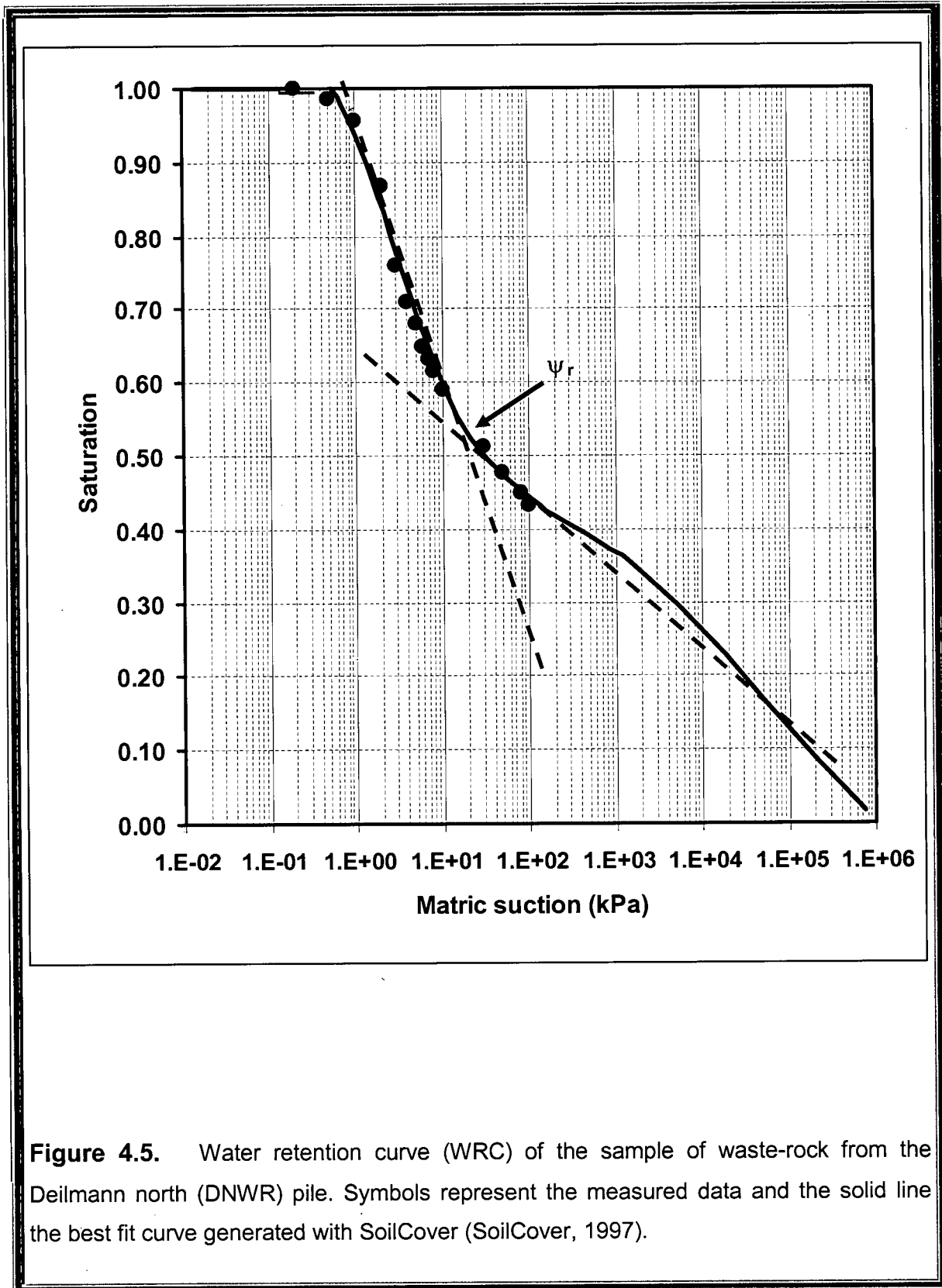


Figure 4.5. Water retention curve (WRC) of the sample of waste-rock from the Deilmann north (DNWR) pile. Symbols represent the measured data and the solid line the best fit curve generated with SoilCover (SoilCover, 1997).

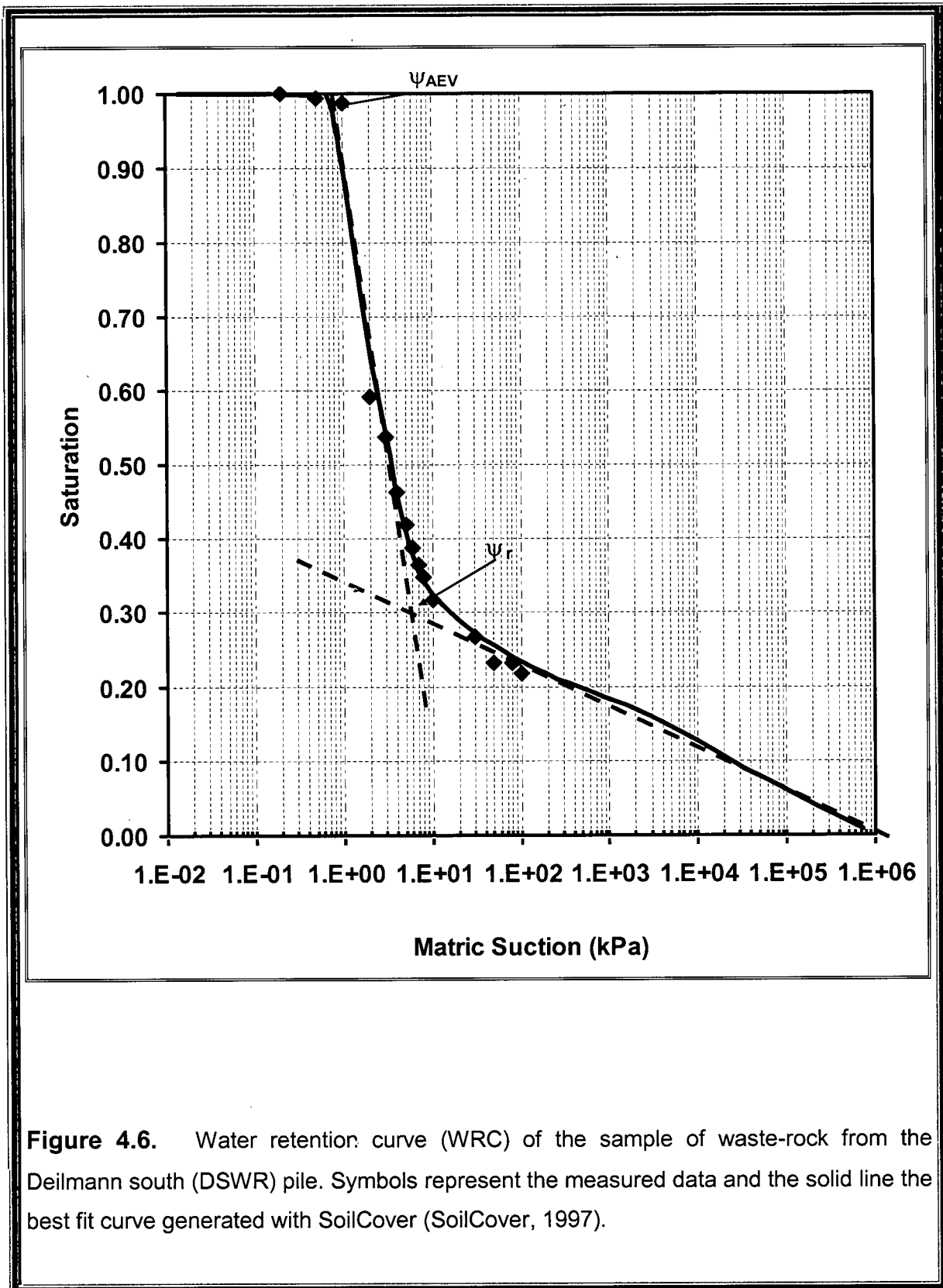


Figure 4.6. Water retention curve (WRC) of the sample of waste-rock from the Deilmann south (DSWR) pile. Symbols represent the measured data and the solid line the best fit curve generated with SoilCover (SoilCover, 1997).

Yanful et al. (2003a) measured the SWCC for fine sand and found an AEV value 3 kPa. This value is close to the value of the DSWR sand sample measured in this thesis (i.e., 2.4 kPa). Wilson et al. (1994) and Newman (1999) also measured the WRCs for fine-grained materials (Beaver Creek sand) and both found an AEV of approximately 3 kPa.

Since the soils are close to saturation up to 2.4 and 1.3 kPa suctions for the DNWR and DSWR, respectively, almost all the pore spaces are filled with water and thus the CO₂ flux is expected to be significantly reduced. It should be noted that the free diffusion coefficient of CO₂ is about four orders of magnitude larger in air than in water, diffusive transport in the water-filled pores is much slower than that in the air-filled voids.

The results show that above the AEVs, the water contents (or saturation) decrease rapidly with matric suction. The WRCs show the two samples drain rapidly between values of matric suctions of 2.4 and 10 kPa and 1 and 10 kPa for the DNWR and DSWR, respectively. At 10 kPa suction, the samples retained about 20% and 10% water for the DNWR and DSWR samples, respectively. This behavior is characteristic of uniform sand and sand/silt materials and has been also described by others (Wilson et al., 1994; Barbour, 1998).

As the matric suction increased the samples reach slow residual values. The residual water content is controlled primarily by the fine fraction and the surface area of the sample. The residual suctions (Ψ_r) (suction at residual water content) were determined using the tangent method applied to the WRCs as described by Fredlund and Xing (1994) and were found to be 11 and 6 kPa for the DNWR and DSWR, respectively (Figures 4.5 and 4.6).

Aubertin et al. (2003) provides also the following expression to evaluate Ψ_r

$$\Psi_r = \frac{0.42}{(eD_H)^{1.26}} \quad [4.1]$$

and also Ψ_{AEV} (suction at AEV):

$$\Psi_{AEV} = \frac{b}{(eD_H)^x} \quad [4.2]$$

where e is the void ratio, and D_H is an equivalent particle diameter for a heterogeneous mixture and b and x are fitting parameters. For practical geotechnical applications, the value of D_H can also be approximated using the following function (Aubertin et al., 1998; Mbonimpa et al., 2000, and 2002):

$$D_H = [1 + 1.17 \log(C_u)] D_{10} \quad [4.3]$$

where D_{10} is the diameter corresponding to 10% passing on the cumulative grain-size distribution curve, and C_u is the coefficient of uniformity ($C_u = D_{60}/D_{10}$). For the equivalent capillary rise in granular soils b can be approximated using the following function (Aubertin et al., 1998):

$$b = \frac{0.75}{1.17 \log(C_u) + 1} \quad [4.4]$$

Using the values of C_u and D_{10} for the DNWR and DSWR samples (see Section 4.1.1) of this thesis), the D_H for the DSWR and DNWR were found to be 0.02478 cm and 0.03488 cm, and b for the DSWR and DNWR were found to be 0.143 and 0.388, respectively. Equation 4.2 yielded values of Ψ_r of 22.07 cm (9.21 kPa) and 55.90 cm (5.59 kPa) for the DNWR and DSWR, respectively. These values are close to those determined graphically using the tangent method (11 and 6 kPa for the DNWR and DSWR, respectively). Similarly, Equation 4.2 yielded values of Ψ_{AEV} of 18.8 cm (1.88

kPa) and 10.36 cm (1.04 kPa) for the DNWR and DSWR, respectively. These values are very close to those determined graphically using the tangent method (1.5 and 1 kPa) for the DNWR and DSWR, respectively. It should be noted that Equation 4.1 is frequently quite practical for fine-grained soils because D_{10} and C_u are often unknown.

4.1.3 Hydraulic conductivity

The hydraulic conductivity is a measure of the ability of the soil to transmit water and depends upon both the properties of the soil and the fluid (Klute and Dirksen, 1986). Total porosity, pore-size distribution, and pore continuity are the important soil characteristics affecting hydraulic conductivity and SWCC. The hydraulic conductivity at or above the saturation point (e.g., AEV) is referred to as saturated hydraulic conductivity (K_{sat}), and for water contents below saturation, it is called the unsaturated hydraulic conductivity 'K' (Figures 4.7 and 4.8). Laboratory tests described in the previous section were conducted to determine the saturated hydraulic conductivity ' k_{sat} ' using the falling-head permeability tests. The tests yielded values of ' K_{sat} ' of $1.20 \times 10^{-6} \text{ m s}^{-1}$ and $1.49 \times 10^{-5} \text{ m s}^{-1}$ and for the DNWR and DSWR near-ground surface (0 - 0.15 m) samples, respectively. These values are characteristic of sand and sand/silt materials. The nature and origin of various data of K are given in Table 4.1. Wilson et al. (1994) measured a value of $3.9 \times 10^{-6} \text{ m s}^{-1}$ for Beaver Creek sand using the falling-head permeability tests. Newman (1999) also measured value of saturated hydraulic conductivity of $6.2 \times 10^{-5} \text{ m s}^{-1}$ for Beaver Creek sand. Yanful et al. (2003) obtained values of K_{sat} of $1.9 \times 10^{-6} \text{ m s}^{-1}$ and $7.3 \times 10^{-6} \text{ m s}^{-1}$ for fine sand and coarse sand, respectively. Hatanaka et al. (1997) measured values of $1.5 \times 10^{-5} - 4.3 \times 10^{-4} \text{ m s}^{-1}$ for undisturbed sands (12 results). Mbonimpa (1998) determined values of $8.2 \times 10^{-5} - 1.1$

$\times 10^{-3} \text{ m s}^{-1}$ for uniform sand (30 results). These values are very similar to those obtained in this work for DNWR and DSWR. The DNWR contained more fine sand (52%) than the DSWR (25%) and had a comparatively lower K_{sat} . The hydraulic conductivity 'K' of an unsaturated soil is a function of matric suction ' ψ '. Laboratory testing was not conducted to measure 'K' at different values of matric suction. Various methods of calculating the hydraulic conductivity 'K' were described above. The relation between the 'K' and ' ψ ' derived from the Brooks and Corey (1964) model for the samples is shown in Figures 4.7 and 4.8. The 'K' of the samples from DNWR and DSWR decreased rapidly with increasing ψ past the AEVs at 1.3 and 2.4 kPa suctions, respectively. As suction was increased by two orders of magnitude, the ' K_s ' are predicted to decrease by more than 10 orders of magnitude. At $\psi = 100 \text{ kPa}$, both K values decreased to $<10^{-15} \text{ m s}^{-1}$.

In summary, the WRCs and associated ' K_{sat} ' of the samples from DSWR and DNWR showed that the near-ground surface (0 - 0.15 m) sample on DNWR retained more water at saturation associated with increasing matric suction than that on DSWR. This behavior is due to slight variations in the waste-rock textures that control soil water.

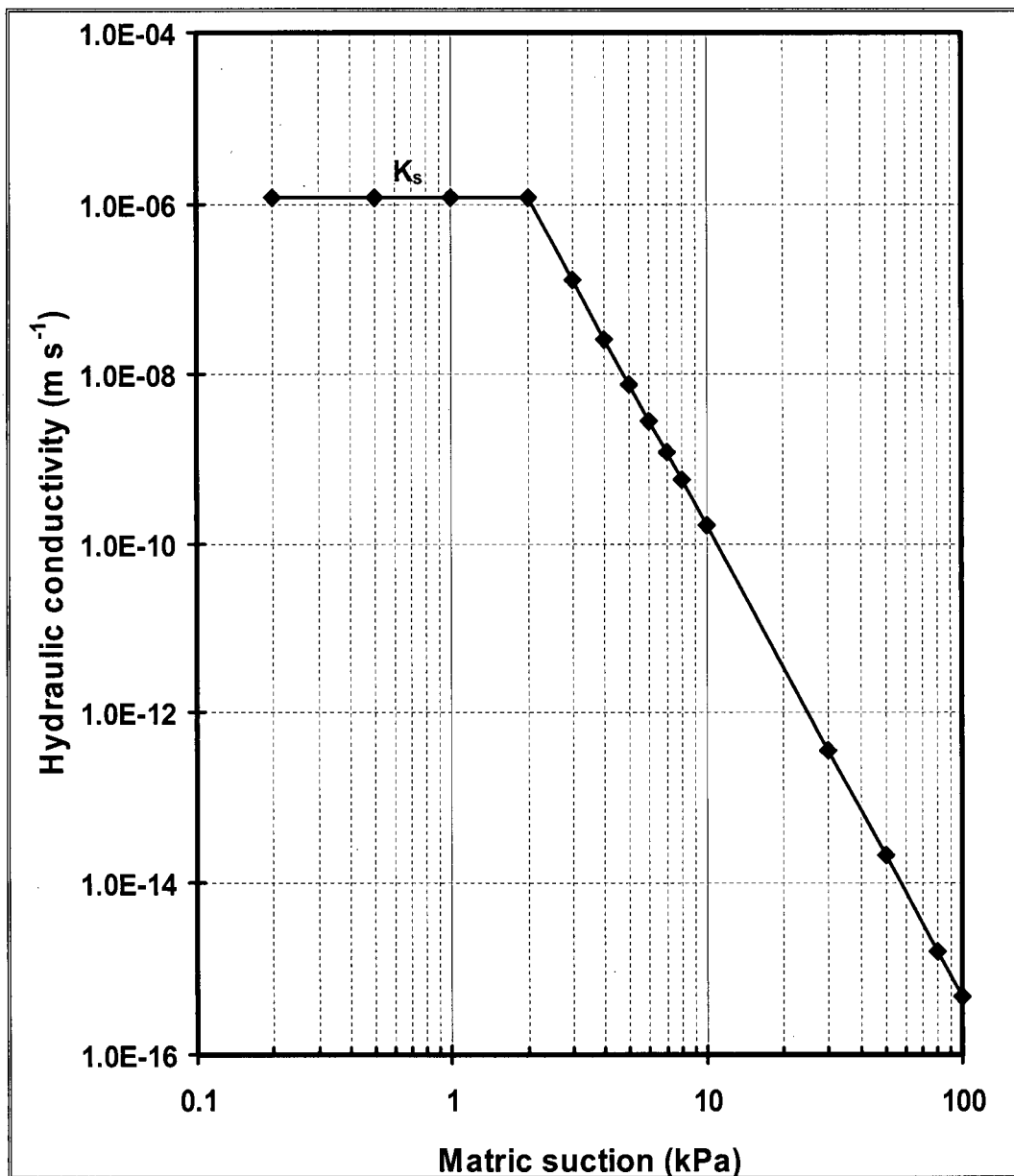


Figure 4.7. Characteristic of the sample of the waste-rock from the Deilmann north waste-rock pile (DNWR): hydraulic conductivity curve (K). The value of saturated hydraulic conductivity (K_{sat}) was measured in the laboratory but the unsaturated hydraulic conductivity (K) was derived from the Brooks and Corey mode (Brooks and Corey, 1964).

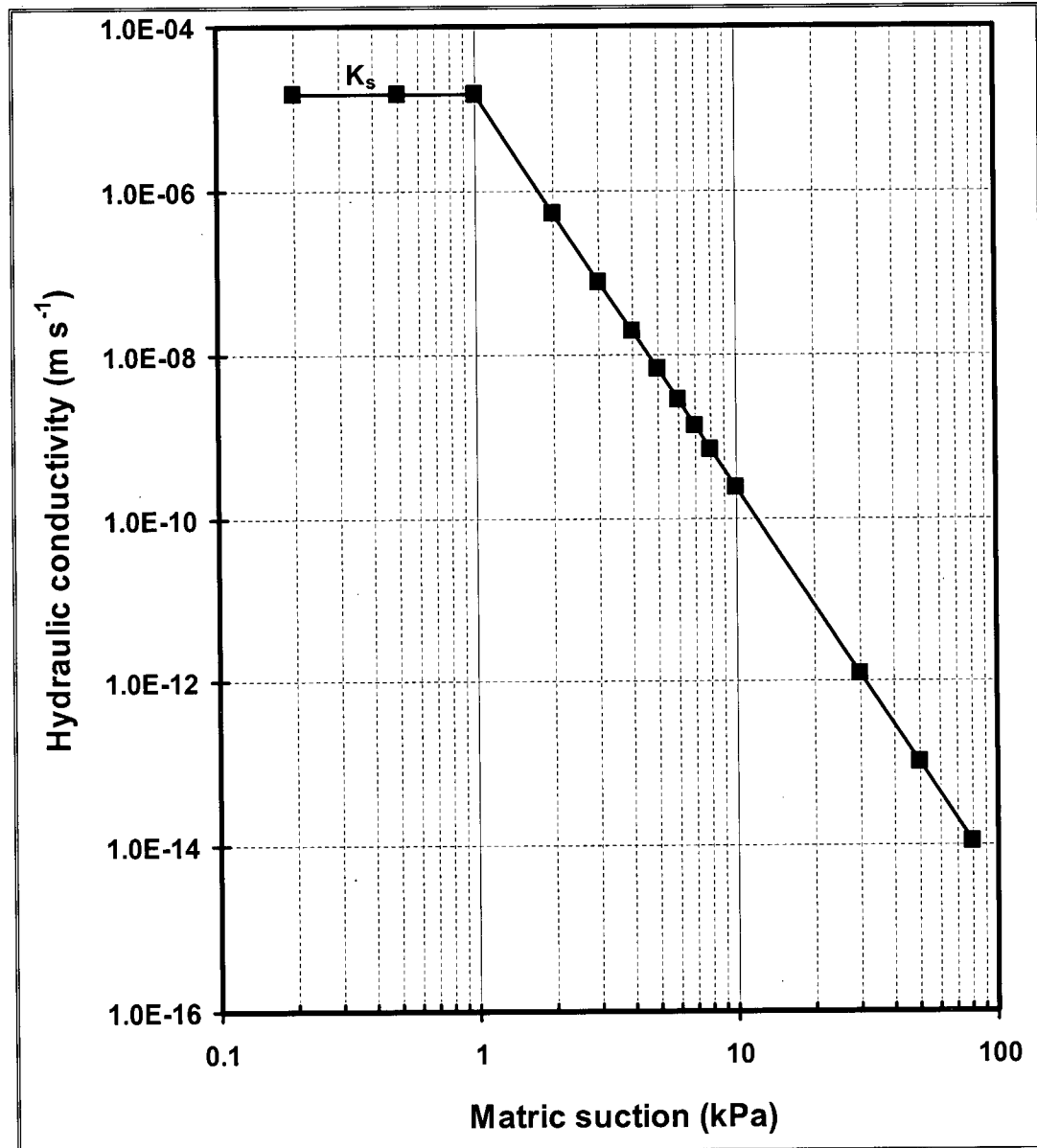


Figure 4.8. Characteristic of the sample of the waste-rock from the Deilmann south waste-rock pile (DSWR): hydraulic conductivity curve (K). The value of saturated hydraulic conductivity (K_{sat}) was measured in the laboratory but the unsaturated hydraulic conductivity (K) was derived from the Brooks and Corey mode (Brooks and Corey, 1964).

Table 4.2. Nature and origin of data for the K value of various granular materials

Source of results	Type of material (number of results)	Range of K values measurd ($m s^{-1}$)
Wilson et al. (1993)	Beaver Creek sand	3.9×10^{-6}
Hatanaka et al. (1997)	Undisturbed sands (12 results)	$1.5 \times 10^{-5} - 4.3 \times 10^{-4}$
Mbonimpa (1998)	Uniform sand (30 results)	$8.2 \times 10^{-5} - 1.1 \times 10^{-3}$
Newman (1999)	Beaver Creek sand	6.2×10^{-5}
Yanful et al. (2003)	. Fine sand.....	1.9×10^{-6}
	. Coarse sand.....	7.3×10^{-6}

4.2 Field Tests Program

This section presents the results of the field tests described in the previous sections. The tests were conducted at the Deilmann north waste-rock (DNWR) and Deilmann south waste-rock (DSWR) piles at the Key Lake uranium mine, northern Saskatchewan, over a period of two years (summers of 2000 and 2002).

The CO₂ flux results were obtained using the DCC and compared to those obtained using two other methods: dynamic closed chamber (DCC), static closed chamber (SCC), and eddy covariance (EC) methods. The data presented include the results of:

1. Diurnal variation in CO₂ flux measured with the DCC at the Deilmann south waste-rock (DSWR) pile.
2. Quantification of spatial and temporal variations in CO₂ flux using the DCC at the Deilmann north waste-rock (DNWR) and DSWR piles.
3. Measurements of CO₂ flux using SCC at the DSWR.
4. Measurements of CO₂ flux using EC at the DSWR.
5. Measurements of near- and surface-water contents and associated CO₂ fluxes after heavy rainfall events at the DNWR and DSWR piles.

4.2.1 Diurnal variation in CO₂ flux

Temporal variability was addressed on a diurnal and long-term basis. The short-term (hourly) variations in the CO₂ flux was measured using the DCC at a single sampling station (DSF1) (Figure 3.8) over a 9-h period (09:00 to 17:00) on August 6, 2000 at the DSWR. The corresponding average hourly air temperature was recorded from the weather station installed on DSWR. The measurements were repeated two to

three times during the test period to reflect the diurnal variation in CO₂ flux due to perturbations in daily weather conditions such as cloudy and rainy days. Representative results of both the CO₂ flux measurements and air temperature are presented in Figure 4.9.

The CO₂ flux ranged from 219 to 250 mg CO₂ m⁻² h⁻¹ (Figure 4.9), with a mean value of 235 (± 14) mg CO₂ m⁻² h⁻¹. Coefficients of variation (CV) for the individual sampling periods ranged from 4.6 to 6.5% and were comparable to those reported under more controlled conditions in laboratory mesocosms (Kabwe et al., 2002). Short-term (hourly) variations in the flux were not significant ($P \leq 0.05$) (e.g., P is test statistic on which a decision rule is based for a test of hypotheses). At DSF1, both the magnitude of the CO₂ flux and the daily variation in the flux were smaller than the values generally reported for agricultural or forest soils (Brumme & Beese, 1992; Lofffield et al., 1992; Rochette et al., 1992; Ambus & Robertson, 1998; Frank et al., 2002). There was only a weak diurnal pattern to the flux and no correlation between the CO₂ flux and air temperature ($r = 0.548$) (e.g., r is a coefficient of correlation). Parkin and Kaspar (2003) reported that diurnal changes in the soil-to-atmosphere CO₂ flux were strongly correlated with air temperature (more so than with soil temperature) when CO₂ production at the surface was a major component of the total measured CO₂ flux (Wohlfahrt et al., 2005; Shi et al., 2006). This, together with the results of Birkham et al. (2003) and Lee et al. (2003a, 2003b), suggests that the CO₂ flux from the surface waste-rock pile may be a result of the upward migration of gas produced during organic matter oxidation at depth and its subsequent transport to, and diffusion across the waste rock/air interface (see Figure 3.7).

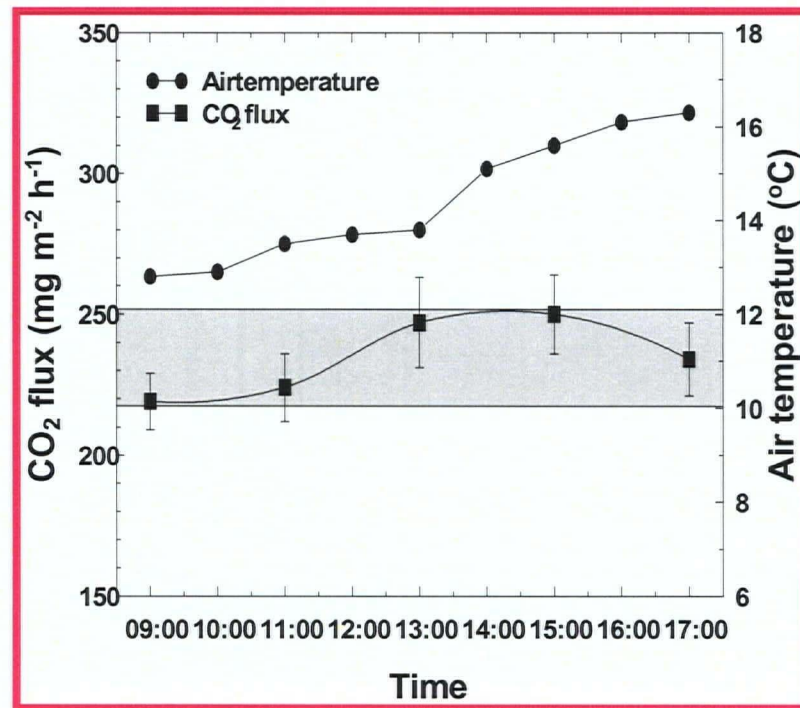


Figure 4.9. Short-term (hourly) variations in the CO₂ flux measured at DSF1 on August 6, 2000. Fluxes were determined using the dynamic closed chamber (DCC) method and averaging a series of four to eight measurement cycles, with each cycle lasting from 2- to 8-min (depending on the magnitude of the flux). The shaded box represents the 95% confidence interval (± 17 mg CO₂ m⁻² h⁻¹) around the calculated daily mean (235 mg CO₂ m⁻² h⁻¹).

4.2.2 Spatial and temporal variation in CO₂ flux measured using the DCC at the Deilmann south waste rock (DSWR) pile

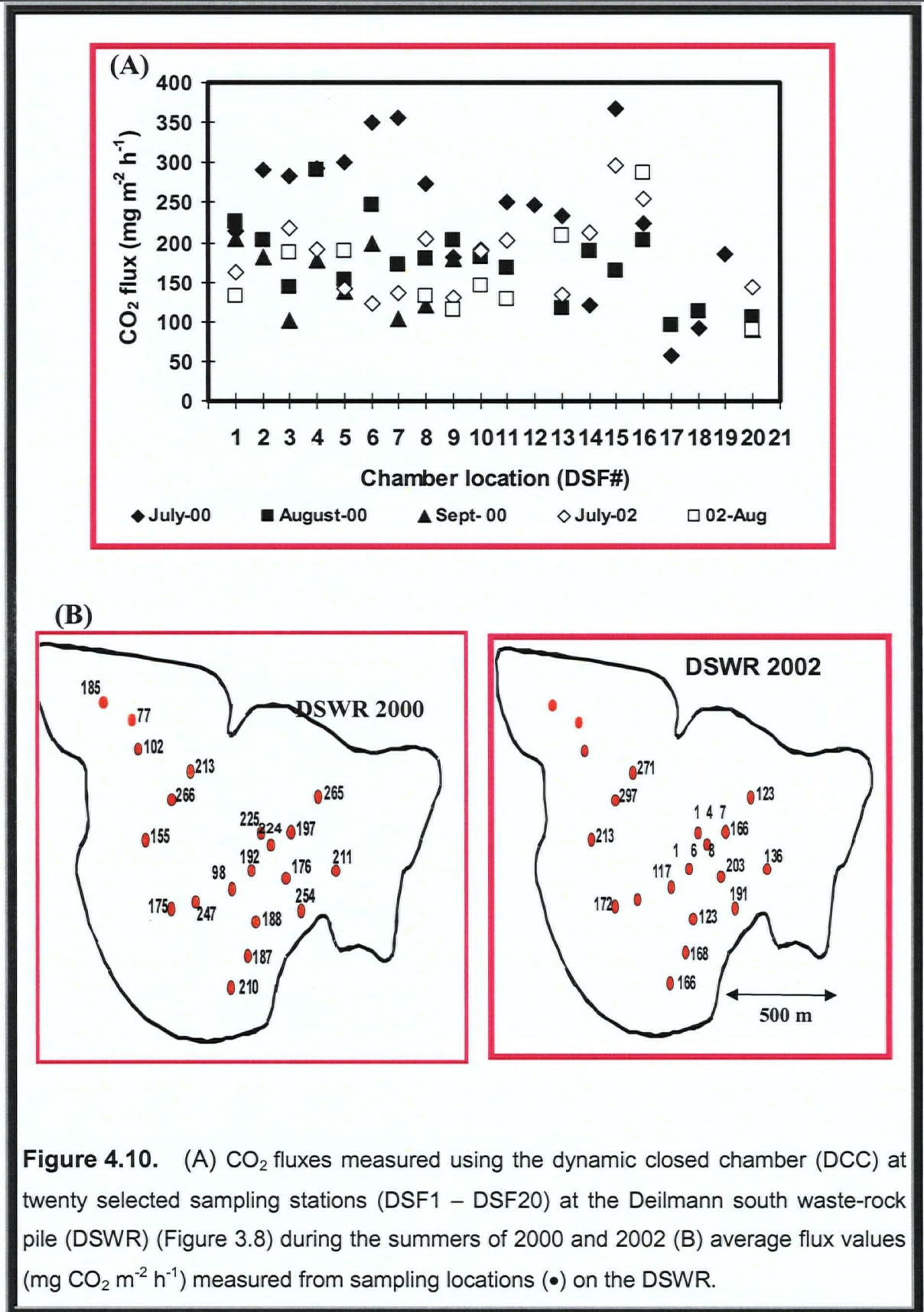
The DCC was used to quantify spatial and temporal variations in the CO₂ flux at 20 sampling stations (DSF1 - DSF20) (Figure 3.8) at the DSWR pile. The measurements were over three periods during summer 2000 (July 1-11; August 1-11, and September 8-16) and twice during summer 2002 (July 13-22 and August 21-26). Results of the CO₂ flux measurements are presented in Figures 4.10A and Figure 4.10B.

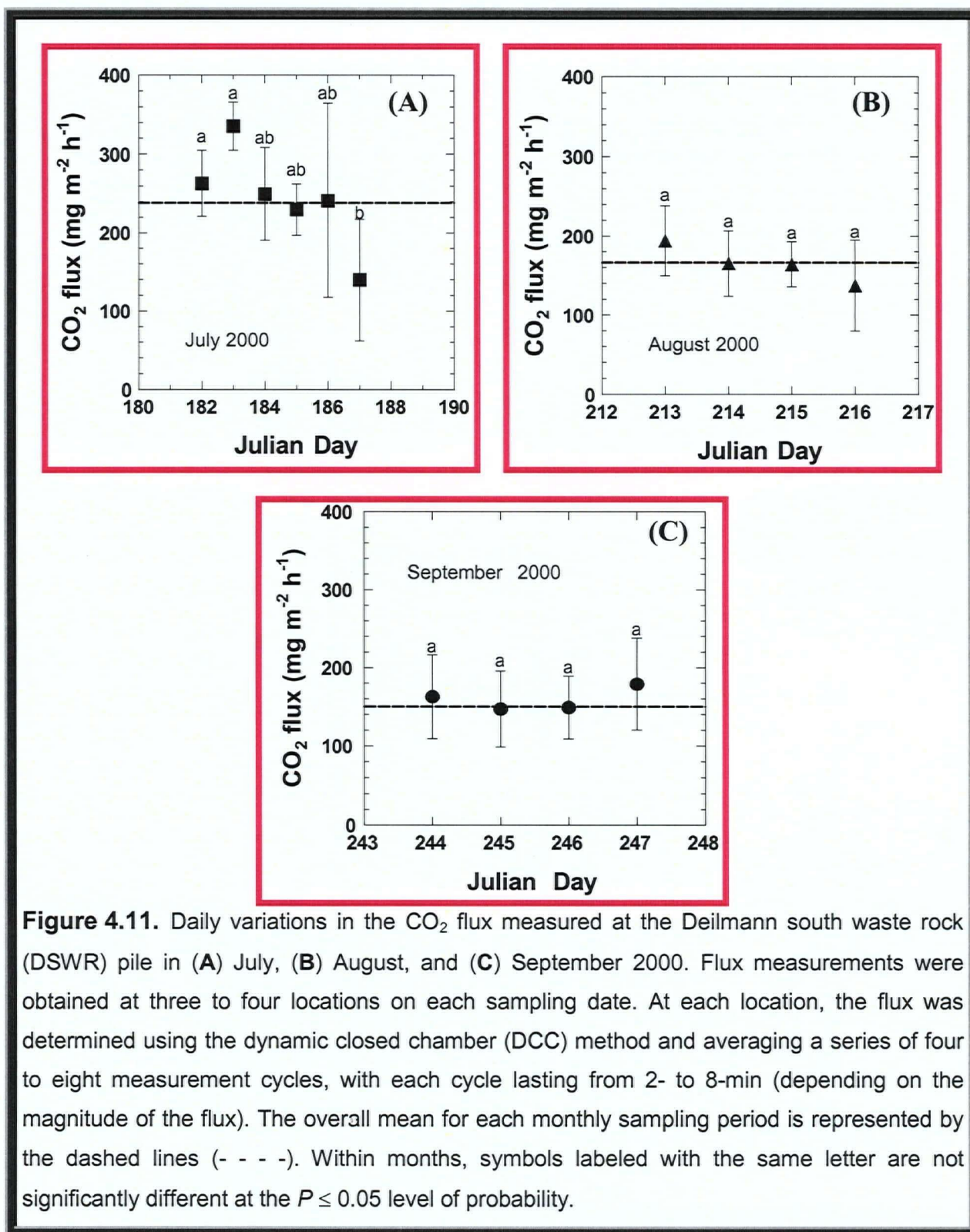
Table 4.1 and Figures 4.11A, 4.11B, and 4.11C present results of statistical analysis of the CO₂ fluxes measured in July, August, and September 2000. During each 4 to 6 day sampling period, the CO₂ flux was measured at a minimum of 12 sampling stations, with three to four stations sampled each day. Differences between sampling stations were generally small (average CV = 24%), indicating that the degree of spatial variability was relatively low. Moreover, the analysis of variance (ANOVA) indicated that within each sampling period differences between the daily CO₂ fluxes were not significant ($F_{Jul} = 2.87$; $F_{Aug} = 1.17$; $F_{Sep} = 0.60$).

The F distribution is the ratio of the variances of two independent samples from normal populations and is given by:

$$F = \frac{\chi_1^2 / \nu_1}{\chi_2^2 / \nu_2}, \text{ and } \chi^2 = \frac{(n-1)S^2}{\sigma^2} \quad [4.5]$$

where S^2 is the variance associated with samples of size n from a normal distribution with variance σ^2 and χ^2 is the chi-square distribution with $\nu = n - 1$ degrees of freedom.





Working under the assumption that both samples are from the same normal population (as was in this case) then Equation becomes:

$$F = \frac{S_1^2}{S_2^2} \quad [4.6]$$

The F ratio was then compared to the expected value of $F(v_1 = n_1 - 1, v_2 = n_2 - 1)$ using the nearest table entry.

With the exception of the July 2000 data set, differences between sampling periods were not significant (average—yielding a long-term average flux of $194 (\pm 75)$ mg CO₂ m⁻² h⁻¹). Again, these results suggest a the laterally extensive source of CO₂ at the base of the pile (see Figure 3.7) and indicate that the production and upward migration of CO₂ through the waste-rock pile is relatively uniform both spatially and temporally.

As noted above, the July 2000 data set yielded a mean CO₂ flux ($238 \text{ mg CO}_2 \text{ m}^{-2} \text{ h}^{-1}$) that was significantly greater ($P \leq 0.05$) than the mean flux calculated for any of the other sampling periods. The flux data collected in July 2000 also exhibited a much wider range in values as indicated by the size of the 'box' and length of the 'whiskers' (Figure 4.12) suggesting a greater degree of spatial and temporal variability during this measurement period.

Flux measurements from across the site also were obtained during the summer of 2002. Differences among sampling stations obtained during the summer 2002 at the DSWR were also relatively small (overall CV = 31 %) and were not significant—yielding an overall average flux $174 (\pm 31) \text{ mg CO}_2 \text{ m}^{-2} \text{ h}^{-1}$. Both calculated mean CO₂ fluxes for the summer 2002 periods were not significantly different from those obtained during the summer 2000 periods at the DSWR, with the exception of the July 2000 data set.

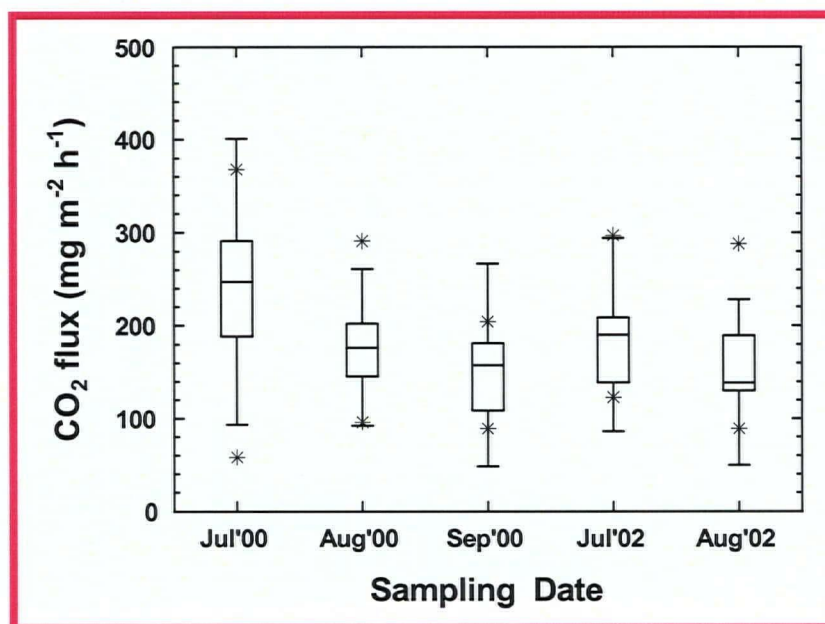


Figure 4.12. Box & Whisker plot characterizing the spatial and long-term temporal variability in the CO₂ flux measured using the dynamic closed chamber (DCC) method at the Deilmann south waste-rock (DSWR) pile in 2000 and 2002. The estimated, time-averaged flux = 170 (± 51) mg CO₂ m⁻² h⁻¹. The minimum and maximum flux values are marked by asterisks (*). Note: values occurring beyond the “whiskers” were identified as outliers and were not included in the analysis of variance.

Table 4.3. Summary of results of CO₂ flux measurements using the dynamic closed chamber system (DCC) for the test period of 2000-2002 at Deilmann south waste-rock pile (DSWR).

	Summer 2000			Summer 2002		
	Mean mg m ⁻² h ⁻¹	Std ^a mg m ⁻² h ⁻¹	CV ^b %	Mean mg m ⁻² h ⁻¹	Std mg m ⁻² h ⁻¹	CV
July	238(n=19)	86	36	185(n=15)	51	28
August	175(n=18)	51	29	162(n=10)	58	36
Sept.	150(n=10)	44	29			
Overall	194	75	39	174	53	31
Overall average (summer 2000 and summer 2002): (188 ± 68 mg m ⁻² h ⁻¹)						

^aStd: standard deviation

^bCV: coefficient of variation

Consequently, the data from each sampling period were pooled and replotted as Box-and Whisker plots (Figure 4.12) to better illustrate the relative consistency of the spatial and short-term temporal variability associated with CO₂ flux measurements at the DSWR.

4.2.3 Spatial and temporal variations in CO₂ flux measured using the DCC at the Deilmann north waste-rock (DNWR) pile

The spatial and temporal variations in the CO₂ flux were measured at the Deilmann north waste-rock (DNWR) pile using the DCC at 9 sampling stations (DNF1 – DNF9) (Figure 3.8). The measurements were assessed three times during summer 2000 (July 1-11; August 1-11, and September 8-16) and twice during summer 2002

Table 4.4. Summary of results of CO₂ flux measurements using the dynamic closed chamber system (DCC) for the test period of 2000-2002 at Deilmann north waste-rock pile (DNWR).

	Summer 2000			Summer 2002		
	Mean	^a Std	^b CV	Mean	Std	CV
	mg m ⁻² h ⁻¹	mg m ⁻² h ⁻¹	%	mg m ⁻² h ⁻¹	mg m ⁻² h ⁻¹	%
July	159(n=9)	41	25	302(n=9)	83	27
August	203(n=9)	50	18	249(n=9)	91	37
Sept.	169(n=9)	52	31			
Overall	177	50	28	276	89	32
Overall average (summer 2000 and summer 2002): (217 ± 83 mg m ⁻² h ⁻¹)						

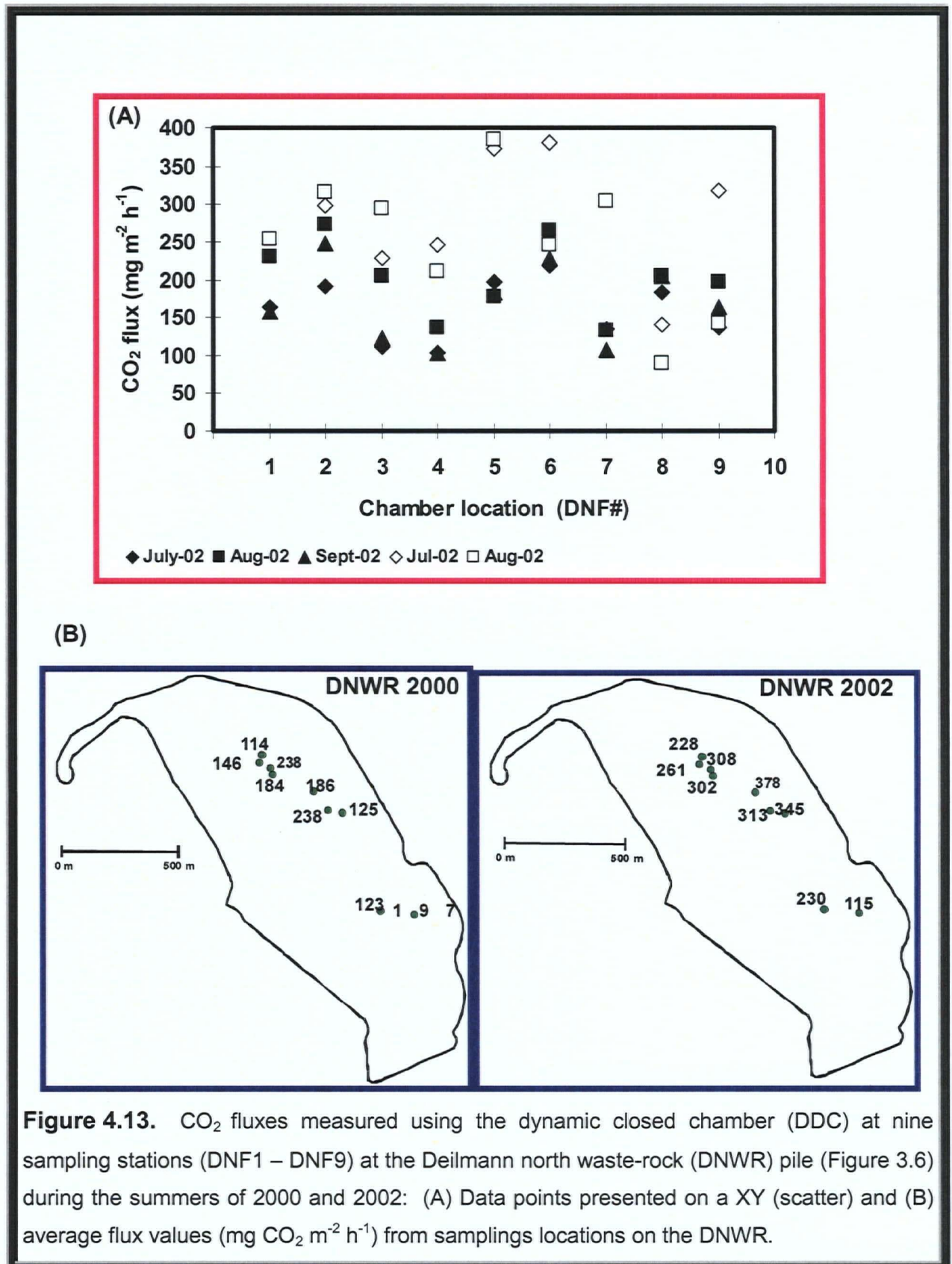
^aStd: standard deviation

^bCV: coefficient of variation

Data of the CO₂ flux measurements are presented in Figures 4.13A and 4.13B.

Table 4.4 and Figure 4.14 summarize the results of statistical analysis of the CO₂ fluxes measured during the summer of 2000 (July to September) and during the summer of 2002 (July to August 2002) at the DNWR. Differences among sampling stations obtained during the summer of 2000 were small (overall CV = 28%) and were not significant, yielding an overall average flux of 177 (± 50) mg m⁻² h⁻¹. Similarly, differences among sampling stations obtained during the summer of 2002 were also relatively small (overall CV = 32%) and were not significant, yielding an overall average flux of 276 (±89) mg m⁻² h⁻¹. However, both calculated mean CO₂ fluxes for the summer of 2002 were significantly different from the mean flux calculated for other sampling periods in the summer of 2000 at the DNWR.

To better illustrate the relative consistency of the spatial and short-term temporal variability associated with CO₂ flux measurements at the DNWR, the data from each



sampling period were also pooled and re-plotted as Box-and-Whisker plots (Figure 4.14). As indicated by the size of the “boxes” and length of the “whiskers” the fluxes data obtained in July and August 2002 also exhibited much wider ranges in values--suggesting a greater degree of spatial and temporal variability during these measurement periods.

4.2.4 Cross-statistical comparison between CO₂ fluxes measured from across the DNWR and DSWR piles

Results of cross-statistical comparison tests between the overall averages CO₂ fluxes calculated for the summers of 2000 and 2002 at the DSWR and the DNWR (Tables 4.1 and 4.2) showed that only the summer 2002 data set for the DNWR yielded an overall average CO₂ flux that was significantly different from other summer sampling periods. Differences among the remaining sampling periods were not significant. The degree of spatial variability at both sites was generally small (average CV is 28%-39%). These minor differences were attributed to slight variations in the waste-rock textures that control soil water. The overall averages of CO₂ fluxes at the DNWR and the DSWR over the 2-year test period (summer 2000 and summer 2002) were $217 \pm 83 \text{ mg m}^{-2} \text{ h}^{-1}$ and 188 ± 68 , respectively.

In summary, the above results appear to reflect the laterally extensive source of CO₂ determined to originate in the dewatered organic-rich lake-bottom sediments at the base of the piles (Figures 3.7 and 3.8) (Birkham et al., 2003; Lee et al., 2003) and suggest that the production and upward migration of CO₂ through the waste-rock piles is relatively uniform both spatially and temporally. At the DSWR the dominant oxidation reactions occur in the organic material underlying the waste rock, the more minor gas reactions in the waste rock are masked (Birkham et al., 2003). However, it should be noted that the acid-base accounting and humidity test results (Cameco, unpublished)

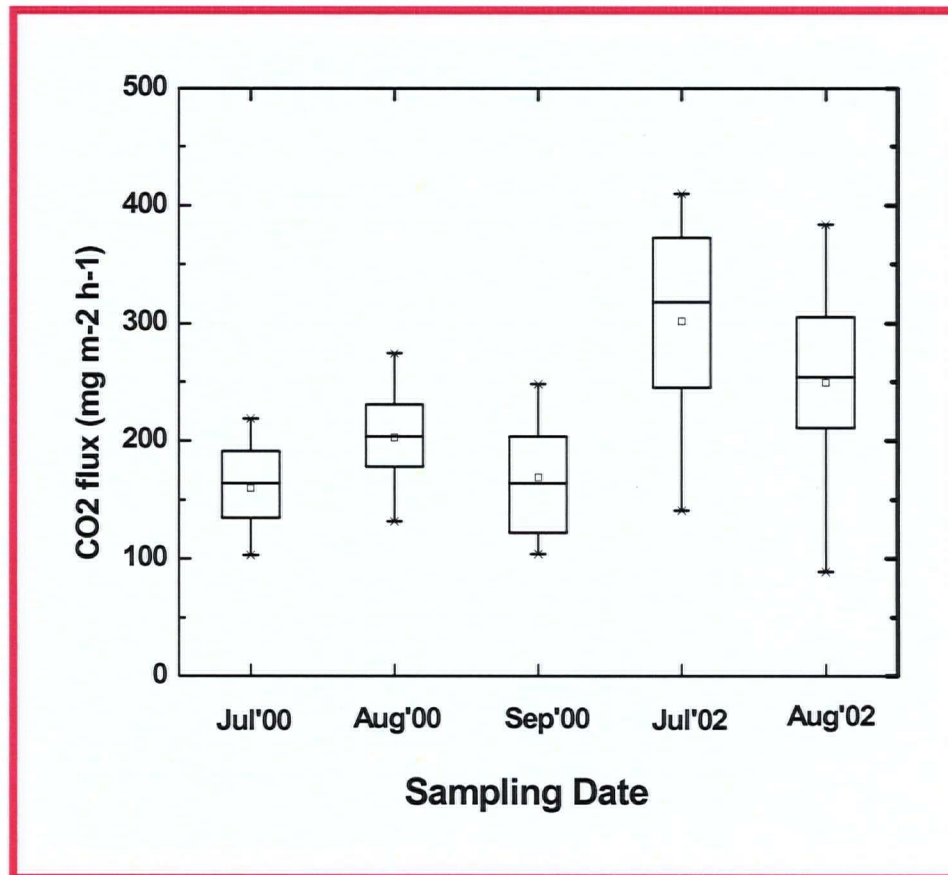


Figure 4.14. Spatial and temporal variations in CO₂ fluxes measured during the summer of 2000 and summer 2002: box-and-whisker plots showing the mean, standard deviation, and extreme values for Deilmann north waste-rock (DNWR) pile data.

suggested that pyrite oxidation-carbonate buffering and the resulting O₂ consumption and CO₂ production are more likely to be observed in the gneissic waste rocks at the DNWR that yielded much greater acid generating potential (AP) (3-11.2 kg CaCO₃ eq./tonne) and acid neutralizing potential (NP) (3.1-4.2 kg CaCO₃ eq./tonne) than sandy waste rocks (AP: 0.9-1.2 kg CaCO₃ eq./tonne; NP: 0.9-1.1 kg CaCO₃ eq./tonne). It may be concluded that the difference between the overall averages CO₂ fluxes calculated for the summer of 2000 and 2002 at the DNWR could be the result of sulphide oxidation and carbonate buffering. Birkham et al. (2003) also concluded that the sulphide oxidation and carbonate buffering may have been dominant reactions within the DNWR.

4.3 Comparison of CO₂ Fluxes Measured using the DCC to those Measured using Static Closed Chamber (SCC) and Eddy Covariance (EC) Methods on the Deilmann South Waste-Rock Pile (DSWR)

4.3.1 Introduction

In a previous study using large-scale laboratory mesocosms filled with sand the DCC method was shown to accurately measure CO₂ fluxes from ground surface to the atmosphere over the range of CO₂ fluxes reported for field conditions (Kabwe et al., 2002). However, to ascertain whether the DCC best approximated field CO₂ fluxes, the DCC measurements were compared to those obtained from across the DSWR using static closed chamber (SCC) and Eddy covariance (EC) methods. The comparison was based on flux data measured on the same period (August 24 to 25, 2002).

4.3.2 DCC fluxes

Subsets of the DCC data obtained during the period from August 24 to 25, 2002, were pooled and replotted as Box-and-Whisker plot (Figure 4.15) for comparison with those obtained using SCC and EC methods. The ANOVA indicated that differences between the daily CO₂ fluxes measure using the DCC from August 24 and 25th 2002 were not significant ($P \leq 0.05$)—yielded an average flux of 162 ± 58 mg CO₂ m⁻² h⁻¹ (n=12) for the 2-d period.

4.3.3 SCC fluxes

Flux measurements using SCC were conducted on August 24, 2002. Headspace gas samples were collected in both the morning (between 10:00 and 11:00) and afternoon (between 16:30 and 17:30).

Flux measurements obtained in both the morning (between 10:00 and 11:00) and afternoon (between 16:30 and 17:30) on August 24, 2002 are presented in Figures 4.16 and 4.17. Results of statistical analysis are presented as box-and-whisker plots in Figure 4.18.

Temporal variations were generally small and there was no significant difference between the average CO₂ flux measured in the morning (181 ± 60 mg CO₂ m⁻² h⁻¹) and that measured in the afternoon (173 ± 62 mg CO₂ m⁻² h⁻¹). Presumably, this reflects the fact that the morning and afternoon measurement periods occurred at the beginning and end of the diurnal cycle. Nevertheless, these results support those obtained earlier using the DCC method, which indicated that the spatial and short-term temporal variability associated with the CO₂ flux was relatively small. Flux measurements of both

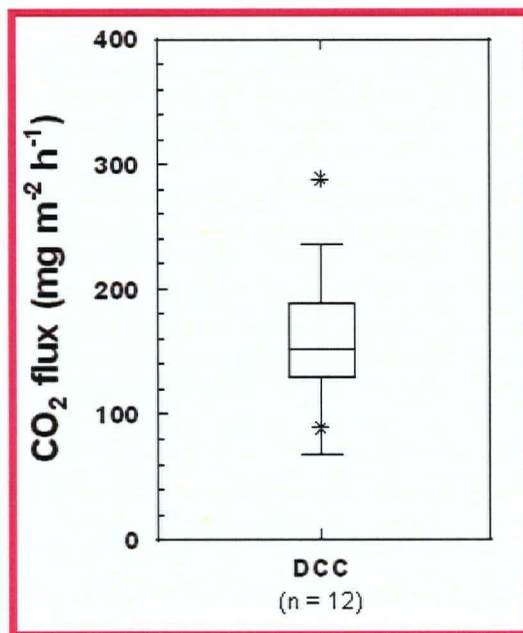


Figure 4.15. Box-and-wisker plot for flux measurements obtained using the DCC method at the Deilmann south waste-rock (DSWR) pile during the period from August 24th to August 25th, 2002 (set of data for comparison with the other two methods: SCC and EC). The minimum and maximum flux values are marked by asterisks (*). Note: values occurring beyond the “whiskers” were identified as outliers and were not included in the analysis of variance.

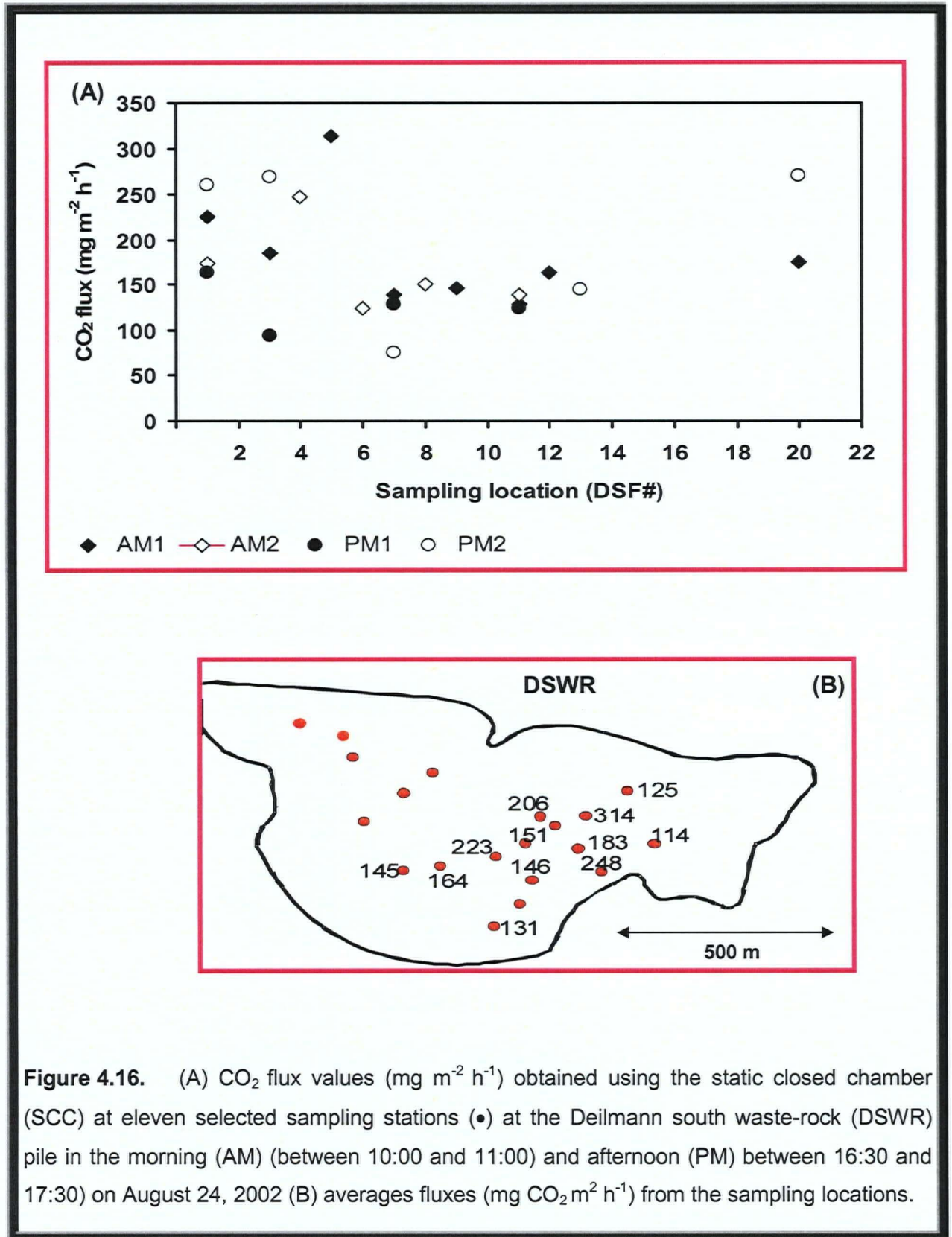


Figure 4.16. (A) CO₂ flux values (mg m⁻² h⁻¹) obtained using the static closed chamber (SCC) at eleven selected sampling stations (•) at the Deilmann south waste-rock (DSWR) pile in the morning (AM) (between 10:00 and 11:00) and afternoon (PM) between 16:30 and 17:30) on August 24, 2002 (B) averages fluxes (mg CO₂ m⁻² h⁻¹) from the sampling locations.

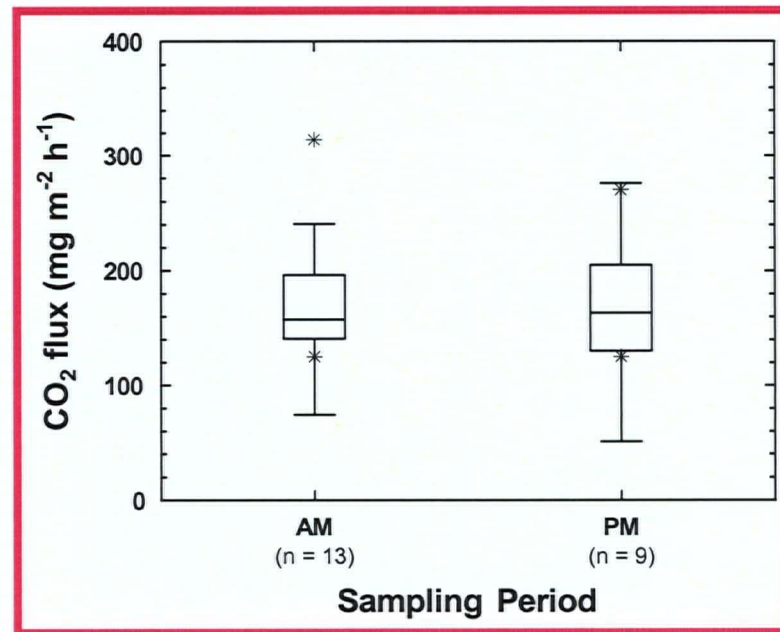
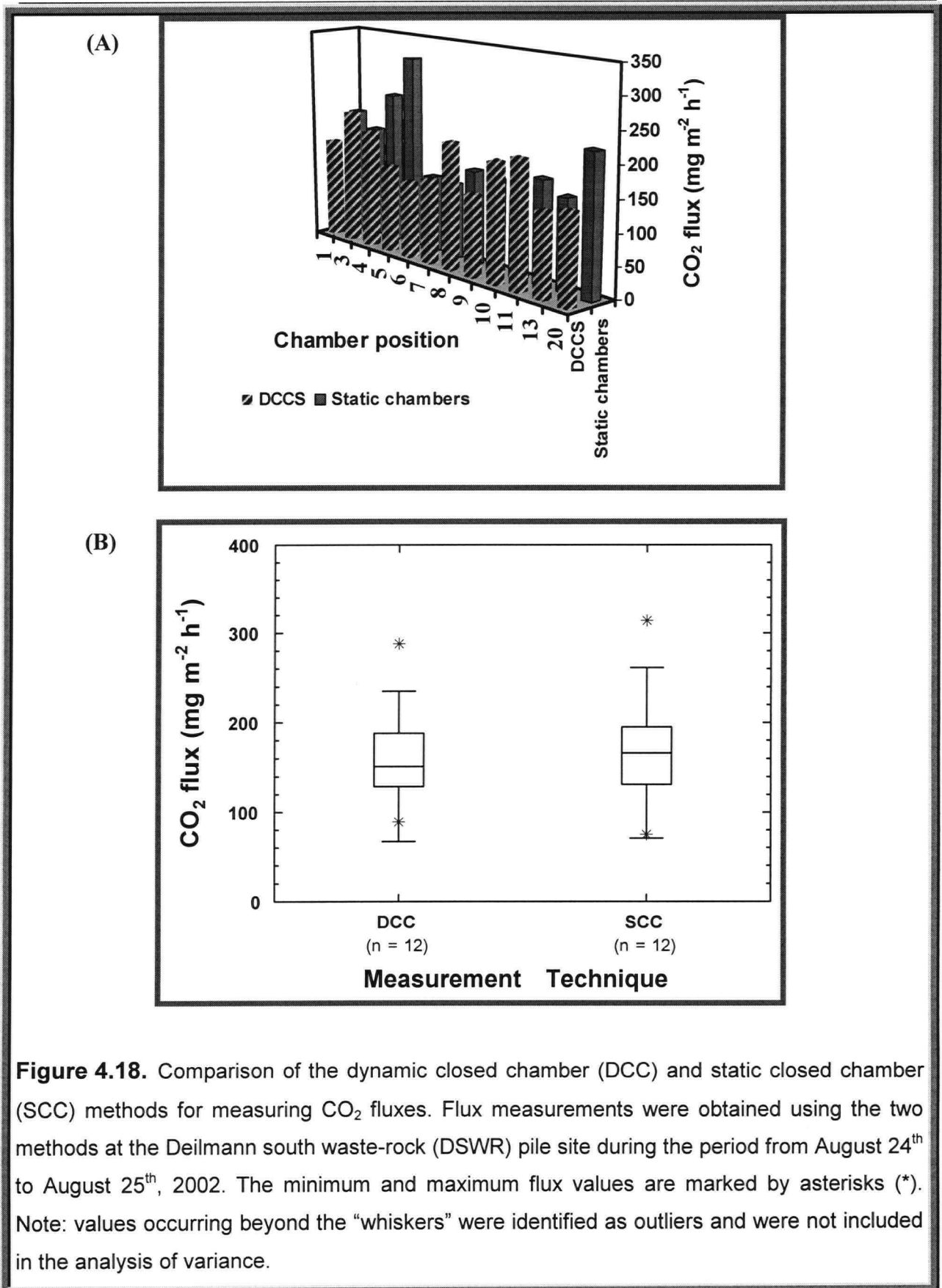


Figure 4.17. Box-and-whisker plots for CO₂ flux measurements obtained from the Deilmann south waste rock (DSWR) pile on August 24, 2002. Measurements were obtained using the static closed chamber (SCC) method between the hours of 10:00 and 11:00 (AM) and 16:30 and 17:30 (PM). The minimum and maximum flux values are marked by asterisks (*). Note: values occurring beyond the “whiskers” were identified as outliers and were not included in the analysis of variance.



the SCC and DCC methods yielded comparable results (Figure 4.19) during the August 2002 test period, with no significant difference ($P \leq 0.05$) between the mean CO₂ fluxes obtained using the two methods. These results demonstrate that both the SCC and DCC methods are equally applicable to the measurement of CO₂ fluxes from the surface of the waste-rock pile.

4.3.4 EC fluxes

Near-continuous measurements of the CO₂ flux were obtained using the EC method during the period from June 25th to August 25th 2002. Measurements were recorded on a data logger installed on the weather station on DSWR. At the end of the test period the data logger was shipped to the Department of Geography of the University of Saskatchewan for data analysis.

It should be noted that data collected during precipitation events by the EC system are no useful (Carey et al., 2005). Subsets of the data were then used to assess the magnitude of the diurnal cycle and compare the EC and chamber-based methods (DCC and SCC). Figure 4.20 shows the diurnal variation in CO₂ flux measured from 10:00 to 17:00 on August 25, 2002 using the EC at the DSWR

The greater temporal resolution provided by the EC system revealed that the CO₂ flux exhibited a distinct diurnal pattern in Figure 4.20. As was the case in August 2000, there was no correlation between the magnitude of the CO₂ flux and air temperature—again suggesting that temperature—induced changes in CO₂ production at the surface of the waste-rock pile were not a major contributor to the total measured CO₂ flux. Compared to the diurnal variations in the CO₂ flux (average s.d. = ± 48 mg CO₂ m⁻² h⁻¹), day-to-day variations in the average flux were generally small (average

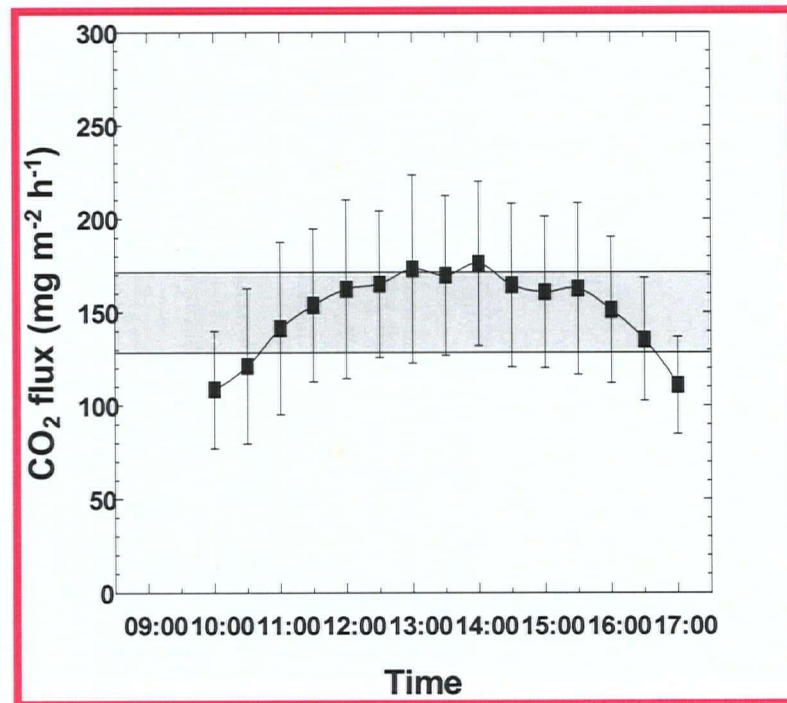


Figure 4.19. Diurnal variations in the CO₂ flux measured from 10:00 to 17:00 on August 25, 2002 using the EC method at the Deilmann south waste-rock (DSWR) pile. The shaded box represents the 95% confidence interval (± 24 mg CO₂ m⁻² h⁻¹) around the calculated daily mean (150 mg CO₂ m⁻² h⁻¹).

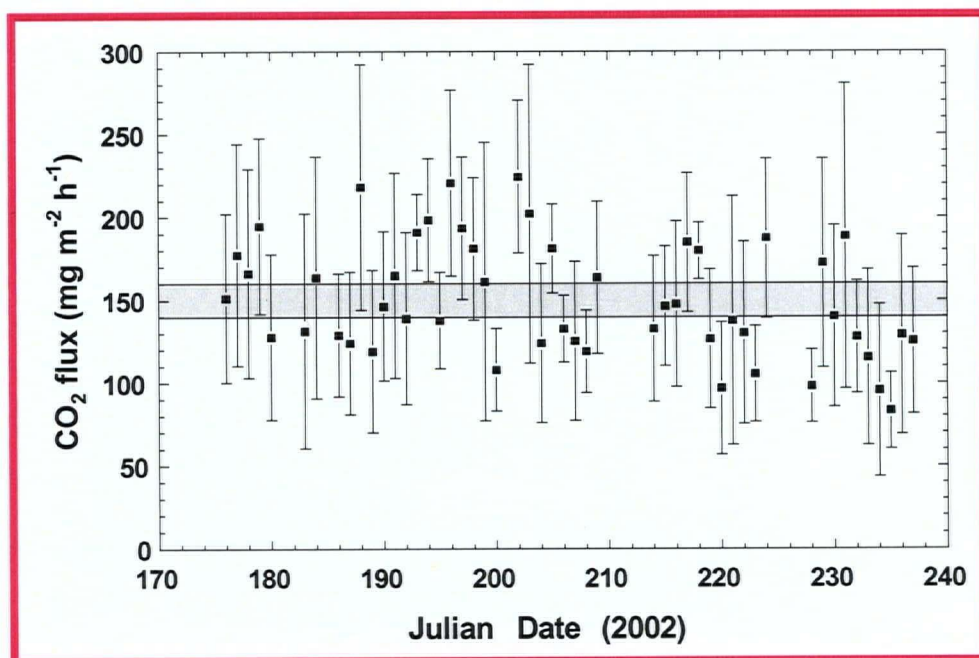


Figure 4.20. Measured CO₂ fluxes using Eddy covariance (EC) at the Deilmann south waste-rock (DSWR) pile. Measurements were obtained on a continuous basis during the period from June 25th to August 25th 2002. Each data point represents the daily mean value averaged over the period from 10:00 to 17:00 hours: The shaded box (B) represents the 95% confidence interval (± 10 mg CO₂ m⁻² h⁻¹) around the overall mean (150 mg CO₂ m⁻² h⁻¹). Note: gaps in the data set represent precipitation events during which no useful data were collected by the EC system.

s.d. = ± 35 mg CO₂ m⁻² h⁻¹). The near-continuous measurements of the CO₂ flux obtained during the period from June 25th to August 25th 2002 are shown in Figures 4.21 and 4.22. Despite a slight downward trend in the daily CO₂ flux with time, the ANOVA revealed that there was no significant difference ($P \leq 0.05$) between the averages for July (160 ± 36 mg CO₂ m⁻² h⁻¹) and August (136 ± 32 mg CO₂ m⁻² h⁻¹). A monthly similar trend was observed in 2000 (using the DCC method), which suggests that there may be a small, but distinct seasonal fluctuation in the CO₂ flux.

Flux measurements obtained using both the EC and chamber-based methods occurred on six occasions during July and August 2002 are presented in Figure 4.23. Differences in the CO₂ flux measured on individual sampling dates, though sometimes large, were not significant ($P \leq 0.05$).

There was no consistent trend; i.e., the chamber-based methods yielded daily flux values that were less than those obtained using the EC method on the first three sampling dates and greater than those obtained using the EC method on the last three sampling dates. As a result, the time-averaged CO₂ flux calculated from the EC data (171 ± 39 mg CO₂ m⁻² h⁻¹) was comparable to that calculated from the corresponding chamber data (178 ± 31 mg CO₂ m⁻² h⁻¹).

In summary, the DCC results showed that the flux of CO₂ from the surface of the waste-rock pile to the atmosphere as relatively uniform, both spatially and temporally. Presumably, this reflects the combined influence of a relatively constant rate of CO₂ production in the organic-rich zone at the base of the waste-rock pile (Birkham et al., 2003) and the textural uniformity of the overburden material (sand) used to construct the pile (Birkham, 2002). That is, these factors combine to exert a controlling influence on the composition and upward migration of pore gases and, in turn, the efflux of gases

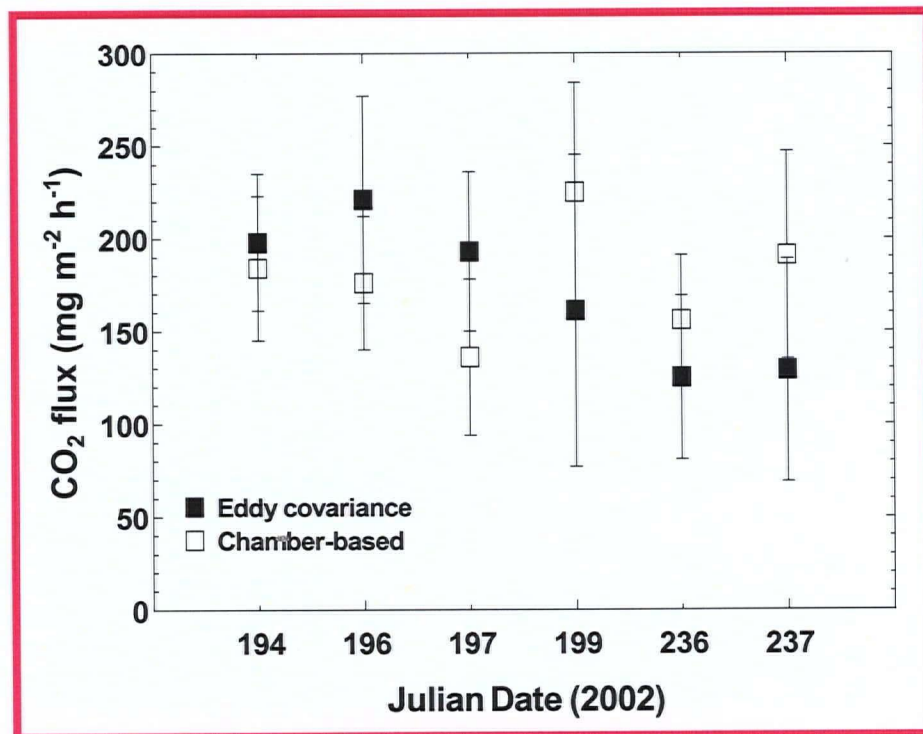


Figure 4.21. Comparison of the eddy covariance (EC) and chamber-based methods for measuring the CO₂ flux from the Deilmann south waste-rock (DSWR) pile.

from the surface to the atmosphere.

Whereas the chamber-based (DCC and SCC) methods yielded comparable data, with an overall time-averaged CO₂ flux of $171 \pm 54 \text{ mg CO}_2 \text{ m}^{-2} \text{ h}^{-1}$; the EC method than that calculated from the chamber data. Underestimation of the F_{CO_2} associated with soil respiration by EC-based methods relative to chamber-based methods has been reported widely in the literature (e.g., Goulden et al., 1996; Norman et al., 1997; Law et al., 1999; Janssens et al., 2000; Davidson et al., 2002). Though not excessively large, these differences presumably reflect the different processes measured by the two methods.

The chamber data exhibited slightly greater standard deviations than the EC data (i.e., DCC = $\pm 58 \text{ mg CO}_2 \text{ m}^{-2} \text{ h}^{-1}$; SCC = $\pm 59 \text{ mg CO}_2 \text{ m}^{-2} \text{ h}^{-1}$; EC = $\pm 32 \text{ mg CO}_2 \text{ m}^{-2} \text{ h}^{-1}$). This most likely reflects the fact that the variability associated with the chamber-based measurements includes both a spatial and temporal component, whereas the variability associated with the EC method is primarily temporal in nature. Thus, it was concluded that both chamber types were suited to the quantification and spatial resolution of CO₂ fluxes associated with waste-rock piles at the Key Lake mine and that the EC method provided the best estimate of the temporal variability in the CO₂ flux.

It is important to note that no single method of measuring soil-atmosphere gas exchanges can meet all objectives. Thus, the choice of method will depend on the type of information required and the characteristics of the site being investigated. Chamber-based methods are especially useful for characterizing spatial variability as well as providing more detailed information regarding local-scale processes. Though more expensive and technically more complex, the eddy covariance method (and other micrometeorological techniques) provides a powerful tool

that allows for spatial integration and near-continuous, long-term monitoring of the soil-atmosphere flux.

Finally, the presence of oxygen in the waste-rock atmosphere is critical for the determination of reaction rates within waste-rock piles. Measurements of surface O_2 fluxes is required to complement the field CO_2 flux data.

4.3.4 Summary of the advantages and disadvantages of the dynamic closed chamber method (DCC)

Some of the advantages of the DCC method can be summarized as follow:

1. The DCC method presents a relatively fast method of measuring field CO_2 fluxes (2 to 10 min. depending on the magnitude of the fluxes).
2. It is a direct method and provides an almost instantaneous indication of the flux measurements regardless of climatic or moisture conditions in the waste dumps.
3. The DCCS uses a portable CO_2 analyzer and can be used to measure the CO_2 fluxes in situ at the same locations using the same chambers with minimal disturbance of the soil.

The disadvantages of the DCC method can be summarized as follow:

1. The method requires a very sensitive CO_2 gas analyzer, thus high initial capital investment (\$19,000 CDN).
2. The CO_2 flux measurements can be influenced by solar radiation and strong wind, and to changes in chamber pressure and temperature during longer measurement cycles (> 1 h).
3. Although the actual measurement time of change in concentrations in the chamber headspace was short in most cases, the set up of the experiment that include

the attachment of the lid to the chamber prior to measurement was labour intensive, taking several minutes to attach the lid. This long time period was due to the size of the chamber and large number of bolts ($n=24$) required to ensure a gas-tight seal between the collar and the lid.

CHAPTER V

Analysis and Discussion

5.1 Introduction

The previous chapter was directed at the primary objective of the present study with respect to the development of a reliable apparatus (i.e., the dynamic closed chamber (DCC) method) for measuring CO₂ fluxes from waste rock. This chapter extends the application of the DCC method and presents the results of the investigation for the influence of a short-term, multi-day (29 July to 5 August 2002) heavy rainfall event on waste-rock water conditions and associated CO₂ fluxes from Deilmann north (DNWR) and Deilmann south (DSWR) waste-rock piles at the Key Lake uranium mine in northern Saskatchewan. The partial differential equation used for the CO₂ model used in this thesis to quantify CO₂ production and diffusion through unsaturated soils is also described. Results of the model validation and its application on mine waste-rock piles are presented. The main objectives of this chapter were to predict the influence of soil water on CO₂ fluxes from mine waste-rock piles and to validate and apply the "CO₂" model to predict concentration-depth profiles and surface CO₂ fluxes in the waste-rock piles.

5.2 Effects of Rainfall Events on Waste-Rock Surface Water Conditions and CO₂ Fluxes Across the Surfaces of the Deilmann North (DNWR) and Deilmann South (DSWR) Waste-Rock Piles

CO₂ fluxes from both the DNWR and the DSWR were measured three times during the summer of 2000 (July to September 2000) and twice during the summer of 2002 (July to August 2002) as described in the previous sections. The total precipitation recorded for each year from 2000, 2001 and 2002 were 483.4, 524.6, and 548.9 mm, respectively. During this period, the year 2002 recorded the greatest precipitation (approximately 1.13 times higher) than that of 2000. From 1977 to 1998, average winter precipitation (October to April inclusive; predominantly as snow) was 163.6 mm, average summer precipitation (May to September inclusive; predominantly rain) was 294.8 mm (data obtained at Key Lake mine site). In general, rainfall accounts for approximately 64% of the average total precipitation at the Key Lake mine site. The effects of the rainfall events on the DNWR and the DSWR surface-water conditions and surface CO₂ fluxes are discussed in the following sections.

5.2.1 Short-term effects of rainfall events on near surface-water conditions

Figures 5.1 and 5.2 show the changes of measured volumetric (θ) water contents at near ground surfaces (0 – 0.15 m) with time, following the cessation of 75.9 mm rainfall over an initial 48-h period [July 30 (day 1) to July 31 (day 2)] with a gradual decrease in rainfall from August 1 (day 3) to August 3 (day 5), at the DNWR and the DSWR. Results show that the ground surfaces of the piles (0 m, open circles) dried rapidly, whereas the drying rates at greater depths (0.05 m and below) decreased slowly with time (Figures 5.1 and 5.2) (see data in Appendix E). The ground surface of the DSWR (Figure 5.2) drains more rapidly than that at the DNWR. For example, on 31 July 2002 (day 3) the ground surface water content on the DSWR was about 0.06 compared with 0.23 on the DNWR. Both ground surfaces continued to dry rapidly with

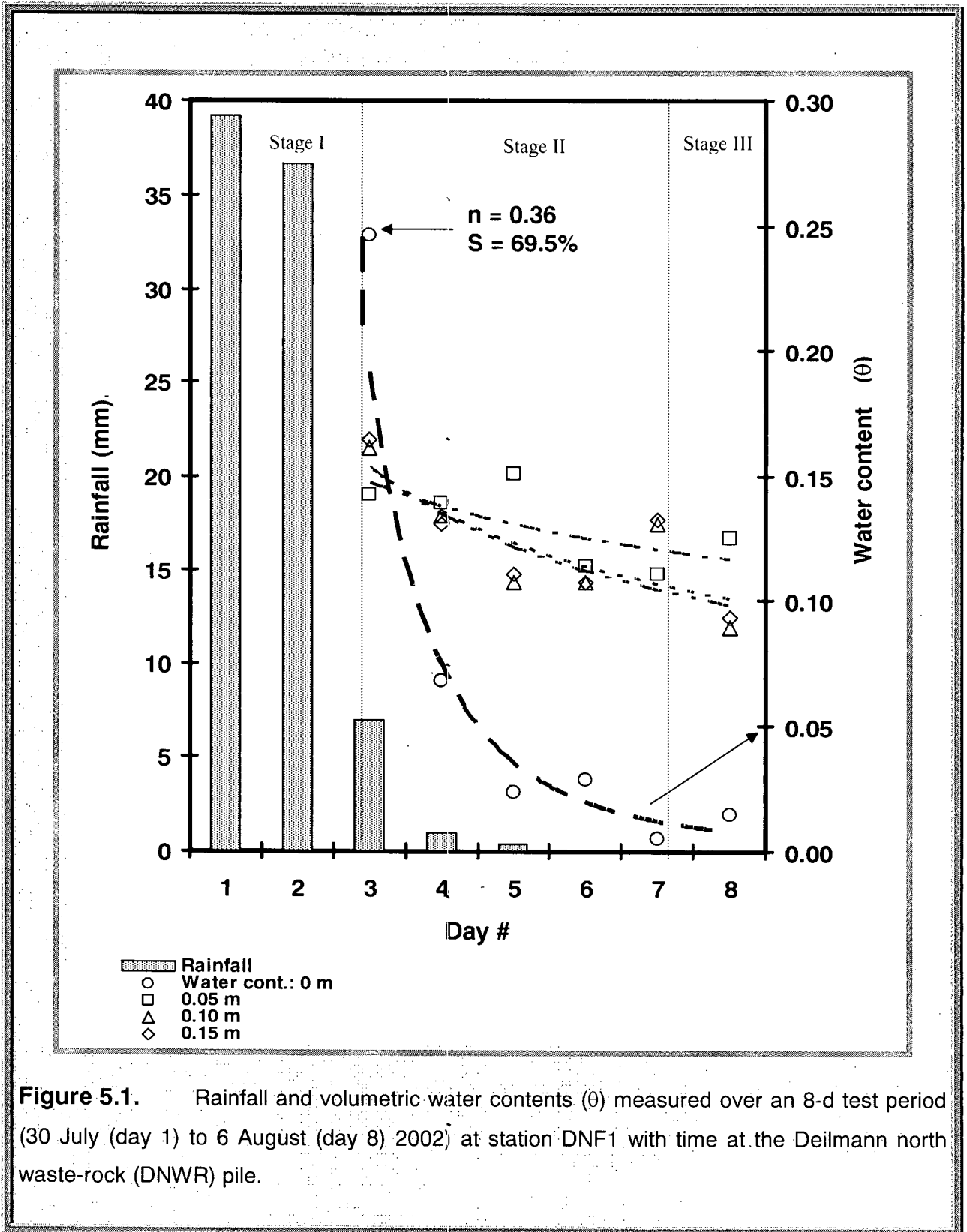


Figure 5.1. Rainfall and volumetric water contents (θ) measured over an 8-d test period (30 July (day 1) to 6 August (day 8) 2002) at station DNF1 with time at the Deilmann north waste-rock (DNWR) pile.

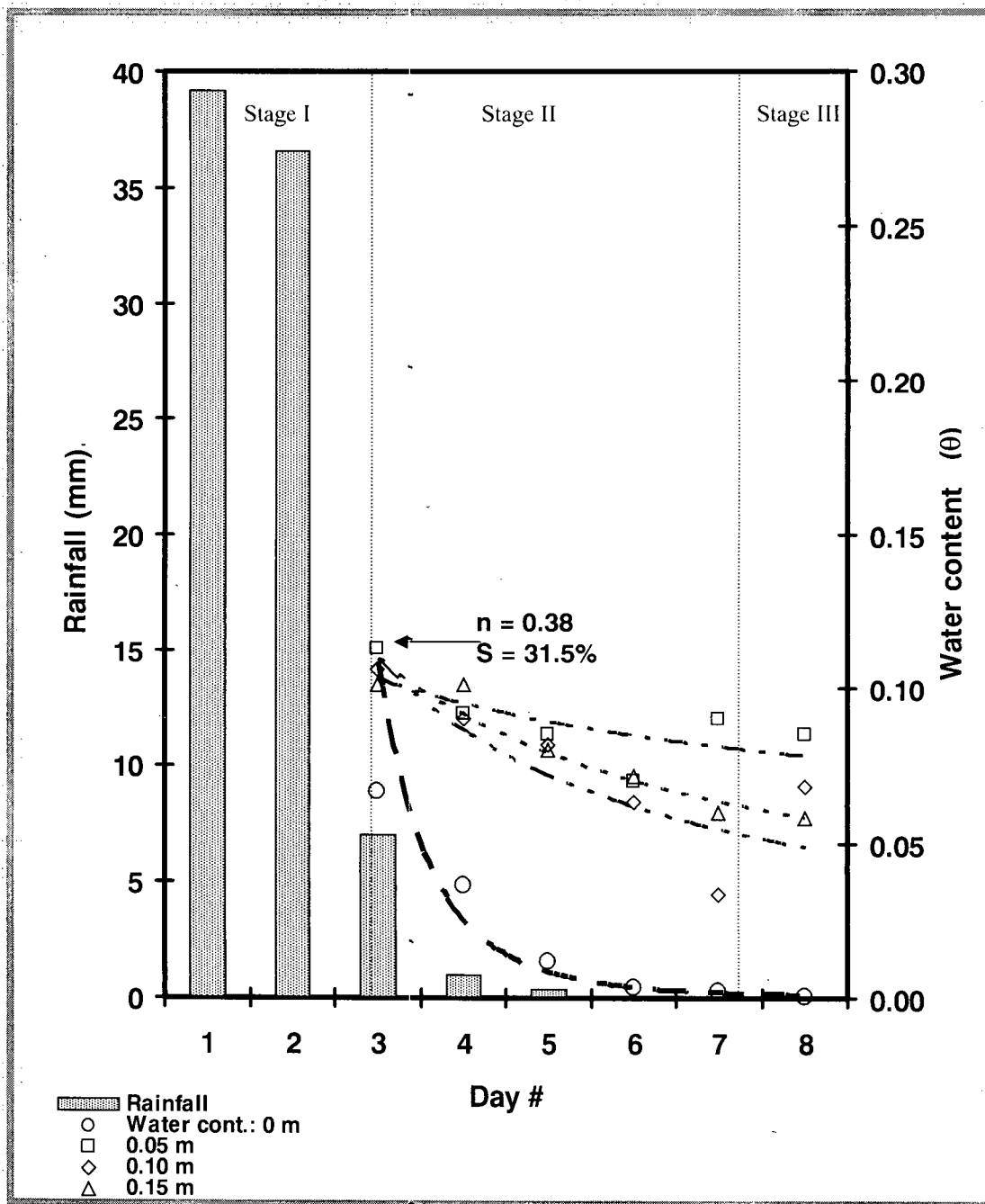


Figure 5.2. Rainfall and water contents measured over an 8-d test period (30 July (day 1) to 6 August (day 8) 2002) at sampling station DSF1 with time at the Deilmann south waste-rock (DSWR) pile. The porosity $n=0.38$.

time to water content values of about 0.10 and 0.004 (day 8), respectively, on the DNWR and the DSWR. The drying rates eventually diminished with time, although at greater depths (0.05 m and below), water contents remained elevated at the end of the test period (day 8). This behavior is caused by the reduction of the unsaturated hydraulic conductivity due to the decrease in surface-water content as evaporation continues (Shuttleworth, 1993; Wilson et al., 1994; Capehart and Carlson 1994; Ek and Cuenca 1994; Capehart and Carlson 1997). The soil surface curves can be described as having three stages of drying as described in Hillel (1980) and Wilson et al. (1994). Stage I drying occurred during the wet period from day 1 to day 3 when the soil surfaces were nearly saturated. Stage II drying starts from day 3 after the cessation of heavy rainfall events. The beginning of the second stage of drying occurs rather abruptly (see Figures 5.1 and 5.2) as the soil surfaces rapidly dried out. The length of time for the second stage of drying lasts depends upon the intensity of the meteorological factors that determine atmospheric evaporativity, as well as upon the conductive properties of the waste-rock itself. The soil surface at the DNWR (Figure 5.1) dried out more slowly than that at the DSWR (Figure 5.2). For example, on day 3 (August 1, 2002) the surface-water content on the DNWR was about 0.23 as compared to 0.06 on the DSWR.

The empirical rate of the decrease of ground soil surface-water (0 m) content ($d\theta_w/dt$) can be described by (Gray, 1995):

$$-\frac{d\theta_w}{dt} = a * t^{-b} \quad [5.1]$$

where θ_w is the volumetric water content (cubic metre of water per cubic meter of air), t is the time, and a and b are parameters related to the boundary conditions and conductance properties of the soil, respectively. The exponent b , which is related to soil diffusivity, is obviously most important, and the greater its value, the greater the decrease in water content. The use of this model to develop descriptive equations for the rate of drying of the ground surface at the DSWR ($-\frac{d\theta_w}{dt} = 28.67 * t^{-5.08}$, $R^2 = 0.948$) and the DNWR ($-\frac{d\theta_w}{dt} = 7.19 * t^{-3.30}$, $R^2 = 0.826$) yielded high correlation coefficients (using Microsoft Excel). The drying equations indicate that the drying rate at the DSWR is greater than that at the DNWR (e.g., the exponent b for DSWR is greater than that for the DNWR).

Gray (1995) pointed out that, if the drying rates were limited only by a diffusion-limited process (i.e. vapor diffusion across the drying zone), the exponents in the drying rate functions would be 0.5. Equation 5.1 is purely empirical and does not attempt to account for flow mechanisms. For example, during drying, the water is simultaneously redistributing away from the waste-rock ground surfaces (e.g., Figures 5.3) because of both upward flow due to evaporation and downward drainage due to gravity; thereby speeding decay of the surface drying rates. The redistribution tends to persist longer in the waste rock at the DNWR than that at the DSWR. The time-variable rate of redistribution depends not only on the hydraulic properties of the waste rocks, but also on the initial wetting depth, as well as on the relative dryness of the bottom layers (Hillel, 1980).

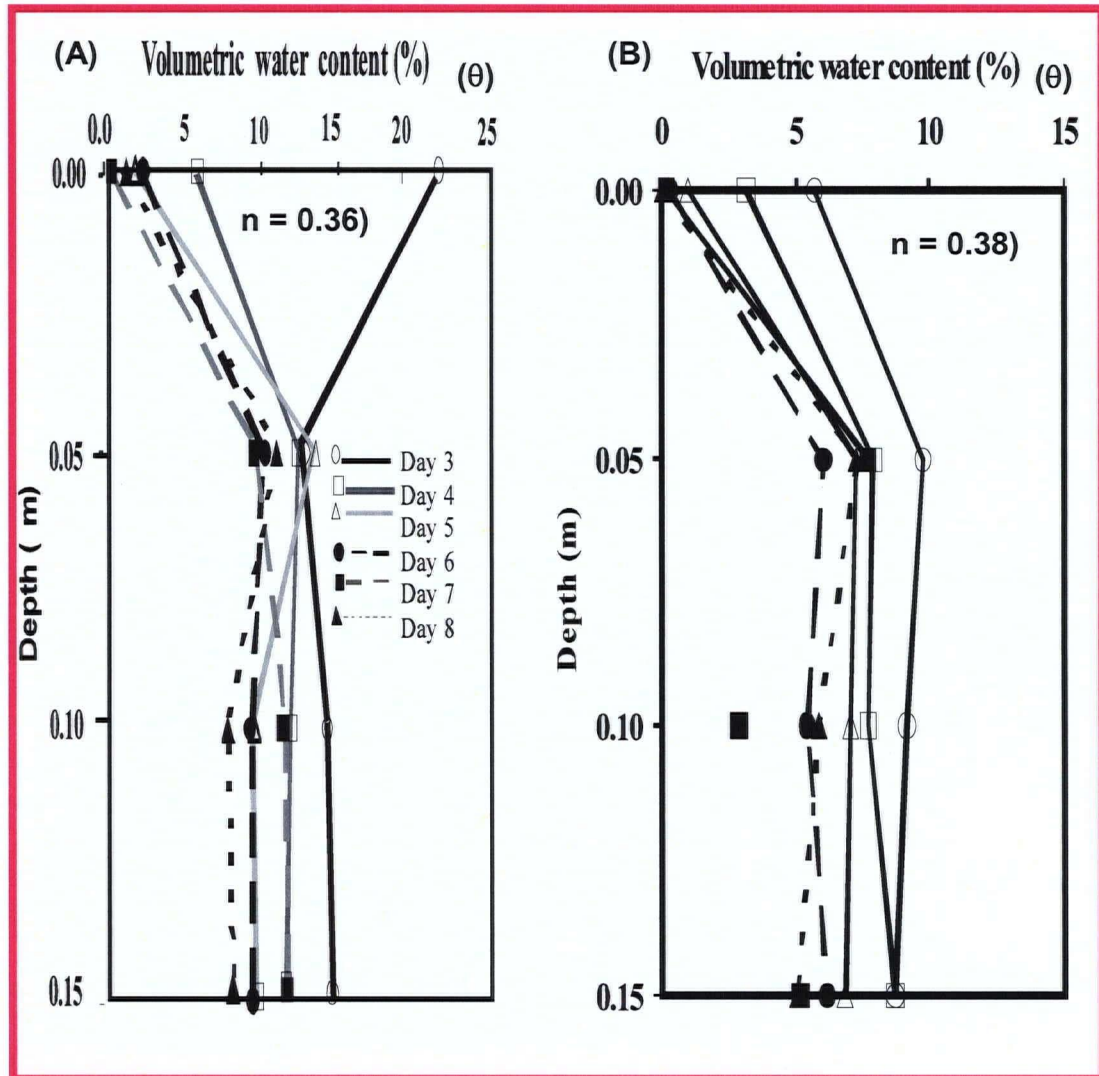


Figure 5.3. Volumetric water content (θ) profiles measured over an 8-d test period [30 July (day 1) to 6 August (day 8) 2002] at (A) station DNF1 at the Deilmann north waste-rock (DNWR) pile and (B) station DSF1 at the Deilmann south waste-rock (DSWR) pile with time.

5.2.2 Short-term effects of rainfall events on CO₂ fluxes

The changes in measured CO₂ fluxes from ground surface following the cessation of 75.9 mm rainfall over the initial 48-h period [July 30 (day 1) to July 31 (day 2)] are presented in Figures 5.4 and 5.5 (solid circles). On 31 July 2002 (day 3), CO₂ fluxes measured from the DNWR and the DSWR were 3% and 36 % of their initial average values of 217 and 188 mg m⁻² h⁻¹, respectively. The figures showed that the changes of surface CO₂ fluxes with time were negatively correlated with measured surface water contents for the waste rock sand.

As the water contents at ground surfaces decreased exponentially, the surface CO₂ fluxes increased exponentially from day 3 to day 8. These inverse linear relationships yielded correlation coefficients of $R^2 = -0.997$ and $R^2 = -0.820$ (using Microsoft Excel) for the DNWR and the DSWR, respectively. By the end of the 8-d test period, the surface CO₂ fluxes had increased by factors of 4 and 45 while the ground surface water contents had decreased from 6.7% to 0.04% and from 25.0% to 1.5% at the DNWR and the DSWR, respectively, and the measured CO₂ gas fluxes approximated their initial mean flux values. This observation suggested that it takes about 5 to 6 d after a heavy rainfall event for the gas fluxes to approach pre-rainfall values. In addition it is further suggested that the impact of rainfall events on CO₂ fluxes from the waste-rock piles is of relative short duration.

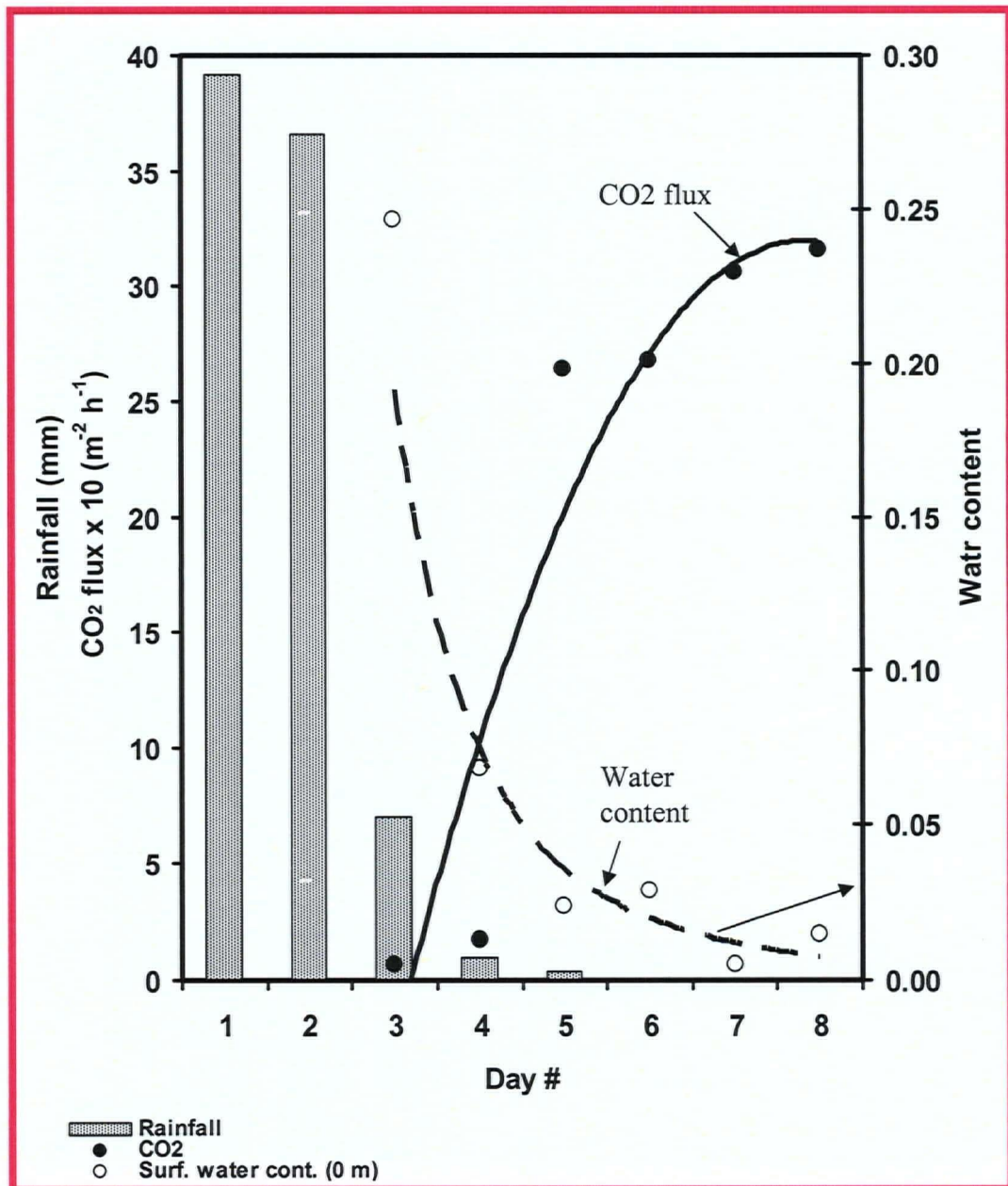


Figure 5.4. Rainfall, water contents, and CO₂ fluxes measured at station DNF1 over an 8-d test period [30 July (day 1) to 6 August (day 8) 2002] at the Deilmann north waste-rock (DNWR) pile with time.

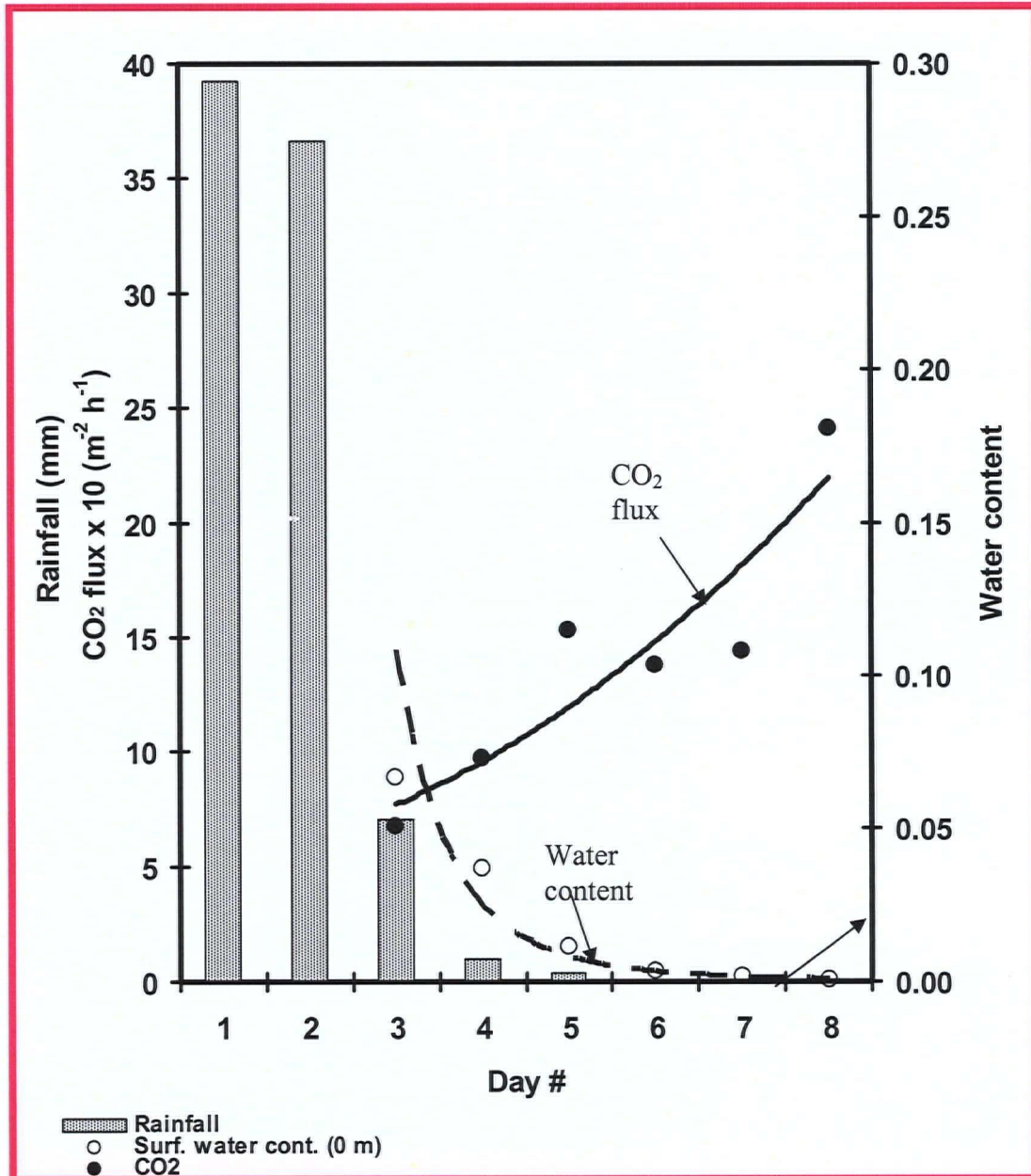


Figure 5.5. Rainfall, water contents, and CO₂ fluxes measured at the DSF1 over an 8-d test period [30 July (day 1) to 6 August (day 8) 2002] at the Deilmann south waste-rock (DSWR) pile with time.

The functional relationship between the measured surface CO₂ flux and the surface-water content is also shown in Figure 5.6. Results showed that the surface CO₂ flux is sensitive to changes of waste-rock surface-water content after heavy rainfall event, exhibiting a power decrease with surface-water content of the form:

$$F_{\text{CO}_2} = a * \theta_w^{-b} \quad [5.2]$$

where F_{CO_2} is the surface CO₂ flux (milligrams per square meter per hour), θ_w is the volumetric water content (cubic metre of water per cubic metre of air), and a and b are parameters related to the boundary conditions and conductance properties of the porous media, respectively. The use of this model to develop descriptive equations showed that a good relationship between the surface CO₂ flux and the ground surface water content of the waste rock at the DNWR ($F_{\text{CO}_2(\text{N})} = 4.71 * \theta_w^{-1.15}$, $R^2 = 0.790$) and DSWR ($F_{\text{CO}_2(\text{S})} = 53.50 * \theta_w^{-0.21}$, $R^2 = 0.846$) (Figure 5.6). The difference in the coefficients a and b between the two piles is attributed to textural variability that affects the water content and the diffusivity of CO₂, which is also a function of water content.

In summary, measurements showed that the gas-flow conditions at the ground surfaces of the DNWR and DSWR were transient after a heavy rainfall. The transient effects were attributed to rapid drainage and evaporation. The effect of heavy rainfall on water-content profiles and CO₂ fluxes was of a relatively short duration.

5.3 Predictions of Evaporative Fluxes and Near-Surface Water Contents Profiles

It was noted from the previous sections that rainfall events can create changes in soil water content and CO₂ gas profiles within unsaturated zones and that the extent of the effect depends on the intensity and duration of the rainfall. Evaporation from mine wastes is a crucial component of the water balance (Carey et al., 2005). Similarly, soil water evaporation significantly affects water content, and as a results, the degree of saturation of the soil and the gas diffusion. Knowledge of the rate of evaporation at the soil-atmosphere interface is required to estimate the water content of candidate cover soils. The one-dimensional SoilCover computer model (Unsaturated Soils Group, 1997) was used to estimate evaporative fluxes at the DNWR and the DSWR over the 8-d test period [(30 July (day 1) to 6 August, 2002 (day 8)]. The model calculates daily evaporation on a site-specific basis, using weather data collected at the site as a boundary condition for the calculation of actual evaporation. The weather data (radiation, air temperature, humidity, and wind speed, etc.) is used in combination with soil characteristics and the calculated changes in soil moisture (details data input, output and results are also presented in Appendix H). The SoilCover predicted evaporative fluxes at the DSWR were compared to published measured values obtained by Carey et al. (2005) from the DSWR during the same test period.

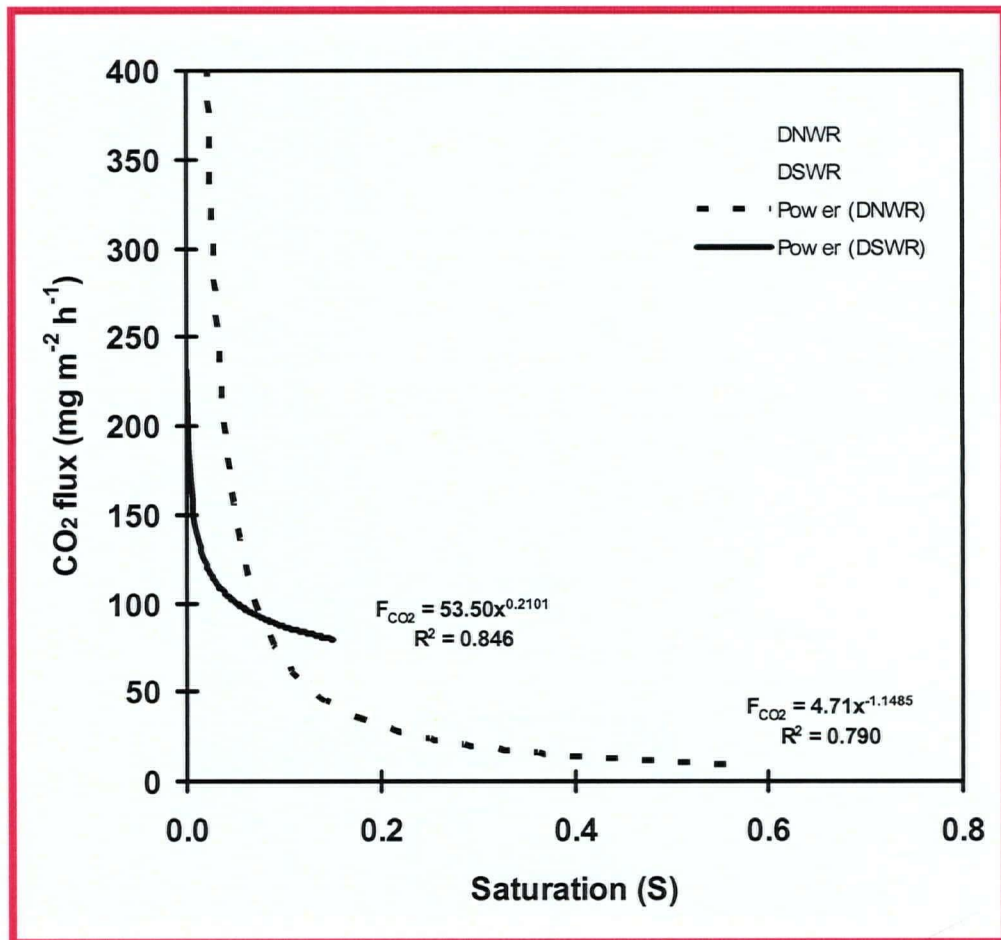


Figure 5.6. Variations in CO₂ flux measurements with surface-water saturation ($S=\theta/n$) measured over an 8-d test period [30 July (day 1) to 6 August (day 8) 2002] at stations DNF1 and DSF1 of the DNWR ($n=0.36$) and DSWR (0.38) piles, respectively.

5.3.1 Short-term predictions of evaporative fluxes

Figures 5.7 and 5.8 show the SoilCover model predictions of cumulative evaporative fluxes and the ratio of actual (AE) and potential (PE) evaporation (AE/PE) as a function of time for the 8-d test period at the DNWR and the DSWR, respectively. Simulations results indicated that during the period of heavy rainfall events from day 1 to day 3 the evaporation rate was relatively low. During this period the cumulative PE and AE were equal at both the DNWR and the DSWR. This stage is being referred as stage I drying (Wilson et al., 1994). Wilson et al. (1997) noted that the AE is approximately equal the PE rate of evaporation until the value of matric suction reaches approximately 3000 kPa. During this period the evaporation is controlled by external meteorological conditions (Hilled, 1980; Wilson et al., 1994).

As the ground surfaces continued to dry from day 3 to day 5 the rate of evaporation started increasing rapidly. The cumulative evaporation was slightly higher at the DSWR (PE = 5.3 mm) than at the DNWR (PE = 4.5 mm) on day 5. After day 5, the values of Actual rate of evaporation and Potential rate of evaporation started to progressively diverge with AE less than PE, but slight faster at the DSWR than at the DNWR (Figures 5.7B and 5.8B). Moreover, results showed that during the separation of the AE and PE, the water contents had dropped dramatically from 0.25 on day 3 to about 0.003 on day 5 at the DNWR and from 0.07 on day 3 to about 0.001 on day 5 at the DSWR, respectively. At the end of the 8-d test period the model simulation results indicated 9.5 and 10.9 mm cumulative PEs for the DNWR and the DSWR. These values represent averages daily evaporation rate of 1.2 and 1.4 mm d⁻¹ for the 8-d test period for the DNWR and DSWR respectively. Carey and co-workers (Carey et al., 2005) directly measured summer evaporation (6 June to 25 August, 2002) using eddy (EC)

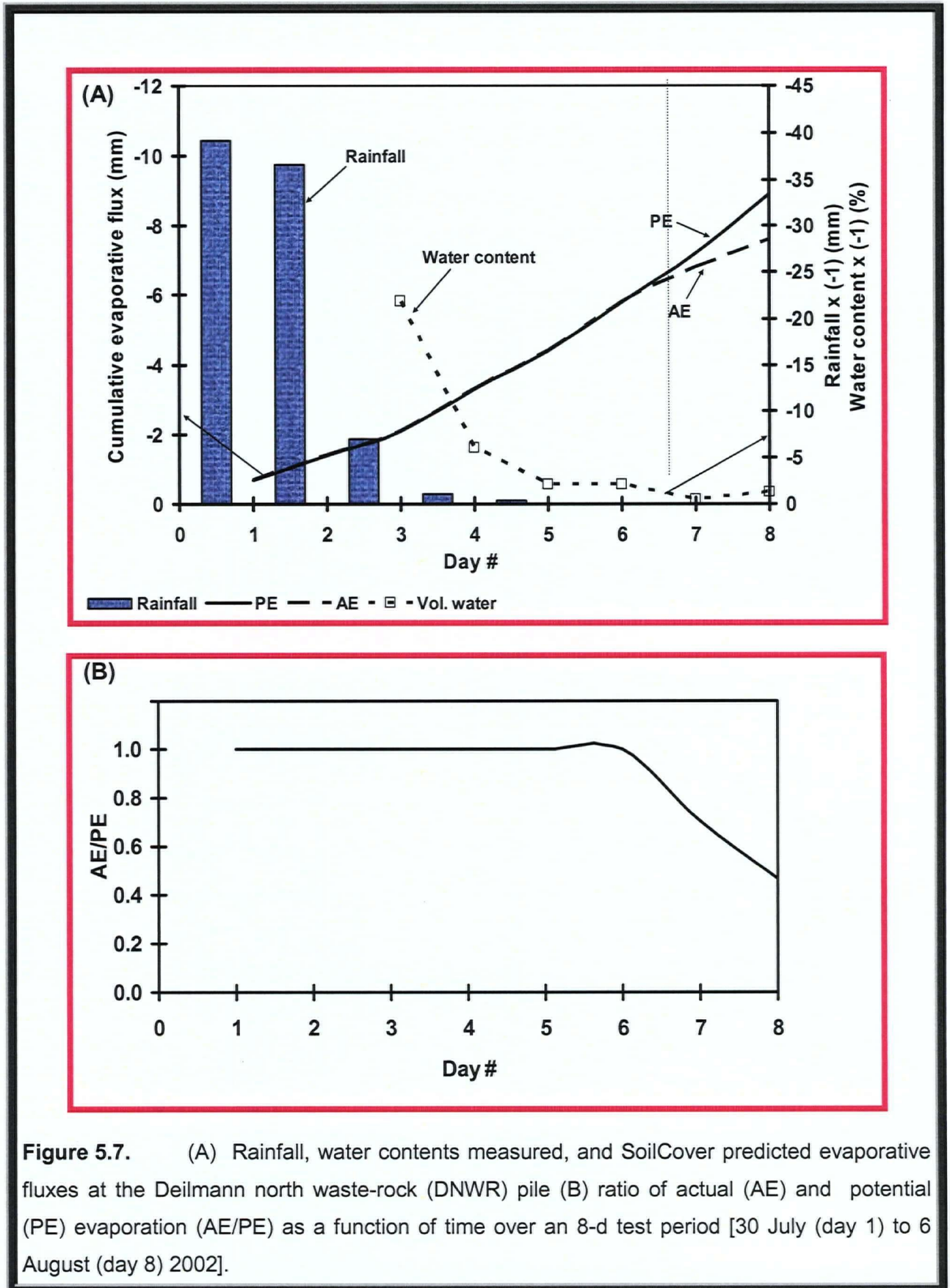


Figure 5.7. (A) Rainfall, water contents measured, and SoilCover predicted evaporative fluxes at the Deilmann north waste-rock (DNWR) pile (B) ratio of actual (AE) and potential (PE) evaporation (AE/PE) as a function of time over an 8-d test period [30 July (day 1) to 6 August (day 8) 2002].

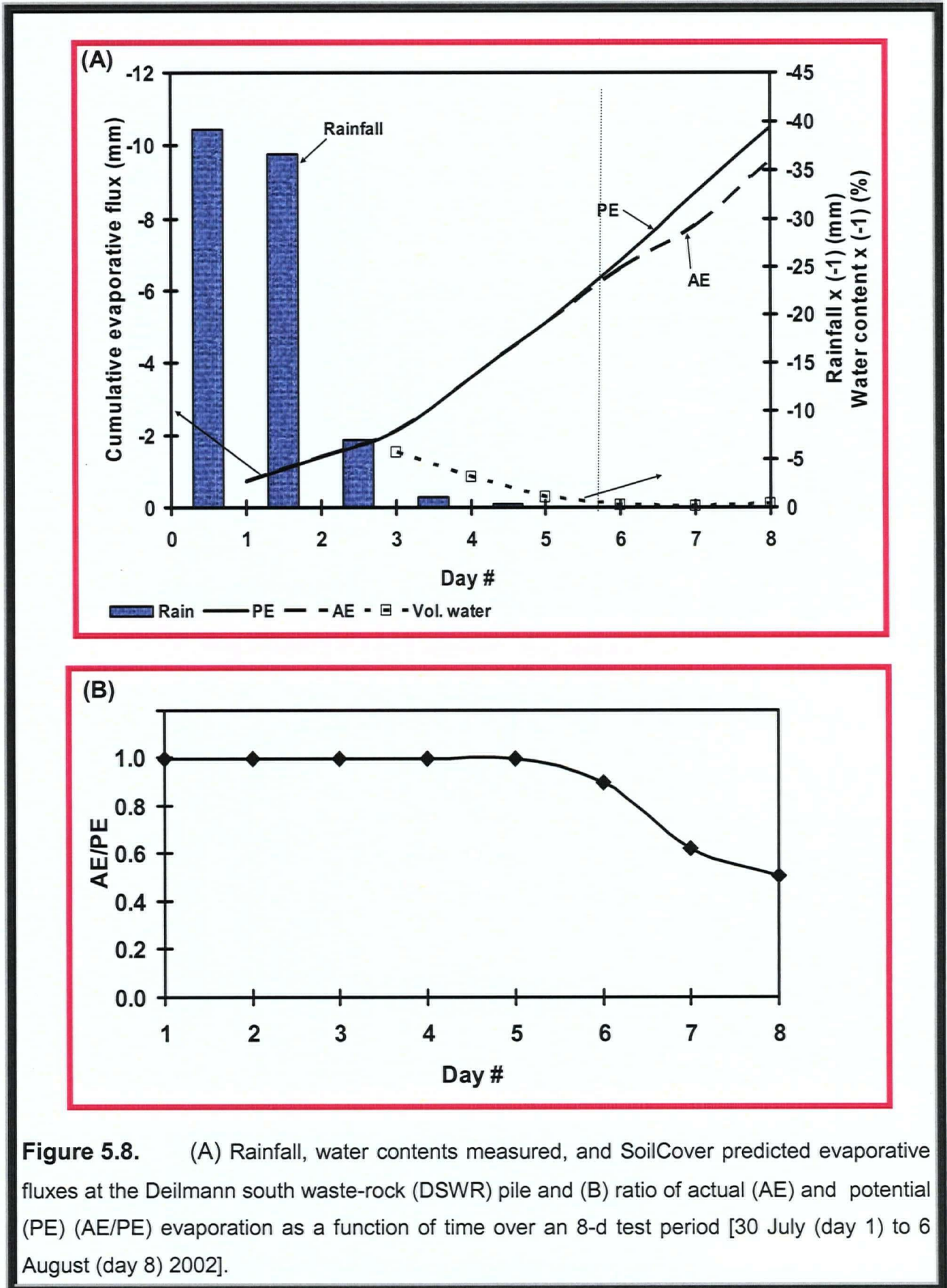


Figure 5.8. (A) Rainfall, water contents measured, and SoilCover predicted evaporative fluxes at the Deilmann south waste-rock (DSWR) pile and (B) ratio of actual (AE) and potential (PE) (AE/PE) evaporation as a function of time over an 8-d test period [30 July (day 1) to 6 August (day 8) 2002].

covariance method at the DSWR. They measured the cumulative AEs (data not shown here) for the 8-day test period and found the cumulative AE of 8.0 mm with an average evaporation of 1 mm d^{-1} at the DSWR (Carey et al., 2005). The results showed good agreement between SoilCover model predicted and EC measured AEs data for the 8-d test period at the DSWR. Carey et al. (2005) also noted that the measured AE was significantly less than the PE at the DSWR due to high surface albedo that reduce available energy for evaporation.

Figures 5.9 and 5.10, respectively, show SoilCover model simulation results of cumulative PE and AE for a 27-d period (July 29 to August 24, 2002) for the DNWR and the DSWR. During this period subsequent rainfall events occurred between day 16 and day 19 where a total of 26.9 mm fell at the sites. These rainfall events are depicted in Figures 5.9B and 5.10B where the ratios AE/PE equal to unit (AE/PE=1).

At the end of the 27-d simulation period the model results yielded cumulative AEs of 32 and 35.6 mm with ratio of PE/AE of 1.44 and 1.37 for the DNWR and the DSWR, respectively. These results represent averages AE evaporation of 1.2 and 1.3 mm d^{-1} at the DNWR and DSWR respectively.

Carey et al. (2005) field-measured data indicated cumulative AE of 37 mm with an average of 1.4 mm d^{-1} for the 27-d test period at the DSWR. These results show good agreement between model (SoilCover) simulations and measured AEs values for the 27-d test period at the DSWR.

In summary, the comparison between the SoilCover predicted AE evaporation and the EC measured AE (Carey et al., 2005) indicated the ability of the SoilCover model to predict, with sufficient accuracy the AE at the surfaces of the waste-rock materials.

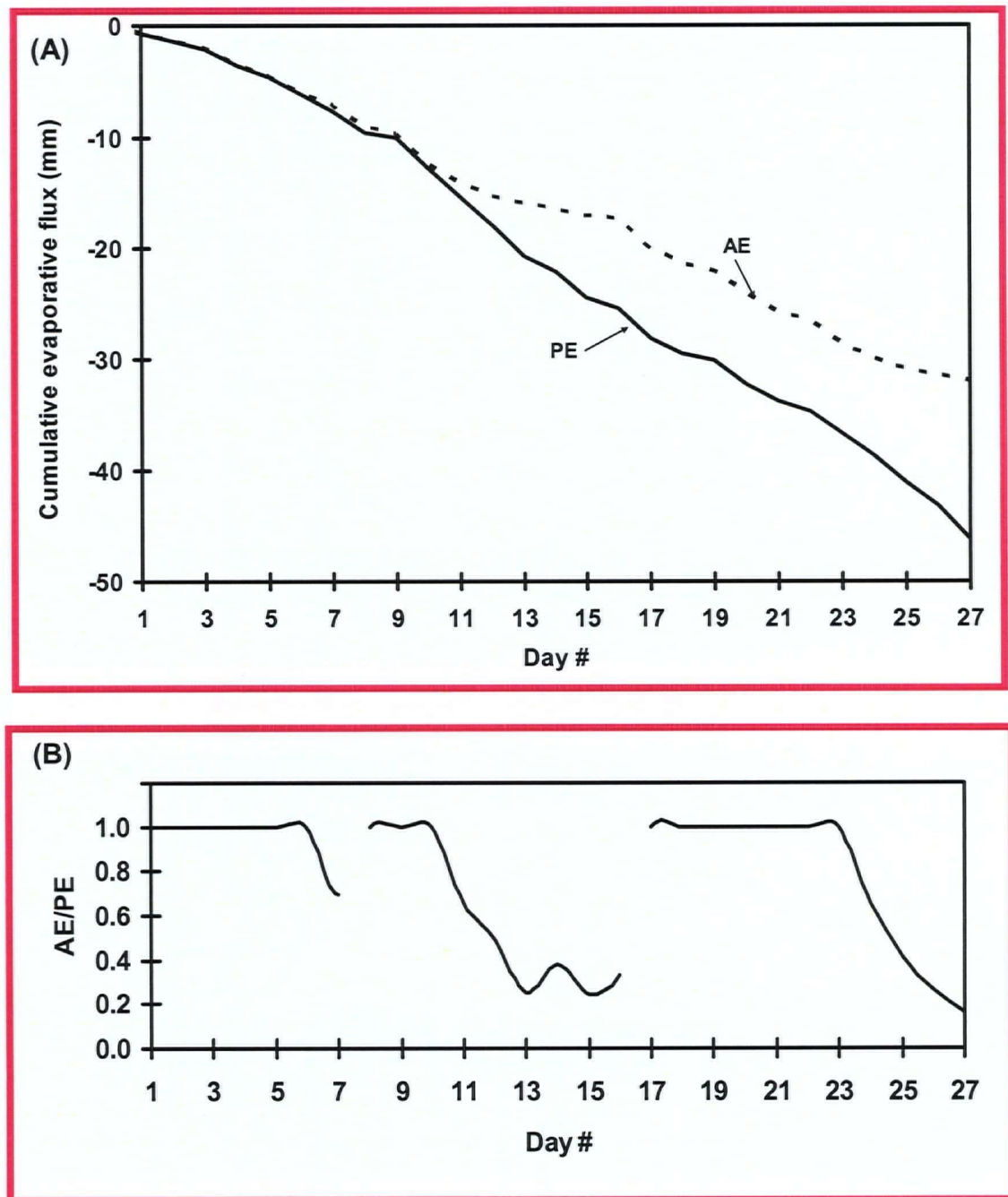


Figure 5.9. SoilCover predicted evaporative fluxes (A) actual AE and potential PE and (B) the ratio of AE/PE at the Deilmann north waste-rock (DNWR) pile over a 27-d test period [29 July (day 1) to 24 August (day 27) 2002] with time.

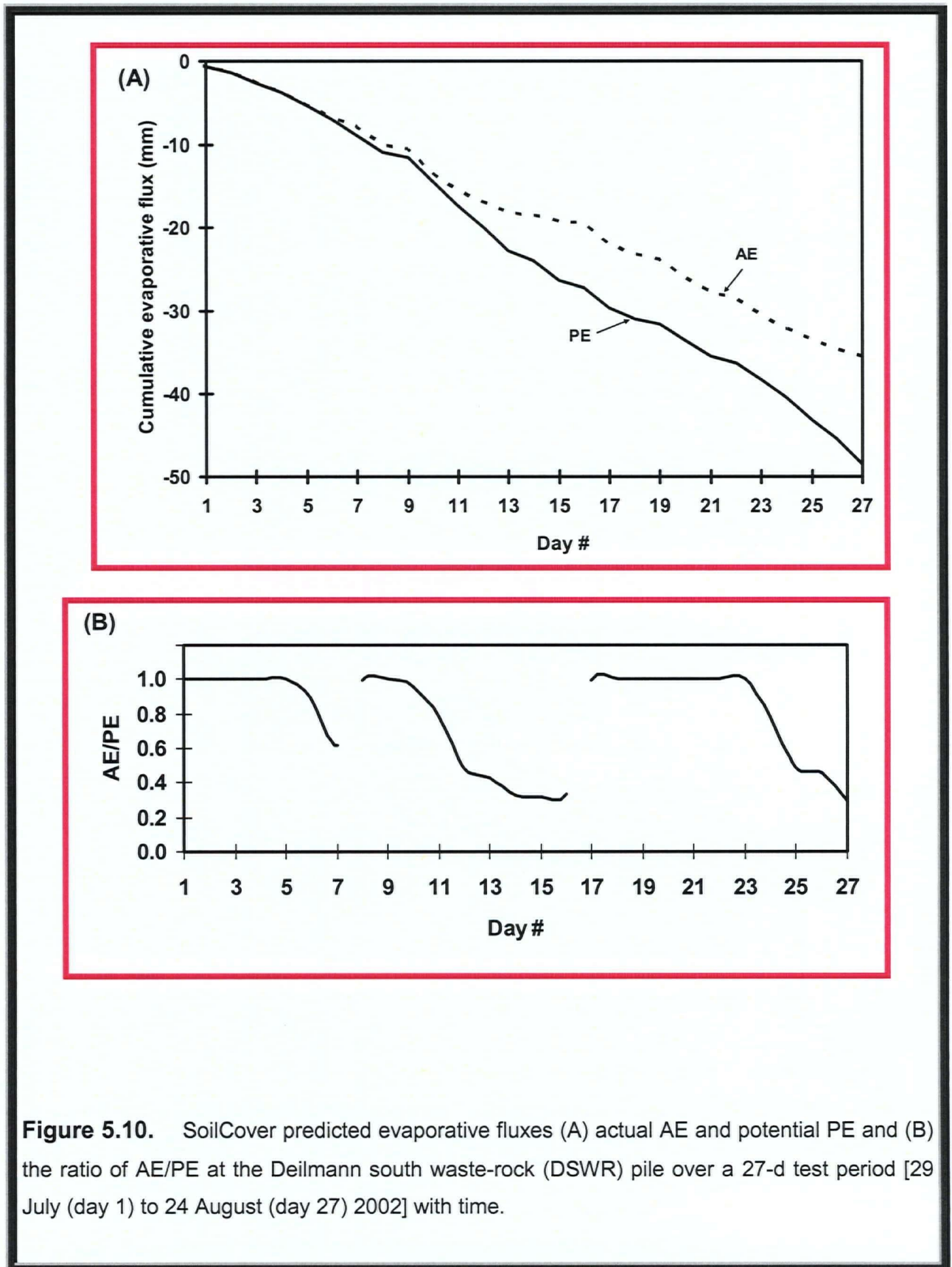


Figure 5.10. SoilCover predicted evaporative fluxes (A) actual AE and potential PE and (B) the ratio of AE/PE at the Deilmann south waste-rock (DSWR) pile over a 27-d test period [29 July (day 1) to 24 August (day 27) 2002] with time.

5.3.2 Short-term predictions of near-surface water contents profiles

SoilCover was also used to predict the changes in water content profiles after the rainfall events over the 8-d test period [(30 July (day 1) to 6 August, 2002 (day 8)] at the DNWR and DSWR. In the simulations, the initial water content profile was required in order to predict the subsequent water profiles. The initial measured water contents profiles and the soil properties of the DNWR and DSWR were used as inputs data for the model simulations. The upper boundary value of water content of 0.03 (3%) was also specified in the model as initial water conditions during the simulations.

Figures 5.11A and 5.12A present the measured water contents profiles and Figures 5.11B and 5.12B present the SoilCover predicted water contents profiles at the DNWR and DSWR piles. Both the measured and SoilCover predicted data show that the water contents conditions at the ground surfaces of the DNWR and the DSWR were transient after the heavy rainfall events. The transient conditions at both the ground surfaces were attributed to the sandy texture of the waste-rock piles and their associated high saturated hydraulic conductivities. The water redistribution appears to persist longer in the waste rock at the DNWR than at the DSWR and this was attributed to slight variations in the waste-rock textures that control soil water.

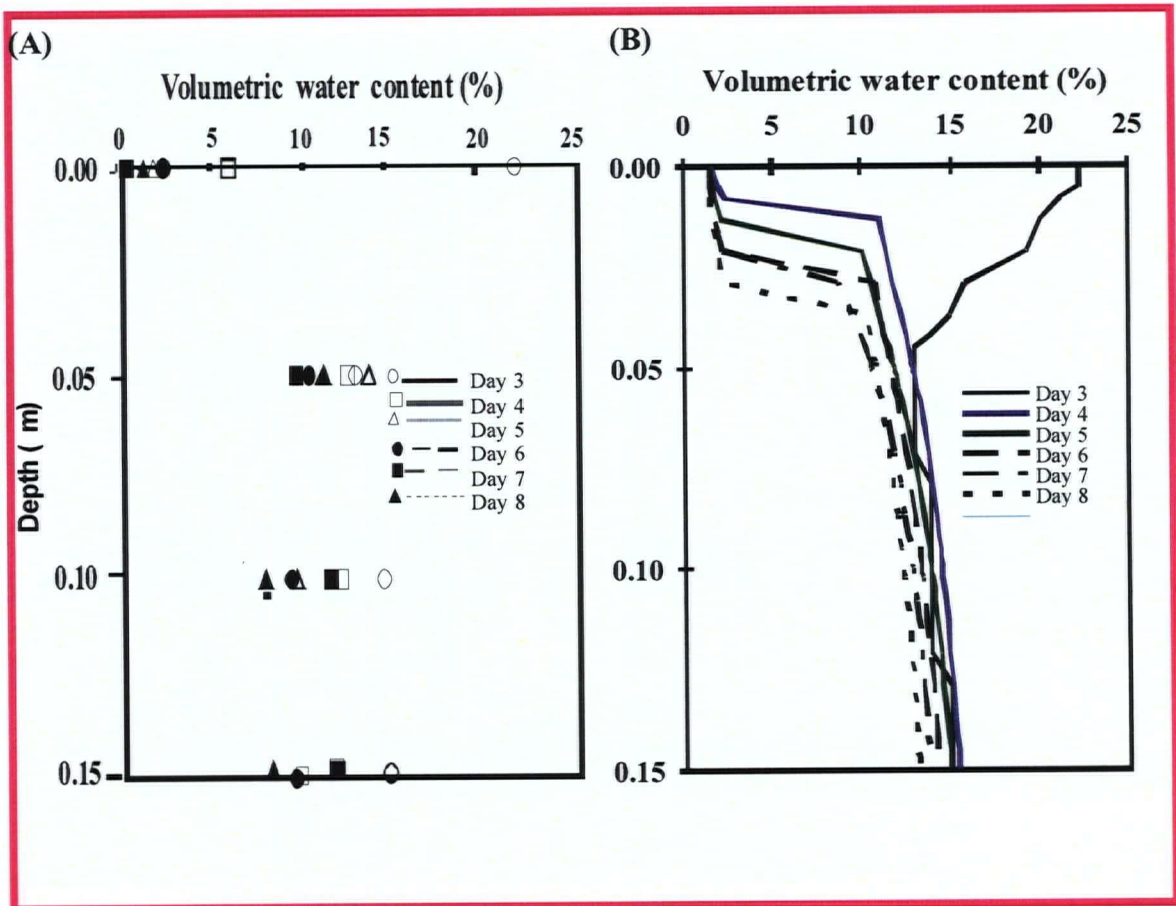
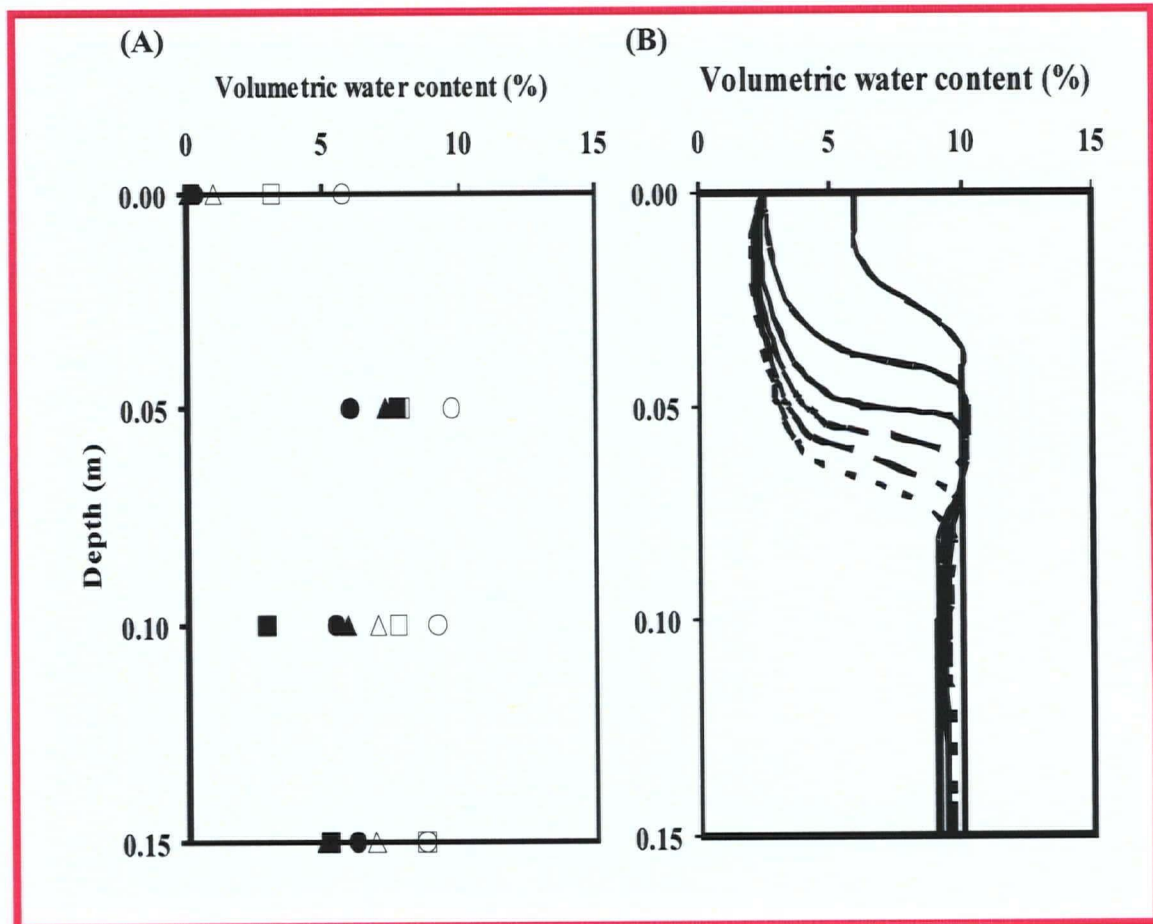


Figure 5.11. Comparison of (A) measured and (B) SoilCover predicted water content profiles for the 8-day test period [July 30 (day 1) to August 6 (day 8), 2002] at the Deilmann north waste-rock (DNWR) pile.



Δ ○ — Day 3
 □ — Day 4
 △ — Day 5
 ● — Day 6
 ■ — Day 7
 ▲ — Day 8

Figure 5.12. Comparison of (A) measured and (B) SoilCover predicted water content profiles for the 8-day test period [July 30 (day 1) to August 6 (day 8), 2002] at the Deilmann south waste-rock (DSWR) pile.

5.4 CO₂ Diffusion Prediction and Model Proposed

This section presents the important theoretical relationships used to quantify CO₂ production and diffusion through unsaturated geologic media. The theoretical of the partial differential equation describing the change in CO₂ concentration with depth and time as a function of CO₂ production and diffusion is also presented. The section is concluded with the description of a relatively simple computer code program used to solve the finite difference formulation of the governing equation of the model developed in this work. The processes of diffusion, production of CO₂, the equations describing one-dimensional transient CO₂ diffusion and production are described below.

5.4.1 CO₂ diffusion

Gas dynamics in most soil systems is a three-dimensional problem, but the use of one-dimensional models is generally accepted (de Jong and Schappert, 1972; Collin and Rasmuson, 1988). One-dimensional CO₂ diffusion in a gaseous environment is commonly described by Fick's First Law that defines the mass flux of CO₂ in a given direction as directly proportional to the negative of the concentration gradient in that direction (Fetter, 1993):

$$F_{\text{CO}_2} = -D \frac{\partial C}{\partial z} \quad [5.3]$$

where: F_{CO_2} = mass flux of CO₂ (kg m⁻² s⁻¹),

D = the free air diffusion coefficient (m² s⁻¹),

C = CO₂ concentration (kg m⁻³), and

Z = depth (m).

The use of Equation 5.3 assumes that Fick's law adequately describes the diffusive gas flux. For gases such as CO_2 , which have sources or sinks in the system and constitute a small fraction of the total system pressure, this appears to be true (Thorstenson and Pollock, 1989). The diffusion coefficient in air (similar to atmospheric composition) for CO_2 is $1.39 \times 10^{-5} \text{ m}^2 \text{ s}^{-1}$ (at 0°C) (Weast and Astle, 1981). The diffusion coefficient increases with increasing temperature and decreasing molecular weight (Fuller et al., 1966).

Aubertin et al. (2000) described the use of an equivalent porosity to represent the effective porosity available for the diffusion of oxygen. Applying this relationship for CO_2 diffusion transforms the water porosity into an equivalent air porosity by partitioning it with Henry's Law coefficient as follows:

$$\theta_{\text{eq}} = \theta_{\text{a}} + \theta_{\text{w}}H \quad [5.4]$$

where: θ_{eq} = equivalent porosity ($\text{m}^3 \text{ m}^{-3}$),

θ_{a} = air porosity ($\text{m}^3 \text{ m}^{-3}$),

θ_{w} = water porosity ($\text{m}^3 \text{ m}^{-3}$), and

H = Henry's Law coefficient (approximated as 0.03 for CO_2 in air and water at 25°C) (Hendry et al., 1993).

Increasing water saturation decreases the equivalent and effective porosity and reduces CO_2 diffusion. Using Henry's law to represent phase partitioning of a reactive gas, such as CO_2 , is an approximation of the true process (Hendry et al., 1993).

Fick's First Law defining CO₂ diffusion through porous media as a function of the equivalent porosity is defined by:

$$F_{\text{CO}_2} = -\theta_{\text{eq}} D^* \frac{\partial C}{\partial z} \quad [5.5]$$

where: F = mass flux of CO₂ (Kg m⁻² s⁻¹),
 θ_{eq} = equivalent porosity (m³ m⁻³),
 D^* = bulk diffusion coefficient (m² s⁻¹),
 C = CO₂ concentration (Kg m⁻³), and
 Z = depth (m).

The equivalent porosity and the bulk diffusion coefficient (D^*) are often combined into a variable D_e , the effective diffusion coefficient, to give:

$$D_e = \theta_{\text{eq}} D^* \quad [5.6]$$

Then Equation 5.5 can be written in terms of the effective diffusion coefficient as:

$$F_{\text{CO}_2} = -D_e \frac{\partial C}{\partial z} \quad [5.7]$$

In soils both diffusion and chemical reactions will determine the CO₂ gradient as described by Fick's second law. Assuming steady state conditions, this law can be written as (Hendry et al., 1999):

$$D_e \frac{\partial^2 C}{\partial z^2} = -G \quad [5.8]$$

where G is a reaction rate ($\mu\text{g CO}_2 \cdot \text{g dry soil}^{-1} \cdot \text{d}^{-1}$).

Aubertin et al. (2000) and Mbonimpa et al. (2003) also defined the effective diffusion coefficient (D_e) from Equation 5.6 as a function of the components of the diffusion in the air and water phase as represented in Equation 5.9.

$$D_e = D_a + HD_w \quad [5.9]$$

Where: D_a = diffusion coefficient component through air phase ($\text{m}^2 \text{s}^{-1}$),
 D_w = diffusion coefficient component through water phase ($\text{m}^2 \text{s}^{-1}$),
 H = Henry's coefficient as defined above.

$$D_a = \theta_a D_a^0 T_a \quad \text{and} \quad D_w = \theta_w D_w^0 T_w \quad [5.10]$$

where: D_a^0 = diffusion coefficient of CO_2 through air ($\text{m}^2 \text{s}^{-1}$),
 D_w^0 = diffusion coefficient of CO_2 through water ($\text{m}^2 \text{s}^{-1}$),
 T_a = tortuosity coefficient for air phase, and
 T_w = tortuosity coefficient for water phase.

The tortuosity coefficients are related to the properties of the material through the following equations (Collin and Rasmuson, 1988; Mbonimpa et al., 2003):

$$T_a = \frac{\theta_a^{2x+1}}{\theta^2} \quad [5.11]$$

$$T_w = \frac{\theta_w^{2y+1}}{\theta^2} \quad [5.12]$$

$$\theta_a^{2x} + (1 - \theta_a)^x = 1 \quad [5.13]$$

$$\theta_w^{2y} + (1 - \theta_w)^y = 1 \quad [5.14]$$

where: θ = total porosity.

Mbonimpa et al. (2003) noted that a reasonable estimation of the value of the variables x and y is 0.75. Using this value for x and y and combining Equations 5.9 – 5.12, the diffusion coefficient equation can be simplified to the Equation 5.15 (Aachib et al., 2002, 2004).

$$D_e = \frac{1}{\theta^2} \left[D_a^0 \theta_a^{3.5} + H D_w^0 \theta_w^{3.5} \right] \quad [5.15]$$

Equation 5.15 was used in the model adopted in this thesis for the evaluation of CO_2 diffusion.

An example of the variation of the effective diffusion coefficient D_e as a function of water porosity θ_w is illustrated in Figure 5.13B. The water contents profiles in Figure 5.13A represent hypothetical drying forcing conditions generated in unsaturated sand material. The initial water-depth profile (curve d1, Figure 5.13A), however, represents

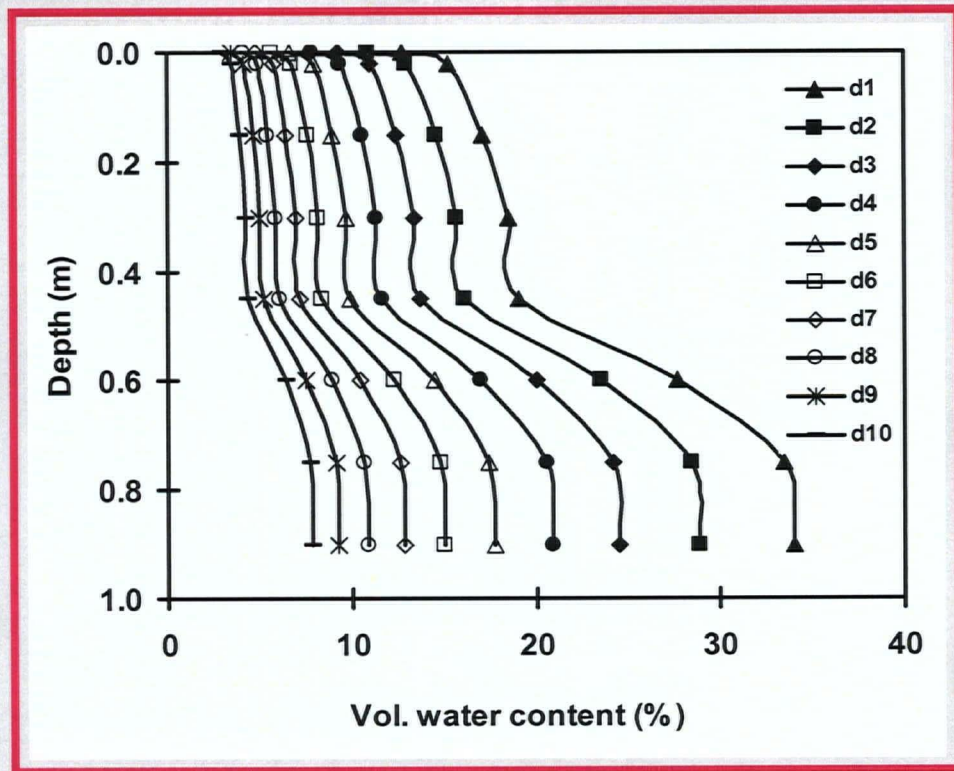


Figure 5.13A. Hypothetical water content profiles in unsaturated sand Material. Curve d1 is an actual measured water profile in the HT minicosm.

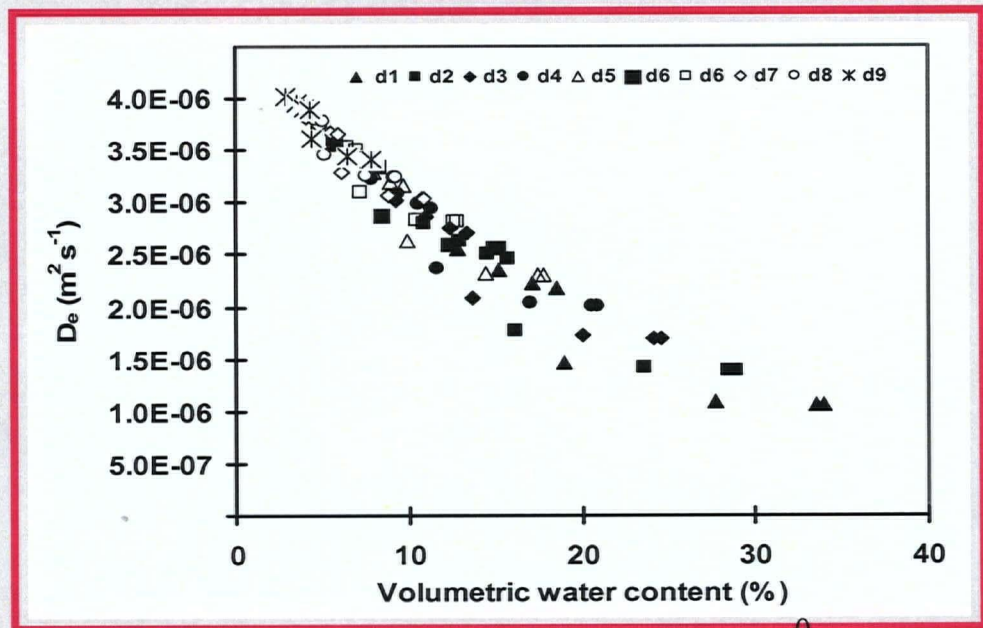


Figure 5.13B. Simulated effective diffusion coefficient (D_e) of CO_2 as a function of water content using hypothetical data presented above.

the measured mean water-depth profile in the HT minicosm column described in Section 3.3 of Chapter 3 of this thesis and in Kabwe et al. (2002). The subsequent profiles were generated by reducing the initial water-depth profile (curve d1) by a factor of 0.1 consecutively. The corresponding simulated changes of the effective diffusion coefficient D_e of CO_2 was computed using Equation 5.15 with the parameters: $\theta = 0.40$ and $D_a^0 = 1.39 \times 10^{-5} \text{ m}^2 \text{ s}^{-1}$ and $H = 0.03$. The general trend shows an increase in the D_e with a decrease in water content or vice versa, as shown in Figure 5.13B. The dependency of the D_e on soil water content for different textured soils is well documented (Klute and Letey, 1958; Rowell et al., 1967; Collin and Rasmuson, 1988; Mbonimpa et al., 2003). The diffusion coefficient of CO_2 in water is about four orders of magnitude slower than that in the air-filled voids.

5.4.2 Biotic CO_2 production rate

As discussed in the previous chapter CO_2 can be produced in biotic reaction (e.g., microbial respiration) or in abiotic (e.g., carbonate buffering) reactions. However the model developed in this thesis will only be focused on biotic reaction. It should be noted that the DCC method was tested and verified in mesocosms filled with fine-grained sand excavated from the C-horizon of an unsaturated zone at a local field site located near Saskatoon, Saskatchewan (Hendry et al., 1993; Kabwe et al., 2002). Studies on microbial aspects of the mesocosm indicated that biological activity within the mesocosm was likely sufficient to account for the generation of CO_2 throughout the profile (Hendry et al., 2001; Lawrence et al., 1993). The "CO₂" model described in this thesis will be also tested and validated with mesocosms measured data.

The CO₂ production (microbia) rate (G) can be described by a function similar to that used by Hendry et al. (1999):

$$G = \theta_a^2 G_o [g(T)g(\theta_w)g(z)] \quad [5.16]$$

Where: G = CO₂ production rate (kg C kg⁻¹ dry soil day⁻¹),
 G_o = reference production rate (kg C kg⁻¹ dry soil day⁻¹),
 $g(T)$ = the production contribution based on temperature,
 $g(\theta_w)$ = the production contribution based on soil moisture content,
 $g(z)$ = the production contribution based on depth.

The function provides the option of determining the G term as a function of temperature, soil moisture content, and/or depth. The functional dependence of production upon temperature, soil moisture content and depth are (Hendry et al., 1999):

$$g(T) = e^{k(T-\bar{T})} \quad [5.17]$$

when: $T > T_{\min}$ and k is arbitrary

The lowest temperature at which CO₂ production occurs is T_{\min} .

$$g(T) = 0 \quad [5.18]$$

When: $T < T_{\min}$

$$g(\theta_w) = \theta_w^a \quad [5.19]$$

where: $a = \text{arbitrary}$

$$g(z) = e^{-bz} \quad [5.20]$$

where: $b = \text{arbitrary.}$

These functions represent the influence of the primary independent variables (Hendry et al., 1999): $g(T)$ is the Arrhenius equation, where a $Q_{10}(=e^{10k})$ value determines the degree to which respiration increases with a 10°C increase in temperature; $g(z)$ represents the commonly observed (e.g., Simunek and Suarez, 1993) exponential decrease in productivity with depth; and the combination of $\theta_a g(\theta_w)$ serves to reflect the reduction in activity which typically occurs at high and low water contents (Ekpete and Cornfield, 1965; Rixon, 1968; Grant and Rochette, 1994; Hendry et al., 1999).

The biotic production rate used in the model developed in this thesis was represented by a function similar to that used by Hendry et al., 1999 (the Equation 5.21):

$$G = G_o \theta_a^a \theta_w^b e^{k_r(T-\bar{T})} \quad [5.21]$$

where: $k_r = \text{constant in the Arrhenius equation } (^\circ\text{C}^{-1}) (k_r=0.044^\circ\text{C}^{-1}),$
 $T = \text{measured temperature } (^\circ\text{C}), \text{ and}$

\bar{T} = reference temperatures ($^{\circ}\text{C}$).

The parameters a and b are fitting parameters. Note that the coefficient $Q_{10}(=e^{10kr})$ is often used to represent the relative increase in respiration intensity per 10°C increase in temperature. The value of $k=0.044^{\circ}\text{C}$ indicates an average Q_{10} of 1.6. The variability in Q_{10} is most likely attributed to differences in microbial community structure. It is acknowledge that sensitivity analysis demonstrated that G is only weakly dependent on $1 < b < 3$ (Hendry et al., 1999).

Figure 5.14 illustrates the simulated microbial respiration rates as a function of temperature and water content using Equation 5.21. Values of the parameters in Equation 5.14 used in the simulations were specified by Hendry et al. (2001): $a = 2$; $b = 1.25$, $k = 0.044^{\circ}\text{C}$; $G_o = 207 \mu\text{g C.g}^{-1}.\text{d}^{-1}$ when $T = 6.17^{\circ}\text{C}$. The production of CO_2 was attributed to microbial activity in the C-horizon sand (Hendry et al., 2000).

The simulated results show that at low water content (θ_w), CO_2 production decreases because of a lack of water; at high θ_w , production also decrease because of excess water filling the pore spaces. The model simulation shows that the maximum microbial CO_2 production occurred at a water content of 0.25 that corresponds to a water saturation of 70% (e.g., for $\theta = 0.40$). This is within values reported in the literature. Linn and Doran (1984) observed that soil incubated with 60% soil pore space filled with water, supported maximum aerobic microbial activities.

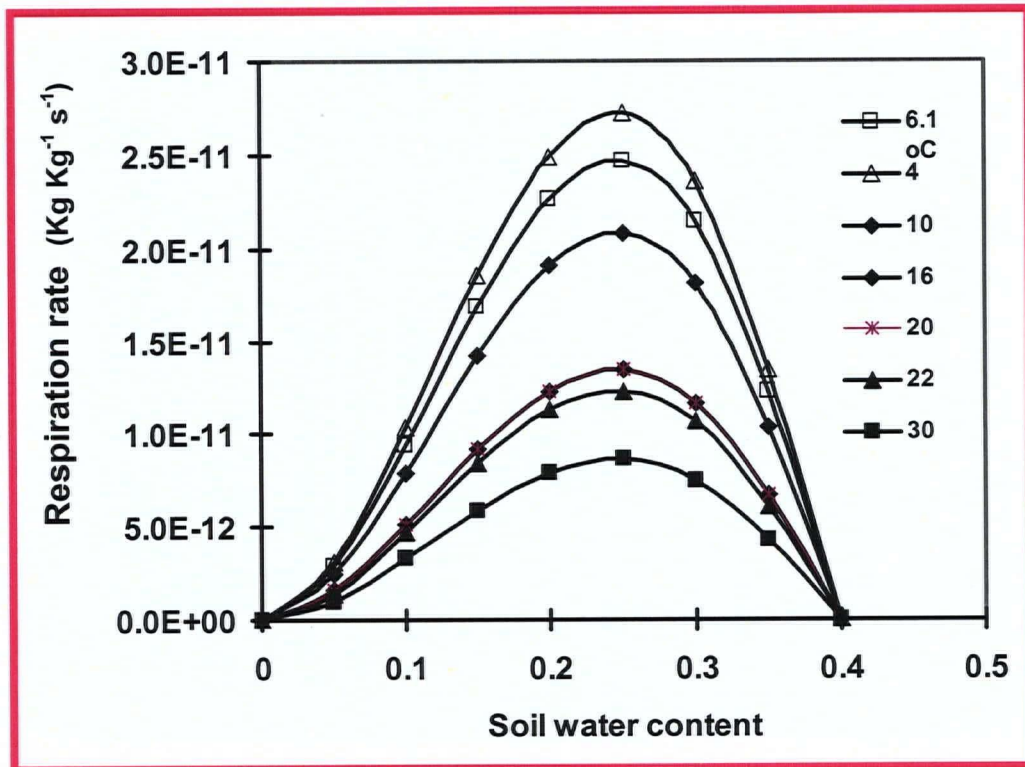


Figure 5.14. Simulated microbial respiration rates as a function of temperature and water content using Equation 5.21.

5.4.3 Development of the partial differential equation

The following section presents the development of the partial differential equation describing the change in CO_2 concentration with depth and time as a function of CO_2 diffusion and production.

Let's consider a representative elementary volume (REV) for derivation of the partial differential equation as illustrated in Figure 5.15.

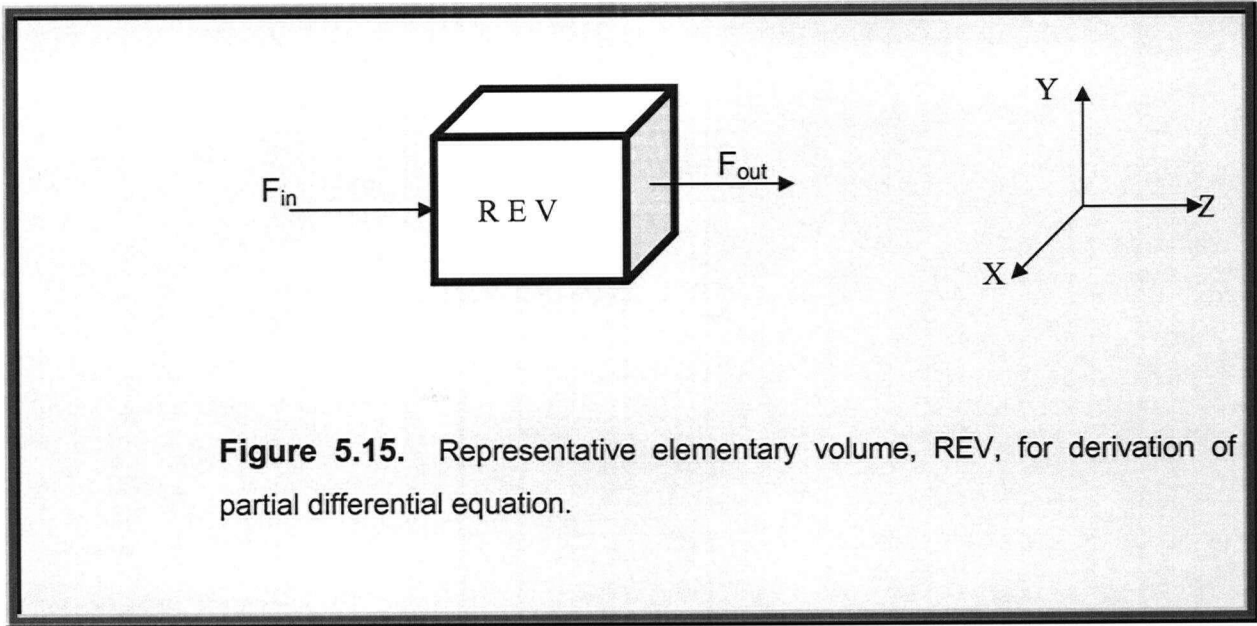


Figure 5.15. Representative elementary volume, REV, for derivation of partial differential equation.

By applying the conservation of mass principle to a porous, cubic volume (dimensions: dx , dy , dz) through which a gaseous species is diffusing (the mass flux entering the volume (F_{in}) minus the mass flux exiting the volume (F_{out}) must equal the change in storage ($\partial m/\partial t$): where F = mass of gaseous species per unit of area per unit of time in the z direction.

$$(F_{in} - F_{out})dx dy + G(dx dy dz) = \frac{\partial m}{\partial t} \quad [5.22]$$

where: G = production rate of gaseous species within cubic volume (kg C kg^{-1} dry soil day^{-1}),
 m = total mass of gaseous species within cubic volume (kg m^{-3}), and
 t = time (s).

Equation 5.22 can be rewritten as:

$$\left(F_{in} - \left(F_{in} + \frac{\partial F}{\partial z} dz \right) \right) dx dy + G(dx dy dz) = \frac{\partial m}{\partial t} \quad [5.23]$$

The mass of gaseous species found in the pore gas and pore water of the cubic volume can be represented by:

$$m = (C_a \theta_a dx dy dz) + (H C_a \theta_w dx dy dz) \quad [5.24]$$

where: C_a = mass of gaseous species /volume of pore gas (kg m^{-3}),

H = Henry's law coefficient,

θ_a = air porosity ($\text{m}^3 \text{m}^{-3}$), and

θ_w = water porosity ($\text{m}^3 \text{m}^{-3}$).

Considering Equations 5.8 ($F = -D_e \frac{\partial C}{\partial z}$) and 5.24, Equation 5.23 can be rewritten:

$$\frac{-\partial \left(-D_e \frac{\partial C_a}{\partial z} \right) dx dy dz}{\partial z} + G(dx dy dz) = \frac{\partial (C_a \theta_a dx dy dz + H C_a \theta_w dx dy dz)}{\partial t} \quad [5.25]$$

Assuming that θ_a and D_e do not vary over the depth interval ∂z and that θ_a , θ_w , H , dx , dy , and dz do not vary over time interval ∂t , Equation 5.25 can be simplified to Equation 5.26 similar to Hendry et al. (2001):

$$D_e \frac{\partial^2 C_a}{\partial z^2} + G = (\theta_a + H\theta_w) \frac{\partial C_a}{\partial t} \quad [5.26]$$

Equation 5.26 is the governing equation used in the model.

5.4.4 Finite difference formulation

The simple model developed in this thesis used a finite difference numerical method to solve the partial differential equation given by Equation 5.26. The numerical method offers a discrete approximation to problems with complex physical properties and geometry, but requires numerous calculations, which are lessened by the use of digital computers capable of performing numerous calculations quickly. The finite difference formulation of Equation 5.26 is a simple calculation based on approximating the derivatives of the function, resulting in a solution only at the discrete points (Lin et al., 1997). For a number of nodes there will be n linear equations, hence the problem may be solved (Freeze and Cherry, 1979). The finite difference method has many advantages, including: simple problems are easily solved, abundance of literature, successful algorithms are available to solve the system of equations and the accuracy is good.

To develop the finite difference formulation defining the change in concentration at a given node, three nodes were defined as shown in Figure 5.16. The nodes represent the center of the finite difference element. The three mass fluxes (F_{in} , F_{out} , and F_{prod}) are defined in Equations 5.27, 5.28, and 5.29:

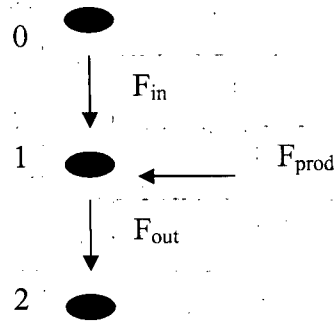


Figure 5.16. Three nodes and the mass fluxes entering and exiting node1 for development of the finite difference formulation.

$$F_{\text{out}} = -D_e \frac{\partial C}{\partial z} = -D_{e1,2} \frac{(C_2 - C_1)}{(z_2 - z_1)} \quad [5.27]$$

$$F_{\text{in}} = -D_e \frac{\partial C}{\partial z} = -D_{e0,1} \frac{(C_1 - C_0)}{(z_1 - z_0)} \quad [5.28]$$

$$F_{\text{prod}} = G\Delta z_{0,1,2} \quad [5.29]$$

Substituting these three equations and Equation 5.23 into Equation 3.19 results in Equation 5.30

$$-D_{e0,1} \frac{(C_1 - C_0)}{(z_1 - z_0)} + D_{e1,2} \frac{(C_2 - C_1)}{(z_2 - z_1)} + G = \frac{\theta_{\text{eq}} \Delta C_1 |\Delta z_{0,1,2}|}{\Delta t} \quad [5.30]$$

and solving Equation 5.30 for the change in concentration (ΔC_1) gives Equation 5.31, which defines the change in concentration at node 1 over a given time-step (Δt):

$$\Delta C_1 = \frac{\Delta t}{|\Delta z_{0,1,2}| \theta_{eq}} \left[-D_{e0,1} \frac{(C_1 - C_0)}{(z_1 - z_0)} + D_{e1,2} \frac{(C_2 - C_1)}{(z_2 - z_1)} + G \right] \quad [5.31]$$

where: $C_0(t)$, $C_1(t)$ and $C_2(t)$ are the concentrations of CO_2 at time (t) at three adjacent nodes of increasing depth numbered 0, 1 and 2; z_0 , z_1 and z_2 are the depths below ground surface of the three nodes; $D_{e0,1}(t)$ and $D_{e1,2}(t)$ are the effective diffusion coefficients between nodes 0 and 1, and 1 and 2 respectively, determined at time (t); $\theta_{eq1}(t)$ is the equivalent porosity at node 1 at time t and; $\Delta z_{0,1,2}$ is the distance between the midpoint between nodes 0 and 1 and the midpoint between nodes 1 and 2. $D_{en,n+1}(t)$ is calculated from the mean of $D_{en}(t)$ and $D_{en+1}(t)$. The maximum length of each time step within the diffusion model was determined by:

$$\frac{D_e \Delta t}{\Delta z^2} = 0.5 \quad [5.32]$$

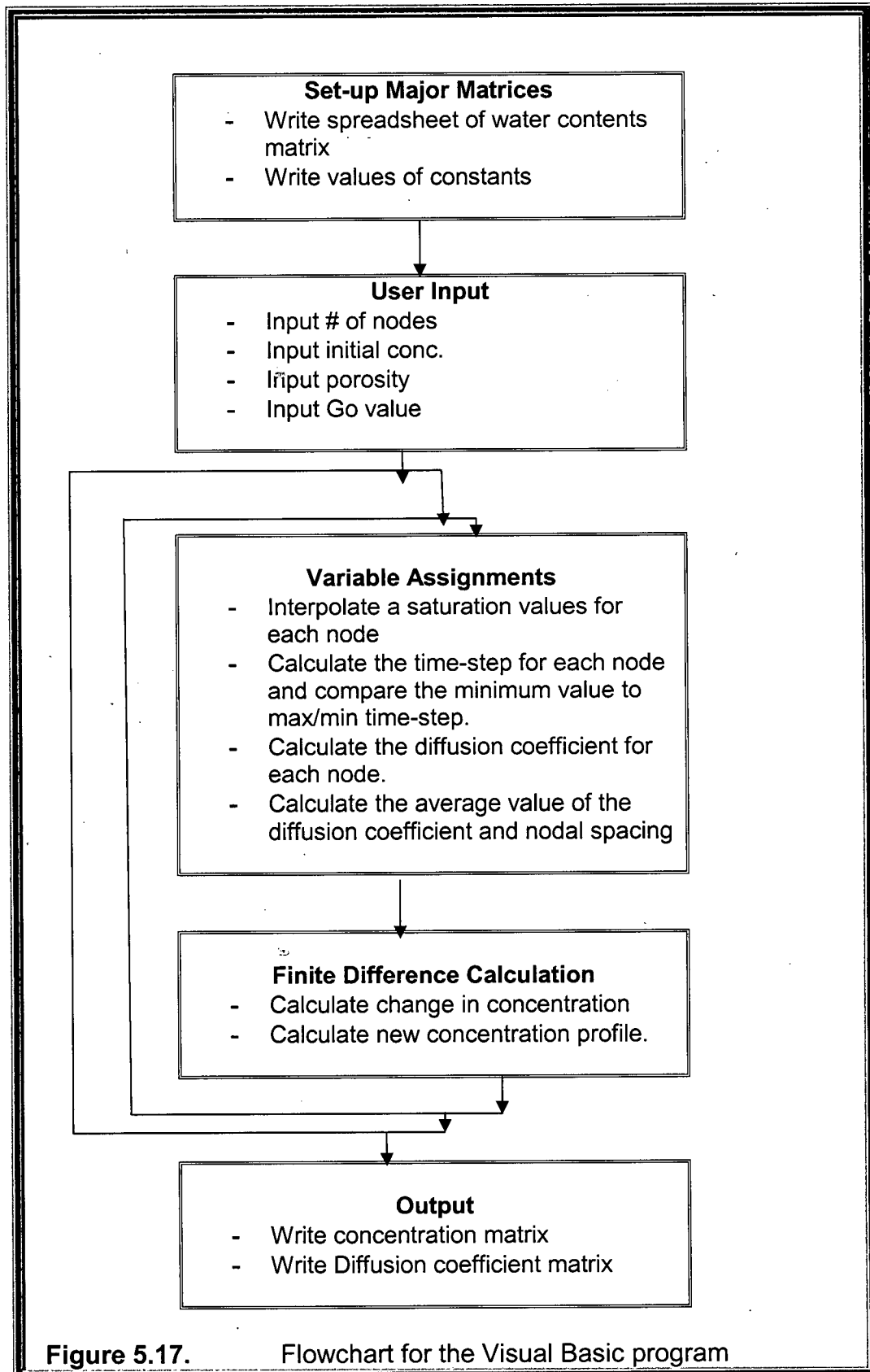
The variable defined as $\Delta z_{0,1,2}$ in Equation 5.31 is the average of the two spaces on either side of the node 1. A value of Δt was calculated at every node in the profile, and the smallest time step was used. For all the variables, the subset numbers separated by commas indicate the node(s) from which the variable must be calculated. Values of T and θ_w were interpolated onto the grid in both time and space.

The boundary condition for the finite difference solution is a constant concentration at the top. Atmospheric concentration is the constant value for the surface node (e.g., 0.036% CO₂ atmospheric concentration).

5.5 Computer Code Program

A simple computer program called "CO2" was written using Macro Visual Basic of Microsoft Excel to solve Equation 5.30. The full Visual Basic codes for the model is provided in Appendix B. A flow chart for the program is shown in Figure 5.17. The model uses water content matrix (depth and time) as the input for the diffusion and production calculations. The model is therefore, able to use the SoilCover water content (or saturation) output as input to the "CO2" model to calculate the change in CO₂ concentration with depth and time as a function of CO₂ diffusion and production.

The upper boundary condition (depth of 0 m) of the model was constrained to volumetric concentration of 0.036 % for CO₂. This represents the relative concentration of CO₂ in the atmosphere. The model required values for soil porosity (bulk), volumetric water contents profile and temperature. CO₂ concentration profiles were also required to run the model. Initial concentration depth profiles provided a starting point for the model while concentration profiles at a later time provide the model with values it could attempt to match. CO₂ production was determined as a function of G_o , soil air porosity (θ_a), and soil moisture content (θ_w) with G_o being the only fitted parameter. The arbitrary parameter "a" was set at 2 which maximized the product of θ_a^2 and θ_w^2 at a degree of saturation of 0.70 (where degree of saturation is the ratio of the volume of water-filled voids to the volume of total void space). Maximum reactivity at a degree of saturation of 0.70 was reasonable because ample amounts of both water and CO₂ (from pore gas)



for reactions would be available. A degree of saturation of 0.70 also agreed with literature values of maximum respiration rates.

The program structure consisted of two nested loops: the innermost loop and the outer loop (Figure 5.17). The innermost loop occurs for each time-step and is where the finite difference calculation takes place. The outer loop occurs for each “day” where the program starts by creating all major matrices. The user uses the input spreadsheet (described later in this section) to input the initial concentration profile and the total porosity (assume to be the same throughout the profile). The minimum and maximum time-step value is specified but can be changed if desired. These values limit how small or how large the time-step value get. The time-step is calculated as a function of the coefficients in the finite difference equation. The formula used to calculate the time-step is given in Equation 5.30 that defines the time-step required for mathematical stability (Zill and Cullen, 1992). It was determined from trial simulations that for most modeling scenarios, 350 iterations were required to reach stability (See Figure 5.18). The model calculates the time-step for each node then takes the minimum value and compares it to the maximum and minimum time-step specified by the program or the user. As noted in the Figure 5.18, convergence was achieved after 350 iterations. The stability was poor below 200 iterations. Hence, 350 iterations were performed for each simulation.

The output of the model is a spreadsheet file containing the: day #, iteration #, nodes, new concentration, concentration changes, diffusion, saturation and time difference calculated values are presented in Appendix B.

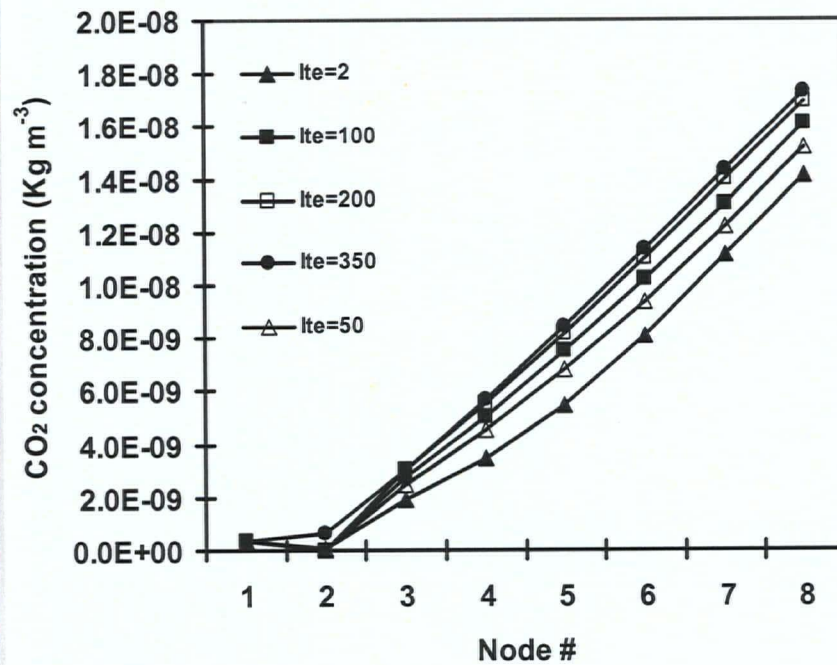


Figure 5.18 Stability curves generated by the model for different iterations using time steps of 0.05 day.

5.6 Application of the CO₂ Model Using Measured Values in Sand Minicosms

The theory and development of a numerical model for CO₂ diffusion and transport were presented in the previous sections. The model was based on the finite difference method to solve the one-dimensional diffusion equation using the program Macro Visual Basic.

The experiments for the dynamic closed chamber (DCC) method were designed and carried out to evaluate the ability and accuracy of the DCC to measure CO₂ fluxes under actual field conditions on the surfaces of the DNWR and DSWR. However, no instrumentation was installed to measure CO₂ concentrations and gradients in the shallow profile within the upper meter of the waste rock piles. Therefore, it is not possible to rigorously test the full utility of the CO₂ model following the heavy rainfall event similar to the SoilCover modeling that was conducted to predict changes in soil water content. The "CO₂" model is evaluated in this section for the prediction of CO₂ concentrations measured in the minicosms experiments previously described in section 3.3 (Kabwe 2001 and Kabwe et al., 2002). The simulation results are interpreted and discussed in the following sections.

5.6.1 Prediction of CO₂ concentration profiles in response to changes in water contents profiles

It was shown in the previous sections that changes in microbial respiration can result from changes in temperature and water content. In the following simulations hypothetical water content profiles for the sand column were used to illustrate the

effects of water content on the effective diffusion coefficient and CO₂ gas concentration depth- profiles in the sand column. Figure 5.19A shows the hypothetical water profiles in a sand column. These profiles were generated by progressively reducing the initial water content profile (curve d1) by a factor of 0.8 consecutively. It should be noted that the initial water content profile (curve d1) is a real measured water profile of a sand column (HT) described in Kabwe (2001) and Kabwe et al.(2002).

In this example, the initial water contents at 0, 0.45 and 0.9 m depths (curve d1) were 12, 20 and 34 % respectively. The final hypothetical water contents at 0, 0.45 and 0.9 m depths (curve d10) were 3, 4 and 8 % respectively.

The corresponding starting CO₂ concentration profile (Figure 5.19B, curve d1) represented the actual measured CO₂ concentrations for the sand column described in Kabwe et al. (2002). In this example, the CO₂ concentrations at 0.15, 0.30 and 0.60 m depths were 0.082, 0.14 and 0.15% respectively. The subsequent simulated changes in CO₂ profiles in the column in response to changes in the water contents profiles presented in Figure 5.19A are shown in Figure 5.19B (curves from d1 to d10). As the soil water content changes from wet to dry conditions (Figure 5.19, curves from right to the left) the CO₂ concentration profiles also increase proportionally (Figure 5.19B, curves from left to the right). At the end of the simulation the CO₂ concentration at 0.15, 0.30 and 0.60 m depths were 0.13, 0.17 and 0.20 %, respectively. Since a constant CO₂ flux was applied to the base of the HT column during the simulation, the change in the CO₂ concentrations profiles was due to the change in the effective diffusion coefficient (D_e) (Equation 5.15) for CO₂, which is a function of water content. The general trend showed a decrease in the D_e with an increase in water content.

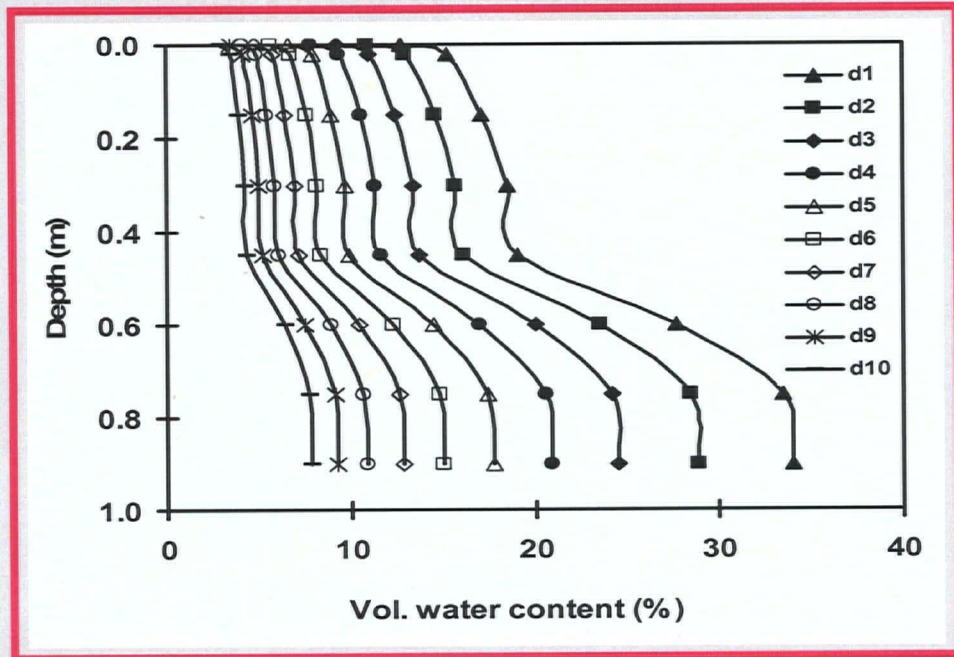


Figure 5.19A. Hypothetical water contents profiles in a sand material described in Figure 5.13A.

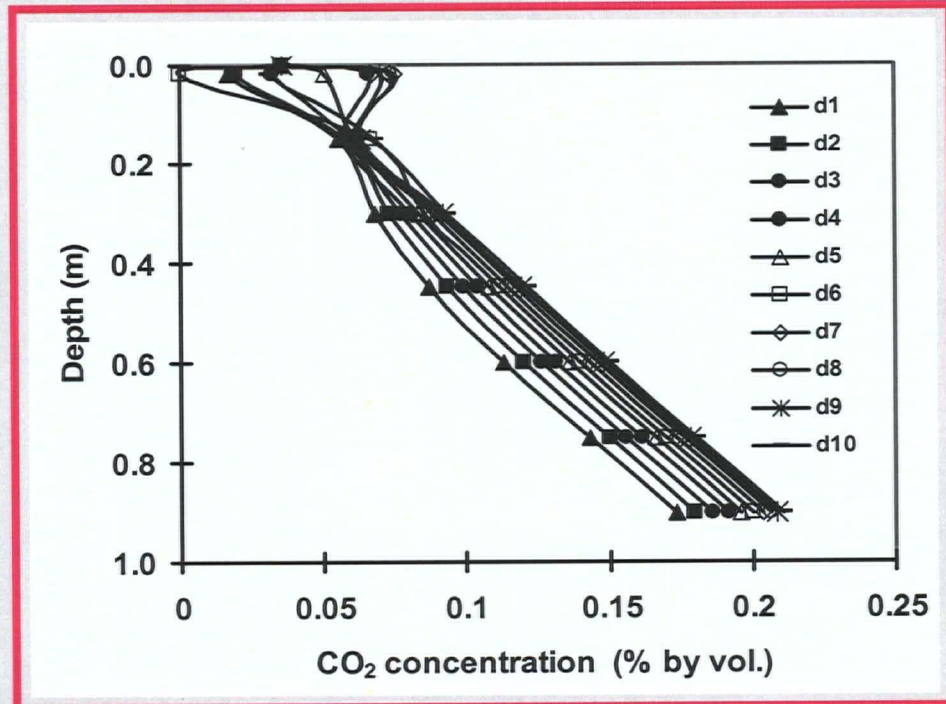


Figure 5.19B. Model predicted CO₂ concentrations profiles in a HT sand column obtained with hypothetical simulated water contents profiles (Figure 5.19A) and an initial measured CO₂ concentrations profile (d1) in HT column (Kabwe et al., 2002).

5.6.2 Simulations of CO₂ Concentration Profiles using Sand Minicosm-Measured Data

In order to test the ability of the "CO₂" model to predict the CO₂ diffusion in sand material, simulations were performed using the minicosm-measured data described in section 3.3 of Chapter 3 of this thesis and in Kabwe (2001), Kabwe et al. (2002) and Richards (1998). One minicosm was kept at room temperature (18 - 23 °C) (HT) and another at 5 °C (LT) (see Appendix F). The minicosm experiments started after the minicosms were filled with about 634 kg of sand excavated from an unsaturated C-horizon at a field described in Kabwe et al. (2002) and Richards (1998).

A constant application rate of water (2 L l/week) was applied to the minicosms from the beginning of the experiments. However, each minicosm demonstrated relatively high water release rates during the first 70 days of experiments (Richards, 1998). Effluent rates stabilized after 60 days from the beginning of the experiment. The water contents profiles shown in Figures 5.20A and 5.20B represent mean values of measured water profiles in the minicosms for the period of 100 days from the start of experiments. As expected, the water content increases with increasing depth to the water table. These water profiles were used to predict the changes of CO₂ concentrations profiles in high (HT) (21 – 23 °C) and low (LT) (5 °C) temperature minicosms (Kabwe et al., 2002; Richards, 1998). The measured temperature profiles in the HT (18 – 23 °C) and LT (5 °C) minicosms over the first 100 days after filling are presented in Appendix X. Temperatures remained near constant and the standard deviation was < 1.0 °C (Richards, 1998).

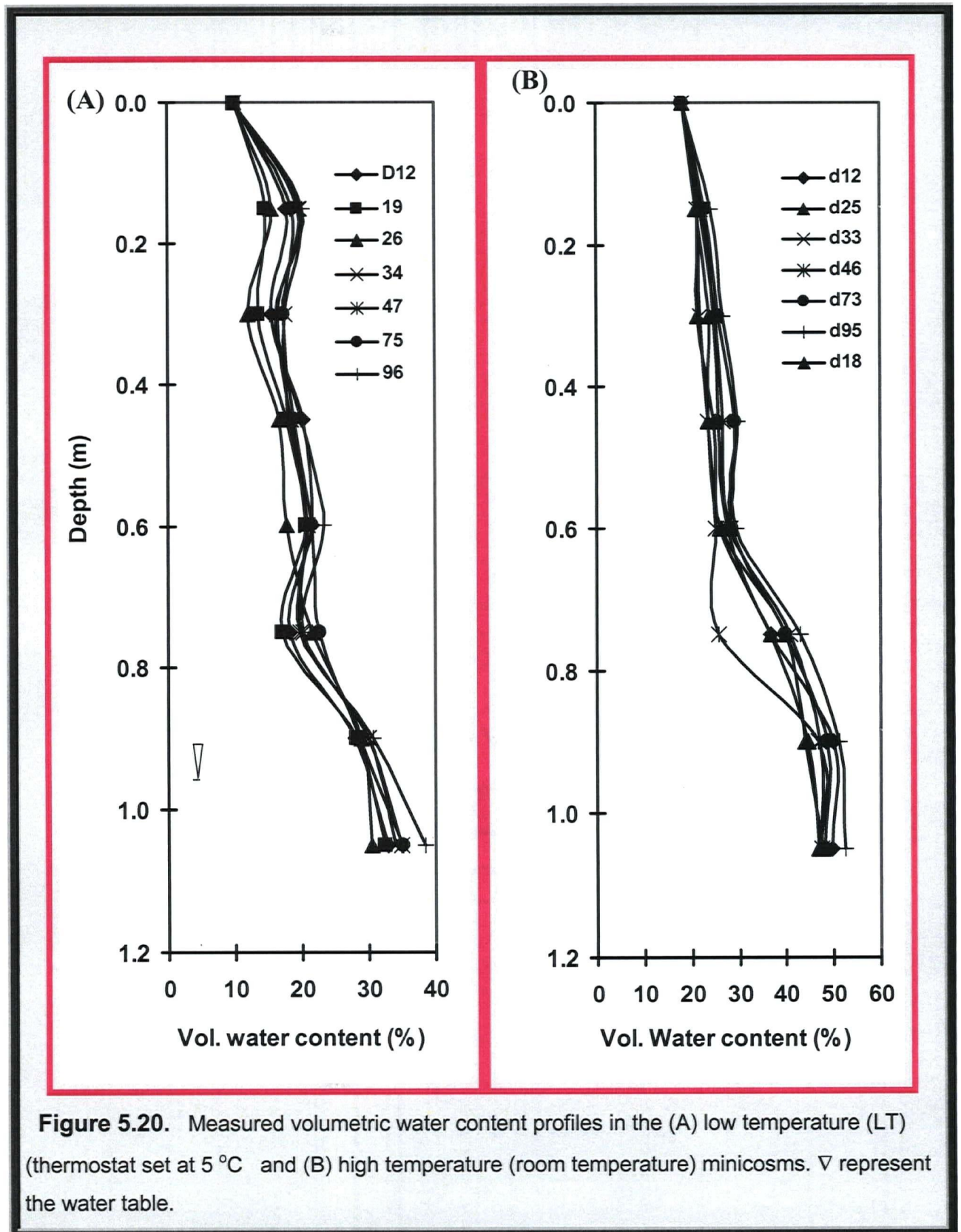


Figure 5.20. Measured volumetric water content profiles in the (A) low temperature (LT) (thermostat set at 5 °C) and (B) high temperature (room temperature) minicosms. ▽ represent the water table.

Responses to short-term fluctuations in room temperature for both LT and HT minicosms were observed only at the 0.02 m depth. For simulation purposes, the average temperatures profiles were used for each minicosm.

Figures 5.21A and 5.21B show the CO₂ concentration profiles for the HT and LT minicosms respectively, measured during the first 100-d period from the beginning of the experiments (Kabwe (2001) and Richards (1998)). The CO₂ concentrations increased with depth, reaching the greatest concentrations at the capillary fringes. During approximately the first 60 days of the experiment, CO₂ concentrations were not yet stable. The generally higher concentrations during the first 60 days were attributed to the disturbance of the soil at the time of excavation and minicosms fillings (Lawrence et al., 1993; Chappelle, 1996). Stable concentration profiles were reached after 80 days at 0.75 m depth (Richards, 1998) but after the initial period of stabilization, CO₂ concentrations at all positions tended to decrease at a low constant rate. The "CO₂" model was used to predict the minicosms concentrations profiles due to changes in the water content profiles described above (Figure 5.20).

To simulate the CO₂ concentrations profiles, the starting CO₂ concentrations profiles and the reference production rate (G_0) were required for the minicosms. The initial concentrations profiles on day 12 (Figures 5.21A and 5.21B) for the LT and HT were used as inputs to predict subsequent concentrations profiles due to changes in water contents profiles (Figure 5.20).

Figures 5.22A and 5.22B show model simulated CO₂ profiles within the LT and HT minicosms respectively, for the case where G^* was characterized by constraining $a = 2$, $b = 1.25$, $k = 0.04$ °C in Equation 5.21, and $G_0 = 270$ µgC g d⁻¹. (Hendry et al., 1999).

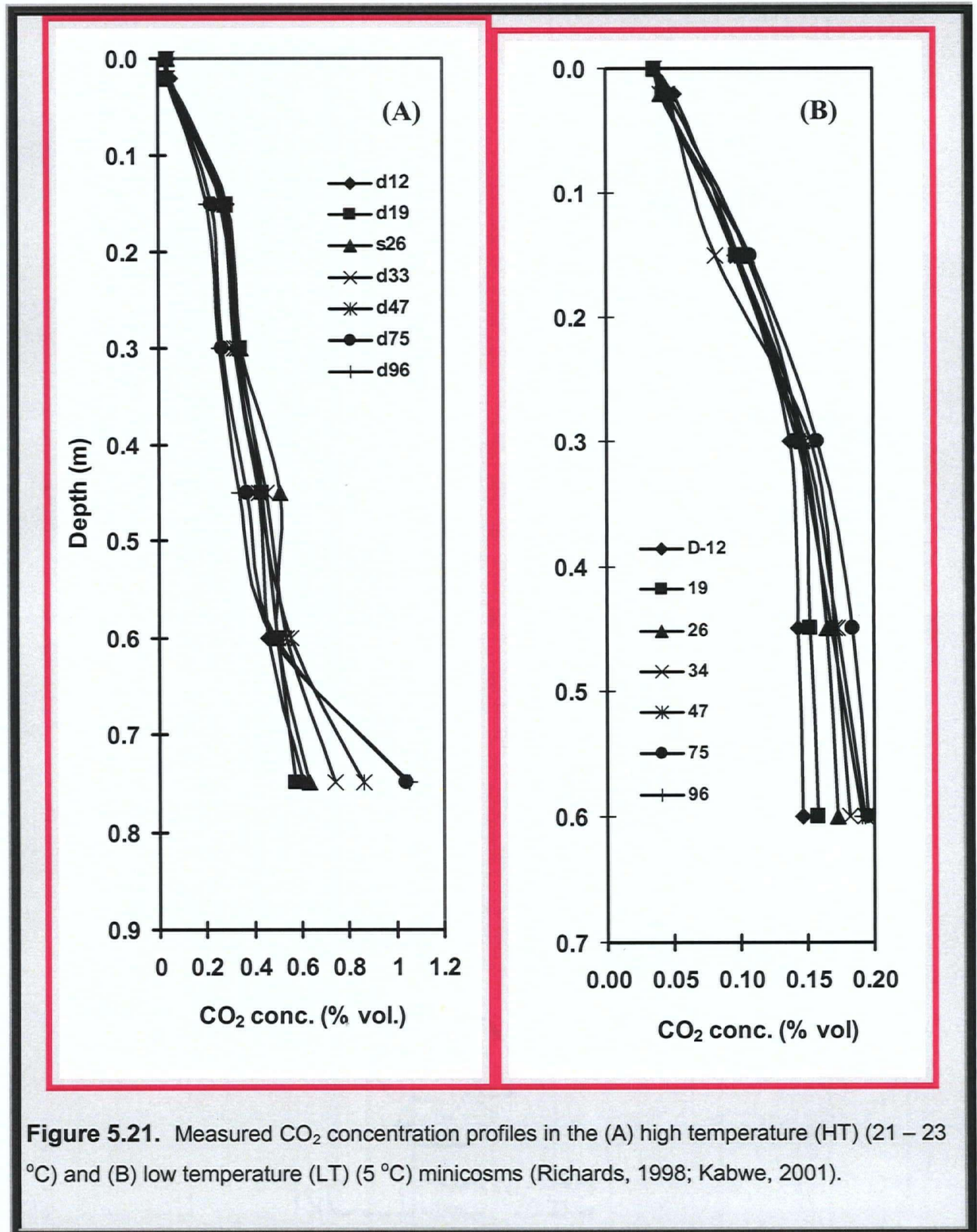


Figure 5.21. Measured CO₂ concentration profiles in the (A) high temperature (HT) (21 – 23 °C) and (B) low temperature (LT) (5 °C) minicosms (Richards, 1998; Kabwe, 2001).

Comparison between the measured (Figures 5.21A and 5.22A) and predicted CO₂ concentration profiles (Figures 5.21B and 5.22B) shows that the model closely approximates the measured CO₂ concentration profiles in both the LT and HT minicosms, except in the region between 0.2 and 0.4 m depth. The relationship between measured and model prediction is shown in Figure 5.23 for the LT and HT minicosms, respectively. Data for the LT minicosm yield a good correlation ($R^2 = 0.98$) between measured and model prediction as compared to $R^2 = 0.74$ for the HT minicosm.

In summary, a simple one-dimensional numerical model for the prediction of changes in the effective diffusion coefficient of CO₂ and its redistribution in subsurface sand material due to changing water contents was developed and validated using minicosm-measured data for unsaturated sand columns. The match between the simulated and the measured concentration profiles for the two minicosms was good. The LT minicosm yielded the best fit ($R^2=0.98$) between the measured and simulated profiles as compared to $R^2=0.79$ for the HT minicosm. It should also be noted that the change in CO₂ concentration profile in the LT minicosm was smaller than that in the HT minicosm over the 100-day test period.

5.7 Prediction of CO₂ Diffusion and Concentration-Depth Profiles in Response to Changes in Water-Depth Profiles in the DSWR

The "CO₂" model was also used to predict CO₂ diffusion and concentration-depth profiles in the DSWR pile. The DSWR was selected for simulations because it has a grain size similar to that of the sand used in minicosms and mesocosm to verify the DCC method (Kabwe et al., 2002). Moreover, the model was also constrained to biotic production rate and that the DSWR pile was controlled by the oxidation of organic

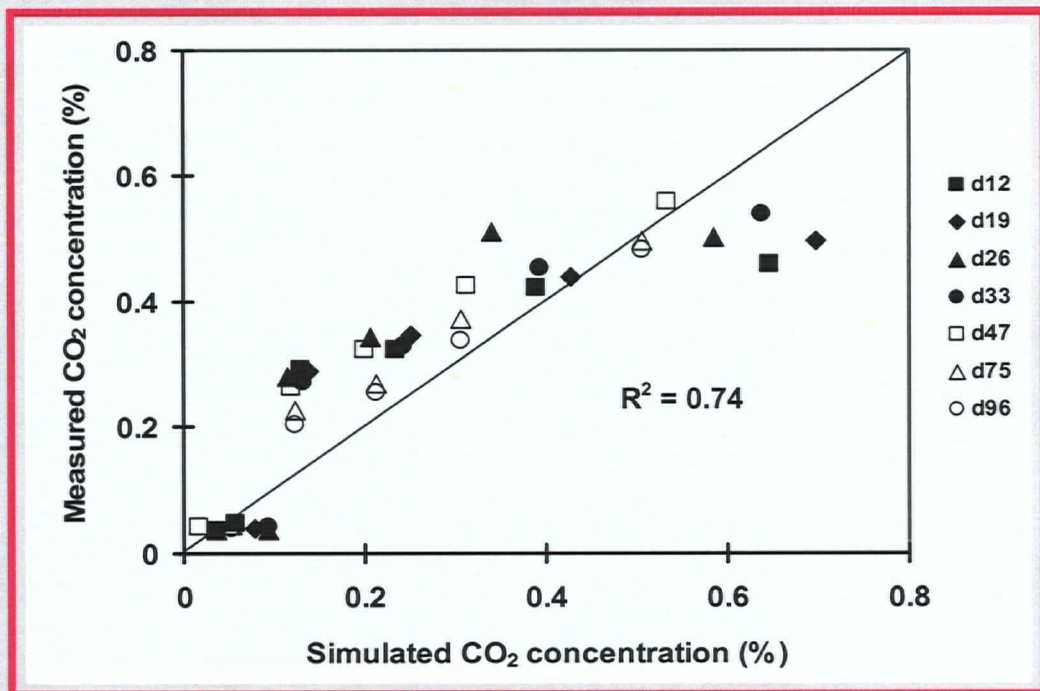
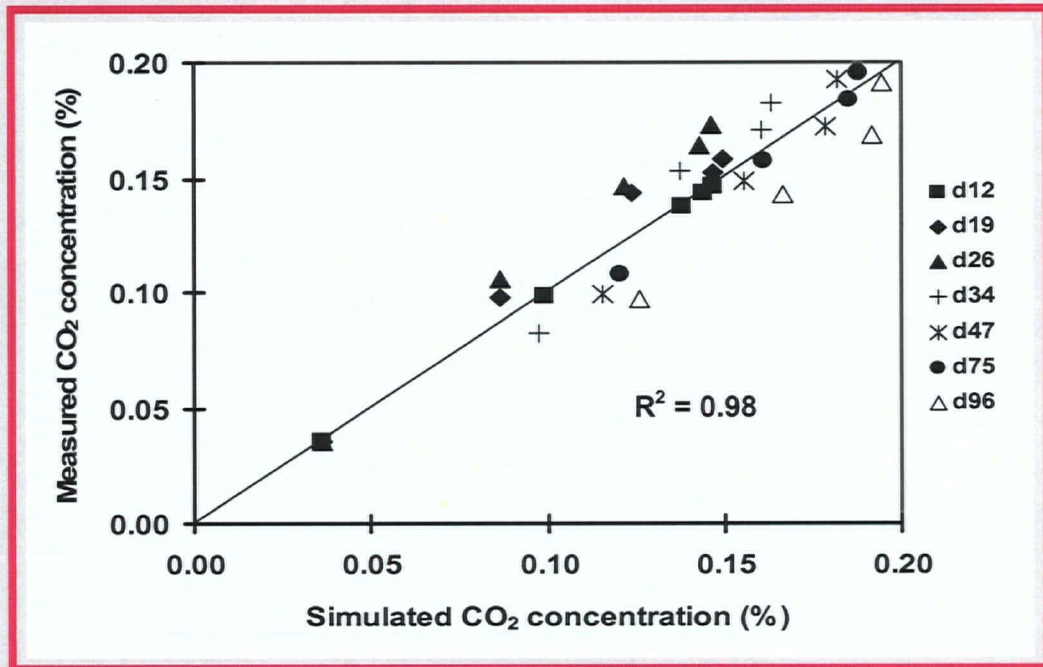


Figure 5.23. (A) Relationship between measured and simulated CO₂ concentrations in the low temperature (LT) (5 °C) minicosm plotted on a 1:1 scale.

carbon present in the lake-bottom sediments (Birkham et al., 2003; Lee et al., 2003) which are at a constant temperature (0 - 1 °C) and moisture content (25 Vol. %) (Birkham et al., 2003) (see also Figure 5.24).

Figure 5.24 shows the geologic profile, and the mean CO₂ concentration- and water content-depth profiles for DSWR (Birkham et al., 2003). Birkham et al. (2003) reported that the trends of CO₂-depth profile was stable over time, suggesting near steady-state conditions with respect to gas concentrations, and thus, reaction rates. The CO₂ concentration increases with increasing depth up to the organic layer of the pile (Figure 5.24B) and suggested that the dominant sites of reaction occurred below the pile. Below the organic layer the more vertical CO₂ concentration-depth profile is observed and that supported the interpretation that the dominant site of production was from the organic-rich material at the base of the pile (Birkham et al., 2003). The volumetric water content (Figure 5.24C) values generally ranged from 2 to 30%, with standard deviations at each depth generally less than 2%, suggesting near steady-state water conditions (Birkham et al., 2003). Zone of increased water contents (>20%) were measured at the natural ground surface between 18 and 20 m, and near the original ground surface. The deepest zones of elevated water content corresponded to the underlying organic layer (Figure 5.24C).

Since the CO₂- and water-depth profiles were stable over time (Birkham et al., 2003) with small variations in measured values, it was not possible to simulate or predict subsequent changes in CO₂-depth profiles associated with changes in water content. For illustration purposes, hypothetical drying forcing conditions were generated in the pile by reducing the initial measured mean water-depth profile (Figure 5.24B and Figure 5.25(A), curve d0) by a factor of 0.1 consecutively as illustrated in Figure 5.25A.

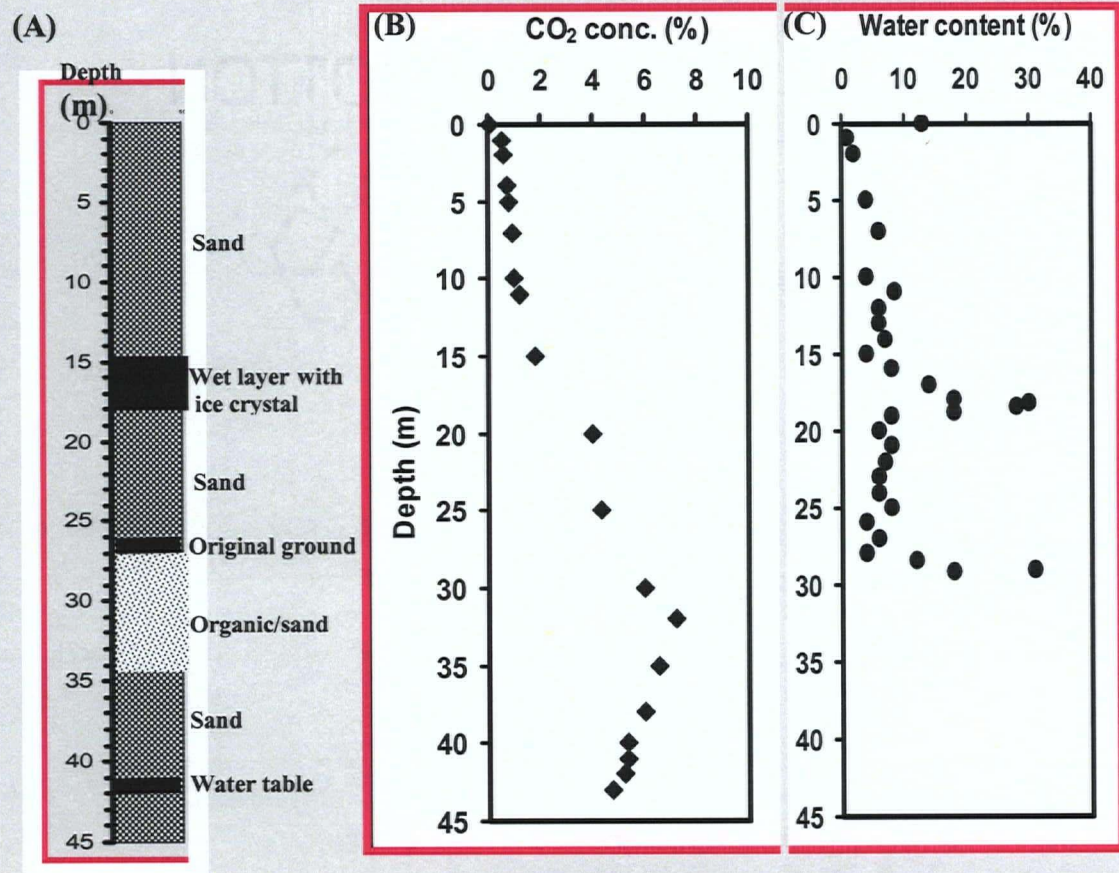


Figure 5.24. Depth profiles for Deilmann south waste-rock (DSWR) pile (A) Geologic profile (B) mean CO₂ concentration (Vol.) and (C) mean volumetric Water contents values (Adapted from Birkham et al, 2003).

Because of the unsaturated condition in the waste-rock pile, the variations in water contents were relatively small, except near the original ground and between 18 and 20 m depth. Figure 5.25B shows the model predicted effective diffusion coefficients D_e -profiles in response to changes in water-depth profiles (hypothetical) (Figure 5.25A) within the DSWR pile. The modeling approach incorporated oxidation reactions limited to the organic-rich material at the base of the pile (up to 30 m depth) (Birkham et al., 2003). The water content-depth profiles values were also limited to the organic layer. Since the production rate of the waste-rock material was not known or determined, an arbitrary number was used instead. This may cause some errors in the values.

The plots in Figure 5.25B show a decrease in D_e -depth profiles with decreasing water-depth profiles through the pile. These profiles trends are also illustrated in Figure 5.26A for the plots of the D_e as a function of water content. As expected the D_e decreases with increasing water content. The model predicted changes in CO_2 concentration-depth profiles are shown in Figure 5.26B. The changes in CO_2 concentration-depth profiles in response to changes in hypothetical water-depth profiles were not significant due to the low initial starting water-depth profile values in the waste-rock pile. This interpretation is supported by the measured standard deviations of less than 2% (Birkham et al., 2003), suggesting near steady-state water conditions in the pile over time. However, the trends showed that as the soil water-depth profiles changes from wet to dry conditions (Figure 5.25A, curves from right to the left) the CO_2 concentration-depth profiles also increase proportionally (Figure 5.26B, curves from left to the right).

In summary, the model was used to estimate CO_2 diffusion and concentration-depth profiles in DSWR in response to changes in water-depth profiles. Because of the unsaturated condition of the waste-rock pile and the near steady-state conditions with

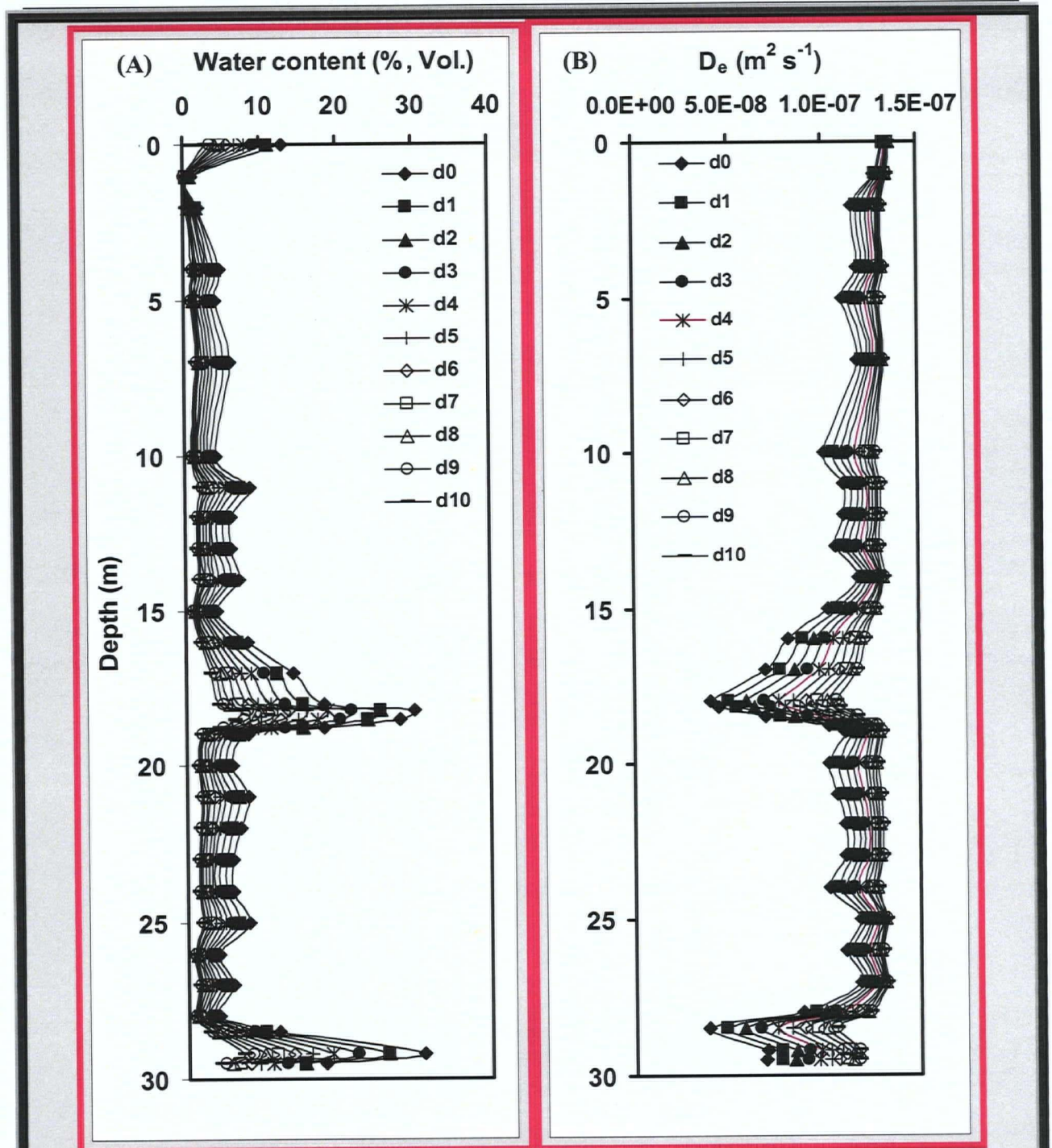


Figure 5.25. (A) Hypothetical water-depth profiles in DSWR pile and (B) model predicted effective diffusion coefficients (D_e) in response to changes in water contents in Figure 5.32A. Curve d0 in Figure 5.32A represents the actual measured mean water-depth profile in Figure 5.31C in the DSWR (Birkham et al., 2003). The subsequent profiles (hypothetical water profile) were generated by reducing the initial measured water-depth profile by a factor of 0.1 consecutively.

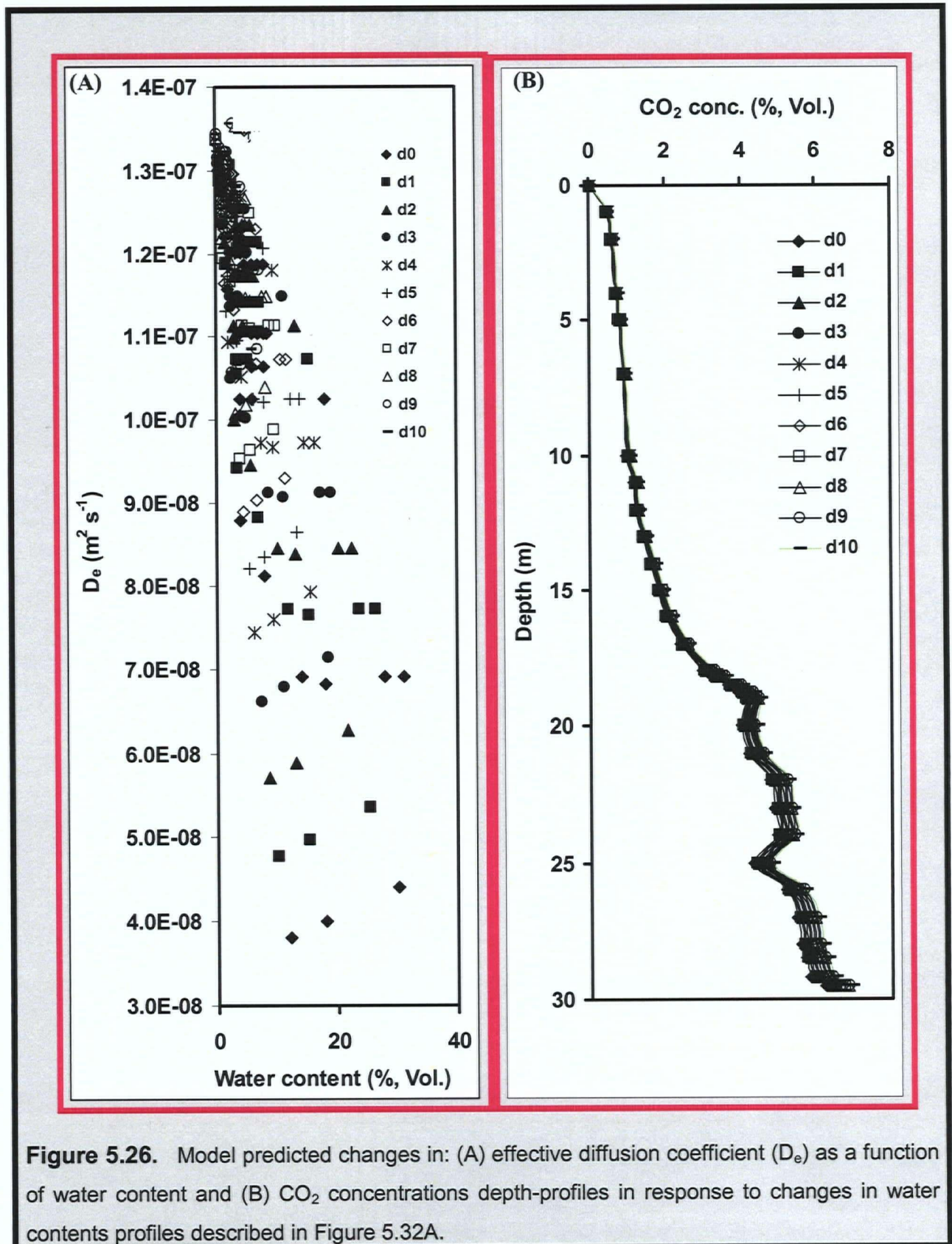


Figure 5.26. Model predicted changes in: (A) effective diffusion coefficient (D_e) as a function of water content and (B) CO₂ concentrations depth-profiles in response to changes in water contents profiles described in Figure 5.32A.

respect to gas concentrations and water content profiles in the DSWR simulations results showed relatively small variations in predicted values.

5.8 Predictions of CO₂ Diffusion and Surface CO₂ Flux from the DNWR and DSWR Piles Following Rainfall Events

A simplified form of the "CO₂" model was also used to predict the effects of rainfall events on the surface effective diffusion coefficient (D_e) and surface CO₂ flux at the DNWR and DSWR during the 6-day test period [August 1 (day 3) to August 6 (day 8) 2002] following 75.9 mm rainfall event over the initial 48-h period [July 30 (day 1) to July 31 (day 2) 2002]. It should be noted that the effects of rainfall events on surface water conditions and CO₂ fluxes at the DNWR and DSWR were discussed in details in Section 5.2 of Chapter 5 of this thesis.

Figures 5.27 and 5.28 show the measured surface water contents, CO₂ fluxes and rainfall events during the 8-d test period as discussed in Chapter 5, along with the model predicted surface D_e and CO₂ fluxes from the DNWR and DSWR piles, respectively. The model was simulated using the measured surface water contents (curves with broken lines and open marks) for each day of the 6-d (day 3 to day 8) test period. Figure 5.27 shows that as the DNWR ground surface continued to dry gradually from day 3 to day 8, the model predicted surface D_e (curve with solid line with triangle marks) also continued to gradually increase with time. It should be noted that the predicted surface D_e and measured surface CO₂ flux exhibit very similar trends. They both increased initially at a fast rate from day 3 to day 5, then at a slow rate and eventually reached a plateau on day 7. At the end of the test period on day 8 the surface D_e at the DNWR was found to be $4.25 \times 10^{-6} \text{ m}^2 \text{ s}^{-1}$. The similar trends were also

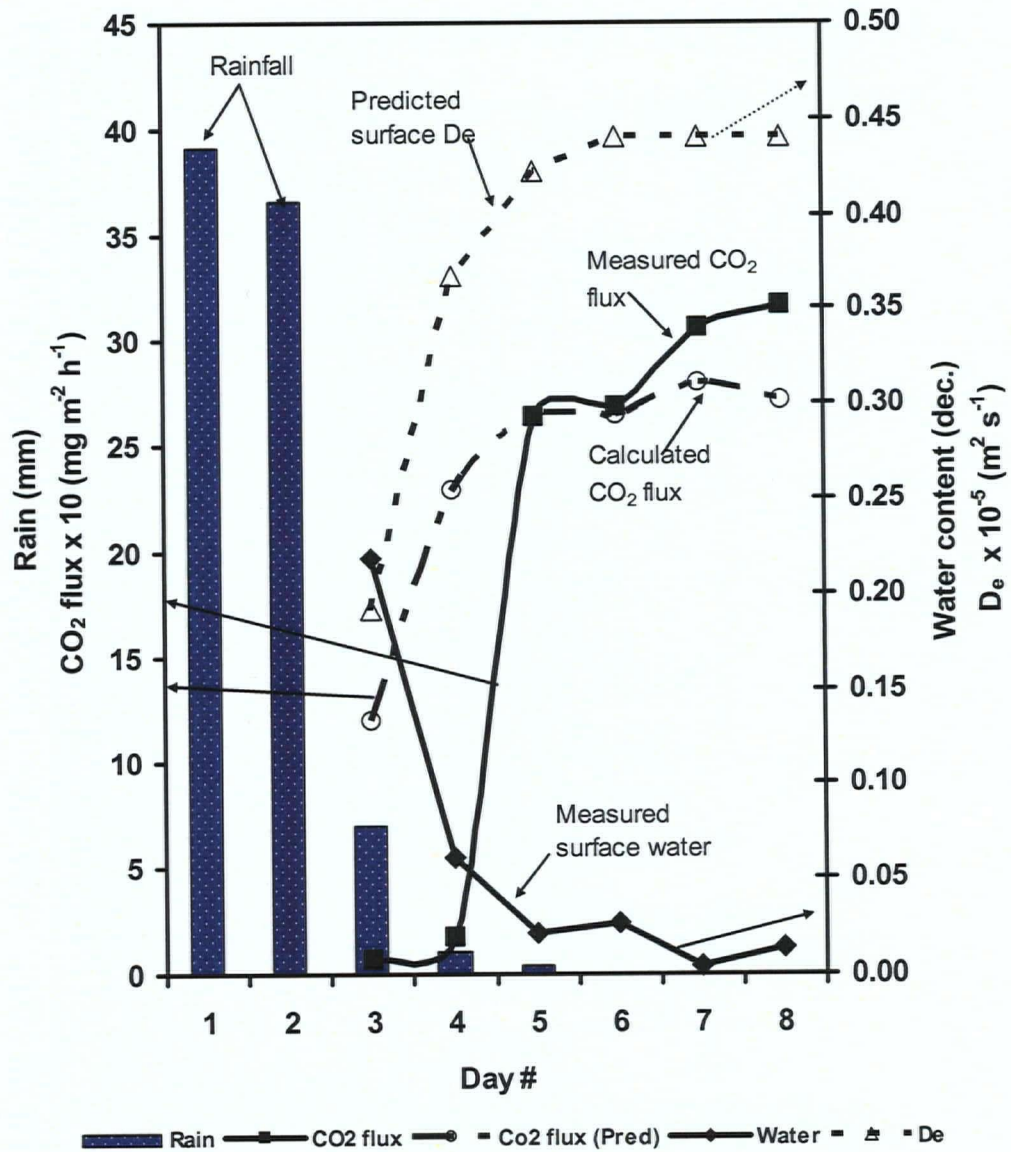


Figure 5.27. Rainfall, measured surface water content and CO₂ flux and predicted effective diffusion coefficient (D_e) and surface CO₂ flux at the Deilmann North waste-rock (DSWR) pile over an 8-day test period [30 July (day 1) to 6 August (day 8) 2002] with time.

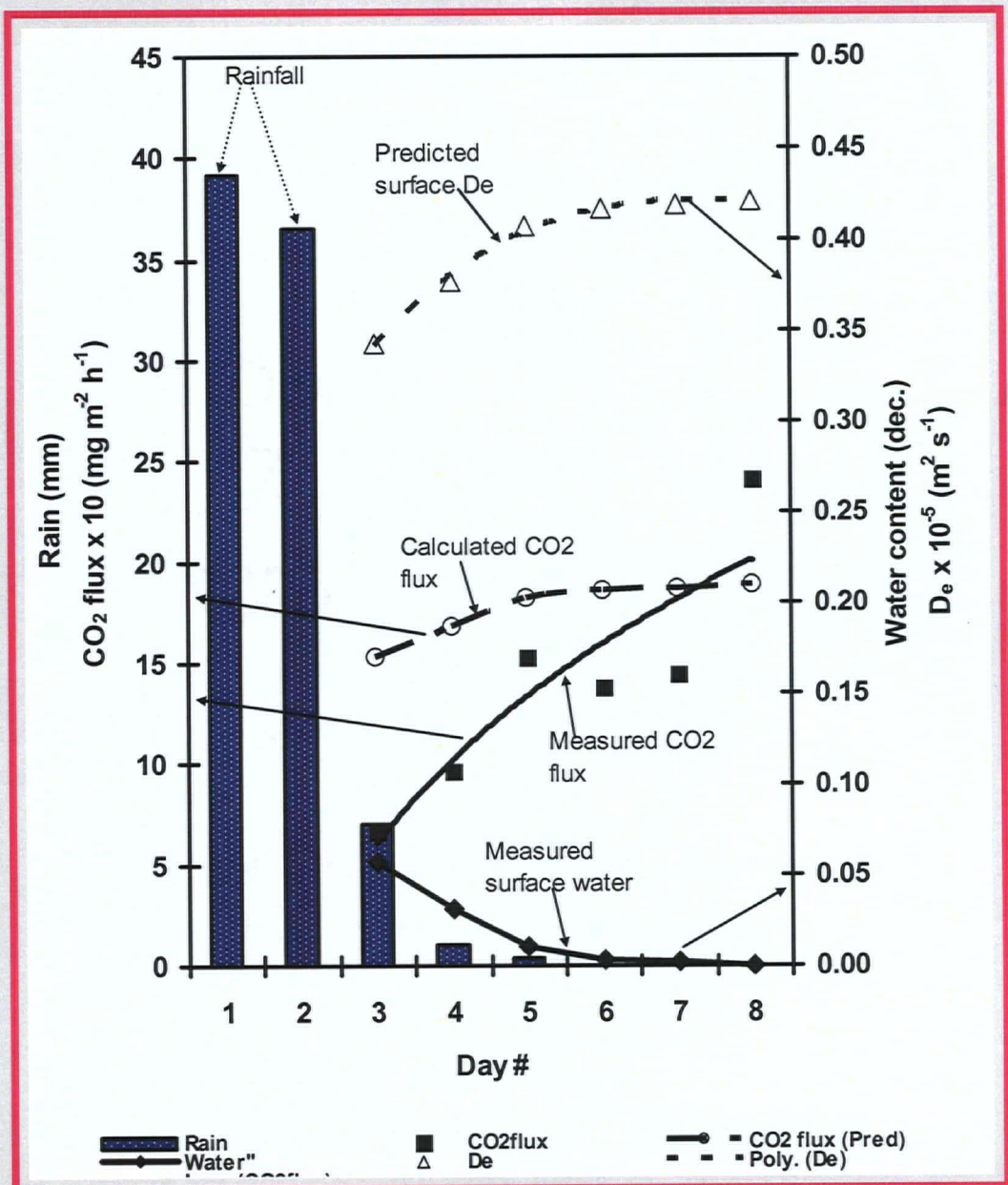


Figure 5.28. Rainfall, measured surface water content and CO₂ flux and predicted effective diffusion coefficient (D_e) and surface CO₂ flux at the Deilmann North waste-rock (DNWR) pile over an 8-day test period [30 July (day 1) to 6 August (day 8) 2002] with time.

observed at the DSWR in Figure 5.28. Similarly, both the measured surface CO₂ flux and predicted surface D_e initially increased at a fast rate from day 3 to day 5 and eventually reached a plateau on day 7. At the end of the test period the surface D_e at the DSWR was found to be $4.40 \times 10^{-6} \text{ m}^2 \text{ s}^{-1}$.

To predict the surface CO₂ flux using Fick's 1st and 2nd law (e.g., Equation 5.3 used in the model) the concentration gradient (e.g., dC/dz) must be known. The concentration gradients, however, were not measured during the test period. But based on the measured average surface CO₂ flux and the corresponding model predicted surface D_e from the DNWR and DSWR piles, the concentration gradients can be estimated using Fick's first law (e.g., Equation 5.3). The concentration gradients were found to be:

$$\frac{\partial C}{\partial z} = 2.03 \times 10^{-2} \left(\frac{\text{kg}}{\text{m}^3 * \text{m}} \right) \text{ and } \frac{\partial C}{\partial z} = 1.24 \times 10^{-2} \left(\frac{\text{kg}}{\text{m}^3 * \text{m}} \right), \text{ for the DNWR and DSWR}$$

piles respectively. It was assumed in the model simulations that the CO₂ was produced at a steady rate below the piles (e.g., the dominant sites of reactions) (Birkham et al., 2003) and that the shallow CO₂ gradient near the ground surface would remain constant during the relatively short-term wetting event. It should be pointed out that this assumption is not completely valid; however actual CO₂ measurements in the sand profiles immediately below the ground surfaces of the waste-rock piles were not obtained and thus it is not possible to accurately constrain the lower boundary of the transient model. Based on this simplifying assumption, the calculated surface CO₂ fluxes during the 6-d test period at the DNWR and DSWR are also shown respectively in Figures 5.27 and 5.28 (curves with solid lines with circle marks) along with the predicted surface D_es. Results showed that the calculated (predicted) and measured

CO₂ fluxes exhibited very similar trends. These trends supported the interpretation that the flux is proportional to the D_e times the concentration gradient.

5.9 Chapter Summary

In summary, results showed that the water content at ground surface is transient after a heavy rainfall and is an important factor in controlling CO₂ fluxes.

Both the EC measured AE and PE (Carey et al., 2005) and SoilCover predicted AE and PE values showed good agreement.

The "CO₂" model predicted, as expected, a decrease in D_e -depth profiles and increase in the CO₂ concentration-depth profiles with decreasing water-depth profiles through the DSWR pile. The model also predicted surface CO₂ fluxes trends that were very similar to the measured surface CO₂ fluxes during the 6-d test period from the DNWR and DSWR following heavy rainfall events.

CHAPTER VI

Summary and Conclusions

A recently developed and laboratory-verified dynamic closed chamber (DCC) method has been tested under field conditions on waste-rock piles at the Key Lake uranium mine. The method has been used to quantify the magnitude of spatial and temporal variations in the CO₂ flux on the Deilmann north (DNWR) and Deilmann south (DSWR) waste-rock piles over a period of two years (summer 2000 – summer 2002). The ability of the DCC to accurately quantify field respiration was demonstrated by comparing the DCC fluxes to those obtained using two other field CO₂ flux measurement techniques: the static closed chamber (SCC) and eddy covariance (EC) methods.

The main advantage of this direct technique is that it provides an almost instantaneous indication of the reaction rate under field conditions, regardless of climatic or moisture conditions in the waste dumps.

The DCC was also used to investigate the effects of climatic variables (e.g., rainfall and evaporation) on near-surface waste-rock-water conditions which also affect surface CO₂ gas fluxes.

A relatively simple "CO₂" model was developed to predict the changes in the effective diffusion coefficient of CO₂, surface CO₂ flux and its redistribution in subsurface material in response to changes in soil water contents.

At the DSWR site the DCC was used to demonstrate that the CO₂ flux was relatively uniform across the pile (with a CV of only about 30%). This CV reflects the combined influence of a relatively constant rate of CO₂ production in the organic-rich

zone at the base of the waste-rock pile and the textural uniformity of the overburden material (sand) used to construct the DSWR pile (Birkham, 2002). That is, these factors combine to exert a controlling influence on the composition and upward migration of pore gases and, in turn, the flux of gases from the surface to the atmosphere.

Comparison between the DCC and the static closed chamber (SCC) showed that there was no significant difference ($p \leq 0.05$) between the mean CO_2 fluxes obtained using the two methods at the DSWR. Whereas the chamber-based (DCC and SCC) methods yielded comparable data from the DSWR, with an overall time-averaged CO_2 flux of $171 \pm 54 \text{ mg CO}_2 \text{ m}^{-2} \text{ h}^{-1}$; the eddy covariance (EC) method yielded a time-averaged CO_2 flux ($150 \pm 35 \text{ mg CO}_2 \text{ m}^{-2} \text{ h}^{-1}$) that was about 12% lower than that calculated from the chamber data. Underestimation of the CO_2 flux associated with soil respiration by EC-based methods relative to chamber-based methods has been reported widely in the literature [e.g., Goulden et al., 1996; Norman et al., 1997; Law et al., 1999; Janssens et al., 2000; Davidson et al., 2002]. Though not excessively large, these differences presumably reflect the different processes measured by the two methods. The chamber data exhibited slightly greater standard deviations than the EC data (i.e., DCC = $\pm 58 \text{ mg CO}_2 \text{ m}^{-2} \text{ h}^{-1}$; SCC = $\pm 59 \text{ mg CO}_2 \text{ m}^{-2} \text{ h}^{-1}$; EC = $\pm 32 \text{ mg CO}_2 \text{ m}^{-2} \text{ h}^{-1}$). It is believed that this likely reflects the fact that the variability associated with the chamber-based measurements includes both a spatial and temporal component, whereas the variability associated with the EC method is primarily temporal in nature.

The overall averages of CO_2 fluxes at the DNWR and DSWR measured with the DCC over the 2-year test period (summer 2000 and summer 2002) were 188 ± 68 and $217 \pm 83 \text{ m}^{-2} \text{ h}^{-1}$, respectively.

Based on these results, it was concluded that the DCC is well-suited to the quantification and spatial resolution of CO₂ fluxes associated with waste-rock piles.

This work showed that the effects of heavy rainfall events on the CO₂ flux and near-surface water conditions were of short duration. The short-term effects of rainfall events were reflected in the lack of long-term spatial and temporal variations in CO₂ fluxes (average CV is 28%-39%) at both sites over a 2-year test period (summer 2000 and summer 2002). Because of lack of temporal and spatial variation in CO₂ fluxes, it is concluded that rainfall events had little long-term effects on CO₂ flux from waste-rock piles.

During the test period, SoilCover was used to predict the rate of evaporation on the DSWR and results were compared to published field-measured evaporation using eddy covariance (EC) method on the DSWR (Carey et al., 2005). Results showed very good agreement between the model predicted and EC measured values. Both the field-measured and predicted data indicated an average evaporation rate of approximately 1.1 mm per day at the DSWR for the 8-day test period.

Verification of the "CO₂" model developed showed good agreement between predicted and sand column-measured data. Simulations results for the deep profile in DSWR showed relatively small variations in predicted CO₂ concentration-depth profiles associated with change in water content during a simulated drying event. A simplified model was also used to predict surface CO₂ fluxes on the DNWR and DSWR at the Key Lake mine following rainfall events. Results showed the model predicted surface D_e and CO₂ fluxes that exhibited very similar trends with measured data. In summary, the CO₂ model, along with others capable of predicting changes in water content profiles with time such as SoilCover, can be of value in the prediction and monitoring of

biogeochemical processes occurring in the unsaturated geologic material and natural soils.

Finally, the field results showed that the DCC method is especially useful for characterizing spatial variability as well as identifying zones of sulphide oxidation and carbonate buffering in the waste-rock piles. The method has distinct advantages over the traditional methods in terms of accuracy, speed, and repeatability and it can be used to measure the CO₂ fluxes in situ at the same locations using the same chambers with minimal disturbance of the soil. The method can be extended to any other mine waste dumps to quantify biogeochemical reaction rates in unsaturated geologic media and soils elsewhere in Canada.

In conclusion, it is believed the objectives of this thesis work were met as stated in the introduction.

References

- Aachib, M., Aubertin, M., Mbonimpa, M. 2002. Laboratory measurements and predictive equations for gas diffusion coefficient of unsaturated soils. Proceedings of the 55th Canadian Geotechnical and Joint IAH-CNC and CGS Groundwater Speciality. Niagara Falls Ont.. Canadian Geotechnical Society, Ottawa: 156-171.
- Aachib, M. Mbonimpa., Aubertin, M. 2004. Measurement and Prediction of Oxygen Coefficient in Unsaturated Media, with Application to Soil Covers. *Water, Air and Soil Pollution* 156: 163-193.
- Affek, H., Ronen, D., and Yakir, D. 1998. Production of CO₂ in the capillary fringe of a deep phreatic aquifer. *Water Resour. Res.* 34 (5), 989-996.
- Ahuja, L.R., Ross, J.D., Bruce, R.R., and Cassel, D.K. 1988. Determining unsaturated Hydraulic conductivity from tensiometric data alone. *Soil Sci. Soc. Am. J.* 52: 27-34.
- Ambus, P. and Robertson, G.P. 1998. Automated near-continuous measurement of carbon dioxide and nitrous oxide fluxes from soil. *Soil Sci. Soc. Am. J.* 62: 394-400.
- Amundson, R.G., Chadwick, O.A., Sowers, J.M., and Doner, H.E. 1988. Relationship between climate and vegetation and the stable carbon isotope chemistry of soils in the eastern Mojave desert. *Nevada. Quat. Res.* 29: 245-254.
- Atkinson, T.C. 1977. Carbon dioxide in the atmosphere of the unsaturated zone: an important control of groundwater hardness in limestones. *J. Hydrol.* 35, 111-123.
- Aubertin, M., Ricard, J.-F., and Chapuis, R.P. 1998. A predictive model for the water retention curve: application to tailings from hard-rock mines. *Can. Geotech. J.* 35: 55-69.

- Aubertin, M., Aachib, M., and Authier, K. 2000. Evaluation of diffusive flux through covers with a GCL. *Geotextiles and Geomembranes* 18:215-233.
- Aubertin, M., Mbonimpa, M., and Chapuis, R.P. 2003. A model to predict the water retention curve from basic geotechnical properties. *Can. Geotech. J.* 40: 1104-1122.
- Aubertin, M., Molson, J., Bussière, B., and Dagenais, A.M. 2006. Investigations of layered cover acting as oxygen barriers to limit acid mine drainage. *Proc. 5th ICEG Environmental Geotechnics: Challenges and Responsibilities for Environmental Geotechnics*, Thomas H.R. (ed.) 26-30 June 2006 Thomas Telford, vol. 2, pp 827-835.
- Baldocchi, D.D., Hicks, B.B., and Meyers, T.P. 1988. Measuring biosphere atmosphere exchanges of biologically related gases with micrometeorological methods. *Ecol.* 69: 1331-1340.
- Barbour, S.L. 1998. Nineteenth Canadian Geotechnical Colloquium: The soil-water characteristic curve: a historical perspective. *Can. Geotech. J.* 35(5): 873-894.
- Barr, A.G., Griffis, T.J., Black, T.A., Lee, X., Staebler, R.M., Fuentes, J.D., Chen, Z., and Morgenstern, K. 2002. Comparing the carbon budgets of boreal and temperate deciduous forest stands. *Can. J. For. Res.* 32: 813-822.
- Bell, A.V., Mills, A.L., and Herman, J.S. 1991. An update of the acid waste rock field trials at heath Steele Mine, New Brunswick. *Second International Conference on the Abatement of Acidic drainage*: 321-340.
- Bennett, J.W. and Ritchie, A.I.M. 1990. "Measurements of the Transport of Oxygen into Two Rehabilitated Wasye-Rock dumps". In: *Proceedings of the Second International Conference on the Abatement of Acidic Drainage*. MEND 3 pp 289-298 September 16-18, 1990, Montreal, Canada.

- Bennett, J.W. and Ritchie, A.I.M. 1992. The installation of monitoring sites in waste rock at the Aitik Mine site August-September (1991). Austral. Nuclear Sci. Technology Org. Report ANSTO/C263.
- Bennett, J. W., Comarmond, M. J., and Jeffery, J. J. 2000. Comparison of sulfidic oxidation rates measured in the laboratory and the field. International Conference on Acid Rock Drainage (ICARD) 2000 Proceedings, Denver, Colorado. The Society for Mining, Metallurgy, and Exploration, Inc., 171-180.
- Black, T.A., Chen, W.J., Barr, A.G., Arain, M.A., Chen, Z., Nesic, Z., Hogg, E.H, Neumann, H.H., and Yang, P.C. 2000. Increased carbon sequestration by a boreal deciduous forest in years with warm spring. *Geophys. Res. Lett.* 27: 1271-1274.
- Blowes, D.W., Al, T., Lortie, L., Gould, W.D., and Jambor, J.L. 1995. Microbial, chemical, and mineralogical characterization of the Kidd Creek mine tailings impoundment, Timmins area, Ontario. *Geomicrobiol. J.* 13: 13-31.
- Bigham, J.M., Schwertmann, U., Carson, L., and Murad, E. 1990. A poorly crystallized oxyhydroxysulfate of iron formed by bacterial oxidation of Fe(II) in acid mine waters. *Geochim. Cosmochim. Acta* 54: 2743-2758.
- Birkham, T.K., M.Sc. Dissertation, University of Saskatchewan 2002.
- Birkham, T.K., Hendry, M.J., Wassenaar, L.I., Mendoza, C.A., and Lee, E.S. 2003. Characterizing Geochemical Reactions in Unsaturated Mine Waste-Rock Piles Using Gaseous O₂, CO₂, ¹²CO₂, and ¹³CO₂. *Environ. Sci. Technol.* 37: 496-501.
- Brooks, R.H., and Corey, A.T. 1964. Hydraulic properties of porous media. Hydrology Paper, No. 3, Colorado State University, Fort Collins, Colorado.
- Brierley, C.L. 1978. Bacterial leaching. *CRC Critical Rev. Microbiol.* 6: 207-262.
- Brumme, R., and Beese, F. 1992. Effects of liming and nitrogen-fertilization on

- emissions of CO₂ and N₂O from a temperate forest. *J. Geophys. Res.* 97(D12): 12851-12858.
- Buchmann and Ernst-Detlef Schulze, 1999. Net CO₂ and H₂O fluxes of terrestrial ecosystems. *Global Biogeochemical Cycles*, 3, 743-750.
- Buchmann, N. 2000. Biotic and Abiotic factors controlling soil respiration rates in *Picea abies* stands. *Soil Biol. Biochem.* 32: 1625-1635.
- Burkins, M.B., Virginia, R.A. and Wall, D.H. 2001. Organic carbon cycling in Taylor Valley, Antarctic: quantifying soil reservoirs and soil respiration. *Global Change Biology* 7: 113-125.
- Burman, R., and Pochop, L.O. 1994. Evaporation, evapotranspiration, and climatic data (Developments in Atmospheric Science 22). Elsevier Science, Amsterdam, The Netherlands.
- Bussi re, B., Dagenais, A., Mbonimpa, M., and Aubertin, M. 2002. Modification of oxygen-consumption testing for the evaluation of oxygen barrier performance. Proceedings of the 55th Canadian Geochemical and 3rd Joint CGS Groundwater Special Conference, Niagara Falls, Ontario, pp. 139-146.
- Bussi re, B., Aubertin, M., and Chapuis, R.P. 2003. The behavior of inclined covers used as oxygen barrier. *Can. Geotech. J.* 40: 512-535.
- Buyanovsky, G. A., Wagner, G. H., and Gantzer, C. J. 1986. Soil respiration in a winter wheat ecosystem. *Soil Sci. Soci. Am. J.* 50: 338-344.
- Capehart, W.J., and Carlson, T.N. 1994. Estimating near-surface soil-moisture availability using a meteorologically driven soil water profile model. *J. Hydrol.* 160(1-4): 1-20.
- Capehart, W.J., and Carlson, T.N. 1997. Decoupling of surface and near-surface soil water content: A remote sensing perspective. *Water Resour. Res.* 33(6): 1383-

1395.

- Carey, S.K., Barbour, S.L., and Hendry, M.J. 2005. Evaporation from a waste-rock surface, Key Lake, Saskatchewan. *Can. Geotech. J.* 42: 1189-1199.
- Cerling, T.E., Solomon, D.K., Quade, J., and Bowman, J.R. 1991. On the isotopic composition of carbon in soil carbon dioxide. *Geochim. et Cosmochim. Acta* 55: 3404-3405.
- Clark, I. and Fritz, P. 1997. *Environmental Isotopes in Hydrology*. Lewis Publishers.
- Collin, M. and Rasmuson, A. 1988. Gas Diffusivity Models for Unsaturated Porous Media. In *Soil Science America Journal*. 52: 311-333.
- Conen, F., and Smith, K.A. 2000. An explanation of linear increases in gas concentration under closed chambers used to measure gas exchange between soil and atmosphere. *Eur. J. Soil Sci.* 51: 111-117.
- Cook, F.J., Dobos, S.K., Carlin, G.D., and Millar, G.E. 2004. Oxidation of pyrite in acid sulfate soils: in situ measurements and modeling. *Australian Journal of Soil Research* 42: 499-507.
- Craig, H. 1953. The geochemistry of the stable carbon isotopes. *Cosmochimica et al.* 3, 53-92.
- Davidson, E.A., and Trumbore, S.E. 1995. Gas diffusivity and production of CO₂ in deep soils of the eastern Amazon. *Tellus Ser. B* 47: 550-565.
- Davidson, E.A., Belk, E., Boone, R.D. 1998. Soil water content and temperature as independent or confounded factors controlling soil respiration in a temperate mixed hardwood forest. *Global Change Biol.* 4, 217-228.
- Davidson, E.A., Savage, K., Bolstad, P., Clark, D.A., Curtis, P.S., Ellsworth, D.S., Hanson, P.J., Law, B.E., Luo, Y., Pregitzer, K.S., Randolph, J.C., and Zak, D. 2002. Belowground carbon allocation in forests estimated from litterfall and

-
- IRGA-based soil respiration measurements. *Ag. For. Met.* 113: 39-51.
- Davidson, J.M., Stone, L.R., Nielsen, D.R., and Larue, M.E. 1969. Field measurement and use of soil-water properties. *Water Resour. Res.* 5: 1312-1321.
- Davis, G.B., and Ritchie, A.I.M. 1987. A model of oxidation in pyretic mine wastes: Part 3. Importance of particle size distribution. *Appl. Math. Model.* 11 (December): 417-422.
- Dawson, R., and Morgenstern 1995. *Liquifaction Flowslides in Rocky Mountain and Mine Waste Dumps, Phase 3, Final Report.* Natural Resources Canada, Ottawa, Ontario. Contract Report 23440-9135/01.
- de Jong, E., and Schappert, H. J. V. 1972. Calculation of soil respiration and activity from CO₂ profiles in the soil. *Soil Sci.* 113(5): 328-333.
- Delleur, J.W. 1999. *The Handbook of Groundwater Engineering.* CRC Press, New York.
- Drever, J.I. 1997. *The Geochemistry of Natural Waters*, 3rd ed. Prentice Hall. Upper Saddle River, NJ. 436 pp.
- Ek, M., and Cuenca, R.H. 1994. Variation in soil parameters: Implications for modeling surface fluxes and atmospheric boundary layer development. *Boundary Layer Meteorol.* 70(4): 369-383.
- Elberling, B., Nicholson, R.V. and David, D.J. 1993. Field evaluation of sulphide oxidation rates. *Nordic Hydrology* 24: 323-338.
- Elberling, B., Nicholson, R.V., Reardon, E.J., and Tibble, P. 1994. Evaluation of sulfide oxidation rates: laboratory study comparing oxygen fluxes and rates of oxidation product release. *Can. Geotech. J.* 31: 375-383.
- Elberling, B., and Nicholson, R.V. 1996. Field determination of sulfide oxidation rates in mine tailings. *Water Resour. Res.* 32: 1773-1784.
- Elberling, B., and Jakobsen, B.H. 2000. Soil solution pH measurements of using in-line

-
- chambers with tension lysimeters. *Canadian J. Soil Sci.* 80: 283-288.
- Elberling, B. 2003. Seasonal trends of soil CO₂ dynamics in a soil subject to freezing. *J. Hydrol.* 276: 159-175.
- Elberling, B. 2005. Temperature and oxygen control on pyrite oxidation in frozen mine tailings. *Cold Regions Science and Technology* 41: 121-133.
- Enoch, C.W. and Dasberg 1971. The occurrence of high CO₂ concentrations in soil air. *Geoderma* 6: 17-21.
- Fahnestock, J.T., Jones, M.H., Brooks, P.D., Walker, D.A., Welker, J.M. 1998. Winter and early spring CO₂ efflux from tundra communities of northern Alaska. *J. Geophys. Res.* 103: 29023-29027.
- Fala, O., Molson, J.W., Aubertin, M., Bussière, B. 2005. Numerical Modeling of Flow and Capillary Barrier Effects in Unsaturated Waste Rock Piles. *Mine Water and Environment* 24(4): 172-185.
- Farrell, R.E., de Jong, E., and Elliott, J.A. 2002. Gas Sampling and Analysis. Pp. 1075-1111. In: J.H. Dane and G.C. Topp (eds.) *Methods of Soil Analysis. Part 4. Physical Methods.* SSSA Book Series, no. 5. Soil Sci. Soci. of Am. J., Madison, WI.
- Frank, A.B., Liebig, M.A., and Hanson, J.D. 2002. Soil carbon dioxide fluxes in northern semiarid grasslands. *Soil Biol. Biochem.* 34: 1235-1241.
- Freeze, R.A. 1969. The mechanism of natural ground-water recharge and discharge 1. One-dimensional, vertical, unsteady, unsaturated flow above a recharging ground-water flow system. *Water Resour. Res.* 153-171.
- Freeze, R.A., and Cherry, J.A. 1979. *Groundwater.* Prentice-Hall, Inc.
- Fredlund, D.G., and Rahardjo, H. 1993. *Soil mechanics for unsaturated soils.* John Wiley & Sons, Inc., New York.

- Fredlund, D.G., and Xing, A. 1994. Equations for the soil-water characteristic curve. *Can. Geotech. J.*, vol. 31, pp. 521-532.
- Fuller, E. N., Schettler, P. D., and Giddings, C. J. 1966. A new method for prediction of binary gas-phase diffusion coefficients. *Industrial and engineering chemistry* 58(5), 19-27.
- Gardner, W.R. 1956. Calculation of capillary conductivity from pressure plate outflow data. *Soil Sci. Soc. Am. Proc.* 20: 317-320.
- Gelinas, P., Lefebvre R., and Choquette M. 1992. Monitoring of acid mine drainage in a waste rock dump. In *Environmental Issues and Waste Management in Energy and Minerals Production* (ed. S. e. al.), pp. 747-756. Balkema.
- Goulden, M.L., Munger, J.W., Fan, S.M., Daube, B.C., and Wofsy, S.C. 1996. Measurements of carbon sequestration by long-term eddy covariance: methods and a critical evaluation of accuracy. *Glob. Change Biol.* 2: 169-182.
- Grable, A.R. 1966. Soil aeration and plant growth, *Adv. Agron.* 18: 57-106.
- Granger, R.J. 1989. A complementary relationship approach for evaporation from nonsaturated surfaces. *J. Hydrol*, 111: 31-38.
- Gray, D.M. 1995. *Handbook of Hydrology*, University of Saskatchewan, Saskatoon, SK, Canada.
- Haddadin, J., Morin, D., Ollivier, P. & Fick, M. 1993. Effect of different carbon dioxide concentration on ferrous iron and pyrite oxidation by a mixed culture of iron and/or sulfur-oxidizing bacteria. *Enzyme Microbiol. Technology* 15, 832-841.
- Hass, H., Fisher, D.W., Thorstenson, D.C., and Weeks, E.P. 1983. $^{13}\text{CO}_2$ and $^{14}\text{CO}_2$ measurements on soil atmosphere sampled in the subsoil unsaturated zone in the western Great Plains of the U.S. *Radiocarbon* 25: 301-314.

- Harries, J. R. and Ritchie, A.I.M. 1981. "The use of temperature profiles to estimate the pyretic oxidation rate in a waste-rock dump from an opencut mine". *Water, Air and Soil Pollution* 15: 405-423.
- Harries, J. R. and Ritchie, A.I.M. 1983. The microenvironment within waste rock dumps undergoing pyritic oxidation. In recent Progress in Biohydrometallurgy (G. Rossi & A.E. Torma, eds.) Assoc. Minereria Sarda, Iglesias, Italy, 377-392
- Harries, J. R. and Ritchie A.I.M. 1985. Pore gas composition in waste rock dumps undergoing pyritic oxidation. *Soil Sci.* 140(2), 143-152.
- Hanson, P.J., Wullschleger, S.D., Bohlman, S.A., and Todd, D.E., 1993. Seasonal and topographic patterns of forest floor CO₂ efflux from an upland oak forest. *Tree Physiology*, 13, 1-15.
- Hatanaka, M., Uchida, A., and Takehara, N., 1997. Permeability characteristics of high-quality undisturbed sands measured in a triaxial cell. *Soils and Foundation, Japanese Society of Soils Mechanics and Foundation Engineering* 37(3): 129-135.
- Helgen, S., Davis, A., and Byrns, C. 2000. Measurement of oxygen, temperature, and geochemical profiles in sulfide and oxide waste rock dumps of different ages. *International Conference on Acid Rock Drainage (ICARD) 2000 Proceedings*, 269-275.
- Herasymuik, G.M, Wilson, G.W., Barbour, S.L., and Smith, T., 1995. The characterization of hydrologic properties and moisture migration pathways of a waste rock dump. *Proceedings of the Nineteenth Annual British Columbia Mine Reclamation Symposium*.
- Hendry, M.J., Lawrence, J.R., Zanyk, B.N., and Kirkland, R. 1993. Microbial production of CO₂ in unsaturated geologic media in a mesoscale model. *Water Resour. Res.*

29: 973-984.

- Hendry, M.J., Mendoza, C.A., Kirkland, R.A., and Lawrence, J.R. 1999. Quantification of transient CO₂ production in a sandy unsaturated zone. *Water Resour. Res.* 35 (7): 2189-2198.
- Hendry, M.J., Mendoza, C.A., Kirkland, R., Lawrence, J.R. 2001. An assessment of a mesocosm approach to the study of microbial respiration in a sandy unsaturated zone. *Groundwater* 39 (3): 391-400.
- Hendry, M.J., Wassenaar, L.I., and Birkham, T.K. 2002. Microbial respiration and diffusive transport of O₂, ¹⁶O₂, and ¹⁸O₂, in unsaturated soils: A mesocosm experiment. *Geochim. et Cosmochim. Acta*, Vol. 66, No. 19, pp. 3367-3374.
- Hillel, D. 1980. *Applications of Soil Physics*, Academic Press, Inc., New York.
- Hobbie, S.E., Schimel, J.P., Trumbore, S.E., Randerson, J.R. 2000. Controls over carbon storage and turnover in high-latitude soils. *Global Change Biology* 6: 196-210.
- Hockley, D., Smolensky, J., Jahn, S., and Paul, M. 2000. Geochemical investigations and gas monitoring of an acid generating waste rock pile. *International Conference on Acid Rock Drainage (ICARD) 2000 Proceedings*, 181-189.
- Holland, E.A., Townsend, A.R., Vitousek, P.M., 1995. Variability in temperature regulation of CO₂ fluxes and N mineralization from five Hawaiian soils: Implications for a changing climate. *Global Change Biol.*, 1, 115-123.
- Hollings, P., Hendry, M.J., and Kirkland, R.A. 2000. Quantification of oxygen consumption rates for gneissic waste rock piles, Key Lake uranium mine, northern Saskatchewan, Canada: application of the kinetic cell technique. *International Conference on Acid Rock Drainage (ICARD) 2000 Proceedings*, 163-169.

- Hutchinson, G.L., Livingston, G.P., Healy, R.W., and Striegl, R.G. 2000. Chamber measurement of surface-atmosphere trace gas exchange: numerical evaluation of dependence on soil, interfacial layer, and source/sink properties. *J. Geophys. Res.* 105: 8865-8875.
- Janssens, I.A., Kowalski, A.S., Longdoz, B., and Ceulemans, R. 2000. Assessing forest soil CO₂ efflux: an in situ comparison of four techniques. *Tree Phys.* 20: 23-32.
- Jaynes, D.B., and Rogowski, A.S. 1983a. Applicability of Fick's law to gas diffusion. *Soil Sci. Soc. Am. J.* 47: 425-430.
- Jaynes, D.B., Rogowski, A.S., Pionke H.B., and Jacoby, Jr. E.L. 1983b. Atmosphere and temperature changes within a reclaimed coal strip mine. *Soil Sci.* 136(3), 164-177.
- Kabwe, K.L. M.Sc., Dissertation, University of Saskatchewan, 2001.
- Kabwe, K.L., Hendry, M.J., Wilson, G.W., and Lawrence, J.R. 2002. Quantifying CO₂ fluxes from soil surfaces to the atmosphere. *J. Hydrol.* 260: 1-14.
- Keen, B.A. 1931. *The Physical Properties of Soils*, Longman, London.
- Keith, C.N., and Vaughan, D.J. 2000. Mechanisms and rates of sulphide oxidation in relation to the problems of acid rock (mine) drainage. In *Environmental Mineralogy: Microbial Interactions, Anthropogenic solution and the influences, Contaminated Land and Waste Management*. Mineralogical Society Special Publication.
- Keller, K. C. and Bacon D. H. 1998. Soil respiration and georespiration distinguished by transport analyses of vadose CO₂, ¹³CO₂, and ¹⁴CO₂. *Glob. Biogeochem. Cycles* 12(2), 361-372.
- Key Lake Mining Corporation 1979. *Environmental Impact Statement for the Key Lake Project*.

- Klute, A., and Letey, J. 1958. The dependence of ionic diffusion on the moisture content of non-adsorbing porous media. *Soil Sci. Soc. Am. Proceedings*, 22: 213-215.
- Klute, A., and Dirksen, C., 1986. "Hydraulic Conductivity and Diffusivity-Laboratory Methods," in A. Klute, ed., *Methods of Soil Analysis, Part I=Physical and Mineralogical Methods*, American Society of Agronomy Monograph 9, 2d ed., pp. 687-734.
- Kovacs, G. 1981. *Seepage Hydraulics*. Elsevier Science Publishers, Amsterdam.
- Law, B.E., Baldocchi, D.D., and Anthoni, P.M. 1999. Belowcanopy and soil CO₂ fluxes in a ponderosa pine forest. *Agric. For. Meteorol.* 94: 171-188.
- Lawrence, J.R., Zanyk, B.N., Wolfaardt, G.M., Hendry, M.J., Robarts, R.D., and Caldwell, D.E. 1993. Design and evaluation of a meso scale model vadoze zone and ground water system. *Ground Water* 31, 446-455.
- Lawrence, J.R., and Hendry, M.J. 1995. Mesocosms for subsurface research. *Water Quality Research J. Canada* 30, no. 3:493-512.
- Lee, E.S., Birkham, T.K., Wassenaar, L.I., and Hendry, M.J. 2003a. Microbial respiration and diffusive transport of O₂, ¹⁶O₂, and ¹⁸O₂ in unsaturated soils and geologic sediments. *Environ. Sci. and Technol.* 37: 2913-2919.
- Lee, E.S., Hollings, P., and Hendry, M.J. 2003b. Use of O₂ consumption and CO₂ production in kinetic cells to delineate pyrite oxidation-carbonate buffering and microbial respiration in unsaturated media. *J. Cont. Hydro.* 65: 203-217.
- Lee, R. W. 1997. Effects of carbon dioxide variations in the unsaturated zone on water chemistry in a glacial -outwash aquifer. *Applied Geochemistry* 12, 347-366.
- Lefebvre, R., Hockley, D., Smolensky, J., and Lamontagne, A. 2001. Multiphase Transfer processes in waste rock piles producing acid mine drainage 2: applications of numerical simulation. *J. Cont. Hydro.* 52: 165-186.

- Linn, D.M., and Doran, J.W. 1984. Effect of water-filled pore space on carbon dioxide and nitrous oxide production in tilled and non tilled soils. *Soil Sci. Soc. Am. J.* 48, 1267-1272.
- Lorenz, W.C. and Tarpley, E.C. 1963. Oxidation of coal mine pyrite. US Bureau of Mines Report, Inv. 6247. Pittsburgh, PA.
- Looney, B.B., and Falta, R.W. 2000. Vadoze Zone. Science and Technology Solutions, Vols. I and II, Battelle Press, Columbus, Ohio.
- Lowson, R.T. 1982. Aqueous oxidation of pyrite by molecular oxygen. *Chemical Reviews, American Chemical Society*, 82(5): 462-496.
- Lofffield, N.S., Brumme, R., and Beese, F. 1992. Automated monitoring of nitrous oxide and carbon dioxide flux from forest soils. *Soil Sci. Soc. Am. J.* 56: 1147-1150.
- Martin, V., Aubertin, M., Buissiere, B., Mbonimpa, M., Dagenais, A.M., and Gosselin, M. 2006. Proc. Of the 7th International Conference on Acid Rock Drainage (ICARD), March 26-30, 2006, St Louis MO. R.I. Barnhisel (ed.) Published by the American Society of Mining and Reclamation (ASMR), 3134 Montavesta Road, Lexington, KY 40502.
- Marshall, T.J., Holmes, J.W., and Rose, C.W. 1996. *Soil physics*. 3rd ed. Cambridge University Press, Cambridge, U.K.
- Matson, P.A., and Harris, R.C. 1995. *Biogenic Trace Gases: Measuring Emissions from Soil and Water*. Blackwell Scientific.
- Mbonimpa, M., 1998. Injizierfahigkeit von Feinstbindemittelsuspensionen zur Abdichtung von Lockergesteinen, *Mitteilungen des Instituts von Grundbau, Bodenmechanik and Energieasserbau (IGBE), Universitat*.
- Mbonimpa, M, Aubertin, M., Aachib, M., and Bussiere, B. 2002. Interpretation of field tests to determine oxygen diffusion and reaction rate coefficients of tailings and

- soil covers. Proceedings of the 55th Canadian Geotechnical Conference – 3rd Joint International Association of Hydrogeologists – Canadian National Chapter – Canadian Geotechnical Society (IAH-CNC/CGS) Conference: Ground and Water: Theory to Practice, Niagara Falls, pp. 147-154. CD-ROM.
- Mbonimpa, M, Aubertin, M., Aachib, M., and Bussi re, B. 2003. Diffusion and consumption of oxygen in unsaturated cover materials. *Can. Geotech. J.* 40: 916-932.
- MEND Secretariat CANMET, 2001, Manual Report 5.4.2, vol. 3 – Prediction, vol. 4 – Prevention and control, vol. 5 – Treatment, vol. 6 Monitoring.
- Moloson J.M., Fala O., Aubertin M., Bussi re B. 2005. Numerical simulations of pyrite oxidation and acid mine drainage in unsaturated waste rock piles. *J. Cont. Hydrol.* 78 (4): 343-371.
- Moncrieff, J.B., and Fan, C. 1999. A model for soil CO₂ production and transport 2: Application to a Florida Pinus elliotte plantation. *Agric. For. Met.* 95: 237-256.
- Moore, C.J. 1986. Frequency response corrections for eddy correlation systems. *Boundary-Layer Met.* 37: 17–35.
- Mualem, Y. 1978. Hydraulic conductivity of unsaturated porous media: generalized macroscopic approach. *Water Resour. Res.* 14: 325-334.
- Mualem, Y. 1986. Hydraulic conductivity of unsaturated soil: Prediction and formulas. In *methods of soil analysis, Part I: Physical and mineralogical methods*. Edited by A Klute. American Society of Agronomy (ASA) and Soil Science Society of America (SSSA), Madison, Wis. Agronomy Monograph No. 9. pp. 799-823.
- Nakayama, F.S. 1990. Soil respiration. *Remote Sensing Rev.* 5:311-321.
- Neal, C., Whitehead, P.G., 1988. the role of CO₂ in long term stream acidification processes: a modeling viewpoint. *Hydrological Science J.* 33: 103-108.

-
- Newman, L., M.Sc. Dissertation, University of Saskatchewan 1999.
- Nicholson, R.V., Gillham, R.W., Cherry, J.A., and Reardon, E.J. 1989. Reduction of acid generation in mine tailings through the use of moisture-retaining cover layers as oxygen barriers. *Can. Geotech. J.* 26: 1-8.
- Nicholson, R.V. 1994. Iron-sulfide oxidation mechanisms: laboratory studies.. In *Short Course Handbook on Environmental Geochemistry of Sulfide Mine-Wastes*. Vol. 22 (ed. J.L. Jambor and D.W. Blowes), pp. 163-183. Mineralogical Association of Canada.
- Noel, M., M., Rykaart, E.,M 2003. Comparative Study of Surface Flux Boundary Models to Design Soil Covers for Mine Waste Facilities. 6th International Conference on Acid Rock Drainage (ICARD), Cairns, QLD, 12-18 July 2003.
- Nordstrom, D.K., and Alpers, C.N. 1999. Geochemistry of acid mine waters. In *Environmental Geochemistry of Mineral deposit* (eds. G.S. Plumlee and M.J. Logsdon), pp 133-160. Society of Economic Geologists, Little, CO.
- Norman, J.N., Garcia, R., Verma, S.B. 1992. Soil CO₂ fluxes and the carbon budget of a grassland. *J. of Geophys. Res.* 97(17): 18,845-18,853.
- Norman, J.M., Kucharik, C.J., Gower, S.T., Baldocchi, D.D., Crill, P.M., Rayment, M., Savage, K., and Striegl, R.G. 1997. A comparison of six methods for measuring soil-surface carbon dioxide fluxes. *J. Geophys. Res.* 102: 28771-28777.
- Norris, P.R. 1989. Factors affecting bacterial mineral oxidation: the example of carbon dioxide in the context of bacterial diversity. In *Proceedings Internat. Symp. On Biohydrometallurgy* (J. Salley, R.G..I. McReady & P.L. Wichllacz, eds.). CANMET Report SP 89-10, 3-14. Dept. Energy Mines Resources Canada.
- O'Kane, M., Wilson, G.D., Barbour, S.L., and Swanson, D.A. 1995. Aspects on the

- performance of the till cover system at Equity Silver Mines Ltd. Proceedings of the Conference on Mining and the Environment, Sudbury, ON, Canada.
- Osozawa, S., and Hasegawa, S. 1995. Diel and seasonal changes in carbon dioxide concentration and flux in an Andisol. *Soil Sci.* **160**: 117-124.
- Pantelis, D., and Ritchie, A.I.M., 1991. Macroscopic transport mechanisms as a rate-limiting factor in dump leaching of pyrite ores. *Applied Mathematics Modelling*, **15**:136-143.
- Pantelis, G., Ritchie, A.I.M. and Stepanyants, Y.A. 2002. A conceptual model for the description of oxidation and transport processes in sulfidic waste rock dumps. *Appl. Math Model*, **26**(7): 751-770.
- Penman, H.L. 1948. Natural evaporation from open water, bare soil and grass. *Proc. R. Soc. London Ser. A* **193**, 120-146.
- Philip, J.R. 1986. Linearized unsteady multidimensional infiltration. *Water Resour. Res.* **22**: 1717-1727.
- Piñol, J., Alcañiz, J.M., Rodà, F. 1995. Carbon dioxide effluxes and pCO₂ in soils of three *Quercus ilex montana* forest. *Biochemistry* **30**: 191-215.
- Priestley, C.H.B., and Taylor, R.J. 1972. "on assessment of the surface heat flux and evaporation using large-scale parameters", *Mon. Weather Rev.*, **100**: pp. 81-92.
- Rankama, K. 1954. *Isotope Geology*. McGraw-Hill Book Co., Inc.
- Rayment, M.B., Jarvis, P.D. 1997. An improved open chamber system for measuring soil CO₂ effluxes of a Boreal black spruce forest. *J. Geophys. Res.* **102**: 28779-287884.
- Reardon, E.J., Allison G.B., and Fritz P. 1979. Seasonal chemical and isotopic variations of soil CO₂ at Trout Creek, Ontario. *J. hydrol.* **43**, 355-371.
- Richards, L.A. 1931. Capillary conduction of liquid through porous medium. *Journal of*

Physics 1: 318-333.

- Richards, G.J. 1998. Minicosm scale investigations into natural biogeochemical processes in a sandy vadose zone. Master of Science Thesis, Department of Geological Sciences, University of Saskatchewan, Saskatoon, Saskatchewan, Canada.
- Rightmire, C. T., and Hanshaw B. B. 1973. Relationship between the carbon isotop composition of soil CO₂ and dissolved carbonate species in groundwater. *Water Resour. Res.* 9(4): 958-967.
- Rightmire, C.T. 1978. Seasonal variation in PCO₂ and ¹³C content of soil atmosphere. *Water Resour. Res.* 14(4): 691-692.
- Rimstidt, J.D., Vaughan, D.J. 2003. Pyrite oxidation: a state-of-the-art assessment of the reaction mechanism. *Geochim. Cosmochim. Acta* 67, 873-880.
- Ritchie, A.I.M. 1994. Short Course Handbook on Environmental Geochemistry of sulfide Mine-Wastes; Jambor, L., Blowes, D. W., Eds.; Mineralogical Association of Canada: Waterloo, Ontario, 1994.
- Ritchie, A.I.M. 1994a. The waste-rock environment. In Short Course Handbook on Environmental Geochemistry of Sulfide Mine-Wastes, Vol. 22 (ed. J.L. Jambor and D.W. Blowes), pp. 201-245. Mineralogical Association of Canada.
- Ritchie, A.I.M. 1994b. Sulfide oxidation mechanisms: controls and rates of oxygen transport. In Short Course Handbook on Environmental Geochemistry of Sulfide Mine-Wastes, Vol. 22 (ed. J.L. Jambor and D.W. Blowes), pp. 201-245. Mineralogical Association of Canada.
- Rochette, P., Gregorich, E.G., and Desjardins, R.L. 1992. Comparison of static and dynamic closed chambers for measurement of soil respiration under field conditions. *Can. J. Soil Sci.* 72(4): 605-609.

- Rowell, D.L., Martin, M.W., and Nye, P.H. 1967. The measurement and mechanism of ion diffusion in soils. III. The effect of moisture content and soil solution concentration on the self diffusion of ions in soils. *J. Soil Sci.* 18: 204-222.
- Russell, C.A., and Voroney, R.P. 1998. Carbon dioxide from the floor of a boreal aspen forest, 1, relationship to environmental variables and estimates of C respired, *Can. J. Soil Sci.* 78: 301-310.
- Russell, E.J. and Appleyard, A. 1915. The atmosphere of the soil: its composition and the causes of variation. *J. Agric. Sci.* 7, 1-48.
- Rykaart, E.M., Wilson, G.W., Fredlund, D.G., and Currey, N.A. 2001. A spatial flux boundary model for tailings dams. *Proceedings of the 54th Annual Canadian Geotechnical Conferences*, 1102-1109.
- Scanlon, B.R., Christman, M., Reedy, R.C., Porro, I., Simunek, J., and Flerchinger, G.N. 2002. Intercode comparisons for simulating water balance of surficial sediments in semiarid regions. *Water Resour. Res.* 38(12): 59-16.
- Scott-Denton, L.E., Sparks, K.L., and Monson, R.K. 2003. Spatial and temporal controls of soil respiration rate in a high-elevation, subalpine fores. *Soil Biol. Biochem.* 35: 525-534.
- Sellers, P., Hall, F., Margolis, H., Kelly, B., Baldocchi, D., den Hartog, G., Cihlar, J., Ryan, M.J., Goodison, B., Crill, P., Jon Ranson, K., Lettenmair, D., and Wickland, D.E., 1995. The Boreal Ecosystem-Atmosphere Study (BOREAS): an overview and early results from the 1994 field year. *Bull. Am. Meteorol. Soc.*, 76, 1549-1577.
- Shi, Pei-Li, Zhang, X.Z., Zhong, Z.M., and Ouyang, H. 2006. Diurnal and seasonal variability of soil CO₂ efflux in acropland ecosystem on the Tibetan Plateau. *Agric. For. Meteorol.* 137: 220-233.

- Schuepp, P.H., Leclerc, M.Y., Macpherson, J.I., and Desjardins, R.L. 1990. Footprint prediction of scalar fluxes from analytical solutions of the diffusion equation. *Boundary Layer Meteorology*, 50: 355-376.
- Schuman, G., Caruccia, F.T. & Bradham, W.S. 1992. Assessment of factors affecting pyrite reactivity. U.S. Government Report PB 92-140227.
- Shuttleworth, W.J. 1993. Evaporation, in *Handbook of Hydrology*, McGraw-Hill, D.R. Maidment, New York.
- Smolensky, J., and Hockley, D. 1999. Oxygen Transport Processes in the Nordhalde of the Ronnenburgh Mining District, Germany Mining and the Environment II. *Sudbury' 99 Conference Proceedings*, p271.
- Solomon, D.K., Cerling, T.E. 1987. The annual carbon dioxide cycle in a montaine soil: observations, modeling, and implications for weathering. *Water Resour. Res.* **23** (12): 2257-2265.
- Steffen, Robertson, and Kirsten (Canada) Inc. 1993. Key Lake Waste Rock Characterization prepared for Cameco Corp.
- Stumm, W., and Morgan, J.J. 1981. *Aquatic Chemistry*. Wiley-Interscience. alpine-subalpine sites. *Global Biogeochem. Cycles* 10(3), 473-482.
- Sunquist, E.T., 1993. The global carbon dioxide budget, *Science* (Washington, D. C.), 259, 934-941.
- Sydor, R.C. 1992. Engineered mine tailings cover: verification of drainage behaviour and investigations of design. M.Sc. thesis, University of Waterloo, Waterloo, Ont.
- Thierron, V., Laudelout, H., 1996. Contribution of root respiration to total CO₂ efflux from the soil of a deciduous forest. *Can. J. For. Res.*, 26, 1142-1148.
- Thorstenson, D.C., and Pollock, D.P. 1989. Gas transport in unsaturated zones: multicomponent systems and the adequacy of Fick's law. *Water Resour. Res.*

25: 477-507.

- Timms, G.P., and Bennet, J.W. 2000. In Proceeding of the International Conference on Acid Rock Drainage (ICARD), Denver, Colorado 2000: 841-849.
- Trumbore, S. E., Davidson E. A., de Camargo, P. B., Nepstad D. C., and Martinelli L. A. 1995. Belowground cycling of carbon in forests and pastures of Eastern Amazonia. *Global Biogeochemical Cycles* 9(4), 515-528.
- Twine, T.E., Kustas, W.P., Norman, J.M., Cook, D.R., Houser, P.R., Meyers, T.P., Prueger, J.H., Starks, P.J., and Wesely, M.L. 2000. Correcting eddy-covariance flux underestimates over a grassland. *Agri. For. Meteorol.* 103: 279-300.
- Unsaturated Soils Group 1997, *SoilCover User's Manual*, Department of Civil Engineering, University of Saskatchewan, Saskatoon, Saskatchewan, Canada.
- Vermaak, R., and Bezuidenhout 2003. The performance of trial cover used for the rehabilitation of acid generating coal reject dumps in Northern Kwazulu-Natal, South Africa. *Proceedings Sixth International Conference on Acid Rock Drainage (ICARD)*, 399-410.
- Wallick, E.I. 1983. Gas composition in the unsaturated zone as an index of geochemical equilibrium in reclaimed landscapes. In *Assessment of Reclamation Potential and Hydrologic Impact of Large-Scale Surface Mining of Coal in Plains Areas of Alberta: Summary Report of Activities 1982-1983*, Vol. Appendix H. Alberta Chapter C.L.R.A., Reclamation Conference, 24-25 February, 1983.
- Wang, Y., Amundson, R., and Trumbore, S. 1999. The impact of land use change on C turnover in soils. *Global Biogeochem. Cycles* 13(1): 47-57.
- Weast, R. and Astle, M.J. 1981. *CRC Handbook of Chemistry and Physics*. CRC Press, Inc.
- Webb, E.K., Pearman, G.I., and Leuning, R.L. 1980. Correction of flux measurements

- for density effects due to heat and water vapour transfer. *Quarter. Journal of the Royal Meteorological Society* 106: 85-100.
- Weeks, E.P., Earp, D.E., and Thompson, G.M. 1982. Use of atmospheric fluorocarbons F-11 and F-12 to determine the diffusion parameters of the unsaturated zone in the southern High Plains of Texas, *Water Resour. Res.* 18: 1365-1378.
- Welles, J.M., Demetriades-Shah, T.H., and McDermitt, D.K., 2001. Considerations for measuring ground CO₂ effluxes with chambers. *Chemical Geology* 177: 3-13.
- Wickland, K. P., Striegl, R. G., 1997. Measurements of soil carbon dioxide and methane concentrations and fluxes, and soil properties at four ages of jack pine forest in the Southern Study, Saskatchewan, Canada, 1993-1995. U.S. Geol. Surv. Open-File Rep., 97-49.
- Wiersma, C.L., Rimstidt, J.D., 1984. Rates of reaction of pyrite and marcasite with ferric iron at pH 2. *Geochim. Cosmochim. Acta* 48: 85-92.
- Wilson, M. R. 1987. Petrogenesis of fluids associated with unconformity-type uranium deposits in Saskatchewan, and with the Zortman-Landusky Au-Ag deposits in Montana. Ph.D., University of Saskatchewan.
- Wilson, G.W. 1990. Soil Evaporative fluxes for Geotechnical Engineering problems. Ph.D. thesis, University of Saskatchewan, Saskatoon, Saskatchewan, Canada.
- Wilson, G.W., Fredlund, D.G., and Barbour, S.L. 1994. Coupled soil-atmosphere modeling for soil evaporation. *Can. Geotech. J.* 31: 151-161.
- Wilson, G.W., Fredlund, D.G., and Barbour, S.L. 1997. The effect of soil suction on evaporative fluxes from soil surfaces. *C. Geotech. J.*, 34: 145-155.
- Wind, G.P. 1955. Field experiment concerning capillary rise of moisture in heavy clay soil. *Netherlands Journal of Agricultural Science* 3: 60-69.
- Wohlfahrt, G., Anfang, C., Bahn, M., Haslanter, A., Neesely, C., Schmitt, M., Drosler,

-
- M., Pfdenhauer, and J., Cernusca, A. 2005. Quantifying nighttime ecosystem respiration of a meadow using eddy covariance, chambers and modeling. *Agri. For. Meteorol.* 128: 141-162.
- Wood, B.D., and Petraitis, M.J. 1984. Origin and distribution of carbon dioxide in the unsaturated zone of the southern High Plains of Texas. *Water Resour. Res.* 20 (9): 1193-1208.
- Wood, B. D., Keller K. C., and Johnstone, D. L. 1993. In situ measurement of microbial activity and controls on microbial CO₂ production in the unsaturated zone. *Water Resour. Res.* 29(3), 647-659.
- Yanful, E.K., and Aube, B.C. 1993a. Modelling moisture retaining soil covers. In *Proceedings of the 1993 Joint CSCE-ASCE Na- © 2005 NRC Canada 1198 Can. Geotech. J. Vol. 42, 2005 © 2005 NRC Canada.*
- Yanful, E.K., Mousavi, S.M., and Yang, M. 2003a. Modeling and measurement of evaporation in moisture-retaining soil covers. *Advances in Environmental Research*, 7: 783–801.
- Yanful, E.K. and Mousavi, S.M. 2003b. Estimating falling rate of evaporation from finite soil columns. *The Science of the Total Environment* 313: 151-152
- Yong, R.N. 2001. *Geoenvironmental engineering – Contaminated soils, pollutant fate, and mitigation.* CRC Press, Boca Raton, Fla.
- Zill, D.G. and Cullen, M.R. 1992. *Advanced Engineering Mathematics.* PWS Publishing Company, Boston, MA.

APPENDIX A

Measuring O₂ Fluxes Using the Dynamic Closed Chamber (DCC) System

NOTE: This section is out of scope of this thesis. This is an on-going research work being carried out by the author of this thesis in the Department of Mining Engineering at UBC, under the supervision of Prof. Ward Wilson.

A1. Design of the dynamic closed chamber (DCC)

Full details of the design, fabrication, and description of the DCC chamber are presented in section 3.4.2.1 of this thesis, and in Kabwe (2001) and Kabwe et al. (2002).

The dynamic closed chamber (DCC) used in this work was initially designed for measuring CO₂ fluxes (Kabwe, 2001 and Kabwe et al., 2002). It consists of an open-ended rim (collar) with a lid. Full details of the design, construction, and operation are presented in Kabwe et al. (2002). Chamber collars were fabricated from fiberglass rims (0.76m dia. × 0.15m height); the chamber lid (0.76m dia. × 0.05m thick) was fabricated from Plexiglas. The lid was attached to the collars with nuts and bolts.

The changes of mass of O₂ within the chamber was measured using an Oxymax ER-10 oxygen gas analyzer.

A2. Principle of operation

The rate of changes of the mass of O₂ within the chamber placed on the surface of the waste-rock dump can be described by:

$$\frac{dm}{dt} = FA \quad (A1)$$

where F is the flux of O_2 through the surface of the waste-rock and A is the area of the base of the chamber. The rate of change of O_2 concentration within the chamber, dC/dt , is given by (Timms and Bennett, 2001):

$$\frac{dC}{dt} = \frac{1}{V} \frac{dM}{dt} \quad (A2)$$

where V is the volume of the chamber. The O_2 flux can then be calculated from the rate of change of O_2 concentration within the chamber. Combining Equations 1 and 2 gives:

$$\frac{dC}{dt} = \frac{F}{h} \quad (A3)$$

where $h = V/A$, the height of the chamber. The critical aspect of the flux chamber design is the need to be able to measure the low fluxes typical of covered systems.

A3. Description and measurement principle of the Oxymax ER-10 oxygen gas analyzer

O_2 was analyzed using an O_2 -Gas Respirometer (Micro-Oxymax ER-10, Columbus Instruments, Ohio USA). The ER-10 is a computerized apparatus for measuring very low levels of gaseous oxygen uptake. An IBM-PC compatible computer maintains and displays the operation of the Micro-Oxymax instrument. Before starting the measurement, the system needs only the time interval between samples to be specified and the chamber volume which is computed automatically during system calibration. When the experiment is started, the software assumes control of the acquisition of information and storage of results and/or presentation to the printer.

Oxymax ER-10 can measure liquid or solid samples from 50 mL to 10 L in volume. The principle of measurement, involves air sampling from the head space of the chamber, circulating it through the gas analyzer and returning back to the sample chamber without any contact with the sample. Samples are continuously aerated with adjustable airflow (100 mL/min. to 1,500 mL/min.), except for the short time interval when a particular sample is being measured by the gas analyzer. Calibration of O_2 gas analyzer is performed automatically at specific time interval with ambient air, thus,

removing the need for the mixed gas bottle. Results of measurements are presented in $\mu\text{lO}_2/\text{min}$ or as an accumulated (total in μl) value of O_2 consumed from the beginning of the experiment. The Oxymax ER10 operates on the principle of using gas sensor to measure the change in the oxygen in the head space of a measuring cell and using this information to calculate how much oxygen the sample is consuming (oxygen uptake). To compute the oxygen consumption requires two measurements of the head space separated by a span of time. The oxygen sensor operates as an oxygen battery (fuel cell), and measures oxygen percentage directly.

The sensitivity of the system to oxygen consumption (uptake) is dependent on two factors: the volume of the headspace gas in the measuring cell, and the span of time between measurements. In general, the smaller the head space volume, the higher the sensitivity. Also, the longer the time between measurements, the higher the sensitivity. The volume of the headspace in the cell is automatically measured by the apparatus. The apparatus uses a direct method to detect and correct errors in the sensor outputs (resulting from environmental temperature changes, barometric pressure changes, or changes in the sensor), and thereby raises the system's measuring accuracy.

The Micro-Oxymax instrument also contains a feature called 'automatic refresh' which allows the gas in the headspace of the measuring cell to be replaced periodically with fresh air or other gas mixtures. This feature is important if the level of oxygen consumption by the sample is high enough that the oxygen becomes depleted in the headspace gas.

A4. Preliminary Results and Discussion

A4.1 Site Location

The Syncrude Canada Ltd (SCL) mine is located 30 km north of Fort McMurray, Alberta, Canada. The regional climate is continental. The mean annual precipitation is approximately 440 mm of which 310 mm is rain (Meiers et al., 2006). The mean annual potential evaporation (Penman) is in the range of 600 to 700 mm/year (Boese, 2003; Babour et al., 2001; Elshorbagy et al., 2005).

Mildre Lake Mine surface dump and other referred to as SW30 dumps were constructed with marine saline-sodic shale overburden removed during mining of soil sands. The SCL mine produces over 200,000 barrels of oil per day (Meiers et al., 2006). Up to 14 tonnes of overburden is excavated for each cubic meter of oil produced. These overburden deposits are salt rich (saline) and sodic. The glacial soil consists of approximately 2% gravel, 38% sand, and 60% silt and clay sized particles while the shale consists of approximately 0.5% gravel, 14.5% sand, and 85% silt and clay sized particles (Meiers et al., 2006).

A4.2 Selection of the height of the DCC chamber

The height of the chamber was selected based on the test results conducted on SWD30 dump at Syncrude on August 12, 2001. The rate of change in oxygen concentration within the chamber described by Equation 3A shows that the smaller the height, the greater the rate of change of oxygen concentration. However, a smaller height also results in a smaller gas volume and a greater relative uncertainty on the volume, due to the irregular profile of the cover surface (Timms and Bennett, 2001). Fig. 1 shows the changes in oxygen concentration measured using three different chamber volumes of 2.5, 4.5, and 6.3 L with the corresponding chamber heights of 0.01, 0.015 and 0.02 m, respectively. Results clearly indicated that the smaller volume of 2.5 L (e.g., $h = 0.01$ m) yielded the smaller rate of change of concentration (e.g., a nearly flat slope).

However, the chamber volume of 4.5 L ($h = 0.015$ m) yielded the greater rate of change of oxygen concentration (e.g., steeper slope) than the chamber volume of 6.3 L ($h = 0.02$ m). The height ($h = 0.015$ m) for the headspace of the chamber presented here, was therefore selected as a compromise between maximizing the rate of change of oxygen concentration and minimizing the uncertainty on the gas volume of the chamber.

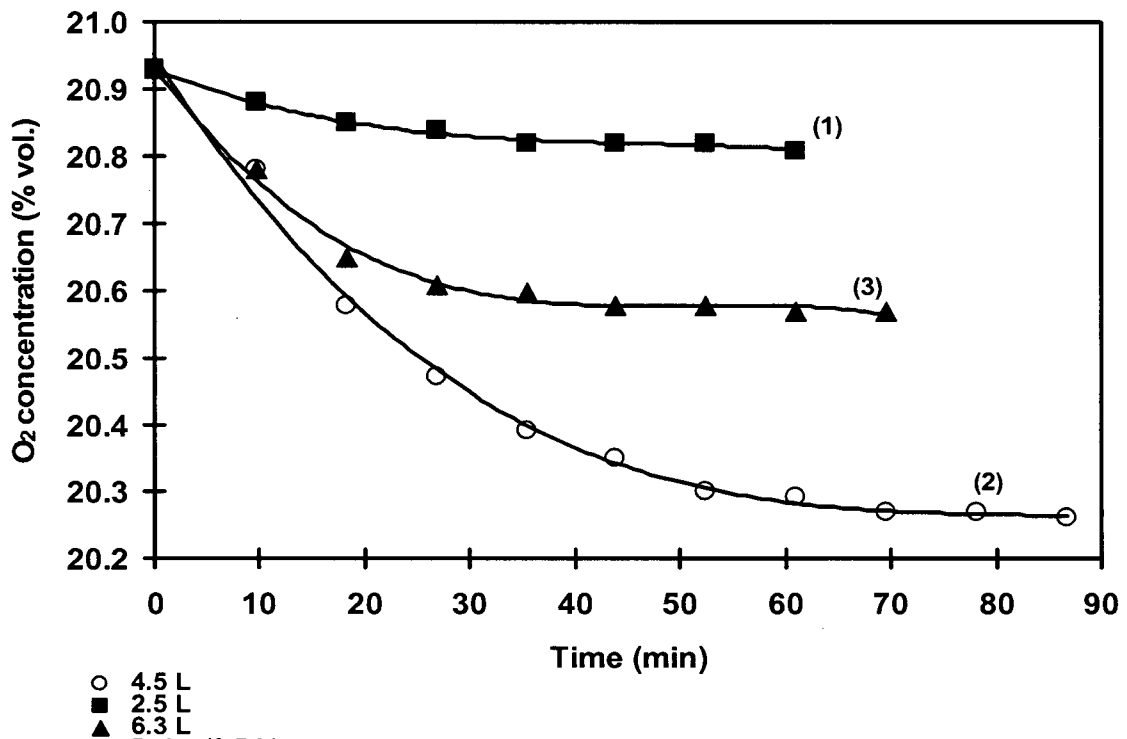


Fig. 1. Changes in oxygen concentrations in chambers with volume of (1) 2.5 L and (2) 4.5 L and (3) 6.3 L as a function of time. Measurements were done at the SWD30 dump at the Syncrude mine on 19 July, 2001.

A4.3 Effect of Relative Humidity

Fig. 2 showed the oxygen concentration and oxygen consumption rate measured on 12 August, 2001 at the DSWR as a function of time. The measurements results yielded a linear decrease in oxygen concentration of the form: $y = -0.0012x + 20.905$ ($R^2 = 0.9934$). The plot revealed a slight large initial drop in oxygen concentration within the chamber during the first 10 min time-interval followed by a more gradual decrease in O₂ concentration. The initial larger drop in O₂ concentration is likely due to the effect of relative humidity. The effect of relative humidity on oxygen concentration within the chamber is well documented in literature. Timms and Bennett (2001) indicated that early measurements with the surface chamber device revealed a large initial drop in oxygen concentration within the chamber when it was placed on the ground, followed by a more gradual decrease. ER-10 employs a drying agent

(Anhydrous Magnesium Perchlorate) in port in which gas is drawn to remove water vapor.

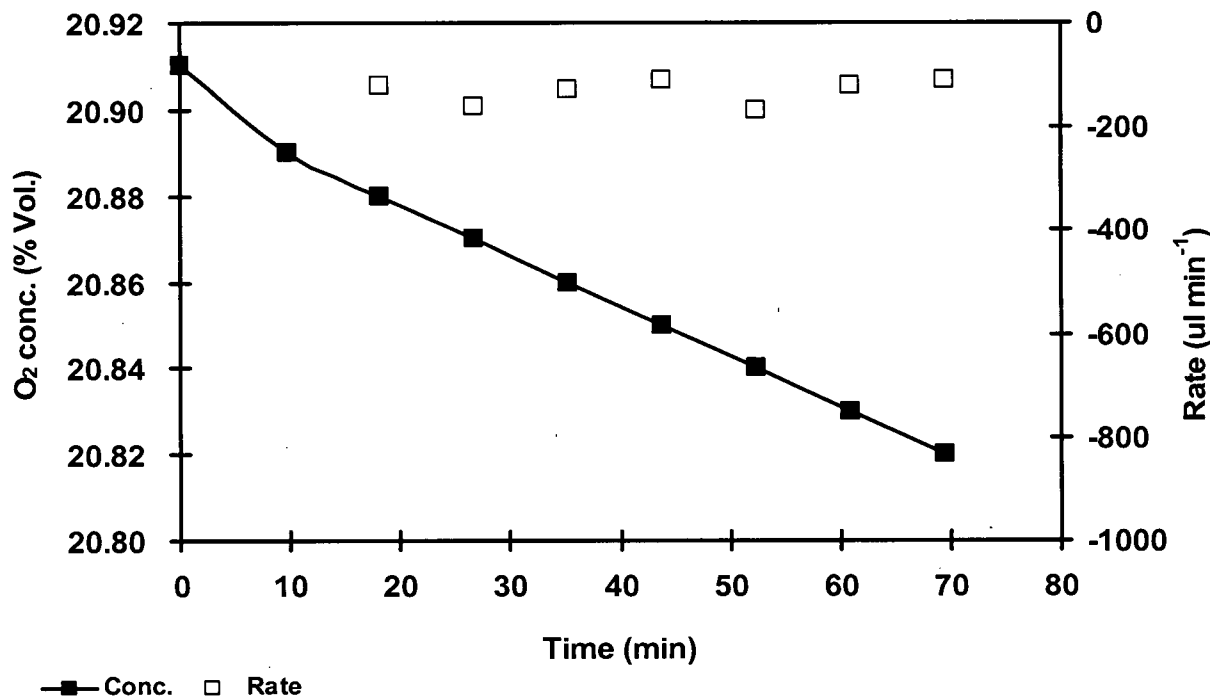


Fig. 2. Change in oxygen concentration and oxygen consumption rate in a chamber installed at the Deilmann south waste-rock (DSWR) as a function of time. Measurements were done on August 9, 2001.

Water removal capacity depends on the type and size of the drying agent employed. Fig. 2 showed the oxygen consumption rate (open symbols) measured within the chamber. The degree of variation was small (covariance, CV = 17.6) with a mean rate of $133 \pm 23.4 \mu \text{ min}^{-1}$. During the measurements the chamber temperature decreased from 17.1 to 15.5 °C. Results also showed that the sensor's pressure remained constant (797.9) throughout the duration of the measurements. Moreover the ER-10 detects and corrects errors in the sensors outputs resulting from environmental temperature changes and barometric pressure changes. The effect of high CO₂ concentration was eliminated by including soda lime in the drying column.

A.5 Effect of soil cover system on O₂ diffusion

Fig. 3 shows the measured oxygen concentrations in the chambers installed on a cover (curve with broken line) and non-cover (curve with solid line) sections of the D30 Dumps using the ER-10 Respirometer. The measurements were done on July 18, 2001. Results showed that the oxygen concentration in the headspace of the chamber installed on the cover section did not change significantly throughout the duration of 86 min test-period. The plot, however, revealed a slight drop in oxygen concentration from 20.91 to 20.87% during the first 10 min time-interval.

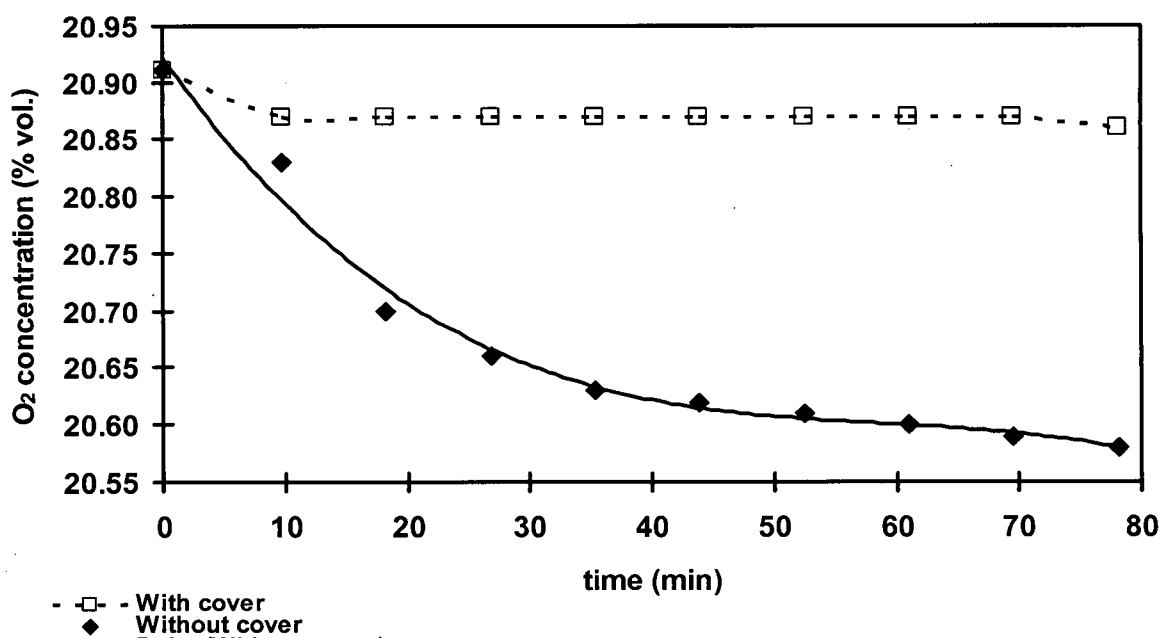


Fig. 3. Changes in oxygen concentrations in the chambers installed on (1) a cover and (2) uncover portions of the D30 dump at Syncrude on July 8, 2001.

The slight decrease in concentration is likely related to the effect of relative humidity on oxygen concentration within the chamber.

The oxygen concentration in the chamber installed on uncover section of the Dumps decreased initially at a faster rate followed by a gradual decreased with time. The decrease in oxygen concentration was represented by the function $y = -10^{-6}X^3 + 0.0003X^2 - 0.0244X + 20.948$ ($R^2 = 0.9948$). At the end of the 86-min test period the concentration decreased from 20.91 to 20.58%.

Finally, the above results indicated that the DCC chamber with the ER-10 Respirometer can be suitable for assessing the performance of the cover placed on mine waste dumps.

APPENDIX B

Eddy Correlation (EC) Method

B.1 Introduction

This section presents a brief theory and derivation of basic equations describing the Eddy correlation (EC) method.

B.2 Theory and basic equations

The eddy correlation flux, is expressed as

$$Flux (kg m^{-2} s^{-1}) = \rho . w . c \quad [A1]$$

where: ρ is the density of the air ($kg m^{-3}$); w is the vertical wind ($m s^{-1}$); c is the mass concentration of substance ($kg kg^{-1}$) i.e., molecular weights for CO_2 and air (m_c/m_a).

Eddy correlation when standard micrometeorological criteria are met [Hicks et al. 1989] will provide absolute evaluations of vertical fluxes in natural environments without making assumptions associated with diffusivities or the nature of the surface cover. In addition, the exchange rate measured represents a spatially integrated flux and the technique is unobtrusive, therefore not disturbing the environment under study. If we write each term of the right-hand side of the above equation [A1] as the sum of a mean value and an instantaneous departure from that mean, i.e.

$$\rho = \bar{\rho} + \rho'; \quad w = \bar{w} + w'; \quad c = \bar{c} + c' \quad [A2]$$

then the equation becomes:

$$\overline{flux} = \bar{\rho}\bar{w}\bar{c} + \bar{\rho}\bar{w}c' + \bar{\rho}w'\bar{c} + \bar{\rho}w'c' + \rho'\bar{w}\bar{c} + \rho'\bar{w}c' + \rho'w'\bar{c} + \rho'w'c' \quad [A3]$$

since

$$\overline{\rho'} = \overline{w'} = \overline{c'} = 0 \quad [A4]$$

the average value of the flux reduces to:

$$\overline{flux} = \overline{\rho w c} + \overline{\rho' w' c'} + \overline{w \rho' c'} + \overline{c \rho' w'} + \overline{\rho' w' c'} \quad [A5]$$

If one ignores density fluctuations (small near the surface) and puts $\overline{\rho} = \rho$:

$$\overline{flux} = \rho \overline{w c} + \overline{\rho' w' c'} \quad [A6]$$

where the first term is the flux due to the mean vertical flow and the second is that due to the eddies.

Over uniform surfaces this further reduces to:

$$F = \rho \overline{w' c'} \quad [A7]$$

Application of this method requires measurement of the vertical wind and the substance concentration (i.e. temperature for the heat flux, vapor pressure for the water vapor flux, CO₂ concentration for the carbon dioxide flux) with sensors of time response short enough to respond to all eddies (fluctuations) (typically a fraction of a second or less). The two instantaneous measurements must be multiplied and their products summed to give flux totals over a period. This is most efficiently done by a measurement system incorporating a small computer.

The eddy correlation method derived the latent and sensible heat fluxes using the following relationships:

$$H = \rho C_p \overline{w' T'} \quad [A8]$$

$$E = L_v \overline{w' q'} \quad [A9]$$

where w , T , q , and C_p are the vertical velocity, temperature, humidity, and specific heat capacity of air respectively.

B.3. Wind profile and the transfer of momentum

The wind profiles above a stand can be represented by the simple logarithmic equation:

$$u_z = \frac{u_*}{k} \ln\left(\frac{z}{z_o}\right) \quad [A10]$$

where u_z is the velocity at height z , u_* is the friction velocity, z_o is the roughness parameter and k is Von Karman's constant ($k = 0.4$, average size of the eddy). Since momentum equals to mass times velocity, a decrease in wind speed represents a decrease of momentum. This decrease or loss of momentum may be thought of as a downward flux of momentum from the air towards the surface. The momentum flux (τ) is expressed as:

$$\tau = \rho K_M \frac{du}{dz} \quad [A11]$$

where, K_M is eddy transfer for momentum and τ is also called dynamic viscosity.

The kinematic viscosity is expressed as:

$$\frac{\tau}{\rho} = K_M \frac{du}{dz} \quad [A12]$$

Assume: $K_M = k u_* (z - D)$ and $\frac{\tau}{\rho} = u_*^2$

where D is zero-plane displacement,

Equation [A12] becomes:

$$\frac{du}{dz} = \frac{u_*}{k(z - D)} \quad [A13]$$

This expression represents the wind shear at height z over an aerodynamically rough surface.

Rearranging and integrating the above equation

$$\int_{u=0}^{u=u} du = k \int_{z=D+z_o}^{z=z} \frac{dz}{z - D} \quad [A14]$$

gives

$$u = \frac{u_*}{k} \ln\left(\frac{z - D}{z_o}\right) = \frac{u_*}{k} \ln(z - D) - \ln(z_o) \quad [A15]$$

If one measure the wind speed u , at several heights, z , and plotting $\ln(z - D)$ as a function of u , one can calculate u_* and z_0 .

Equation [14] could also be reported as:

$$\Delta u = \frac{u_*}{k} \ln\left(\frac{z_2 - D}{z_1 - D}\right) \Rightarrow u_* = \frac{k \Delta u}{\ln\left(\frac{z_2 - D}{z_1 - D}\right)} \quad [\text{A16}]$$

The sensible heat and latent heat fluxes can also be expressed as

$$H = -\rho C_p K_h \frac{dT}{dz} \quad [\text{A17}]$$

$$LE = -\rho \lambda K_v \frac{de}{dz} \quad [\text{A18}]$$

where, ρ is air density, C_p is the specific heat capacity of air, K_h is the eddy diffusivity for heat, and $\Delta\theta/\Delta z$ is the potential temperature gradient, K_v is the eddy diffusivity for water vapour, and $\Delta e/\Delta z$ is the vapor pressure gradient.

Similar expressions can be written for gradients of temperature and vapour pressure as follows

$$\frac{dT}{dz} = -\frac{H}{C_p u_* k (z - d)} \quad [\text{A19}]$$

and

$$\frac{de}{dz} = -\frac{\gamma \lambda E}{\rho C_p u_* k (z - d)} \quad [\text{A20}]$$

where γ is the psychrometric constant.

APPENDIX C

Computer code for CO₂ diffusion model

This section presents the computer codes for the "CO₂" diffusion model and spreadsheets describing different function of the program including:

1. Input spreadsheet
2. Water content spreadsheet
3. Temperature spreadsheet
4. Output spreadsheet
5. Results spreadsheet

1. Input spreadsheet

The user uses this spreadsheet to enter the # of nodes and # of simulation days. All constants values are also entered on this spreadsheet. The elevation (in m), porosity, and initial concentrations profile (in Kg/m³) is required to run the program and should be entered on this spreadsheet. The program run button [CO₂] is also located on this spreadsheet.

2. Water content spreadsheet

This spreadsheet contains a table of water content (as %). The Y axis represent the # of node (Elevation) and X axis represents # number of days of simulations. Note that the number of nodes and days are determined in the input spreadsheet.

3. Temperature spreadsheet

This spreadsheet is used to enter the temperature profiles for each day if known. However, the average temperature for the profile can be entered throughout the table.

4. Output spreadsheet

The output spreadsheet presents the complete results of calculations of new concentration and diffusion coefficient for each iteration. The spreadsheet displays the: day #, iteration#, Nodes, new concentration, concentration changes, diffusion coefficient, saturation and time difference calculated values.

5. Results spreadsheet

The new concentrations (in %) and diffusion coefficients (in m/s) for each profile and for each day are printed on this spreadsheet.

C.1. Computer code for "CO2" model

```
Public elev(), por(), oldconc(), daysv() As Double
Public watcont(), temp(), G(), Temperature(), allsatv(), G0, k, a, b As Double
Public Nodes, days, maxdelt, mindelt, starow As Integer
```

```
Sub read_input()
```

```
Nodes = Worksheets("Input").Cells(5, 3).Value
days = Worksheets("Input").Cells(6, 3).Value
maxdelt = Worksheets("Input").Cells(7, 3).Value
mindelt = Worksheets("Input").Cells(8, 3).Value
starow = Worksheets("Input").Cells(9, 3).Value
G0 = Worksheets("Input").Cells(10, 3).Value
k = Worksheets("Input").Cells(11, 3).Value
a = Worksheets("Input").Cells(12, 3).Value
b = Worksheets("Input").Cells(13, 3).Value
Tref = Worksheets("Input").Cells(14, 3).Value
```

```
ReDim elev(Nodes), por(Nodes), oldconc(Nodes), daysv(days)
ReDim watcont(Nodes, days), allsatv(Nodes, days), G(Nodes, days),
Temperature(Nodes, days), temp(Nodes, days)
Worksheets("results").Cells.ClearContents
Worksheets("output").Cells.ClearContents
Worksheets("TempDiff").Cells.ClearContents
```

```
For i = 1 To Nodes
```

```
    elev(i) = Worksheets("Input").Cells(starow + i - 1, 2).Value
    por(i) = Worksheets("Input").Cells(starow + i - 1, 3).Value
    oldconc(i) = Worksheets("Input").Cells(starow + i - 1, 4).Value
```

```
Next i
```

'populates the vector containing saturation, G and daysvector matrixes

```
For i = 1 To Nodes
```

```
  For d = 1 To days
```

```
    daysv(d) = Worksheets("watercont").Cells(4, d + 1).Value
```

```
    watcont(i, d) = Worksheets("watercont").Cells(i + 4, d + 1).Value
```

```
    allsatu(i, d) = watcont(i, d) / 100
```

```
    Temperature(i, d) = Worksheets("Temperature").Cells(i + 3, d + 1).Value
```

```
    Worksheets("TempDiff").Cells(i, d).Value = Temperature(i, d) - Tref
```

```
    temp(i, d) = Worksheets("TempDiff").Cells(i, d).Value
```

```
  Next d
```

```
  Worksheets("results").Cells(i + 2, 2).Value = oldconc(i)
```

```
Next i
```

```
End Sub
```

```
Sub CoCON()
```

```
Dim deltax(), sumdelt() As Double
```

```
Dim diffusion(), timesteps(), waterpor(), airpor() As Double
```

```
Dim eqpor(), avgdiffusion(), concchange(), sctime() As Double
```

```
Dim difffluxin(), satu(), difffluxout(), coflux(), newconc() As Double
```

```
diffcoefair = 0.000018          'diffusion coefficients (De)in m2/s
```

```
diffcoefwater = 0.0000000025    'diffusion coefficients (De)in m2/s
```

```
henry = 0.03
```

```
read_input
```

```
' average of the size of the spaces on either side of a node Delev
```

```
ReDim deltax(Nodes), diffusion(Nodes), timesteps(Nodes)
```

```
ReDim waterpor(Nodes), airpor(Nodes), eqpor(Nodes), avgdiffusion(Nodes)
```

```
ReDim concchange(Nodes), difffluxin(Nodes)
```

```
ReDim difffluxout(Nodes), coflux(Nodes), newconc(Nodes), satu(Nodes), sctime(days)
```

```
For i = 1 To Nodes - 2
```

```
  deltax(i + 1) = Abs(((elev(i + 2) - elev(i + 1)) + (elev(i + 1) - elev(i))) / 2)
```

```
Next i
```

```
deltax(1) = deltax(2)
deltax(Nodes) = deltax(Nodes - 1)
```

```
'calculate time interval in seconds for timesteps
```

```
For d = 1 To days - 1
  sctime(d) = (daysv(d + 1) - daysv(d)) * 86400
Next d
```

```
'main loop to compute Co2 concentration per day
```

```
d = 1
q = 2
While d <= days
  For i = 1 To Nodes
    satu(i) = allsatu(i, d)
  Next i
  countb = 1
  difference = maxdelt + 1
  sumdeltat = 0
```

```
While sumdeltat < sctime(d)
```

```
'statement to avoid extreme values
```

```
For i = 1 To Nodes
  If satu(i) <= 0 Then
    satu(i) = 0.00001
  End If
  If satu(i) >= 1 Then
    satu(i) = 0.9999
  End If
```

```
Next i
```

```
'compute Dw, Da, Eqpor, De
```

```
For i = 1 To Nodes
  waterpor(i) = satu(i) * por(i)
```

```

    airpor(i) = por(i) - waterpor(i)
    eqpor(i) = airpor(i) + henry * waterpor(i)
    diffusion(i) = (1 / por(i) ^ 2) * (diffcoefair * airpor(i) ^ 3.5 + henry * diffcoefwater *
waterpor(i) ^ 3.5)
    timesteps(i) = eqpor(i) * 0.5 * (deltax(i) ^ 2) / diffusion(i)
    G(i, d) = G0 * (airpor(i) ^ a) * (waterpor(i) ^ b) * Exp(k * (temp(i, d)))
    Next i
    deltat = Application.WorksheetFunction.Min(timesteps)
    If deltat > maxdelt Then
        deltat = maxdelt
    End If
    If deltat < mindelt Then
        deltat = mindelt
    End If
    If deltat > difference Then
        deltat = difference
    End If
    sumdeltat = sumdeltat + deltat

' solve finite difference equation
avgdiffusion(1) = 0
For i = 1 To Nodes - 1
    dlev = (elev(i) - elev(i + 1))
    avgdiffusion(i + 1) = dlev / (((dlev / (2 * diffusion(i))) + (dlev / (2 * diffusion(i + 1))))))
Next i

' compute concchange vector to solve the differential equation
concchange(1) = 0
For i = 2 To Nodes - 1
    d1 = (oldconc(i) - oldconc(i - 1)) / (Abs(elev(i) - elev(i - 1)))
    d2 = (oldconc(i + 1) - oldconc(i)) / (Abs(elev(i + 1) - elev(i)))
    concchange(i) = (deltat / (deltax(i) * eqpor(i)) * (-avgdiffusion(i) * d1 +
avgdiffusion(i + 1) * d2 + G(i, d)))
Next i

```

```
concchange(Nodes) = concchange(Nodes - 1)
For i = 1 To Nodes
    newconc(i) = oldconc(i) + concchange(i)
    If newconc(i) < 0 Then
        newconc(i) = 0
    End If
    oldconc(i) = (newconc(i))
Next i
For i = 1 To Nodes - 1
    ' Interpolate new saturation values for the next iteration
    satu(i) = allsatu(i + 1, d) + (allsatu(i + 1, d + 1) - allsatu(i + 1, d)) * deltat /
sctime(d)
Next i
countb = countb + 1
difference = sctime(d) - sumdeltat

For i = 1 To Nodes
Worksheets("output").Cells(q, 1).Value = d
Worksheets("output").Cells(q, 2).Value = countb
Worksheets("output").Cells(q, 3).Value = i
Worksheets("output").Cells(q, 4).Value = newconc(i)
Worksheets("output").Cells(q, 5).Value = concchange(i)
Worksheets("output").Cells(q, 6).Value = diffusion(i)
Worksheets("output").Cells(q, 7).Value = satu(i)
Worksheets("output").Cells(q, 8).Value = difference
q = q + 1
Next i
q = q + 1
Wend
Worksheets("results").Cells(1, 1).Value = "New Concentration"
Worksheets("results").Cells(4 + Nodes, 1).Value = "Diffusion"
For i = 1 To Nodes
    Worksheets("results").Cells(2, d + 1).Value = daysv(d)
```

```
Worksheets("results").Cells(i + 2, d + 1).Value = newconc(i) * 100000000
Worksheets("results").Cells(i + 2, 1).Value = elev(i)
Worksheets("results").Cells(5 + Nodes, d + 1).Value = daysv(d)
Worksheets("results").Cells(i + Nodes + 5, d + 1).Value = diffusion(i)
Worksheets("results").Cells(i + Nodes + 5, 1).Value = elev(i)
```

```
Next i
```

```
d = d + 1
```

```
Wend
```

```
Worksheets("output").Cells(1, 1).Value = "Day"
Worksheets("output").Cells(1, 2).Value = "Iteration#"
Worksheets("output").Cells(1, 3).Value = "Node"
Worksheets("output").Cells(1, 4).Value = "Newconc"
Worksheets("output").Cells(1, 5).Value = "Concchange"
Worksheets("output").Cells(1, 6).Value = "Diffusion"
Worksheets("output").Cells(1, 7).Value = "Saturation"
Worksheets("output").Cells(1, 8).Value = "Time Difference"
End Sub
```

```
Sub UpdateEmbeddedChart() \' attach macro to chart object
    ActiveSheet.DrawingObjects(Application.Caller).Select
    UserForm1.Show
```

```
End Sub
```

```
Sub UpdateChartSheet() \' attach macro to rectangle drawn over chart
    UserForm1.Show
```

```
End Sub
```

C.2. Typical spreadsheets

Table C1. Typical input spreadsheet

The screenshot shows a Microsoft Excel spreadsheet titled "Microsoft Excel - Co2b_v2 (1)UpdatedK2b". The spreadsheet is divided into several sections:

- Constants Table (Rows 4-14):** A table with three columns: Description, Constant, and Value.

Description	Constant	Value
Nodes		8
Days		11
Maxdeltat		8600
Mindeltat		50
Data starts		18
GO		1.00E-15
k		0.044
a		2
b		1.25
Tref		6.17
- Data Table (Rows 17-25):** A table with five columns: i=nodes, Elevation(i), Porosity (i), and OldCone (i).

i=nodes	Elevation(i)	Porosity (i)	OldCone (i)
1	0.00	4.00E-01	3.60E-09
2	0.02	4.00E-01	3.80E-09
3	0.15	4.00E-01	5.70E-09
4	0.30	4.00E-01	7.40E-09
5	0.45	4.00E-01	9.20E-09
6	0.60	4.00E-01	1.10E-08
7	0.75	4.00E-01	1.30E-08
8	0.90	4.00E-01	1.60E-08
- Chart (Bottom Right):** A line graph with a y-axis from 0.00 to 1.00 and an x-axis from 1 to 6. It shows a series of red square markers connected by a black line, representing the data from the 'OldCone (i)' column. The values increase from approximately 0.00 at x=1 to 0.75 at x=6.

The spreadsheet interface includes a menu bar (File, Edit, View, Insert, Format, Tools, Data, Window, Help, Acrobat), a toolbar with various icons, and a status bar at the bottom showing "Ready". The Windows taskbar at the very bottom displays the Start button, several open applications (PhDThesisApp, CO2Program1, Microsoft Exc..., Microsoft Visu...), and the system clock showing 1:02 PM on Friday, 12/01/2007.

Table C2. Typical Water content spreadsheet

The screenshot shows a Microsoft Excel spreadsheet titled "Microsoft Excel - Co2b_v2 (1)UpdatedIK2b". The spreadsheet contains data for "Water concentration" over 11 days for 8 nodes. The columns are labeled A through M, and rows are numbered 1 through 27. The data is organized as follows:

Nodes\days	1	2	3	4	5	6	7	8	9	10	11	12
1	12.8000	10.88	9.248	7.8608	6.68168	5.679428	4.827514	4.103387	3.487879	2.964697	2.519992	3.2759
2	15.2000	12.92	10.982	9.3347	7.934495	6.744321	5.732673	4.872772	4.141856	3.520578	2.992491	3.89023
3	17.1500	14.5775	12.391	10.5322	8.952407	7.609546	6.468114	5.497897	4.673213	3.972231	3.376396	4.38931
4	18.5000	15.725	13.366	11.3613	9.657116	8.208548	6.977266	5.930676	5.041075	4.284914	3.642176	4.73482
5	19.0200	16.167	13.742	11.6807	9.928559	8.439275	7.173384	6.097376	5.18277	4.405354	3.744551	4.86791
6	27.7200	23.562	20.028	17.0235	14.47001	12.29951	10.45458	8.886397	7.553437	6.420422	5.457358	7.09456
7	33.4800	28.458	24.189	20.5609	17.47677	14.85525	12.62697	10.73292	9.122983	7.754535	6.591355	8.56876
8	34.0000	28.9	24.565	20.8803	17.74821	15.08598	12.82308	10.89962	9.264678	7.874976	6.69373	8.70184

The Windows taskbar at the bottom shows the Start button, several open applications (PhDThesisApp..., CO2Program1..., Document3 - ...), and the system tray with the date and time: 1:05 PM, Friday, 12/01/2007.

Table C4. Typical model output spreadsheet

1	Day	Iteration#	Node	Newconc	Concechange	Diffusion	Saturation	Time Difference
2	1	2	1.00E+00	3.60E-09	0.0E+00	2.82E-06	2E-01	8.6E+04
3	1	2	2.00E+00	3.92E-09	1.2E-10	2.56E-06	2E-01	8.6E+04
4	1	2	3.00E+00	5.63E-09	-7.4E-11	2.36E-06	2E-01	8.6E+04
5	1	2	4.00E+00	7.40E-09	3.3E-12	2.23E-06	2E-01	8.6E+04
6	1	2	5.00E+00	9.16E-09	-3.9E-11	2.18E-06	3E-01	8.6E+04
7	1	2	6.00E+00	1.10E-08	-3.4E-11	1.46E-06	3E-01	8.6E+04
8	1	2	7.00E+00	1.30E-08	4.2E-11	1.09E-06	3E-01	8.6E+04
9	1	2	8.00E+00	1.60E-08	4.2E-11	1.06E-06	3E-01	8.6E+04
10								
11	1	3	1.00E+00	3.60E-09	0.0E+00	2.56E-06	2E-01	8.6E+04
12	1	3	2.00E+00	3.78E-09	-1.5E-10	2.36E-06	2E-01	8.6E+04
13	1	3	3.00E+00	5.69E-09	-3.2E-11	2.23E-06	2E-01	8.6E+04
14	1	3	4.00E+00	7.36E-09	-4.3E-11	2.18E-06	2E-01	8.6E+04
15	1	3	5.00E+00	9.11E-09	-4.7E-11	1.46E-06	3E-01	8.6E+04
16	1	3	6.00E+00	1.10E-08	-1.0E-12	1.09E-06	3E-01	8.6E+04
17	1	3	7.00E+00	1.31E-08	5.9E-11	1.06E-06	3E-01	8.6E+04
18	1	3	8.00E+00	1.61E-08	5.9E-11	1.06E-06	3E-01	8.6E+04
19								
20	1	4	1.00E+00	3.60E-09	0.0E+00	2.56E-06	2E-01	8.5E+04
21	1	4	2.00E+00	3.93E-09	1.5E-10	2.36E-06	2E-01	8.5E+04
22	1	4	3.00E+00	5.54E-09	-4.9E-11	2.23E-06	2E-01	8.5E+04
23	1	4	4.00E+00	7.32E-09	-4.2E-11	2.18E-06	2E-01	8.5E+04
24	1	4	5.00E+00	9.07E-09	-4.3E-11	1.46E-06	3E-01	8.5E+04
25	1	4	6.00E+00	1.10E-08	-5.5E-13	1.09E-06	3E-01	8.5E+04
26	1	4	7.00E+00	1.32E-08	5.5E-11	1.06E-06	3E-01	8.5E+04
27	1	4	8.00E+00	1.62E-08	5.5E-11	1.06E-06	3E-01	8.5E+04
28								
29	1	5	1.00E+00	3.60E-09	0.0E+00	2.56E-06	2E-01	8.5E+04
30	1	5	2.00E+00	3.78E-09	1.5E-10	2.36E-06	2E-01	8.5E+04

Table C5. Typical model simulation results spreadsheet

The screenshot displays a Microsoft Excel spreadsheet titled "Microsoft Excel - Co2b_v2 (1)UpdatedIK2b". The spreadsheet is organized into two main sections: "New Concentration" (rows 1-11) and "Diffusion" (rows 12-21). The columns represent time steps from 1 to 11. The "New Concentration" section shows values increasing from 0 to 0.9. The "Diffusion" section shows values in scientific notation, ranging from approximately 2.56E-06 to 1.06E-06. Below the spreadsheet, two line graphs are visible. The left graph plots "Diffusion" values (y-axis: 0.0000025 to 0.0000045) against time steps (x-axis: 1 to 11), showing four distinct series (Series 1-4) that generally decrease over time. The right graph plots "Concentration" values (y-axis: 1.5 to 2.5) against time steps, showing four series that generally increase over time. The taskbar at the bottom shows the Start menu, taskbar with open applications (PhDThesisApp, CO2Program1, Document3, Microsoft Exc, Microsoft Visu), and system tray with date/time 12/01/2007 1:07 PM.

	A	B	C	D	E	F	G	H	I	J	K	L	M	N	O
1	New Concentration														
2		1	2	3	4	5	6	7	8	9	10	11			
3	0	0.36	0.36	0.36	0.36	0.36	0.36	0.36	0.36	0.36	0.36	0.36	0.36	0.36	0.36
4	0.02	0.392039	0.368416	0.497119	0	0.104148	0.729202	2.00E-01	0.198531	0.219773	0.431767	0.431767			
5	0.15	0.526496	0.547786	0.564218	0.624813	0.626609	0.593987	0.654541	0.66548	0.672806	0.655853	0.655853			
6	0.3	0.668966	0.713908	0.756236	0.790302	0.822791	0.852761	0.872405	0.891883	0.908654	0.924551	0.924551			
7	0.45	0.852024	0.912509	0.97024	1.020683	1.063397	1.099365	1.130432	1.156605	1.178888	1.197704	1.197704			
8	0.6	1.106526	1.173726	1.238455	1.294453	1.341775	1.381568	1.41537	1.443958	1.468257	1.488863	1.488863			
9	0.75	1.40201	1.469232	1.534936	1.591763	1.639664	1.679847	1.713982	1.742813	1.76731	1.788067	1.788067			
10	0.9	1.70201	1.769232	1.834936	1.891763	1.939664	1.979847	2.013982	2.042813	2.06731	2.088067	2.088067			
11															
12	Diffusion														
13		1	2	3	4	5	6	7	8	9	10	11			
14	0	2.56E-06	2.81E-06	3.03E-06	3.23E-06	3.41E-06	3.57E-06	3.7E-06	3.82E-06	3.93E-06	4.02E-06	4.02E-06			
15	0.02	2.36E-06	2.62E-06	2.87E-06	3.09E-06	3.28E-06	3.45E-06	3.6E-06	3.74E-06	3.85E-06	3.95E-06	3.95E-06			
16	0.15	2.23E-06	2.5E-06	2.76E-06	2.99E-06	3.19E-06	3.37E-06	3.54E-06	3.68E-06	3.8E-06	3.91E-06	3.91E-06			
17	0.3	2.18E-06	2.46E-06	2.72E-06	2.95E-06	3.16E-06	3.35E-06	3.51E-06	3.65E-06	3.78E-06	3.89E-06	3.89E-06			
18	0.45	1.46E-06	1.78E-06	2.08E-06	2.37E-06	2.64E-06	2.88E-06	3.09E-06	3.29E-06	3.46E-06	3.61E-06	3.61E-06			
19	0.6	1.09E-06	1.41E-06	1.73E-06	2.04E-06	2.33E-06	2.59E-06	2.84E-06	3.06E-06	3.26E-06	3.43E-06	3.43E-06			
20	0.75	1.06E-06	1.38E-06	1.7E-06	2.01E-06	2.3E-06	2.57E-06	2.82E-06	3.04E-06	3.24E-06	3.42E-06	3.42E-06			
21	0.9	1.06E-06	1.38E-06	1.7E-06	2.01E-06	2.3E-06	2.57E-06	2.82E-06	3.04E-06	3.24E-06	3.42E-06	3.42E-06			

APPENDIX D

Waste-rock Sample Analyses Results

D.1 Introduction

This chapter presents the laboratory results of the waste-rock samples described in section 2.2.6 of chapter 2. The data presented includes the results of:

1. Grain size distribution curves for the waste-rock samples from the DSWR and DNWR.
2. Soil water characteristic curves (SWCCs) for the samples from DSWR and DNWR.
3. Saturated hydraulic conductivities for the samples from the DSWR and DNWR.

D.2. Grain-size distribution

Table D1. Grain-size test with dispersing agent

The particle-size analysis of the waste-rock samples was determined according to modified ASTM Designation: D 422-63. Results of the laboratory analysis are presented below:



University of British Columbia
 Department of Mining Engineering
 CO-MIX Laboratory

GRAIN SIZE TEST WITH DISPERSING AGENT

Sample:	TP01	Place:	
Depth:	0.3 - 0.4 m	Date:	10-Dec-03
Hygroscopic moisture		Specific gravity # 2 mm	Soil (g) =

Tare N°				Pycnometer N°					
Tare (g)				Temperature (°C)					
Tare + WS (g)				Pyc. + water (g)					
Tare + DS (g)				Pyc.+water+soil(g)					
Moisture (%)				G (g/cm ³)					
w (%):				1.09				G_s:	2.74

Mass of air dried soil M_t (g) =	90.0	Total mass of dried sample M_{dt} (g)	89.0
---	------	--	------

Coarse screening				
Sieve	Opening (mm)	Retained (g)	Total retained (g)	% passing
2"	50.8	0.00	0.00	100.0
1 1/2"	38.1	0.00	0.00	100.0
1"	25.4	0.00	0.00	100.0
3/4"	19.1	0.00	0.00	100.0
3/8"	9.5	0.00	0.00	100.0
4	4.76	0.00	0.00	100.0
10	2.00	0.00	0.00	100.0

Fine Screening				
Sieve	Opening (mm)	Retained (%)	Total retained (g)	% passing
16	1.19	0.00	0.00	100.0
30	0.59	0.00	0.00	100.0
40	0.42	0.30	0.30	99.7
60	0.25	7.80	8.10	90.9
100	0.149	36.50	44.60	49.9
200	0.074	30.40	75.00	15.8

HYDROMETER							
Mass of wet soil submitted to sedimentation M_{sw} (g)					90.01	Hydrometer N° : 863	
Time	time (s)	temp. (°C)	R (g/cm ³)	Rh (g/cm ³)	a (cm)	QS (%)	d (mm)
30 s	30	18.0	1.014	1.0053	13.8	15.4	0.0719
1 min.	60	18.0	1.013	1.0053	14.1	13.6	0.0513
2 min.	120	18.0	1.013	1.0053	14.1	13.6	0.0363
4 min.	240	18.0	1.013	1.0053	12.8	13.6	0.0245
8 min.	480	18.0	1.012	1.0053	13.1	11.9	0.0175
15 min.	900	18.0	1.012	1.0053	13.1	11.9	0.0128
30 min.	1800	18.0	1.012	1.0053	13.1	11.9	0.0090
1 h	3600	18.8	1.012	1.0051	13.2	11.3	0.0063
2 h	7200	18.8	1.011	1.0051	13.3	10.4	0.0045

4 h	14400	18.8	1.011	1.0051	13.3	10.4	0.0032
8 h	28800	18.8	1.011	1.0051	13.3	10.4	0.0023
24 h	86400	18.8	1.010	1.0051	13.6	8.6	0.0013

D (mm)	% mat. Pass	% mat.ret.	MATERIAL*	% of material
50.80	100.0	0.0	20<Coarse gravel<60	0.0
38.10	100.0	0.0		
25.40	100.0	0.0		
19.10	100.0	0.0	6,0<Median gravel<20,0	0.0
9.52	100.0	0.0		
4.76	100.0	0.0	2,0<Fine gravel<6,0	0.0
2.00	100.0	0.0		
1.190	100.0	0.0	0,60<Coarse sand<2,0	0.0
0.590	100.0	0.0	0,20<Median sand<0,6	29.4
0.420	99.7	0.3		
0.250	90.9	9.1		
0.149	49.9	50.1	0,06< Fine sand <0,20	57.3
0.074	15.8	84.2		
0.0719	15.4	84.6	0,002 < Silt < 0,06	4.0
0.0513	13.6	86.4		
0.0363	13.6	86.4		
0.0245	13.6	86.4		
0.0175	11.9	88.1		
0.0128	11.9	88.1		
0.0090	11.9	88.1		
0.0063	11.3	88.7		
0.0045	10.4	89.6		
0.0032	10.4	89.6		
0.0023	10.4	89.6		
0.0013	8.6	91.4		

Cu = 300

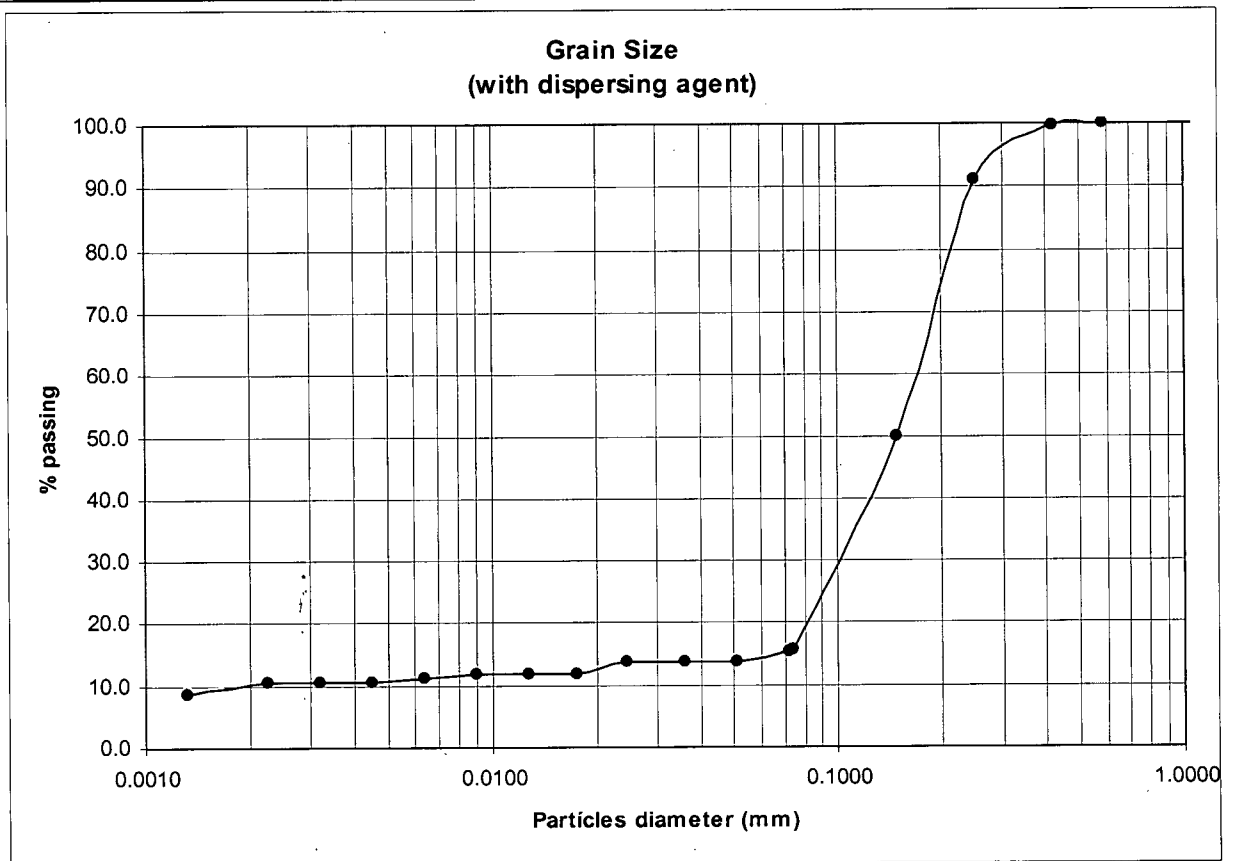


Table D2. Grain-size test without dispersing agent

1. Sample from DNWR:

mesh	Mm	g	%	%retained	Cum. Pas %
	12.5				100
4	4.75	20	8.00	8	92.04
10	2	25	10.00	18.00	82.04
20	0.85	53.1	21.25	39.25	60.79
40	0.417	53.1	21.25	60.50	39.54
60	0.25	54.3	21.73	82.23	17.81
80	0.177	14.9	5.96	88.19	11.85
100	0.15	6.9	2.76	90.95	9.09
140	0.105	6.4	2.56	93.51	6.53
200	0.075	0.8	0.32	93.83	6.21
270	0.053	5.6	2.24	95.76	4.28
-270	-0.053	8.9	3.56	99.32	
Total		250	100.04		

2. Sample from DSWR:

mesh	Mm	g	%	%retained	Cum. Pas %
	12.5				100
4	4.75	3.1	1.24	1.24	98.80
10	2	14.6	5.84	7.08	92.96
20	0.85	34.6	13.85	20.93	79.11
40	0.417	56.2	22.49	43.42	56.62
60	0.25	60.1	24.05	67.47	32.57
80	0.177	33.8	13.53	80.99	19.05
100	0.15	15.9	6.36	87.35	12.69
140	0.105	13.8	5.52	92.88	7.16
200	0.075	5	2.00	94.88	5.16
-200	-0.075	12.9	5.16	100.04	
Total		250	100.04		

D.4 Soil Water Characteristic Curve (SWCC) Test Results

1. Sample from DSWR:

Sample	DSWR							
cell	1660.9		Tare	4.1	diameter	6.9	final ht	4.460
cell+sample	1977.6		Tare+wet	53.6	ht	4.64	Dia	6.900
			Tare+dry	51.8	ini. vol	173.5026	volume	166.7719
sample	316.7							
water	9.4		Water	1.8			Tare	7.9000
soil	307.3		Soil	47.7			tare+wet	328.4800
w.c.	0.030589		w.c.	0.0377			tare+dry	314.2000
	suction	Weight	w.c.	final w.c.	vol. w.c.	%vol. W.c.	water	14.2800
	0.2	2027.1	0.1917	0.2105	0.3716	37.1637	Soil	306.3000
2026.4	0.5	2026.8	0.1907	0.2095	0.3699	36.9908	w.c.	0.0466
2007.4	1	2026.4	0.1894	0.2082	0.3676	36.7603		
							vol.	
1997.3	2	2007.4	0.1276	0.1462	0.2581	25.8094	Water	64.4800
1992.6	3	1997.3	0.0947	0.1132	0.1999	19.9882	vol. Soil	109.0226
1989.7	4	1992.6	0.0794	0.0979	0.1728	17.2793		
1987.7	5	1989.7	0.0700	0.0884	0.1561	15.6078	porosity	0.3866
							void ratio	
1986.2	6	1987.7	0.0635	0.0819	0.1446	14.4551		0.5914

1985.2	7	1986.2	0.0586	0.0770	0.1359	13.5906		
1983.1	8	1985.2	0.0553	0.0737	0.1301	13.0142	Gs	2.8095
1980	10	1983.1	0.0485	0.0669	0.1180	11.8039		
1978.8	30	1980	0.0384	0.0567	0.1002	10.0171		
1977.6	50	1978.8	0.0345	0.0528	0.0933	9.3255		
1976.9	80	1977.6	0.0306	0.0489	0.0863	8.6339		
	100	1976.9	0.0283	0.0466	0.0823	8.2304		

D. Sample from DNWR:

Sample	DNWR							
Cell	1669.2		Tare	4.1	diameter			5
cell+sample	1960.8		Tare+wet	53.6	Ht			6.9
			Tare+dry	51.8	ini. vol			186.964
Sample	291.6							
Water	21.9		Water	1.8	6.9	final ht	Tare	6.9000
Soil	269.7		Soil	47.7	4.64	dia	tare+wet	303.5000
w.c.	0.081201		w.c.	0.0378	173.5026	volume	tare+dry	276.5000
	suction	weight	w.c.	final w.c.	vol. w.c.	% vol. W.c.	Water	27.0000
	0.2	1990.4	0.1910	0.2311	0.3591	35.9072	Soil	269.6000
	0.5	1989.5	0.1876	0.2277	0.3539	35.3885	w.c.	0.1001
	1	1987.6	0.1806	0.2207	0.3429	34.2934		
	2	1982.2	0.1605	0.2007	0.3118	31.1811	vol. Water	62.3000
	3	1975.4	0.1353	0.1754	0.2726	27.2618	vol. Soil	111.2026
	4	1972.3	0.1238	0.1639	0.2548	25.4751		
	5	1970.5	0.1172	0.1573	0.2444	24.4377	porosity	0.3332
	6	1968.5	0.1098	0.1499	0.2328	23.2850	void ratio	0.5602
	7	1967.4	0.1057	0.1458	0.2265	22.6510		
	8	1966.4	0.1020	0.1421	0.2207	22.0746	Gs	2.4244
	10	1964.9	0.0964	0.1365	0.2121	21.2101		2.2700
	30	1960	0.0782	0.1183	0.1839	18.3859		
	50	1957.8	0.0701	0.1102	0.1712	17.1179		
	80	1956.1	0.0638	0.1039	0.1614	16.1381		
	100	1955.1	0.0601	0.1001	0.1556	15.5617		

D.5 Saturated Hydraulic Conductivity Test Results

1. Sample from DSWR:



University of British Columbia
 Department of Mining Engineering
 CO-MIX Laboratory

Falling Head Permeability Test FLUX UPWARD

Sample: PermDSWR1	Golden Sunlight - Tailings		
Place: Area			
Depth: 31" - 43"	State: Loose - Hig Moist. %	Date: 28-Apr-03	

Mold No.	Height (cm)	Diameter (cm)	Volumme (cm3)	Weight (g)	Cylinder
3	11.60	10.10	929.38	3850.7	Small
Mold + Sample (g) =		5122.00	Gsample =		1.62 g/cm3

A_{cross} (m2) = 0.00801		Temp, C: 23.0
L_{sample} (m) = 0.098		
V_{sample} (cm3) = 785.0		

T _{elapsed} (min)	h (cm)	Δt (min)	Δ _t (%)	K (m/s)	k _{avg} (m/s)
0.000	96.0	-			
0.257	51.0	0.257		1.01E-04	
0.000	96.0	-	0.8		1.01E-04
0.259	51.0	0.259		1.00E-04	
0.000	96.0	-			1.01E-04
0.257	51.0	0.257		1.01E-04	
0.000	96.0	-	0.0		
0.257	51.0	0.257		1.01E-04	

2. Sample from DNWR:



University of British Columbia
 Department of Mining Engineering
 CO-MIX Laboratory

**Falling Head Permeability Test
 FLUX UPWARD**

Sample: PermDNWR1	Place: Golden Sunlight - Tailings Area		
Depth: 31" - 43"	State: Loose - Hig Moist. %	Date: 28-Apr-03	

Mold No.	Height (cm)	Diameter (cm)	Volumme (cm3)	Weight (g)	Cylinder
3	11.60	10.10	929.38	3850.7	Small
Mold + Sample (g) =		5083.50	Gsample =		1.73 g/cm3

A_{cross} (m2) = 0.00801	Temp, C: 23.0
L_{sample} (m) = 0.089	
V_{sample} (cm3) = 712.9	

T _{elapsed} (min)	h (cm)	Δt (min)	Δt (%)	K (m/s)	k _{avg} (m/s)
0.000	96.0	-	9.9	1.01E-04	9.41E-05
0.233	51.0	0.233		9.19E-05	
0.000	96.0	-	9.19E-05		
0.256	51.0	0.256			
0.000	96.0	-	0.0	9.19E-05	
0.256	51.0	0.256			
0.000	96.0	-			
0.256	51.0	0.256			

APPENDIX E

CO₂ flux measurement results obtained at the Deilmann south (DSWR) and Deilmann north (DNWR) waste-rock piles using the dynamic closed chamber (DCC), static closed chamber (SCC) and eddy covariance (EC) methods

Table E1. CO₂ fluxes measurements obtained using the dynamic closed chamber (DCC) at the Deilmann south waste rock (DSWR) pile.

Loc. #	Year 2000			Year 2002	
	July	August	Sept.	July	August
1	215	225	204	162	132
2	290	202	182		
3	284	143	102	218	187
4	292	291	178	191	
5	300	154	137	142	190
6	350	246	200	123	
7	356	173	104	136	
8	274	180	121	204	132
9	182	202	179	131	115
10	192	182		190	145
11	250	169		203	129
12	247				
13	234	116		134	209
14	121	189		213	
15	368	164		297	
16	224	203		254	288
17	58	96			
18	91	113			
19	185				
20		106	89	144	89

Table E2. CO₂ fluxes measurements obtained using the dynamic closed chamber (DCC) at the Deilmann north waste rock (DNWR) pile.

Loc. #	Year 2000			Year 2002		
	July	Aug.	Sept	July	Aug.	
1	164	231	158	450	254	
2	191	274	248	298	317	
3	111	205	122	228	294	
4	103	136	104	245	211	
5	197	178	183	373	384	
6	219	266	228	381	246	
7	135	132	107	410	305	
8	183	204	204	141	89	
9	136	198	164	318	142	

Table E3 CO₂ flux measurements obtained using the static closed chamber (SCC) in the morning (between 10:00 and 11:00 on August 24, 2002 at nine selected sampling stations (DSF1 - DSF9).at the Deilmann south waste-rock (DSWR) pile (Figure 4.8A).

Loc. #	AM1	AM2	Avg
	mg m ⁻² h ⁻¹		
1	226	174	200
3	185		185
4		248	248
5	369	260	314
6		125	125
7	139		139
8		151	151
9	146		146
10	129	139	134
11	164		164
13			
20	175		175

Table E4 CO₂ flux measurements obtained using the static closed chamber (SCC) in the afternoon (between 16:30 and 17:30) on August 24, 2002 at six selected sampling stations (DSF1-DSF9) at the Deilmann south waste-rock (DSWR) pile.

Loc.	PM1		PM2	Avg.
#		Mg	m ⁻² h ⁻¹	
1	164		261	212.5
3	94.5		269	181.75
4				
5				
6				
7	128		75	101.5
8				
9				
10	125			125
11				
13			145	145
20			270	270

Table E5. Summary of CO₂ flux measurements obtained using the static closed chamber (SCC) in the morning (between 10:00 and 11:00) and afternoon (between 16:30 and 17:30) at nine selected sampling stations (DSF1-DSF9) at the Deilmann south waste-rock (DSWR) pile on August 24, 2002.

Loc.		AM		PM
#		mg	m ⁻²	h ⁻¹
1		200		213
3		185		182
4		248		
5		315		
6		125		
7		139		102
8		151		
9		146		
10		134		125
11		164		
13				145
20		175		270

Table E6. Temporal variations in the CO₂ flux obtained at the Deilmann south waste-rock (DSWR) pile using the Eddy covariance (EC) method. Measurements were obtained during the period from June 25th to August 25th 2002. Each data point represents the daily mean value averaged over the period from 10:00 to 17:00 hours.

<i>Julian Day</i>	<i>Day</i>	<i>Mean CO₂ Flux mg m⁻² hr⁻¹</i>	<i>CO₂ Flux Standard Deviation mg m⁻² hr⁻¹</i>
176	25-Jun-02	122	51
177	26-Jun-02	143	67
178	27-Jun-02	134	63
179	28-Jun-02	157	53
180	29-Jun-02	103	50
181	30-Jun-02		
182	01-Jul-02		
183	02-Jul-02	106	71
184	03-Jul-02	132	73
185	04-Jul-02		
186	05-Jul-02	104	37
187	06-Jul-02	100	43
188	07-Jul-02	176	74
189	08-Jul-02	96	49
190	09-Jul-02	118	45
191	10-Jul-02	133	62
192	11-Jul-02	112	52
193	12-Jul-02	154	23
194	13-Jul-02	160	37
195	14-Jul-02	111	29
196	15-Jul-02	178	56
197	16-Jul-02	156	43
198	17-Jul-02	146	43
199	18-Jul-02	130	84
200	19-Jul-02	87	25
201	20-Jul-02		
202	21-Jul-02	181	46
203	22-Jul-02	163	90
204	23-Jul-02	100	48
205	24-Jul-02	146	27

206	25-Jul-02	107	20
207	26-Jul-02	101	48
208	27-Jul-02	96	25
209	28-Jul-02	132	46
210	29-Jul-02		
211	30-Jul-02		
212	31-Jul-02		
213	01-Aug-02		
214	02-Aug-02	107	44
215	03-Aug-02	118	36
216	04-Aug-02	119	50
217	05-Aug-02	149	42
218	06-Aug-02	145	17
219	07-Aug-02	102	42
220	08-Aug-02	78	40
221	09-Aug-02	111	75
222	10-Aug-02	105	55
223	11-Aug-02	85	29
224	12-Aug-02	151	48
225	13-Aug-02		
226	14-Aug-02		
227	15-Aug-02		
228	16-Aug-02	79	22
229	17-Aug-02	139	63
230	18-Aug-02	113	55
231	19-Aug-02	152	92
232	20-Aug-02	103	34
233	21-Aug-02	93	53
234	22-Aug-02	77	52
235	23-Aug-02	67	23
236	24-Aug-02	104	60
237	25-Aug-02	101	44

APPENDIX F

Data for measurements of near- and surface-water contents and CO₂ fluxes across the surfaces of the DSWR and DNWR after heavy rainfall events

This section presents results of measurements of near- and surface-water contents (0 – 0.15 m) and associated CO₂ fluxes from the DSWR and DNWR piles over an 8-d test period [30 July (day 1) to 6 August (day 8) 2002] after rainfall events. Waste-rock samples were collected each day during the test period at sampling stations DSF1 and DNF1 (Figure 4.8A) and analyzed for water contents within 24 hours. The gravimetric water contents were measured at 0, 0.05, 0.10, and 0.15 m depths. The gravimetric water contents were converted to volumetric water contents using the waste-rock properties measured in the laboratory (e.g., SWCC, soil specific density and porosity). The climatic parameters for the test site (e.g., rainfall and temperature) were recorded from the weather station installed on DSWR.

Results of volumetric water contents, CO₂ fluxes, rainfall events, and average daily temperatures for the DSWR and DNWR are presented in the Tables below..

Table F1. Water contents and CO₂ fluxes measured over an 8-d test period [30 July (day 1) to 6 August (day 8) 2002] at station DNF1 with time at the Deilmann north waste-rock (DNWR) pile.

Date	Day #	Temp. °C	Rainfall (mm)	CO ₂ Flux	Depth			
					0 m	0.05 m	0.10 m	0.15 m
Jul. 30	1	12.6	39.2					
Jul. 31	2	10.0	36.6	mg m ⁻² h ⁻¹	Water content (vol.)			
Aug. 01	3	11.8	7	7	0.2187	0.1267	0.1432	0.1463
Aug. 02	4	7.5	1	17	0.060	0.1237	0.1191	0.116131
Aug. 03	5	6.5	0.4	264	0.0211	0.1342	0.0950	0.0980
Aug. 04	6	8.4	0	268	0.0256	0.1010	0.0950	0.0950
Aug. 05	7	10.5	0	306	0.0045	0.0980	0.1161	0.1176
Aug. 06	8	13.2	0	316	0.0131	0.1110	0.0794	0.0829

Table F2. Water contents and CO₂ fluxes measured over an 8-d test period [30 July (day 1) to 6 August (day 8) 2002] at station DSF1 with time at the Deilmann south waste-rock (DSWR) pile.

Date	Day #	Temp. °C	Rainfall (mm)	CO ₂ flux	Depth			
					0 cm	5 cm	10 cm	15 cm
Jul. 30	1	12.6	39.2					
Jul. 31	2	10.0	36.6	Mg m ⁻² h ⁻¹	Water content (vol.)			
Aug. 01	3	11.8	7	67	0.0571	0.0970	0.0913	0.0870
Aug. 02	4	7.5	1	97	0.0313	0.0785	0.0770	0.0870
Aug. 03	5	6.5	0.4	153	0.0010	0.0728	0.0699	0.0685
Aug. 04	6	8.4	0	138	0.0029	0.0599	0.0542	0.0613
Aug. 05	6	10.5	0	144	0.0017	0.0770	0.0285	0.0514
Aug. 06	8	13.2	0	241	0.00036	0.0728	0.0585	0.0499

APPENDIX G

Minicosms data used for simulations with CO₂ diffusion model

This section presents measured column data (Kabwe et al., 2002) used for simulation with CO₂ diffusion model developed in this thesis. The data were obtained from two minicosms: one kept at low temperature (LT) at about 5 °C and another one at room temperature (HT). The data presented include: water contents profiles, CO₂ concentrations profiles, and temperatures profiles.

G.1. HT Minicosm (column kept at room temperature)

Table F1. Temperature data from HT minicosm measured from Day 12 to Day 96 after filling the column with sand material.

Depth (m)	Day #						
	D-12	19	26	34	47	75	96
0	9.00	9.02	9.05	9.01	9.02	8.86	8.11
0.02	7.57	7.71	7.71	7.62	7.42	7.21	7.49
0.3	8.34	8.47	8.42	8.35	8.13	8.34	7.74
0.6	8.80	8.91	8.88	8.80	8.65	8.90	8.08
0.9	9.37	9.46	9.44	9.35	9.24	9.52	8.69

Table G2. Volumetric water contents from HT minicosm measured from Day 12 to Day 96 after filling the column with sand material

Depth (m)	Day #						
	11	18	25	32	46	73	95
0	18.29	18.29	18.29	18.29	18.29	18.29	18.29
0.15	22.56	21.03	21.39	21.85	21.32	22.91	24.12
0.30	24.87	23.74	21.43	25.04	21.99	25.63	26.65
0.45	25.89	23.53	24.93	26.61	23.55	29.16	29.69
0.60	27.59	26.38	25.93	28.35	25.12	28.44	29.52
0.7	36.60	39.85	36.65	40.91	25.73	39.98	43.14
0.90	49.80	43.99	44.63	47.12	46.82	48.53	51.31
105	49.52	47.87	46.93	47.58	47.57	48.06	52.46

Table G3. CO₂ Concentration from HT minicosm measured from Day 1 to Day 96 after filling the column with sand material

Depth (m)	Day #						
	D12	d19	d26	d33	d47	d75	d96
0	0.036	0.036	0.036	0.036	0.036	0.036	0.036
0.02	0.048	0.04	0.038	0.041	0.041	0.044	0.04
0.15	0.29	0.288	0.279	0.271	0.263	0.225	0.203
0.3	0.323	0.345	0.343	0.329	0.322	0.269	0.254
0.45	0.422	0.437	0.51	0.452	0.424	0.371	0.337
0.6	0.458	0.495	0.5	0.538	0.556	0.494	0.48
0.75	0.605	0.573	0.63	0.738	0.86	1.041	1.051

APPENDIX H

Climatic parameters used in simulations with SoilCover and recorded at the weather station installed on the Deilmann south waste-rock (DSWR) pile

Simulation of evaporative fluxes [potential (PE) and actual (AE)] using SoilCover numerical model required the site weather parameters as inputs. The weather parameters used in simulations were recorded at a weather station installed on DSWR. The description of the weather station was presented in chapter 4. The weather parameters used in the model simulations are presented in Table G1

Table H1. Weather parameters recorded at the weather station installed on Deilmann south waste-rock (DSWR) pile.

Key Lake, 2002								
		T_Air	RH MAX	RH MIN	Net Rad	Net Rad	WIND	Rain
		oC	Pct.	Pct.	W/m2	MJ	m/s	Mm
205	Jul-24	21.28583	88.7	39.01	91.9805	7.95	4.289375	0
206	Jul-25	21.22417	91.8	39.93	46.53471	4.02	2.788542	1.8
207	Jul-26	22.51708	96.1	39.06	60.10498	5.19	2.620271	0
208	Jul-27	17.78146	98.4	78.7	24.0446	2.08	3.058292	5.4
209	Jul-28	17.15208	100	58.27	70.62138	6.10	3.287375	7.7
210	Jul-29	13.12063	97.7	70.6	21.79919	1.88	5.67475	39.2
211	Jul-30	11.20646	98.9	91.5	31.37233	2.71	6.197479	36.6
212	Jul-31	12.05354	100	83	58.67254	5.07	6.021208	7
213	Aug-01	8.072521	97.4	68.36	44.57667	3.85	8.522083	1
214	Aug-02	7.386729	96	66.55	66.0985	5.71	7.299021	0.4
215	Aug-03	10.02648	91.8	51.57	50.56073	4.37	5.679396	0
216	Aug-04	12.50308	88.8	44.88	50.86933	4.40	3.107708	0
217	Aug-05	14.59542	95.5	47.1	61.26404	5.29	5.039354	2.6
218	Aug-06	14.94688	99.8	87.8	20.31873	1.76	3.40325	13.3
219	Aug-07	19.24146	100	41.11	93.0589	8.04	3.4625	0
220	Aug-08	21.89958	98.1	31.3	86.83577	7.50	2.132104	0
221	Aug-09	22.04375	84.8	35.37	70.22992	6.07	3.077438	0
222	Aug-10	19.66188	77	36.82	65.12854	5.63	4.502417	0
223	Aug-11	14.67708	97.3	51.91	30.10281	2.60	3.830146	0
224	Aug-12	16.47563	90.5	38.84	66.93844	5.78	3.648688	0
225	Aug-13	14.16771	98.5	65.73	19.09198	1.65	2.913188	8.8
226	Aug-14	14.02771	99.7	62.58	48.55794	4.20	3.579667	2.9
227	Aug-15	12.06688	98	69.85	44.98344	3.89	2.106208	7.9
228	Aug-16	11.3225	99.1	81.9	22.15146	1.91	2.743583	7.3
229	Aug-17	11.96729	98.9	48.51	73.07313	6.31	3.738729	0
230	Aug-18	13.00967	95.7	28.92	54.86875	4.74	2.488333	0
231	Aug-19	11.39683	95.6	50.55	13.02202	1.13	4.382563	2.2
232	Aug-20	9.112875	87.3	37.3	59.66702	5.16	5.10575	0
233	Aug-21	15.07235	85.4	38.32	62.63533	5.41	3.510646	0
234	Aug-22	20.53417	72.6	38.08	56.01819	4.84	5.302063	0
235	Aug-23	20.70354	94.1	34.59	56.71417	4.90	2.354833	0
236	Aug-24	21.9425	76.8	25.21	60.14081	5.20	5.660375	0

APPENDIX I

SoilCover run summary page for simulations of evaporative fluxes at the DSWR and DNWR piles during the field tests

The following pages present the daily input and output data and summary pages of SoilCover model simulations results of evaporative fluxes from the DSWR and DNWR piles obtained during the 8-d and 27-d test periods. The climatic parameters for input data were obtained from the weather station installed at the DSWR. The soil properties of the waste rocks were obtained from laboratory tests.

Table I.1 Daily input data for SoilCover simulations for evaporative fluxes during the 8-d test period at the Deilmann south waste-rock (DSWR) pile.

Weather data section							Moisture boundaries section			
Run Day	Max. AirTemp	Min. AirTemp	Net Rad.	Max RH	Min RH	Wind Speed	Top BC	Top BC	Start time	Stop time
	(C)	(C)	(MJ/m ² -day)	(dec)	(dec)	(km/hr)	(Type)	(Value)	(hrs)	(hrs)
1	18.00	10.00	1.8834	0.98	0.71	1.41	3	39.2	0	24
2	15.50	11.00	2.7110	0.99	0.92	0.5918	3	36.6	0	24
3	11.00	5.00	5.069	1.00	0.83	0.793	3	7	0	24
4	10.00	3.00	3.8514	0.97	0.68	1.7391	3	1	0	24
5	13.00	3.50	5.7109	0.96	0.66	2.565	3	0.4	0	24
6	17.00	3.00	4.3685	0.92	0.52	4.4193	3	0	0	24
7	18.50	5.00	4.3951	0.88	0.45	5.6997	3	0	0	24
8	18.50	5.00	4.3951	0.88	0.45	5.6997	3	0	0	24

Moisture boundaries section	Other daily data section
-----------------------------	--------------------------

Bot BC	Bot BC	Top Temp	Bot Temp	Pan Evap	Write Day	Root	Root
(Type)	(Value)	(C)	(C)	(mm/day)	Out	Top (cm)	Bot (cm)
1	0.11	1	14	1	1	1	1
1	0.087	1	13	1	1	1	1
1	0.087	1	8	1	1	1	1
1	0.068	1	6.5	1	1	1	1
1	0.061	1	8.25	1	1	1	1
1	0.051	1	10	1	1	1	1
1	0.05	1	11.7	1	1	1	1
1	0.05	1	11.7	1	1	1	1

Table I2. Daily output data for SoilCover simulations for evaporative fluxes during the 8-d test period at the Deilmann south waste rock (DSWR) pile.

Elapsed Time days	Pot Evap (mm)	Act Evap (mm)	Pot Tran (mm)	Act Tran (mm)	Tot ET (mm)	Water Bal (%)	Spec Flux (mm)	Bottom Flux (mm)
0	0	0	0	0	0	0	0	0
1	-0.72	-0.72	0	0	-0.72	-23.775	39.2	0.28
2	-0.745	-0.745	0	0	-0.745	-81.124	36.6	-0.068
3	-1.239	-1.239	0	0	-1.239	192.386	7	-0.13
4	-1.057	-1.057	0	0	-1.057	212.662	1	-0.137
5	-1.615	-1.615	0	0	-1.615	222.733	0.4	-0.266
6	-1.638	-1.468	0	0	-1.468	222.885	0	-0.747
7	-1.922	-1.189	0	0	-1.189	222.831	0	-0.909
8	-1.933	-0.981	0	0	-0.981	223.142	0	-0.92

Runoff (mm)	Selected Node Flx (mm)	Net Infiltration (mm)	Cum. PE (mm)	Cum. AE (mm)	Cum. PT (mm)	Cum. AT (mm)	Cum. ET (mm)	Cum. Precip. (mm)
0	0	0	0	0	0	0	0	0
22.606	0	15.873	-0.72	-0.72	0	0	-0.72	39.2
0	0	35.855	-1.465	-1.465	0	0	-1.465	75.8
0	0	5.761	-2.705	-2.704	0	0	-2.704	82.8
0	0	-0.057	-3.762	-3.762	0	0	-3.762	83.8
0	0	-1.215	-5.377	-5.377	0	0	-5.377	84.2
0	0	-1.468	-7.014	-6.844	0	0	-6.844	84.2
0	0	-1.189	-8.936	-8.034	0	0	-8.034	84.2
0	0	-0.981	-10.869	-9.015	0	0	-9.015	84.2

Cum. Runoff (mm)	Cum. Infil. (mm)	Cum. Bott Fl. (mm)	Cum. int flx (mm)
0	0	0	0
22.606	15.873	0.28	0
22.606	51.728	0.212	0
22.606	57.489	0.082	0
22.606	57.432	-0.056	0
22.606	56.217	-0.322	0
22.606	54.749	-1.068	0
22.606	53.56	-1.978	0
22.606	52.579	-2.897	0

Table 13. SoilCover simulations summary for evaporative fluxes during the 8-d test period at the Deilmann south waste rock (DSWR) pile.

SoilCover V. 4.01 Run Summary Page

1. Project Name: DSWR2b

2. Project Directory: c:\scv4\

3. Run Parameters:

a) Vegetation: No

b) Freeze-Thaw: No

4. Mesh Information:

a) Convergence Criteria:

Max Iterations	Max Change Suction (%)	Max Change Temperature (°C)	Suction Convergence (%)	Temperature Convergence (%)
50	1	1	0	0

b) Time Step Control:

Max Change Suction (%)	Max Change Temperature (°C)	Minimum Time Step (seconds)	First Time Step (seconds)	Maximum Time Step (seconds)
5	5	2	1	1600

c) Soil Profile Data:

Number of Nodes	Number of Layers	Nodes	Drain Flux (mm/day)
40	3	2	0

5. Soil Property Summary:

Soil Name	Porosity	Spec Grav	D _v (m ² /s)	K _{sat} (cm/s)
cover soil	0.4	2.7	9.10E-06	1.20E-04
waste rock	0.326	2.78	5.00E-05	1.40E-04
waste rock	0.488	2.79	5.00E-05	1.80E-04
waste rock	0.355	2.77	5.00E-05	1.60E-03
name5				
name6				
name7				
name8				

6. Boundary Conditions:

a) First date of run:	01-Apr-96
b) Total run days:	8
c) Top temperature condition:	Computed
d) Bottom temperature (C):	14
e) Day 1 top moisture condition:	Precip.
f) Day 1 bot. moisture condition:	0.11
g) Day 1 bottom moisture value:	0.11

7. Vegetation Summary:

a) Moisture limiting point (kPa):

b) First date of growing season:

c) Moisture wilting point (kPa):

d) Last date of growing season:

e) Grass quality:

f) First day root depth (cm):

8. Run Output Summary:

a) Net cumulative precipitation (mm):	84.2	b) Net cumulative infiltration (mm):	52.579
c) Net cumulative bottom flux (mm):	-2.897	d) Net cumulative runoff (mm):	22.606
e) Net cumulative PE (mm):	-10.869	f) Net cumulative AE (mm):	-9.015
g) Net cumulative PT (mm):	0	h) Net cumulative AT (mm):	0
i) Net cumulative BT (mm):	-5.015	j) Net cum. user monitor flux (mm):	0
k) Net cumulative drain node flux (mm):	0	User Node: 52	
		User Elev: 1.00 cm	

Table I4. Daily input data for SoilCover simulations for evaporative fluxes during the 27-d test period at the Deilmann south waste rock (DSWR) pile.

Weather data section							Moisture boundaries section			
Run Day	Max AirTemp	Min AirTemp	Net Rad	Max RH	Min RH	Wind Speed	Top BC	Top BC	Start time	Stop time
	(C)	(C)	(MJ/m ² -day)	(dec)	(dec)	(km/hr)	(Type)	(Value)	(hrs)	(hrs)
1	11.50	9.00	1.8834	0.98	0.71	1.41	3	39.2	0	24
2	15.50	11.00	2.711	0.99	0.92	0.5918	3	36.6	0	24
3	11.00	5.00	5.069	1	0.83	0.793	3	7	0	24
4	10.00	3.00	3.8514	0.97	0.68	1.7391	3	1	0	24
5	13.00	3.50	5.7109	0.96	0.66	2.565	3	0.4	0	24
6	17.00	3.00	4.3685	0.92	0.52	4.4193	3	0	0	24
7	18.50	5.00	4.3951	0.88	0.45	5.6997	3	0	0	24
8	18.50	5.00	5.29	0.96	0.47	5	3	2.6	0	24
9	17.00	11.00	1.76	1	0.88	3.4	3	13.3	0	24
10	24.00	12.00	8.04	1	0.41	3.5	3	0	0	24
11	26.00	13.50	7.5	0.98	0.31	2.1	3	0	0	24
12	28.00	8.00	6.07	0.85	0.35	3.1	3	0	0	24
13	26.50	11.00	5.63	0.77	0.37	4.5	3	0	0	24
14	21.00	7.00	2.6	0.97	0.52	3.8	3	0	0	24
15	22.00	3.50	5.78	0.91	0.39	3.6	3	0	0	24
16	20.00	6.00	1.65	0.99	0.66	2.9	3	0	0	24
17	17.50	10.50	4.2	0.1	0.63	3.6	3	8.8	0	24
18	15.00	8.50	3.89	0.98	0.7	2.1	3	2.9	0	24
19	12.50	9.00	1.91	0.99	0.82	2.7	3	7.9	0	24
20	15.50	6.00	6.31	0.99	0.49	3.7	3	7.3	0	24
21	17.00	1.00	4.74	0.96	0.3	2.5	3	0	0	24
22	15.00	7.00	1.13	0.96	0.51	4.4	3	0	0	24
23	14.00	0.00	5.16	0.87	0.37	5.1	3	2.2	0	24
24	21.00	0.00	5.41	0.85	0.38	3.5	3	0	0	24
25	24.50	16.00	4.84	0.73	0.38	5.3	3	0	0	24
26	26.50	10.00	4.9	0.94	0.35	2.3	3	0	0	24
27	26.00	15.00	5.2	0.77	0.25	5.7	3	0	0	24

Moisture boundaries section	Other daily data section
------------------------------------	---------------------------------

Bot BC	Bot BC	Top Temp	Bot Temp	Pan Evap	Write Day	Root
(Type)	(Value)	(C)	(C)	(mm/day)	Out	Top (cm)
1	0.11	1	14	1	1	1
1	0.087	1	10	1	1	1
1	0.087	1	13	1	1	1
1	0.068	1	8	1	1	1
1	0.061	1	6.5	1	1	1
1	0.051	1	8.25	1	1	1
1	0.05	1	10	1	1	1
1	0.05	1	11.7	1	1	1
1	0.05	1	15	1	1	1
1	0.05	1	15	1	1	1
1	0.05	1	15	1	1	1
1	0.05	1	15	1	1	1
1	0.05	1	15	1	1	1
1	0.05	1	15	1	0	1
1	0.05	1	15	1	0	1
1	0.05	1	15	1	0	1
1	0.05	1	15	1	0	1
1	0.05	1	15	1	1	1
1	0.05	1	15	1	0	1
1	0.05	1	15	1	0	1
1	0.05	1	15	1	0	1
1	0.05	1	15	1	1	1
1	0.05	1	15	1	0	1
1	0.05	1	15	1	0	1

Table 15. Daily output data for SoilCover simulations for evaporative fluxes during the 27-d test period at the Deilmann south waste rock (DSWR) pile.

Elapsed Time Days	Pot Evap (mm)	Act Evap (mm)	Pot Tran (mm)	Act Tran (mm)	Tot ET (mm)	Water Bal (%)	Spec Flux (mm)	Bottom Flux (mm)
0	0	0	0	0	0	0	0	0
1	-0.633	-0.633	0	0	-0.633	-20.61	39.2	0.291
2	-0.745	-0.745	0	0	-0.745	-75.6	36.6	-0.084
3	-1.239	-1.239	0	0	-1.239	-186.932	7	-0.094
4	-1.057	-1.057	0	0	-1.057	-207.207	1	-0.14
5	-1.616	-1.616	0	0	-1.616	-217.28	0.4	-0.255
6	-1.638	-1.464	0	0	-1.464	-217.44	0	-0.686
7	-1.913	-1.174	0	0	-1.174	-217.384	0	-0.836
8	-1.99	-1.987	0	0	-1.987	-221.791	2.6	-0.901

9	-0.571	-0.571	0	0	-0.571	-225.3	13.3	-1.084
10	-2.927	-2.814	0	0	-2.814	-225.433	0	-1.155
11	-2.91	-2.271	0	0	-2.271	-224.448	0	-1.192
12	-2.717	-1.294	0	0	-1.294	-224.843	0	-1.177
13	-2.781	-1.197	0	0	-1.197	-224.213	0	-1.17
14	-1.282	-0.42	0	0	-0.42	-223.966	0	-1.107
15	-2.294	-0.731	0	0	-0.731	-224.154	0	-1.127
16	-0.862	-0.291	0	0	-0.291	-224.128	0	-1.085
17	-2.536	-2.522	0	0	-2.522	-235.63	8.8	-1.076
18	-1.307	-1.307	0	0	-1.307	-239.589	2.9	-1.085
19	-0.609	-0.609	0	0	-0.609	-243.004	7.9	-1.058
20	-2.046	-2.046	0	0	-2.046	-246.594	7.3	-1.068
21	-1.788	-1.788	0	0	-1.788	-246.637	0	-1.02
22	-0.827	-0.827	0	0	-0.827	-246.737	0	-1.021
23	-1.968	-1.968	0	0	-1.968	-250.723	2.2	-1.004
24	-2.22	-1.74	0	0	-1.74	-250.604	0	-1.056
25	-2.748	-1.347	0	0	-1.347	-250.551	0	-1.169
26	-2.248	-1.022	0	0	-1.022	-249.817	0	-1.178
27	-3.084	-0.903	0	0	-0.903	-249.701	0	-1.187

Runoff (mm)	Selected Node Flx (mm)	Net Infiltration (mm)	Cum. PE (mm)	Cum. AE (mm)	Cum. PT (mm)	Cum. AT (mm)	Cum. ET (mm)	Cum. Precip. (mm)
0	0	0	0	0	0	0	0	0
23.438	0	15.129	-0.633	-0.633	0	0	-0.633	39.2
0	0	35.855	-1.378	-1.378	0	0	-1.378	75.8
0	0	5.761	-2.617	-2.617	0	0	-2.617	82.8
0	0	-0.057	-3.674	-3.674	0	0	-3.674	83.8
0	0	-1.216	-5.29	-5.29	0	0	-5.29	84.2
0	0	-1.464	-6.928	-6.754	0	0	-6.754	84.2
0	0	-1.174	-8.841	-7.928	0	0	-7.928	84.2
0	0	0.613	-10.831	-9.914	0	0	-9.914	86.8
0	0	12.729	-11.402	-10.485	0	0	-10.485	100.1
0	0	-2.814	-14.329	-13.299	0	0	-13.299	100.1
0	0	-2.271	-17.239	-15.57	0	0	-15.57	100.1
0	0	-1.294	-19.957	-16.864	0	0	-16.864	100.1
0	0	-1.197	-22.738	-18.062	0	0	-18.062	100.1
0	0	-0.42	-24.02	-18.481	0	0	-18.481	100.1
0	0	-0.731	-26.314	-19.213	0	0	-19.213	100.1
0	0	-0.291	-27.177	-19.504	0	0	-19.504	100.1
1.136	0	5.142	-29.713	-22.026	0	0	-22.026	108.9
0	0	1.593	-31.02	-23.333	0	0	-23.333	111.8
0	0	7.291	-31.629	-23.942	0	0	-23.942	119.7
0	0	5.254	-33.675	-25.988	0	0	-25.988	127
0	0	-1.788	-35.463	-27.776	0	0	-27.776	127
0	0	-0.827	-36.29	-28.603	0	0	-28.603	127
0	0	0.232	-38.259	-30.571	0	0	-30.571	129.2
0	0	-1.74	-40.479	-32.312	0	0	-32.312	129.2

0	0	-1.347	-43.227	-33.659	0	0	-33.659	129.2
0	0	-1.022	-45.475	-34.681	0	0	-34.681	129.2
0	0	-0.903	-48.559	-35.584	0	0	-35.584	129.2

Cum. Runoff (mm)	Cum. Infil. (mm)	Cum. Bott Fl. (mm)	Cum. int flx (mm)
0	0	0	0
23.438	15.129	0.291	0
23.438	50.985	0.207	0
23.438	56.745	0.113	0
23.438	56.688	-0.027	0
23.438	55.473	-0.282	0
23.438	54.008	-0.968	0
23.438	52.835	-1.805	0
23.438	53.448	-2.705	0
23.438	66.177	-3.789	0
23.438	63.363	-4.944	0
23.438	61.092	-6.136	0
23.438	59.798	-7.313	0
23.438	58.601	-8.483	0
23.438	58.181	-9.59	0
23.438	57.45	-10.716	0
23.438	57.158	-11.802	0
24.573	62.301	-12.877	0
24.573	63.894	-13.962	0
24.573	71.185	-15.02	0
24.573	76.439	-16.088	0
24.573	74.651	-17.109	0
24.573	73.824	-18.129	0
24.573	74.055	-19.133	0
24.573	72.315	-20.189	0
24.573	70.967	-21.357	0
24.573	69.946	-22.536	0
24.573	69.043	-23.722	0

Table 16. SoilCover simulations summary for evaporative fluxes during the 27-d test period at the Deilmann south waste rock (DSWR) pile.

SoilCover V. 4.01 Run Summary Page

1. Project Name: DSWR2cn

2. Project Directory: c:\scv4\

3. Run Parameters:

a) Vegetation: No

d) Freeze Thaw: No

4. Mesh Information:

a) Convergence Criteria:

Max. Suction	Max. Change Suction (%)	Max. Change Temperature (%)	Suction Dispersion (%)	Temperature Dispersion (%)
50	1	1	0	0

b) Time Step Control:

Max. Change Suction (%)	Max. Change Temperature (°C)	Minimum Time Step (seconds)	First Time Step (seconds)	Maximum Time Step (seconds)
5	5	2	1	1000

c) Soil Profile Data:

Number of Nodes	Number of Layers	Nodes/Node	Flux (mm/day)
40	3	2	0

5. Soil Property Summary:

Soil Name	Porosity	Spec. Grav.	Mo (H ₂ O)	Ksat (cm/d)
cover soil	0.4	2.7	9.10E-06	1.20E-04
Waste Rock	0.325	2.78	5.00E-05	1.40E-04
waste rock	0.488	2.73	5.00E-05	1.60E-04
waste rock	0.355	2.77	5.00E-05	1.60E-03
cover				
barren				
cover				
barren				

6. Boundary Conditions:

a) First date of run:	01-Apr-96
b) Total run days:	27
c) Top temperature condition:	Computed
d) Bottom temperature (C):	-14
e) Day 1 top moisture condition:	Precip.
f) Day 1 bot. moisture condition:	0.11
g) Day 1 bottom moisture value:	0.11

7. Vegetation Summary:

a) Moisture limiting point (kPa):

b) First date of growing season:

c) Mass:air wilting point (kPa):

d) Last date of growing season:

e) Grass quality:

f) First day root depth (cm):

8. Run Output Summary:

a) Net cumulative precipitation (mm):	129.2	b) Net cumulative infiltration (mm):	69.043
c) Net cumulative bottom flux (mm):	-23.722	d) Net cumulative runoff (mm):	24.573
e) Net cumulative PE (mm):	-48.859	f) Net cumulative AE (mm):	-35.584
g) Net cumulative PI (mm):	0	h) Net cumulative AI (mm):	0
i) Net cumulative ET (mm):	-35.584	j) Net cum. user monitor flux (mm):	0
k) Net cumulative drain node flux (mm):	0	User Node:	52
		User Elev:	1.00 cul

Table 17. Daily input data for SoilCover simulations for evaporative fluxes during the 8-d test period at the Deilmann north waste rock (DSWR) pile.

Weather data section							Moisture boundaries section			
Run Day	Max. AirTemp	Min. AirTemp	Net Rad.	Max RH	Min RH	Win Speed	Top BC	Top BC	Start time	Stop time
	(C)	(C)	(MJ/m2-day)	(dec)	(dec)	(km/hr)	(Type)	(Value)	(hrs)	(hrs)
1	18.00	10.00	1.8834	0.98	0.71	1.41	3	39.2	0	24
2	18.00	10.00	1.8834	0.98	0.71	1.41	3	36.6	0	24
3	11.50	9.00	2.7106	0.99	0.91	0.5918	3	7	0	24
4	15.50	9.00	5.0693	1	0.83	0.793	3	1	0	24
5	11.00	5.00	3.8514	0.97	0.68	1.7391	3	0.4	0	24
6	10.00	3.00	5.7109	0.96	0.67	2.565	3	0	0	24
7	13.00	3.50	4.3685	0.92	0.52	4.4193	3	0	0	24
8	17.00	3.00	4.3951	0.89	0.45	5.6997	3	0	0	24

Moisture boundaries section	Other daily data section
-----------------------------	--------------------------

Bot BC	Bot BC	Top Temp	Bot Temp	Pan Evap	Write Day	Root	Root
(Type)	(Value)	(C)	(C)	(mm/day)	Out	Top (cm)	Bot (cm)
1	0.3	1	14	1	1	1	1
1	0.3	1	13	1	1	1	1
1	0.23	1	8	1	1	1	1
1	0.146	1	6.5	1	1	1	1
1	0.116	1	8.25	1	1	1	1
1	0.098	1	10	1	1	1	1
1	0.095	1	11.7	1	1	1	1
1	0.118	1	10	1	1	1	1

Table 18. Daily output data for SoilCover simulations for evaporative fluxes during the 8-d test period at the Deilmann north waste rock (DSWR) pile.

Elapsed Time days	Pot Evap (mm)	Act Evap (mm)	Pot Tran (mm)	Act Tran (mm)	Tot ET (mm)	Water Bal (%)	Spec Flux (mm)	Bottom Flux (mm)
0	0	0	0	0	0	0	0	0
1	-0.72	-0.72	0	0	-0.72	-23.775	39.2	0.28
2	-0.745	-0.745	0	0	-0.745	-81.124	36.6	-0.068
3	-1.239	-1.239	0	0	-1.239	192.386	7	-0.13
4	-1.057	-1.057	0	0	-1.057	212.662	1	-0.137
5	-1.615	-1.615	0	0	-1.615	222.733	0.4	-0.266
6	-1.638	-1.468	0	0	-1.468	222.885	0	-0.747
7	-1.922	-1.189	0	0	-1.189	222.831	0	-0.909
8	-1.933	-0.981	0	0	-0.981	223.142	0	-0.92

Runoff (mm)	Selected Node Flx (mm)	Net Infiltration (mm)	Cum. PE (mm)	Cum. AE (mm)	Cum. PT (mm)	Cum. AT (mm)	Cum. ET (mm)	Cum. Precip. (mm)
0	0	0	0	0	0	0	0	0
22.606	0	15.873	-0.72	-0.72	0	0	-0.72	39.2
0	0	35.855	-1.465	-1.465	0	0	-1.465	75.8
0	0	5.761	-2.705	-2.704	0	0	-2.704	82.8
0	0	-0.057	-3.762	-3.762	0	0	-3.762	83.8
0	0	-1.215	-5.377	-5.377	0	0	-5.377	84.2
0	0	-1.468	-7.014	-6.844	0	0	-6.844	84.2
0	0	-1.189	-8.936	-8.034	0	0	-8.034	84.2
0	0	-0.981	-10.869	-9.015	0	0	-9.015	84.2

Cum. Runoff (mm)	Cum. Infil. (mm)	Cum. Bott. Fl. (mm)	Cum. int flx (mm)
0	0	0	0
22.606	15.873	0.28	0
22.606	51.728	0.212	0
22.606	57.489	0.082	0
22.606	57.432	-0.056	0
22.606	56.217	-0.322	0
22.606	54.749	-1.068	0
22.606	53.56	-1.978	0
22.606	52.579	-2.897	0

Table 19. SoilCover simulations summary for evaporative fluxes during the 8-d test period at the Deilmann south waste rock (DNWR) pile.

SoilCover V. 4.01-Run Summary Page

1. Project Name: DNWRP4c

2. Project Directory: c:\scv4\

3. Run Parameters:

a) Vegetation: No

d) Freeze / Thaw: No

4. Mesh Information:

a) Convergence Criteria:

Max. Iterations	Max Change Suction (%)	Max Change Temperature (%)	Radius Dampening (%)	Temperature Dampening (%)
50	1	1	0	0

b) Time Step Control:

Max Change Suction (%)	Max Change Temperature (%)	Minimum Time Step (seconds)	First Time Step (seconds)	Maximum Time Step (seconds)
5	5	2	1	1000

c) Soil Profile Data:

Number of Nodes	Number of Layers	Drain Mode	Drain Flux (mm/day)
40	3	2	0

5. Soil Property Summary:

Soil Name	Porosity	Spec Grav.	Wt (14Pa)	Ksat (cm/s)
Sandy soil	0.4	2.7	9.10E-06	1.50E-04
cover soil	0.325	2.78	5.00E-05	1.40E-04
Waste Rock	0.488	2.79	5.00E-05	1.60E-04
waste rock	0.355	2.77	5.00E-05	1.60E-04
name5				
name6				
name7				
name8				

6. Boundary Conditions:

a) First date of run:	01-Apr-86
b) Total run days:	8
c) Top temperature condition:	User
d) Bottom temperature (C):	14
e) Day 1 top moisture condition:	Precip.
f) Day 1 bot. moisture condition:	0.3
g) Day 1 bottom moisture value:	0.3

7. Vegetation Summary:

a) Moisture limiting point (kPa):

c) Moisture wilting point (kPa):

e) Grass quality:

b) First date of growing season:

d) Last date of growing season:

f) First day root depth (cm):

8. Run Output Summary:

a) Net cumulative precipitation (mm):	84.2
c) Net cumulative bottom flux (mm):	-76.689
e) Net cumulative PP (mm):	-9.456
g) Net cumulative PT (mm):	0
i) Net cumulative ET (mm):	-8.053
k) Net cumulative drain node flux (mm):	0
b) Net cumulative infiltration (mm):	76.147
d) Net cumulative runoff (mm):	0
f) Net cumulative AI (mm):	-8.053
h) Net cumulative AT (mm):	0
j) Net cum. user monitor flux (mm):	0

User Node: 52
User Elev: 1.00 cm

Table I10. Daily input data for SoilCover simulations for evaporative fluxes during the 27-d test period at the Deilmann north waste rock (DNWR) pile.

Weather data section							Moisture boundaries section			
Run Day	Max AirTemp	Min AirTemp	Net Rad.	Max RH	Min RH	Wind Speed	Top BC	Top BC	Start time	Stop time
	(C)	(C)	(MJ/m2-day)	(dec)	(dec)	(km/hr)	(Type)	(Value)	(hrs)	(hrs)
1	18.00	10.00	1.8834	0.98	0.71	1.41	3	39.2	0	24
2	18.00	10.00	1.8834	0.98	0.71	1.41	3	36.6	0	24
3	11.50	9.00	2.7106	0.99	0.91	0.5918	3	7	0	24
4	15.50	9.00	5.0693	1	0.83	0.793	3	1	0	24
5	11.00	5.00	3.8514	0.97	0.68	1.7391	3	0.4	0	24
6	10.00	3.00	5.7109	0.96	0.67	2.565	3	0	0	24
7	13.00	3.50	4.3685	0.92	0.52	4.4193	3	0	0	24
8	17.00	3.00	4.3951	0.89	0.45	5.6997	3	2.6	0	24
9	17.00	11.00	1.76	1	0.88	3.4	3	13.3	0	24
10	18.50	12.00	8.04	1	0.41	3.5	3	0	0	24
11	17.00	13.50	7.5	0.98	0.31	2.1	3	0	0	24
12	24.00	8.00	6.07	0.85	0.35	3.1	3	0	0	24
13	26.00	11.00	5.63	0.77	0.37	4.5	3	0	0	24
14	28.00	7.00	2.6	0.97	0.52	3.8	3	0	0	24
15	26.50	3.50	5.78	0.91	0.39	3.6	3	0	0	24
16	21.00	6.00	1.65	0.99	0.66	2.9	3	0	0	24
17	22.00	10.50	4.2	0.1	0.63	3.6	3	8.8	0	24
18	20.00	8.50	3.89	0.98	0.7	2.1	3	2.9	0	24
19	17.50	9.00	1.91	0.99	0.82	2.7	3	7.9	0	24
20	15	6.00	6.31	0.99	0.49	3.7	3	7.3	0	24
21	12.50	1.00	4.74	0.96	0.3	2.5	3	0	0	24
22	15.5	7.00	1.13	0.96	0.51	4.4	3	0	0	24
23	17.00	0.00	5.16	0.87	0.37	5.1	3	2.2	0	24
24	15.00	0.00	5.41	0.85	0.38	3.5	3	0	0	24
25	14.00	16.00	4.84	0.73	0.38	5.3	3	0	0	23
26	21.00	10.00	4.9	0.94	0.35	2.3	3	0	0	24
27	24.50	15.00	5.2	0.77	0.25	5.7	3	0	0	24

Moisture boundaries section	Other daily data section
-----------------------------	--------------------------

Bot BC	Bot BC	Top Temp	Bot Temp	Pan Evap	Write Day	Root	Root
Type	(Value)	(C)	(C)	(mm/day)	Out	Top (cm)	Bot (cm)
1	0.3	1	14	1	1	1	1
1	0.3	1	13	1	1	1	1
1	0.23	1	8	1	1	1	1
1	0.146	1	6.5	1	1	1	1
1	0.116	1	8.25	1	1	1	1

1	0.098	1	10	1	1	1	1
1	0.095	1	11.7	1	1	1	1
1	0.118	1	10	1	1	1	1
1	0.05	1	15	1	1	1	1
1	0.05	1	15	1	1	1	1
1	0.05	1	15	1	1	1	1
1	0.05	1	15	1	1	1	1
1	0.05	1	15	1	1	1	1
1	0.05	1	15	1	1	1	1
1	0.05	1	15	1	0	1	1
1	0.05	1	15	1	0	1	1
1	0.05	1	15	1	0	1	1
1	0.05	1	15	1	1	1	1
1	0.05	1	15	1	0	1	1
1	0.05	1	15	1	0	1	1
1	0.05	1	15	1	0	1	1
1	0.05	1	15	1	1	1	1
1	0.05	1	15	1	1	1	1
1	0.05	1	15	1	1	1	1
1	0.05	1	15	1	1	1	1
1	0.05	1	15	1	1	1	1

Table I11. Daily output data for SoilCover simulations for evaporative fluxes during the 27-d test period at the Deilmann north waste rock (DNWR) pile.

Elapsed Time days	Pot Evap (mm)	Act Evap (mm)	Pot Tran (mm)	Act Tran (mm)	Tot ET (mm)	Water Bal (%)	Spec Flux (mm)	Bottom Flux (mm)
0	0	0	0	0	0	0	0	0
1	-0.735	-0.735	0	0	-0.735	-7.323	39.2	-11.85
2	-0.727	-0.727	0	0	-0.727	-9.52	36.6	-35.624
3	-0.691	-0.691	0	0	-0.691	-12.549	7	-16.112
4	-1.38	-1.38	0	0	-1.38	-19.872	1	-8.056
5	-1.096	-1.096	0	0	-1.096	-22.03	0.4	-3.075
6	-1.496	-1.496	0	0	-1.496	-22.851	0	-1.683
7	-1.525	-1.069	0	0	-1.069	-23.114	0	-0.854
8	-1.825	-1.825	0	0	-1.825	-23.299	2.6	0.603
9	-0.579	-0.579	0	0	-0.579	-33.409	13.3	-0.072
10	-2.708	-2.708	0	0	-2.708	-47.271	0	-0.163
11	-2.553	-1.681	0	0	-1.681	-59.167	0	-0.177
12	-2.573	-1.254	0	0	-1.254	-64.431	0	-0.152
13	-2.774	-0.687	0	0	-0.687	-67.107	0	-0.122
14	-1.419	-0.536	0	0	-0.536	-68.718	0	-0.095
15	-2.447	-0.594	0	0	-0.594	-69.565	0	-0.074
16	-0.877	-0.295	0	0	-0.295	-70.247	0	-0.055
17	-2.676	-2.664	0	0	-2.664	-70.985	8.8	-0.008
18	-1.415	-1.415	0	0	-1.415	-72.585	2.9	-0.005
19	-0.669	-0.668	0	0	-0.668	-78.405	7.9	-0.063
20	-2.027	-2.027	0	0	-2.027	-98.202	7.3	-0.1

21	-1.629	-1.629	0	0	-1.629	110.986	0	-0.165
22	-0.836	-0.835	0	0	-0.835	120.726	0	-0.168
23	-2.087	-2.087	0	0	-2.087	-127.48	2.2	-0.084
24	-1.991	-1.313	0	0	-1.313	129.965	0	-0.107
25	-2.363	-0.971	0	0	-0.971	131.853	0	-0.105
26	-2.084	-0.561	0	0	-0.561	132.993	0	-0.086
27	-3.03	-0.498	0	0	-0.498	133.788	0	-0.067

Runoff (mm)	Selected Node Flx (mm)	Net Infiltration (mm)	Cum. PE (mm)	Cum. AE (mm)	Cum. PT (mm)	Cum. AT (mm)	Cum. ET (mm)	Cum. Precip. (mm)
0	0	0	0	0	0	0	0	0
0	0	38.465	-0.735	-0.735	0	0	-0.735	39.2
0	0	35.873	-1.461	-1.461	0	0	-1.461	75.8
0	0	6.309	-2.152	-2.152	0	0	-2.152	82.8
0	0	-0.38	-3.532	-3.532	0	0	-3.532	83.8
0	0	-0.696	-4.628	-4.628	0	0	-4.628	84.2
0	0	-1.496	-6.124	-6.124	0	0	-6.124	84.2
0	0	-1.069	-7.649	-7.193	0	0	-7.193	84.2
0	0	0.775	-9.474	-9.018	0	0	-9.018	86.8
0	0	12.721	-10.053	-9.597	0	0	-9.597	100.1
0	0	-2.708	-12.761	-12.304	0	0	-12.304	100.1
0	0	-1.681	-15.314	-13.985	0	0	-13.985	100.1
0	0	-1.254	-17.887	-15.239	0	0	-15.239	100.1
0	0	-0.687	-20.662	-15.926	0	0	-15.926	100.1
0	0	-0.536	-22.081	-16.461	0	0	-16.461	100.1
0	0	-0.594	-24.528	-17.056	0	0	-17.056	100.1
0	0	-0.295	-25.405	-17.351	0	0	-17.351	100.1
0	0	6.136	-28.081	-20.015	0	0	-20.015	108.9
0	0	1.485	-29.496	-21.43	0	0	-21.43	111.8
0	0	7.232	-30.165	-22.098	0	0	-22.098	119.7
0	0	5.273	-32.191	-24.125	0	0	-24.125	127
0	0	-1.629	-33.821	-25.754	0	0	-25.754	127
0	0	-0.835	-34.656	-26.59	0	0	-26.59	127
0	0	0.113	-36.743	-28.677	0	0	-28.677	129.2
0	0	-1.313	-38.735	-29.99	0	0	-29.99	129.2
0	0	-0.971	-41.098	-30.961	0	0	-30.961	129.2
0	0	-0.561	-43.181	-31.522	0	0	-31.522	129.2
0	0	-0.498	-46.211	-32.02	0	0	-32.02	129.2

Cum. Runoff	Cum. Infil.	Cum. Bott Fl.	Cum. int flx
----------------	----------------	------------------	-----------------

(mm)	(mm)	(mm)	(mm)
0	0	0	0
0	38.465	-11.85	0
0	74.339	-47.474	0
0	80.648	-63.586	0
0	80.268	-71.643	0
0	79.572	-74.718	0
0	78.076	-76.4	0
0	77.007	-77.254	0
0	77.782	-76.652	0
0	90.503	-76.724	0
0	87.796	-76.887	0
0	86.115	-77.064	0
0	84.861	-77.216	0
0	84.174	-77.337	0
0	83.639	-77.432	0
0	83.044	-77.506	0
0	82.749	-77.561	0
0	88.885	-77.569	0
0	90.37	-77.575	0
0	97.602	-77.637	0
0	102.875	-77.738	0
0	101.246	-77.903	0
0	100.41	-78.071	0
0	100.523	-78.155	0
0	99.21	-78.262	0
0	98.239	-78.367	0
0	97.678	-78.453	0
0	97.18	-78.52	0

Table I12. SoilCover simulations summary for evaporative fluxes during the 27-d test period at the Deilmann north waste rock (DNWR) pile.

SoilCover V. 4.01 Run Summary Page

1. Project Name: DNWRP4x

2. Project Directory: c:\scv4\

3. Run Parameters:

a) Vegetation: No b) Freeze/Thaw: No

4. Mesh Information:

a) Convergence Criteria:

Max. Iteration	Max. Change Saturation (%)	Max. Change Temperature (°C)	Max. Change Drainage (%)	Max. Change Temperature (°C)
50	1	1	0	0

b) Time Step Control:

Max. Change Saturation (%)	Max. Change Temperature (°C)	Minimum Time Step (seconds)	First Time Step (seconds)	Maximum Time Step (seconds)
5	5	2	1	1000

c) Soil Profile Data:

Number of Nodes	Number of Layers	Drain Mode	Drain Plus (mm/day)
40	3	2	0

5. Soil Property Summary:

Soil Name	Porosity	Depth (cm)	Sp (1/15)	Kst (m/d)
Soil: soil	0.4	2.77	9.10E-06	1.50E-04
cover soil	0.328	2.73	5.00E-05	1.40E-04
Waste Rock	0.488	2.79	5.00E-05	1.60E-04
waste rock	0.355	2.77	5.00E-05	1.60E-03
rock5				
rock7				
rock8				

6. Boundary Conditions:

a) First date of run:	01-Apr-96
b) Total run days:	27
c) Top temperature condition:	User
d) Bottom temperature (°C):	14
e) Day 1 top moisture condition:	Precip.
f) Day 1 top moisture condition:	0?
g) Day 1 bottom moisture value:	0.3

7. Vegetation Summary:

a) Moisture limiting point (LWP):	
c) Moisture cutting point (LCP):	
e) Grass quality:	
b) First date of growing season:	
d) Last date of growing season:	
f) First day root depth (cm):	

8. Run Output Summary:

a) Net cumulative precipitation (mm):	129.2	b) Net cumulative infiltration (mm):	97.18
c) Net cumulative bottom flux (mm):	-79.52	d) Net cumulative runoff (mm):	0
e) Net cumulative PT (mm):	-46.211	f) Net cumulative ΔT (mm):	-32.02
g) Net cumulative PT (mm):	0	h) Net cumulative AT (mm):	0
i) Net cumulative IT (mm):	-32.02	j) Net cum. user monitor flux (mm):	0
k) Net cumulative drain node flux (mm):	0	User Node:	52
		User Elev:	1.00 cm